



**The role of histone Htz1 in
nucleotide excision repair in
*Saccharomyces cerevisiae***

Yanbo Deng

Institute of Cancer & Genetics

School of Medicine

Cardiff University

A Thesis submitted to Cardiff University for the degree of Doctor of

Philosophy

Ph.D. 2013

DECLARATION

This work has not previously been accepted in substance for any degree and is not concurrently submitted in candidature for any degree.

Signed (candidate) Date

STATEMENT 1

This thesis is being submitted in partial fulfillment of the requirements for the degree of PhD

Signed (candidate) Date

STATEMENT 2

This thesis is the result of my own independent work/investigation, except where otherwise stated. Other sources are acknowledged by explicit references.

Signed (candidate) Date

STATEMENT 3

I hereby give consent for my thesis, if accepted, to be available for photocopying and for inter-library loan, and for the title and summary to be made available to outside organisations.

Signed (candidate) Date

ACKNOWLEDGEMENTS

Foremost, I would like to express my sincere gratitude to my supervisor Professor Ray Waters, for the continuous support of my PhD study and research, for his patience, motivation, enthusiasm, and immense knowledge. His guidance helped me in all the time of research and writing of this thesis. Thanks for giving me this opportunity to come here to do this PhD and let me have a wonderful 4 years. I could not have imagined having a better supervisor for my PhD study. I also would like to thank Dr. Yachuan Yu as my original supervisor for his assistance and guidance in getting my graduate career started when I first came to this lab. He taught me all the techniques and led me in to this study and gave me a lot of support even after he had left the group. I am also very grateful to Professor Simon Reed for always being patient and encouraging when I asked for help and he gave me a lot inspiration.

I must give a huge thanks to my colleagues that accompanied and supported me for this memorable period. To Dr. Shirong Yu and Dr. Yumin Teng, their endless kindness made me feel like I was living in my hometown. Shirong also gave a lot of support for the experiments. As the most experienced person in the lab, questions go to her and come back with the perfect solution. To Dr. Katie Evans, who taught me a lot of English and also treated me with quality chocolate cookies, you are the little sunshine in our lab. To Dr Mark Bennett, who is the magician of bioinformatics, thanks for helping out and sorting out that massive datasets in my thesis. I must tell you that I was jealous that you have such big screens and two of them. To Dr. Richard Webster, who was too scared to play tennis with me; you are so funny that actually I wasted a lot of my lab time just laughing at your silly jokes and tricks again and again. To Dr. James Powell, you are calm and considerate when working and extremely funny when relaxed; I always remember that you took the wrong jumper for Katie. To Wenbin Wang, my Chinese buddy in the lab, thanks for sharing leisure time together. A special thanks goes to the lunch-time concourse tour group and all the members of our lab badminton club.

In addition, I must thank my little girlfriend; Cloris Zhang, although I probably could have finished faster if I could have controlled myself and not to talked to you that

much. Thanks for your love and support and the patience for waiting for me to come back, that is always the source that kept me going.

Most of all I would like to thank my Mum and Dad. Your endless love throughout my life give me encouragement to overcome all the difficulties. You are always a call away to give me your sincere love. I also want to thank my uncle Dr. Yilong Ren and my aunt Dr. Lan Wang and cousin Lin Ren; because of you, the UK has become my second home, I will always cherish the happy times we spent together.

I also would like to thank the China Scholarship Council and Cardiff University for offering me the studentship to support my study.

SUMMARY

Nucleotide excision repair (NER) is critical for maintaining genome integrity. How chromatin dynamics are regulated to facilitate this process in chromatin is still under exploration. Htz1 (H2A.Z), a highly conserved histone H2A variant, is incorporated into the nucleosomes around the promoters of many genes in *S. cerevisiae*. Htz1 is involved in the maintenance of genome stability, DNA transcription activation, DNA replication and DNA repair. In this study, I employed *Saccharomyces cerevisiae*, as a model organism.

In this thesis, I examined the role of histone Htz1 in the response to UV light at specific regions using a high resolution approach and throughout the entire yeast genome using chromatin-immunoprecipitation coupled to microarrays. *htz1Δ* and its deposition related mutants are more sensitive to UV and CPD removal was impaired in total DNA from both *htz1Δ* and *swr1Δ* strains. Acetylation of Htz1 at K3, 8, 10, 14 does not contribute to UV sensitivity or CPD removal from total DNA. CPD removal experiments at the *MFA2* promoter and the *HMRa1* coding region have showed that Htz1 has a role in NER and it likely only affects repair at local nucleosomes containing Htz1. My ChIP experiments at *MFA2* and *HMRa1* indicate that Htz1 enhances the binding of the HAT Gcn5 to Htz1 containing chromatin and this promotes histone H3 hyperacetylation in Htz1 nucleosomes in the *MFA2* promoter after UV irradiation. As a result of this optimal level of histone H3 acetylation occur and the binding of Rad14 to damaged DNA is also enhanced at this region. My genome-wide study shows that UV does not influence the localization of Htz1 as it still resides at the pre-UV sites. Htz1 and H3 K9K14 acetylation is found to be associated with each other genome-wide. This is believed to be via the interaction between Htz1 and Gcn5. These results show that there is a positive role of Htz1 in promoting efficient GG-NER.

Abbreviations

(6-4)PP - Pyrimidine (6–4) pyrimidone photoproduct

aa – Amino acid

ATR - Ataxia-telangiectasia mutated and Rad3-related

BER – Base excision repair

CAK- CDK activating kinase

ChIP – Chromatin immunoprecipitation

CPD – Cyclobutane pyrimidine dimer

DBD – DNA binding domain

DSB – Double strand break

dsDNA – Doubled stranded DNA

EDTA - Ethylenediamine tetraacetic acid

GG-NER – Global genome NER

HAT – Histone acetyl transferase

HR – Homologous recombination

IP – Immunoprecipitation

MMR – Mismatch repair

NER – Nucleotide excision repair

NHEJ – Non-homologous end joining

NTS – Non-transcribed strand

ORF – Open reading frame

PCNA – Proliferating nuclear antigen

PCR – Polymerase chain reaction

PIC- Preincision complex

qPCR – quantitative PCR

RFC – Replication factor C

RNAPI - RNA polymerase I

RNAPII - RNA polymerase II

RPA – Replication protein A

SDS – Sodium dodecyl sulphate

ssDNA – Single stranded DNA

TCR – Transcription coupled NER

TF – Transcription factor

TS – Transcribed strand

TSS – Transcription start site

UBA – Ubiquitin associated

UbL – Ubiquitin like

UPP – Ubiquitin proteasome pathway

WCE – Whole cell extract

Chapter 1 Introduction

1. DNA damage and repair

1.1 DNA damage

DNA is the molecule that stores the genetic information passed from generation to generation and it is the blueprint of most biological life. It was assumed that this macromolecule must be extraordinarily stable in order to maintain the high degree of fidelity required of a master blueprint, and it has been something of a surprise to learn that the structure of DNA is in fact quite dynamic and subject to constant change.

Both spontaneous and external factors can lead to DNA damage and alteration. If these damages are not corrected they can result in mis-replication of DNA and a concomitant change in the DNA sequence. Such mutations have enabled the evolution of life, but too much mutation can be deleterious to an organism, for example by causing cancer in higher organisms. Hence there is a delicate balance between DNA and repair and mutation that cells and organisms have to achieve. DNA is the only repairable biomacromolecule and cells/organisms have evolved a number of complex processes to cope with damage to their genome. Before considering these I will first discuss the types of damage to DNA that are frequently encountered.

1.1.1 Spontaneous damage to DNA

The DNA has to be copied with relative accuracy to maintain the genetic code during cell division. The precise base pairing properties of this double helical molecule are required for this (Alberts et al., 2002).

In the absence of any other influences, base pairing errors are around 1% to 10%. With the help of 3'-5' exonuclease of DNA polymerase to remove incorrect nucleotides this proof-reading capacity (DNA polymerases are the enzymes that replicated the genome) increases the efficiency of the polymerase to result in one error per 10^{-5} to 10^{-6} bases (Keohavong and Thilly, 1989). Finally, post-replicative mismatch repair

increases the replicative fidelity even further to result for the yeast *Saccharomyces cerevisiae* in one error in newly replicated DNA per 10^{-6} to 10^{-9} nucleotides (Tran et al., 1999); these rates are similar to those encountered in organisms ranging from *E.coli* to humans (Kunkel, 2004).

1.1.2 Spontaneous chemical alteration

Cellular DNA can undergo a number of spontaneous changes.

(1) Base isomerisation

Isomers of the 4 DNA bases can interconvert. This conversion can change the hydrogen bond between bases and for example result in adenine pairing with cytosine and thymine with guanine. These errors can influence both the parental and filial generations (Friedberg et al., 2005).

(2) Deamination of bases

The loss of these groups from DNA occurs spontaneously, and in a pH and temperature-dependent manner (Kuraoka, 2008). They results in the conversion of the affected bases to uracil, hypoxanthine, xanthine, and thymine respectively

(3) Loss of bases- depurination and depyrimidination

Spontaneous hydrolyses can result in the loss of pyrimidines and purines from DNA which is greater than generally recognized; the loss of bases due to depurination and depyrimidination of DNA amounts to several thousand residues per genome per day for a mammalian cell (Lindahl, 1982).

(4) Oxidative Damage to DNA

There are various intra- and extracellular sources of oxygen radicals, and oxygen has been appropriately called the “sink” for electrons generated in various redox reactions during aerobic metabolism. The major intracellular source of oxygen radicals is probably leakage associated with the reduction of oxygen to water during mitochondrial respiration. Cell respiration co-products are singlet oxygen peroxide radicals (O_2) hydrogen peroxide (H_2O_2) and hydroxyl radicals ($\cdot OH$). They can create thymine ethylene glycol, hydroxymethyl uracil and other base modifications that in

turn provoke DNA single chain breakage.

(5) Other spontaneous changes to DNA

In addition there are DNA methylations that occur post-replication and structural changes that can accumulate; both of these events can influence DNA functionality (Brown, 2002).

1.1.3 Physical factors triggering DNA damage

Radiation damage to DNA .

(1) UV induced DNA damage

The study of DNA damage was first based on the impact of UV on DNA. When DNA is treated with 260nm ultraviolet irradiation (its absorption peak) the most prevalent type of damage is cyclobutane pyrimidine dimers (CPDs). Adjacent pyrimidines absorb UV energy and covalent bonds are formed between these bases in the same DNA strand. These reactions are quite common: in humans each cell in the skin might experience 50-100 reactions during every second of sunlight exposure (Goodsell, 2001). This reaction is limited to skin because of the weak penetration of ultraviolet irradiation. Ultraviolet irradiation also can cause other base damages and DNA breakage. For example, 6-4 photoproducts and pyrimidine hydrates. As UV radiation was employed to study DNA repair in this thesis all of these damages are covered in more detail in the next section.

(2) Ionizing radiation

Ionizing radiation has direct and indirect ways by which it can create DNA damage. DNA can absorb the energy directly from the radiation and it can also be affected by other molecules (mainly H₂O) in close proximity to DNA and which absorb radiation energy to generate highly reactive free radicals that modify DNA.

Types of ionizing radiation-induced DNA damage.

1. Base Changes

These can be induced by OH-free radicals. They include oxidation to DNA strands and formation of peroxide and base ring shedding and destruction. Pyrimidines are

more susceptible than purines to the creation of these damages (Friedberg et al., 2005). Following ionizing radiation these damages can be induced in clusters, and if they occur in close proximity in opposite strands then they can subsequently result in the creation of double strand breaks (Ward, 2000).

2. Deoxyribose changes

Each carbon atom and hydrogen atom on the hydroxyl of deoxyribose can react with OH⁻, leading to deoxyribose decomposition and DNA strand breaks (Ward, 1994).

3. DNA strand breakage

DNA strand breakage can be a biologically serious type of damage caused by ionizing radiation, and the breakage efficiency is related to the radiation dose and the radiation in question (e.g. soft or hard X-rays; high LET such as alpha radiation). Radiation can destroy the deoxyribose directly or break the phosphodiester bond to produce a DNA break. The frequency of single strand breaks (SSBs) is 10-20 times higher than double strand breaks. The former are usually more easily repaired than the latter. There is a good correlation between the frequency of double strand breaks and the lethal consequences of ionizing radiation (Szumiel, 2008).

4. DNA cross-links.

These DNA cross-links include DNA-DNA strands cross-links (inter- and intra strand cross-links) and DNA-protein cross-links. Radiation can result in the cross-linking of duplex DNA molecules whereas the cross-linking of DNA to proteins by covalent bond formation has also been observed (Cecchini et al., 2005). This includes cross-links to histone, non-histone proteins and enzymes related to DNA metabolism.

1.1.4 Chemically induced DNA damage

Alkylating agents

Alkylating agents are electrophilic compounds that can easily react with the DNA macromolecule.

(1) Base alkylations

Alkylating agents can add alkyl groups to the N- or O- atoms of pyrimidines or

purines. Well studied examples include alkylations to the N⁷ of guanine and the N³ of adenine. After alkylation to the O6 of guanine, at replication it will no longer hydrogen bond with cytosine but does so with thymine. Thus this lesion is potentially highly mutagenic (Shrivastav et al., 2010).

(2) Base shedding

After alkylation, guanine's glycosidic bond is less stable and this can result in base loss to create an apurinic site.

(3) Strand breakage

DNA phosphodiester bonds can be alkylated easily to form unstable phosphate triesters which hydrolyse between the phosphoric acid and the deoxyribose to result in DNA breakage.

(4) Cross-links

Monofunctional alkylating agents only alkylate one site in DNA, whereas bifunctional agents can alkylate two sites to form cross-links between DNA strands and/or DNA-proteins (Siddik, 2005)

Base analogs

Some synthetic base analogs damage DNA and serve as anti-cancer drugs e.g. 5-bromouracil, 5-fluorouracil. These analogs are taken up by cells and they can replace the normal base during DNA replication, as their structure is similar to that of the normal base. 5-bromouracil resembles thymine, pairing with adenine when in the keto form and pairing with guanine when in its enolic form. In this way, a thymine-adenine pair can be changed to a guanine-cytosine pair (Rizki and Rizki, 1969)

1.1.5 UV radiation and DNA damage

The similarity of the absorption spectrum of DNA and the action spectra for cell inactivation, induction of chromosome aberrations, and mutation within the wave length region 230-300nm indicates that DNA is the main chromophore for all of these effects. However, in some cases the action spectra are slightly red shifted compared

with the DNA absorption spectrum. This suggests that light absorption by proteins also plays some role. In some cases, such as for isochromatid breaks, UV absorption in proteins seems to play a major role (Hollosoy, 2002). Action spectra of UV damage to functions directly related to proteins, such as sodium or amino acid transport, closely resemble the absorption spectra of proteins.

Historically, the investigation of UV radiation damage to DNA marks the beginning of the study of the repair of DNA damage (Reviewed in Friedberg et al., 2005). Research on the consequences of exposing cells to UV radiation has been central to elucidating the repair and tolerance of DNA damage. The UV radiation spectrum is divided into three wavelength bands designated UV-A (400 to 320nm), UV-B (320 to 290nm), UV-C (290 to 100nm). As stated earlier the action spectrum of damage to a number of cellular processes/molecules resembles the absorption spectrum of DNA within the wavelength region 230-300nm (Friedberg et al., 2005). Most studies have involved germicidal UV light of approximately 260nm (the DNA absorption peak) (Huang et al., 2005). UV light at 260nm induces two major types of damage: cyclobutane pyrimidine dimers (CPDs), which constitute 70%-80% of total damage; and (6-4) pyrimidine-pyrimidone dimers, which cause 20%-30% of the total damage (Rastogi et al., 2010). CPDs also increase linearly with UVB exposure, but the dose–response relationship varies significantly between different species and taxa (Malloy et al., 1997). In the wavelength region above 320nm the number of CPDs per lethal event decreases and practically all action spectrum for UV effects on cell function fall above the absorption spectrum of DNA (Moan and Peak, 1989).

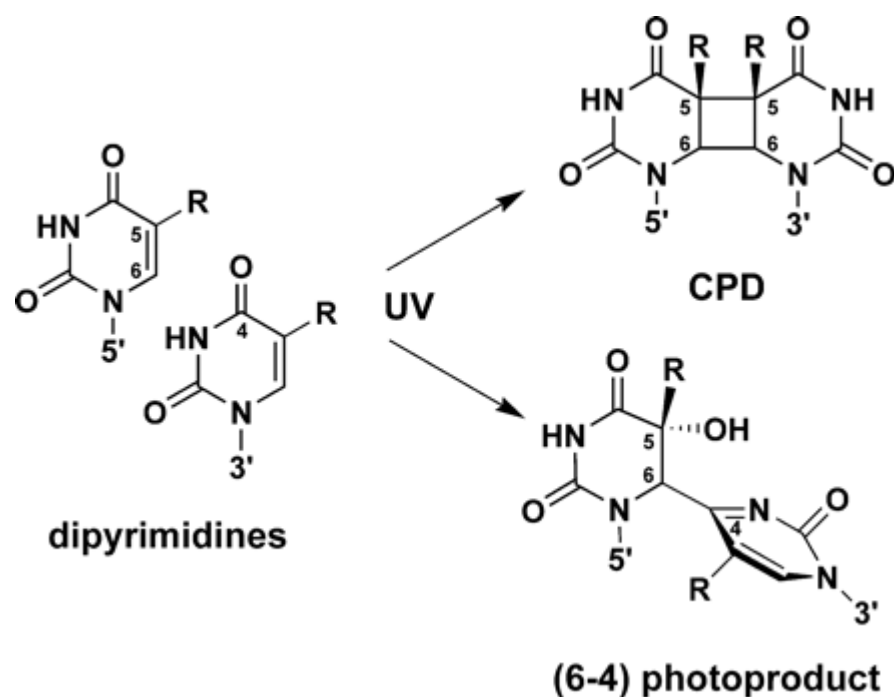


Figure 1.1 The chemical structure of the (6-4) PP and a CPD.

1.1.5.1 Cyclobutyl Pyrimidine Dimers

The formation of pyrimidine photodimers in frozen solutions of thymine was first observed in 1958 (Jagger, 1958). CPDs are formed by covalent bonds between 2 carbon atoms (C-5 and C-6) of adjacent pyrimidines in the same DNA strand, forming a cyclobutyl ring. Only four of the possible isomeric forms of CPDs have been detected with significant yield, namely the cis-syn, the cis-anti, the trans-syn and the trans-anti configurations. Precursors of these isomers may be either excited triplet state pyrimidines or singlet state pyrimidines. The triplet state mechanism probably predominates in solutions of isolated pyrimidines and leads mainly to trans isomers while the singlet state mechanism favours the formation of cis isomers. In native DNA only the cis-syn isomers have been detected (Su et al., 2008). Different types of CPDs can be formed with different probabilities and the yield of CPDs in DNA is influenced by nucleotide locations (Ura et al., 2001). It has been known for years that after moderately high doses of UV radiation the yield of C-C is significantly lower than that of C-T or T-T; there is a ratio of T-T to C-T to T-C to C-C of 68:13:16:3 after the irradiation of plasmid DNA with 254nm. A similar trend has been observed in DNA from irradiated human cells (Friedberg et al., 2005). In HeLa cells exposed to 254nm

light the ratio TT:CT:CC was found to be 30:13:7. The frequency of dimer formation in some sequences is significantly higher than that observed in others (Friedberg et al., 2005). CPDs result in severe helical conformation distortion (Lee et al., 2004).

1.1.5.2 Pyrimidine (6-4) pyrimidone photoproducts

These DNA photoproducts have an action spectrum for formation similar to that for CPDs, and they were first observed in 1965 reviewed in (Rosenstein and Mitchell, 1987). (6-4) pyrimidone photoproducts are formed by a covalent bond between the C-6 position of one pyrimidine and the C-4 position of the adjacent pyrimidine (Pfeifer et al., 1991). They are immunogenic and are usually assayed by radioimmunological methods (Mitchell and Rosenstein, 1987). The yield of (6-4) photoproducts has been reported to be 10%-50% of the yield of CPDs. However, they occur predominantly at TC and CC sequences, and are more frequent at such sites than are CPDs which predominate at TT and CT sequences (Douki and Cadet, 2001).

The formation of a (6-4) photoproduct from two pyrimidines results in a red shift of the absorption spectrum. The (6-4) photoproduct has an absorption maximum at about 310nm and is photolysed with an action spectrum identical with its own absorption spectrum (Yamamoto et al., 2009). Thus, in the wavelength region 290-320nm, (6-4) photoproducts are both formed and photolysed (Mitchell and Rosenstein, 1987). The photolysis product may be the so-called “Dewar valence isomer”, TpT3 (Michaela et al., 2003). Photolysis of a certain fraction of (6-4) photoproducts may also lead to alkali-labile sites which give rise to SSBs in alkali (Moan and Peak, 1989). The (6-4) photoproducts produces even more significant structural distortions in the DNA double helix than the CPD and with a higher yield in linker regions of nucleosomes than in the core (Pfeifer, 1997).

The biological importance of (6-4) photoproducts relative to that of CPDs was determined in an XP revertant cell line that repairs only the (6-4) photoproducts. Contrary to what has been assumed, it was concluded that the majority of the biological effects of UV light, including cell killing, sister chromatid exchanges,

mutagenesis, and inhibition and recovery of DNA and RNA synthesis, appeared to be mainly due to (6-4) photoproducts rather than to CPDs (Moan and Peak, 1989). In agreement with this is the finding that the sensitivities of several mammalian cell lines to UV-induced inactivation correlated better with the capacity to repair (6-4) photoproducts than CPDs (Gale and Smerdon, 1990). However, caution should be applied here as the ability to undertake nucleotide excision repair varies between mammalian species as will the reparability of CPDs or (6-4) photoproducts at different genes (see later section 2).

1.2 DNA repair pathways

DNA is a repairable biomacromolecule and this ability is significant for evolution and the basic maintenance of genetic stability. There are several cellular responses to deal with DNA damage. There are four major categories of repair common to all eukaryotic: base excision repair (BER), nucleotide excision repair (NER) and mismatch repair (MMR) and double strand break repair (reviewed in Friedberg et al. 2005).

1.2.1 Base excision repair

The base excision repair (BER) pathway as shown in Figure 1.2 is a multi-step process important for the repair of a wide variety of chemical lesions at the base of a single deoxyribonucleic acid caused by oxidation, alkylation and base deamination, methylation or spontaneous loss of the DNA base itself (Khobta and Epe, 2012, Fortini et al., 2003). The minimal BER pathway may be reconstituted with only 4 or 5 enzymes, including DNA glycosylase, AP endonuclease, DNA polymerase and a DNA ligase. BER is initiated through the action of a DNA glycosylase, which functions to recognise a lesion and cleaves the N-glycosidic bond between a damaged base and the sugar phosphate backbone to release the excised base and result in an apyrimidinic/apurinic (AP) or abasic site in the DNA (Scharer and Jiricny, 2001). These AP sites can also be generated by the spontaneous hydrolysis of the

N-glycosidic bond. In the second step, the deoxyribose phosphate backbone adjacent to the apyrimidic/apurinic (AP) site is cleaved, either 5' to the AP site by an AP endonuclease or 3' to the AP site via an AP lyase activity present in some AP glycosylases, generating a 3' hydroxyl group and a transient 5' abasic deoxyribose phosphate (dRP). The dRP is then further accomplished by the action of DNA polymerase β by adding one nucleotide to the 3' end of the nick and removes the dRP moiety via its associated AP lyase activity. The missing nucleotide is ultimately replaced by a DNA polymerase (primarily DNA pol β in mammals or pol ϵ in yeast), and the nick is sealed by DNA ligase III (or ligase I, and in yeast Cdc9). There are two subpathways in BER, with different DNA synthesis of either a single nucleotide or multiple nucleotides (Sung and Dimple, 2006). The process of DNA synthesis to add a single nucleotide, is named short-patch BER, or alternatively if a further 1-12 downstream nucleotides are replaced, it is termed long-patch BER. The short-patch BER as described above represents approximately 80-90% of all BER (Friedberg et al., 2005). In long patch BER which is the back-up pathway of BER, DNA is cleaved by the AP endonuclease APE1 (or in yeast Apn1), this is displaced by DNA polymerase in a PCNA dependent manner during replication. This step adds several nucleotides to displace the dRP as a overhang oligonucleotide. The displaced ssDNA fragment then is resolved by the endonuclease FEN1 (Rad27 in yeast) allowing DNA ligation to complete the reaction (Friedberg et al., 2005).

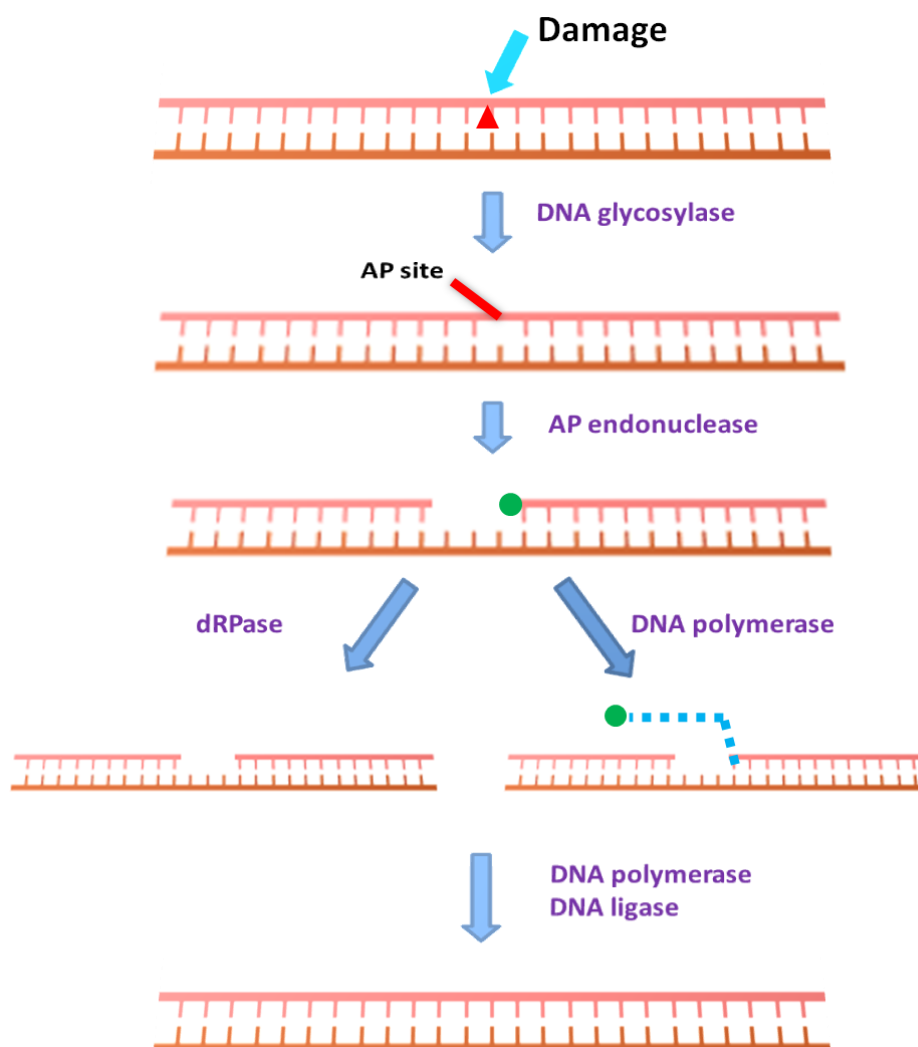


Figure 1.2 The two pathways for base excision repair.

1.2.2 Nucleotide excision repair

NER is perhaps the most flexible of the DNA repair pathways considering the diversity of DNA lesions it acts upon. The most well studied lesions repaired by NER are UV-induced cyclobutane pyrimidine dimers and 6-4 photoproducts (de Boer and Hoeijmakers, 2000). Other NER substrates include bulky chemical adducts, DNA intrastrand crosslinks, and some forms of oxidative damage. The common features of lesions recognized by the NER pathway are that they cause both a helical distortion of the DNA duplex and a modification of the DNA chemistry (Reviewed in Friedberg et al., 2005). The NER repair pathway is highly relevant to my thesis and it is covered in

more detail later (section 2) .

1.2.3 DNA mismatch repair

The Mismatch repair (MMR) pathway is essential in repairing base-base mismatches as well as insertion/deletions loops from replication errors and also base substitution mismatches and insertion-deletion mismatches (IDLs) that are caused by DNA polymerase mis-incorporation and template slippage are generated in organisms from bacteria to mammals (Pluciennik et al., 2010, Jiricny, 2006, Kunkel and Erie, 2005). In the absence of MMR, accumulation of these mutations promotes carcinogenesis. MMR is similar to other excision repair pathways and involves ssDNA resection over the mismatched DNA, followed by DNA polymerase dependent resynthesis.

In eukaryotes, DNA mismatches or IDLs are recognised by MSH2, MSH3 and MSH6 (Kunkel and Erie, 2005). These proteins function as heterodimers of MSH2-MSH6 (MutS α) or MSH2-MSH3 (MutS β), which encircle the DNA at a mismatch in an asymmetric binding manner. Msh2-Msh6 (the yeast homologue of human MSH2-MSH6) can slide along DNA in an ATP independent manner in the absence of rapid deassociation/reassociation events (Gorman et al., 2007). A second heterodimeric complex important for MMR includes the MutL homologues which exist as MutL α (MLH1-PMS2 in humans, Mlh1-Pms1 in yeast), MutL β (MLH1-PMS1, Mlh1-Mlh2 in yeast) and MutL γ (MLH1-MLH3). MutL α has been demonstrated to function as a nicking endonuclease able to produce single stranded nicks in dsDNA (Kadyrov et al., 2006). After DNA mismatches or IDLs are recognised, MutS α translocates along the DNA away from the site of the lesion until MutL α is recruited by MutS α in an ATP-dependent manner (Friedberg et al., 2005). Both PCNA, MutL α and MutS α can form complexes on DNA. MSH3 and MSH6 physically interact with proliferating cell nuclear antigen (PCNA), and this interaction has been predicted to couple MMR with DNA replication (Kunkel and Erie, 2005). In support of this prediction, the interaction with PCNA is found to be necessary to activate the endonucleolytic activity of MutL α (Masih et al., 2008), and it appears that

the orientation upon which PCNA is loaded onto DNA dictates which strand is incised (Pluciennik et al., 2010). The strand containing the mismatch or IDL is excised and resynthesised by factors including PCNA, RPA, RFC, exonuclease I, DNA polymerases delta and epsilon, endonuclease FEN1 (Hays, 2001).

1.2.4 Double strand break (DSB) repair

DSBs are a highly cytotoxic DNA lesion and are the product of multiple sources including ionizing radiation, oxidative stress and replication of damaged DNA. DSB repair can occur via two repair mechanisms; non-homologous end joining (NHEJ) or homologous recombination (HR) (Heyer et al., 2010, San Filippo et al., 2008).

1.2.4.1 Homologous recombination (HR)

HR is initiated by the nucleolytic resection in the 5'→3' direction adjacent to the DSB (San Filippo et al., 2008). 3' single-stranded DNA ends are generated and invade a DNA helix of a homologous sequence and displace the original strand forming a heteroduplex. In *S.cerevisiae* this processing involves four nucleases Mre11-Rad50-Xrs2, Exo1, Dna2 and Sae2 as well as the helicase Sgs1 (Heyer et al., 2010). Single stranded DNA (ssDNA) ends are coated with RPA to prevent secondary structures forming, but subsequent recombination requires the formation of a nucleoprotein filament. The formation of the filament is mediated through Rad51 paralogues, Rad52 and BRCA2 (the latter is only present in higher eukaryotes). After strand invasion the double-stranded DNA helices are linked via a crossing single-strand, generating two Holliday junctions. These junctions may be resolved in a variety of ways to produce both recombinant and non-recombinant dsDNA. Finally, single strand annealing is followed by removal of the 3' ssDNA ends (Heyer et al., 2010, San Filippo et al., 2008).

1.2.4.2 Non-homologous end Joining (NHEJ)

NHEJ is the only DSB repair option in any circumstance where the HR template is

unavailable. NHEJ is a process of direct DNA end-to-end fusion that does not require strand exchanges or the availability of homologous DNA (Reviewed in Friedberg et al., 2005). NHEJ is not a major repair pathway in yeast but it is in mammalian cells. For vertebrate NHEJ, when a DSB breaks forms, the DNA ends are bound by Ku and this complex functions to recruit the nuclease, polymerase and ligase activities (Lieber, 2010). DSB repair in mammalian cells is characterised as having a fast NHEJ component and a slow HR component (Weibezahn et al., 1985). The importance of the NHEJ in mammalian cells compared to yeast may lie in the fact the mammalian genome is so vast and repetitive it is harder to find a suitable partner region for HR. The NHEJ pathway in mammalian cells includes XRCC4, DNA polymerase Pol λ and Pol μ , DNA ligase VI, the Ku70/80 heterodimer and the DNA-dependent protein kinase catalytic subunit (Weterings and van Gent, 2004). The direct joining of two DNA ends will likely involve lesion recognition; forming a bridge to keep the ends near to one another; processing of the DNA ends in a compatible form to be joined together and then the final ligation and sealing of the two ends (Weterings and van Gent, 2004).

1.3 Nucleotide excision repair (NER)

Nucleotide excision repair (NER) is a major DNA repair pathway that ensures that the genome remains functionally intact and is faithfully transmitted to progeny. NER is characterized by the incision of the damaged DNA strand on both sides of the lesion, resulting in eukaryotes in the removal of a fragment approximately 25-30 nucleotides as an oligonucleotide fragment containing the damage. In both prokaryotes and eukaryotes, NER represents an important repair system that is uniquely adapted to remove a large variety of DNA lesions, particularly those that distort the DNA helix; thus, it functions in the removal of damage induced by ultraviolet UV light and the repair of a wide range of helix distorting lesions, including those induced by aromatic hydrocarbons or electrophilic molecules such as cisplatin, as well as intrastrand cross-links (Reviewed in Friedberg et al., 2005).

In humans, a defect in NER results in xeroderma pigmentosum (XP) (Cleaver, 1968). Individuals with XP are extremely sensitive to UV light and the incidence of sunlight induced skin cancers is about 2000 fold higher in XP individuals than in the general population (reviewed in de Boer and Hoeijmakers, 2000). However, defects in NER lead, in addition to cancer and aging, to developmental abnormalities with clinical heterogeneity and varying severities (Kamileri et al., 2012). Recent research has revealed that proteins in NER play distinct roles, and some of them even taken part in other cell process beyond DNA repair. NER factors are components of protein complexes known to be involved in nucleosome remodeling, histone ubiquitination, and the transcriptional activation of genes involved in nuclear receptor signaling, stem cell reprogramming and postnatal mammalian growth (Kamileri et al., 2012).

The NER pathway has two subpathways which are fundamentally identical except in their mechanism of damage recognition. Transcription coupled NER (TC-NER) is initiated through damage mediated inhibition of RNA polymerase II (RNAPII) transcription (reviewed in Hanawalt and Spivak, 2008). TC-NER is confined to only the transcribed strand (TS) of active genes, and promotes rapid repair in these regions in comparison to the remaining genome. The second subpathway, global genome NER (GG-NER), restores DNA damage throughout the entire genome and repairs both active and inactive genes as well as intergenic regions (reviewed in Jazayeri and Jackson, 2002).

I have employed the yeast *Saccharomyces cerevisiae* to examine specific aspect of NER because this mechanism is highly conserved throughout evolution and this yeast has many NER genes homologous to those in humans. Mutations in the NER genes affect both species in a similar fashion. Yeast *rad* mutants (for radiation-sensitive) act like human XP cells and are exceptionally sensitive to UV radiation (reviewed in Friedberg, 2000). As a result, genetic and biochemical studies with the yeast *Saccharomyces cerevisiae* have made major contributions to understand the mechanism of NER in humans. Our current knowledge of NER favours that the NER reaction is mediated through an ordered, stepwise assembly of repair proteins

(reviewed in Friedberg, 2006).

The following sections will detail the specific proteins and processes involved in TC-NER and GG NER in humans and yeast.

In both yeast and humans, the NER process consists of the following steps:

1. Distortion of the DNA helix, rather than specific structural forms of damage suggested to be the common signal for recognition and the initial binding of damage recognition proteins.
2. The DNA helix is unwound around the damaged sites and mediated by the helicase activity of subunits of TFIIH (RNA polymerase Transcription Factor)
3. A dual incision employed by endonucleases creates incisions in the damaged DNA strand both 5' and 3' to the lesion.
4. Excision of the oligonucleotide containing the lesion
5. Synthesis of new DNA fragment using the undamaged strand as a template.
6. DNA ligase anneals the newly synthesized DNA to the existing DNA strand.

1.3.1 NER in humans

For bulky helix-distorting damage, especially lesions induced by UV light, the major repair mechanism is the evolutionarily conserved nucleotide excision repair (NER) pathway. The rate of repair of lesions by NER varies greatly and efforts have been made to determine how much a part distortion plays in lesion recognition rate. For instance, (6-4)PPs distort the DNA to a greater extent than CPDs, and are also repaired 5 to 10 times faster (Friedberg et al., 2005). In humans, it is the only DNA repair mechanism being able to remove UV lesions such as cyclobutane pyrimidine dimers (CPDs) and pyrimidine (6-4) pyrimidone photoproducts (6-4PP) (Gillet and Scharer, 2006). As briefly mentioned, direct evidence of the roles of NER in preventing cancer are found in patients with the autosomal recessive condition xeroderma pigmentosum (XP). These individuals have defects in at least one of the NER genes leading to deficient or no NER and subsequently a 2000 fold higher incidence of skin cancer than in the normal population. The seven NER-deficient

complementation groups representing distinct repair genes XPA–G were identified in XP patients and the NER gene which contains the mutation determines the XP complementation group that the individual belongs to (Cleaver et al., 2009). Patients in these groups are defective in both NER subpathways, except for the XP-C and XP-E groups that are specifically defective in GG-NER (reviewed in Friedberg, 2006).

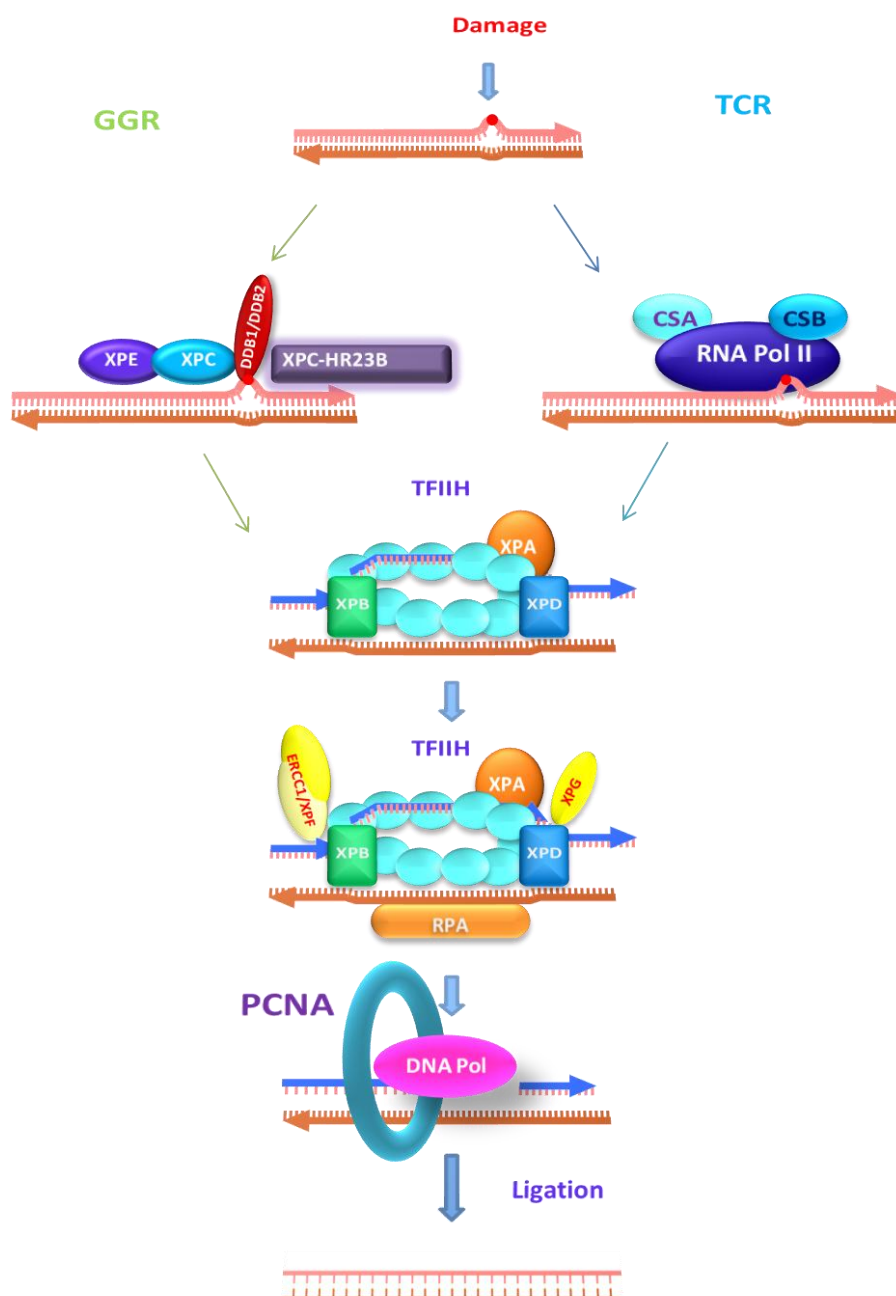


Figure 1.3 The molecular mechanism of the two NER pathways in humans.

(See following text for a description)

1.3.1.1 Global Genome NER (GG-NER) in human

As shown in Figure 1.3, *in vitro* work has determined that the 10 key highly purified components required to process a complete NER reaction are RPA, XPA, XPC-RAD23B, XPG, ERCC1-XPF, TFIIH complex, DNA polymerases δ or ϵ , RFC, PCNA and DNA ligase I. In addition there are less well characterised roles for other stimulatory and regulatory proteins (Araujo et al., 2000). In a stepwise procedure, DNA is first surveyed by the xeroderma pigmentosum complementation group C (XPC)-RAD23-centrin, EF-hand protein, 2 (CETN2) complex (Masutani et al., 1994, Nishi et al., 2005), and the UV damaged DNA-binding protein (UV-DDB) complex (DDB1-DDB2-containing E3-ubiquitin ligase complex) (Lagerwerf et al., 2011). After the complex associates with damaged DNA, RAD23 will dissociate from XPC and does not participate in the next part of the NER process (Bergink et al., 2012). Transcription factor II H (TFIIH) is required to unwind the DNA around the lesion and stabilize the single-stranded DNA. TFIIH is a 10/11-subunit complex including XPB, p62, p52, p44, p34, p8, and XPD in addition to the Cdk-activating-kinase (CAK) complex (released from the core during the NER reaction) and XPG. Unwinding of the DNA relies on the ATPase activity of XPB to form a 27-nucleotide bubble asymmetrically flanking the damage (Oksenysh et al., 2009a). Together with XPA and replication protein A (RPA), XPB and XPD stabilize the damaged DNA for incision (Overmeer et al., 2011). XPG and Complementation group 1 (ERCC1)-XPF are structure-specific endonucleases which cleave the 3' and 5' side of the nucleotide fragment containing damaged DNA. Afterward, RPA is then released from this part of DNA to initiate incision events at other locations (Overmeer et al., 2011). The single-strand gap is then filled by the replicative DNA polymerases δ or ϵ , or the trans lesion DNA polymerase κ ; their polymerase activity is stimulated and coordinated by proliferating cell nuclear antigen (PCNA) loaded onto the DNA by replication factors C (RFC) and A (Kelman, 1997). The nascent DNA fragment is finally sealed by DNA ligase III-XRCC1 (Moser et al., 2007) and DNA ligase I (Araujo et al., 2000, Mocquet et al., 2008).

1.3.1.2 Transcription coupled NER (TC-NER) in humans

The other subpathway of NER, TC-NER, undertakes damage recognition via RNA polymerase II (RNAPII). Stalled RNAPII does not dissociate from the damaged template during assembly of the TCR complex (Fousteri et al., 2006b, Laine and Egly, 2006a). Instead, it colocalizes with Cockayne syndrome B (CSB), a DNA-dependent ATPase (Citterio et al., 1998, Eisen et al., 1995) and CSA, a protein that is part of an E3-ubiquitin ligase complex [containing DDB1, Cul-lin 4A, and ring-box 1 (ROC1/Rbx1)] (Groisman et al., 2003). CSB binds stalled RNAPII and triggers the assembly of the remaining NER factors and histone acetyltransferase p300 (Hasan et al., 2001). CSA recruits (together with CSB) the nucleosomal binding protein high mobility group nucleosome binding domain 1 (HMGN1) (Birger et al., 2003), XPA binding protein 2 (XAB2) (Nakatsu et al., 2000), and TFIIS (Tornaletti et al., 1999). Once chromatin is accessible for TCR, the lesion is removed by the core NER reaction (Laine and Egly, 2006b). Cockayne syndrome is also a recessive genetic disorder yet its patients are not cancer prone, but have multiple health issues and a limited life span.

1.3.1.3 Damage recognition

1.3.1.3.1 Damage recognition during human GG-NER

Human GG-NER damage recognition is facilitated by the XPC-HR23B complex and the UV-DDB protein complex (reviewed in Yeh et al., 2012).

XPC-HR23B-centrin2

Mutations within the XPC genes specifically inhibit GG-NER but do not affect TC-NER (Venema et al., 1991). In vivo, XPC protein is a constituent of a heterotrimeric complex of XPC-HR23B-centrin2, which is known to have a fundamental role in DNA damage detection (Nishi et al., 2005, Volker et al., 2001).

In vitro studies show XPC-HR23B binds dsDNA but has a greater affinity for UV or cisplatin damaged dsDNA or dsDNA containing a (6-4)PP, a platinum crosslink or a cholesterol moiety and elicits the translocation of another NER factor, TFIIH, to damaged DNA (Batty and Wood, 2000, Sugasawa et al., 1998). This DNA binding is mediated by the XPC protein and the second subunit of the XPC complex, HR23B stimulates the *in vitro* NER reaction only in the presence of XPC (Yokoi et al., 2000). The ability of XPC to bind to a broad variety of structurally unrelated DNA lesions suggests that the protein must utilise a non-specific binding mode. This is thought to function by detecting changes in the canonical DNA structure caused by all lesions (Sugasawa, 2009, Bergink et al., 2012). In support of this, a non-lesion containing 5bp mismatch in dsDNA is readily bound by XPC-HR23B, however it is not excised by the NER machinery (Sugasawa et al., 2001). Furthermore, the CPD lesion, which is known to cause more minimal alterations to the DNA helical structure is poorly bound by XPC-HR23B and poorly repaired compared with (6-4)PPs (Batty et al., 2000, Sugasawa et al., 2009). However, if the CPD is incorporated into a mismatch, the binding affinity of XPC-HR23B is higher and the efficiency of repair is dramatically increased (Sugasawa et al., 2001, Mu and Sancar, 1997). XPC binds ss/dsDNA junctions with high affinity and thus separation of the dsDNA by a lesion is considered the primary determinant for damage binding (Sugasawa et al., 2002, Buterin et al., 2005). More studies of DNA adduct structure demonstrated a good correlation between the lesion derived dsDNA separation, XPC binding affinity and NER efficiency (Mocquet et al., 2007). Further studies have shown XPC also has a very high affinity for ssDNA, which is attenuated by UV damage, implying the protein may in fact primarily bind the non-damaged strand at a lesion (Maillard et al., 2007, Bergink et al., 2012). This conclusion is heavily supported by two other recent studies demonstrating that eliminating perturbations in the non-damaged DNA strand suppressed NER damage excision (Buterin et al., 2005, Sugasawa et al., 2009). Remarkably, a study has functionally uncoupled the ability of XPC to bind dsDNA mismatch loops and ssDNA (Camenisch et al., 2009). The two activities lie within

different regions of the XPC DNA-binding domain (DBD), and suggest XPC binds lesions with a bipartite recognition mechanism (Friedberg, 2006). XPC-RAD23B binding is an early event in NER and can also bind to distortions created by 3- to 5-base unpaired bubbles in DNA that do not contain a lesion. This binding of XPC-RAD23B will further distort the structure of the DNA and this could facilitate the entry of XPA, RPA and TFIIH proteins. When ATP-dependent helicases like TFIIH, XPB and XPD encounter a chemical alteration the translocation arrests. During this process of forming an open complex, if no lesions are detected, a stable open complex cannot be formed and NER does not occur. (Friedberg et al., 2005, Sugasawa et al., 2001). XPC binds dsDNA mismatches asymmetrically aligning toward the 5' of such structures (Sugasawa et al., 2002). Damage binding is concurrent with further separation of the dsDNA at a lesion (Evans et al., 1997b, Tapias et al., 2004).

Reciprocal immunoprecipitation and siRNA transfection analysis demonstrated that DNA repair factor XPC is post-translationally modified by ubiquitin and SUMO1 following UV irradiation (Sugasawa et al., 2005, Wang et al., 2005). By using several NER-deficient cell lines, DDB2 (DNA damage binding protein) and XPA are found to be required for both UV-induced XPC modifications. SUMOylation looks to be important for the stabilisation of XPC following UV (Wang et al., 2005). The stability of XPC is reduced significantly following the UV irradiation of XP-A cells and where there is no SUMOylation of XPC. UV, and inactivation of ubiquitylation and the treatment of proteasome inhibitors quantitatively inhibited the UV-induced XPC modifications. Thus these modifications require the functions of DDB2 and XPA and also the the ubiquitin-proteasome system. (Wang et al., 2007). Indeed, XPC ubiquitylation is readily reversible within the cell (Sugasawa et al., 2005). Mutation of lysine 655 to alanine prohibits post-translational modifications of XPC and also its degradation which is essential for recruitment of XPG to UV damage (although XPA and XPB are unaffected). This abolishes GG-NER (Wang et al., 2007).

The roles for HR23B in GG-NER are less clear. In human cells, HR23B is known to express a paralogue called HR23A. Both these proteins have four well-defined functional domains including an N-terminal ubiquitin-like (UbL) domain, the XPC binding domain and two ubiquitin-associated domains (Hiyama et al., 1999). Whilst the two proteins seem to play a functionally redundant role in NER, the majority of XPC complexes are with HR23B (Araki et al., 2001, Ng et al., 2003). *In vitro*, addition of HR23B stimulates NER activity, and both the HR23B N-terminal ubiquitin like domain and the XPC interaction domain are required for this activity (Sugasawa et al., 1996, Masutani et al., 1997). HR23A and HR23B have roles to stabilize the XPC protein by protecting it from 26S proteasome-dependent protein degradation and over-expression of XPC functions to partially relieve the UV sensitivity of mHR23A^{-/-}, mHR23B^{-/-} cell lines (Ng et al., 2003). The protein has also been suggested to contribute to turnover of XPC-HR23B at the pre-initiation complex (PIC) (You et al., 2003).

More recently XPC-HR23B was found to be in a complex with centrin 2 which binds XPC and this contributed to XPC stability, thereby increasing the efficiency of NER (Araki et al., 2001). Centrin 2 is a calcium binding protein, whose affinity for an XPC peptide is strongly promoted by calcium presence (Popescu et al., 2003). Binding of XPC by centrin 2 is necessary for efficient repair *in vivo* and increases damage binding by XPC *in vitro* (Nishi et al., 2005). DNA binding activity of XPC-HR23B is significantly reinforced by the addition of centrin 2. Electrophoretic mobility shift assays showed that centrin 2 stimulates the binding of XPC-HR23B to DNA containing 6-4PP by up to 20-fold, enhances its binding to nondamaged DNA by 4-fold and also increases the ability to recognize a CPD following the addition of centrin 2. (Nishi et al., 2005)

The UV-DDB (DNA damage binding) protein complex

In the global-genome pathway of NER (GG-NER) and as described above, the DNA is initially surveyed for lesions by XPC-RAD23B. The second complex

implicated in damage recognition in human cells is termed the UV damaged DNA binding complex (UV-DDB) (Sugasawa, 2009). The principal complex consisting of the two subunits termed DDB1 (the p127 subunit of DDB) and DDB2 (the p48 subunit of DDB) is able to bind pyrimidine dimers including isomers of a CPD and 6-4PP with the highest reported affinity and specificity of all NER proteins (Wittschieben et al., 2005, Yeh et al., 2012). Compared with DDB, XPC has a substantially lower affinity and specificity for UV lesions (Batty et al., 2000). Mutations in DDB2 give rise to XP complementation group E. These cell lines are known to have defects exclusively in GG-NER (Hwang et al., 1999, Tang and Chu, 2002). XPE lines are known to have highly deficient CPD repair but 6-4PP repair is affected to a lesser extent (Hwang et al., 1999). *In vivo*, the DDB complex has been demonstrated to bind both (6-4)PPs and CPDs, and damage recognition occurs independently of XPC-HR23B-Centrin 2. *In vivo*, DDB2 localizes ahead of XPC to CPD and 6-4PP lesions (Luijsterburg et al., 2007, Moser et al., 2005). In the absence of DDB2, XPC still localizes to 6-4PP and to a lesser extent to CPDs with a substantial delay in kinetics (Fitch et al., 2003, Moser et al., 2005). Despite the molecular defect of XPE, cell-free extracts do not require the UV-DDB complex for efficient NER. However addition of this complex has been shown to have a stimulatory role for the repair of CPDs (Wakasugi et al., 2002). These *in vitro* experiments only employ naked DNA for repair, implying that UV-DDB may have a predominant role in detection of UV-induced lesions in the chromatin (Radic-Otrin et al., 2002).

The X-ray co-crystal structure of UV-DDB explained how the complex is bound to a DNA duplex containing a 6-4PP or an abasic site analog, tetrahydrofuran (Scrima et al., 2008). The study demonstrated DNA damage recognition occurs exclusively through DDB2, but not DDB1. One end of the DDB2 β propeller, opposite the DDB1-binding surface, has an evolutionarily conserved hairpin, which is inserted into the minor groove of the DNA duplex. When bound to DNA containing a 6-4PP, this hairpin insertion leads to flipping out of the two damaged pyrimidine bases and

induces an around 40° kink of the DNA duplex, so separating the DNA strands. Intriguingly, in the co-crystal of UV-DDB and THF-containing DNA, a normal base immediately 3' to THF also is flipped out, suggesting that UV-DDB may have evolved especially to recognize dinucleotide lesions like those induced by UV. Although the structure of UV-DDB bound to a CPD still remains to be solved, this would be expected to explain the very different binding affinities for the two major UV photolesions. Both UV-DDB and XPC-HR23B bind DNA damage, but only XPC is essential for GG-NER (Hwang et al., 1999). Accumulating evidence has indicated that UV-DDB promotes recruitment of XPC to DNA sites containing UV photolesions, especially CPDs which are poorly recognised by XPC thereby enhancing GG-NER. (Scrima et al., 2008, Yeh et al., 2012). As mentioned before, *in vivo*, DDB2 localizes to CPD and 6-4PP lesions faster than XPC and an absence of DDB2 will delay XPC localizing to 6-4PP and CPDs (Moser et al., 2005). These examples demonstrated UV-DDB enhanced damage binding of XPC (Moser et al., 2005, Yasuda et al., 2007). Furthermore, XPC and UV-DDB have been shown to physically interact, this may explain the mechanism of UV-DDB enhancing XPC the binding affinity to DNA damage (Sugasawa et al., 2005).

In vivo the UV-DDB complex is part of an CUL4A-based E3 ligase, including Cul4A, Roc1, and all members of the COP9 signalosome (Groisman et al., 2003, Guerrero-Santoro et al., 2008). The COP9 signalosome functions to negatively regulate the E3 ubiquitin ligase and dissociates from this in response to UV damage. Both UV-DDB and associated E3 ubiquitin ligase subunits are recruited to damage sites as a complex (Luijsterburg et al., 2007). Following UV, The tetrameric E3 ligase, containing UV-DDB is active and able to polyubiquitinate XPC, DDB2 and CUL4A and histones H2A, H3 and H4 around a damaged site (Wang et al., 2006, Kapetanaki et al., 2006). XPC seems to be reversibly ubiquitinated, which is not observed in XP-E cells or Chinese hamster cells without functional DDB2. Cell-free DNA binding assays using paramagnetic beads further revealed that UV-DDB loses its binding activity for UV-damaged DNA upon poly-ubiquitination of DDB2, whereas

polyubiquitinated XPC appears to be still able to bind DNA. In addition to this, DDB2 is degraded in an UV-dose dependent manner, and suggests that polyubiquitination could be involved in a 'lesion handover' mechanism from UV-DDB to XPC. (Kapetanaki et al., 2006, Sugasawa et al., 2005). Since XPC poorly recognizes lesions within the nucleosome core, ubiquitination of histones by the UV-DDB associated E3 ligase may have a role in chromatin remodeling, which destabilize the nucleosome and enable NER factors to get access to lesions. However, the damage binding of UV-DDB is far more rapid than the half life of DDB2 in response to UV, and UV dependent degradation occurs independent of XPC (Alekseev et al., 2008, Luijsterburg et al., 2007). In contrast to DDB2, low-level degradation of XPC occurs in an UV-dose independent manner and a large fraction of the protein is known to be reversibly polyubiquitylated in response to damage (Sugasawa et al., 2005, El-Mahdy et al., 2006). The mechanistic significance of XPC ubiquitylation is unknown, however the post-translationally modified protein is observed to have a higher DNA binding affinity. Ubiquitination of XPC and DDB2 has been suggested to mediate an ubiquitin-dependent handover of the lesion from DDB2 to XPC (Sugasawa et al., 2005) and DDB2-DDB1 forms an E3 ligase in association with CUL4A/B that mediates monoubiquitylation of histones and polyubiquitylation of DDB2 and XPC (Scrima et al., 2011). While autoubiquitylated DDB2 is targeted for degradation, XPC is not because it is protected from proteasome action by RAD23, a proteasome-interacting protein (Sugasawa, 2006). The ubiquitination of histones surrounding the lesions, on the other hand, has been suggested to loosen the nucleosome structure, thereby facilitating the access of the NER repair machinery to the site of damage (Wang et al., 2006).

1.3.1.3.2 Damage recognition during human TC-NER

Defective TC-NER results in the condition termed Cockayne syndrome (CS); a disorder characterised by UV-sensitivity, premature ageing and neurological abnormalities (Nospikel, 2009). RNAPII functions as the initiator of the TC-NER

pathway through its arrest by a lesion during transcription elongation. Chromatin structure is known to strongly influence GG-NER repair kinetics (Waters et al., 2009, Li and Smerdon, 2004), and the damage recognition step is commonly considered to be the rate limiting step in NER (Chaudhuri et al., 2009, Lommel et al., 2000), RNAPII cannot distinguish lesions according to their preferential position in chromatin as it is processive along the DNA, hence another NER protein will promote the recognition step in cooperation with RNAPII.

RNA polymerase II (RNAPII)

RNAPII is a multi-subunit enzyme that catalyzes the synthesis of mRNA from the DNA template. It is proposed to function as the initiator of the TC-NER pathway by stalling at a lesion during transcription elongation. This proposition is based upon a plethora of experimental observations. Firstly, lesions within DNA that function to prohibit transcription elongation by RNAPII are repaired by TC-NER. Such lesions include cisplatin lesions or a CPD (Sarker et al., 2005, Tornaletti, 2009). Conversely, an *N*-2-aminofluorene adduct, which fails to prohibit RNAPII elongation, is not preferentially repaired within the TS of a gene; the operational definition of functional TC-NER (Tang et al., 1989). Secondly, functional TC-NER requires ongoing transcription. Inhibiting RNAPII function either through chemical inhibition or through the use of temperature sensitive RNAPII mutants prohibits preferential repair of the TS of a gene (Christians and Hanawalt, 1992, Sweder and Hanawalt, 1992). Thirdly, using high resolution technologies, it has been observed that preferential repair of the TS begins adjacent to a transcription start site (TSS), and that the kinetics of repair are uniform along the TS (Tijsterman et al., 1999, Teng et al., 1997). Lastly, the incision reaction of TC-NER can be reconstituted *in vitro* at a lesion where RNAPII arrested. This occurred via recombinant NER proteins, but excluding the addition of XPC which is considered a fundamental damage recognition factor in GG-NER (Laine and Egly, 2006a) and is absolutely required for reconstitution of the reaction *in vitro* (Rademakers et al., 2003, Volker et al., 2001).

The current model for TC-NER states that the arrest of RNAPII at a lesion

triggers the downstream recruitment of NER factors (Laine and Egly, 2006a). Other studies have indicated XPG independently recognises and binds RNAPII arrested at a lesion and interact with RNAPII *in vivo* (Sarker et al., 2005).

CSB is a member of the SWI/SNF2 family of DNA-dependent ATPases and contains seven conserved helicase motifs. Members of SWI/SNF chromatin remodelling factors have roles in DNA repair by increasing the accessibility of the lesion in the mononucleosome core particle (Hara and Sancar, 2002). CSB protein is necessary for the molecular mechanism of TC-NER and interacts with RNAPII *in vivo* after UV (Fousteri et al., 2006a, van Gool et al., 1997). CSB was shown to interact with proteins that function in transcription and/or DNA repair, such as histones, XPG, transcription activator p53, hypo- and hyperphosphorylated RNA pol II, together with TFIIE and TFIIH transcription factors (Tantin, 1998, Sarker et al., 2005). It was also confirmed *in vivo*, that CSB is essential for the recruitment of a wide array of NER factors to RNAPII in response to UV damage, including TFIIH, XPG, XPA, ERCC1 and CSA (Fousteri et al., 2006a).

CSA and CSB

Like XP patients, CS patients show hypersensitivity to sunlight but have no predisposition to skin cancer. However, CS patients show a distinctive array of severe developmental and neurological abnormalities as well as premature aging (Friedberg et al., 2005). Classical CS is caused by mutations in either the CSA or CSB genes. CSA- and CSB-deficient cells (CS-A and CS-B, respectively) are proficient in GG-NER but show a defect in TC-NER.

Mfd an important *Escherichia coli* (*E.coli*) TC-NER repair protein is structural similar to CSB. Mfd mediated a coupling mechanism between transcription and repair, and this suggested a potential role of CSB in TC-NER (Selby and Sancar, 1997). Mfd promotes the forward translocation of RNA Pol II when a block in the template is encountered and this translocation is likely to transform the RNA Pol II complex into a more open state that facilitates the access of downstream DNA to the repair factors. CSB is also a member of this ATPases/helicase superfamily like mfd but no helicase

activity has been detected (Selby and Sancar, 1997, Citterio et al., 1998). Thus it has been suggested to similarly function to recruit NER factors by displacing RNAPII (Troelstra et al., 1992, Svejstrup, 2003). However, in contrast to Mfd, CSB cannot displace RNAPII stalled at a lesion, but human RNAP II stalled at a CPD does not inhibit repair (Selby and Sancar, 1997).

A previous report suggested that CSB interacts with RNAPII in the absence of damage, implying that CSB may also have a role in transcription (van den Boom et al., 2004, Malik et al., 2010). Although the repair of 6–4PPs photoproducts and the N-(deoxyguanosin-8-yl)-2-acetylaminofluorene (dG-C8-AAF) adduct occurs without strand bias, the overall repair rate of these lesions by GG-NER is surprisingly delayed in CS cells compared with in wild-type cells. UV causes CSB to have a more stabilised interaction with RNAPII and recruits CSB to chromatin (van den Boom et al., 2004, Fousteri et al., 2006a). CSB has been demonstrated to induce negative supercoiling in dsDNA, it has an ATPase dependent chromatin remodelling activity and the ability to catalyse both ssDNA annealing and strand exchange *in vitro* (Citterio et al., 2000, Beerens et al., 2005). Furthermore, CSB has also been indicated to physically interact with TFIIH, XPA and CSA (Henning et al., 1995, Groisman et al., 2006). In these conditions, CSB might affect the chromatin conformation of both active genes and throughout the genome, enabling the efficient repair of different types of lesions. How each of these properties play a role in recruiting downstream NER factors and/or contribute to as yet undefined molecular mechanisms remains to be seen.

In humans CSA is essential for TC-NER, whilst surprisingly, mutation of the yeast homologue *RAD28* does not seem to affect repair kinetics (Bhatia et al., 1996, Venema et al., 1990). As observed with CSB, CSA binds to RNAPII regardless of DNA damage but this accumulates after UV irradiation (Groisman et al., 2003, Fousteri et al., 2006a). CSA protein is a component of an E3 ubiquitin ligase complex alongside cullin 4A, Roc1 and the COP9 signalosome (CSN) and it was found to associate with RNAP II in a UV-dependent fashion (Groisman et al., 2003). E3

ubiquitin ligases target the covalent addition of an ubiquitin molecule to protein lysines, which often initiates proteasomal degradation of the protein (Finley, 2009). The GG-NER specific factor DDB2 also resides in a similar complex to CSA. TC-NER-associated factor CSA and the GG-NER-associated factor DDB2 form very similar E3 ubiquitin–ligase complexes, establishing a link between these two pathways and ubiquitin-dependent protein degradation (Groisman et al., 2003). COP9 functions to negatively regulate the CSA E3 ubiquitin ligase. To date, the only known substrate of this ligase is CSB (Groisman et al., 2006). CSB is ubiquitinated by the CSA ligase and degraded by the proteasome in a UV-dependent manner at a later time in the repair process, and this activity is necessary for the recovery of RNA synthesis following UV damage. Unlike CSA, deletion of Rad28 (the yeast homolog) does not affect post-UV recovery of RNA synthesis (Reagan and Friedberg, 1997). In addition, CSA is not considered to retain a stable complex with CSB, and a transient interaction of these two was observed *in vivo* (van Gool et al., 1997). Furthermore, CSA is only required for the recruitment of TFIIS, HMG1 and XAB2 to RNAPII for TC-NER, and thus plays a functionally distinguishable role in TC-NER from CSB (Fousteri et al., 2006a).

Ubiquitin

Recent studies raise the importance of post-translational modifications in the molecular mechanism of DNA repair, and the covalent attachment of ubiquitin to repair proteins is highly prevalent via E3 ubiquitin ligases such as the CSA complex, and the structurally related SUMO polypeptides (Bergink and Jentsch, 2009, Jackson and Durocher, 2013). As mentioned before, CSB is a substrate of CSA, and also RNAPII (PolII LS) is known to be ubiquitinated in response to UV damage to result in proteasomal degradation of the protein (Ratner et al., 1998, Woudstra et al., 2002). The identity of the key ubiquitylation event that initiates TC-NER is still unknown, but RNAP II and CSB ubiquitylation are two main candidates. In that regard, CSB possesses a functionally important ubiquitin binding domain (UBD), suggesting that CSB recognizes this key ubiquitylation event (Anindya et al., 2010). Furthermore,

DUB USP7 is recruited to stalled polymerases by UVSSA which is the product of a gene mutated in a CS-like UV-sensitivity syndrome (Cleaver, 2012). UVSSA-USP7 interacts with RNAP II and delays the CSA-dependent degradation of CSB by the proteasome. CSB was identified to possess an ubiquitin binding domain (UBD) at its C-terminus (Anindya et al., 2010). In the absence of this domain, CSB is unable to dynamically associate with TC-NER complexes that result in sequestration of the protein at a lesion. Amazingly, the truncated protein can still function to recruit all the proteins necessary for DNA incision and oligonucleotide extrusion at a lesion, however neither activity can be detected (Laine and Egly, 2006a). Thus an ubiquitylation event seems absolutely required for TC-NER via a CSB directed regulation mechanism. Arrest of an elongating RNAPII (by DNA damage or through chemical inhibition) appears to be the primary stimulus for PolII LS ubiquitylation, thus DNA damage per se is not necessarily required (Lee et al., 2002, Somesh et al., 2005). It was hypothesised that in the absence of successful TC-NER, an arrested RNAPII may be removed through degradation of PolII LS by the proteasome as ‘a last resort’ mechanism (Svejstrup, 2007, Somesh et al., 2005). In fact the E3 ubiquitin ligase that targets PolII LS is conserved from *S.cerevisiae* to humans and the repair proteins are not required for this activity. Mutations in CSA/CSB that function to delay recovery of RNAPII transcription after UV treatment do so by causing a reduction of the substrate of PolII LS ubiquitylation (Anindya et al., 2007). Despite this abundance of data, and the fact that RNAPII does not sterically inhibit TC-NER *in vitro*, the degradation of PolII LS and subsequent elimination of RNAPII for TC-NER is still a working model (Malik et al., 2010, Tremeau-Bravard et al., 2004). The covalent modification does not seem to influence TC-NER or degradation but instead looks to mediate activation of downstream DNA damage response pathways (Chen et al., 2009). The degradation of RNAP II by the proteasome can be seen as a measurement and provides a potential opportunity to study the role of ubiquitin chain editing.

1.3.1.4 Formation of the preincision complex

Following DNA damage recognition, an open complex formation occurs around a lesion, with an unwound open complex spanning around 25 nucleotides for lesion verification. After that a collection of factors associate with the lesion forms a multi-protein complex termed the preincision complex (PIC) (Mu et al., 1997, Wakasugi and Sancar, 1998). The recognition of damaged DNA and remodeling of chromatin is a rate-limiting step for repair, and the high specificity complex PIC facilitates the remodeling of chromatin in this step (Evans et al., 1997a, Mu et al., 1996b). After recognition, GG-NER and TC-NER require identical factors to compete NER (Guthrie, 2008).

TFIIH

The multisubunit complex TFIIH is necessary for the transcription of RNA polymerase I and II genes (Thomas and Chiang, 2006) and originally it was discovered as a transcription factor that also takes part in cell cycle control (Matsuno et al., 2007). In mammalian cells, TFIIH comprises ten sub-units, XPB, XPD, GTF2H1 (aka p62), GTF2H4 (p52), GTF2H2 (p44), GTF2H3 (p34), GTF2H5 (TTDA), CDK7, CCNH (cyclin H) and MNAT1 (Mat1). CDK7, CCNH and MNAT1 (Bedez et al., 2013). They form a complex which can phosphorylate the C-terminal domain (CTD) of RNAPII. These sub-units and the CTD kinase activity are not required for NER *in vitro*. However as they are present in the native TFIIH complex, they may play roles in modulating the process (Araujo et al., 2000, Svejstrup et al., 1996). Co-immunoprecipitation of TFIIH, using an antibody against the CDK7 sub-unit, obtains about 30% of the XPC in a cell and a small amount of XPG, but no other NER proteins (Araujo et al., 2001). This may indicate that TFIIH and XPC interact in the early stages of NER. Following damage recognition, *in vitro* binding of the three factors TFIIH, XPA and RPA to a lesion are partially interdependent both for GG-NER and TC-NER (Lainé and Egly, 2006, Mu et al., 1997). However, more sensitive *in vitro* studies and *in vivo* evidence strongly suggest TFIIH is the first protein complex to join a damage site following detection (Riedl et al., 2003, Tapias et

al., 2004). Subunits XPD and XPB possess 5' → 3' and 3' → 5' helicase activity respectively which is responsible for unwinding the DNA helix (Sung et al., 1993, Schaeffer et al., 1993, Schaeffer et al., 1994). XPD's helicase activity is only required for its roles in NER and is dispensable for proper transcription, but mutations of the *XPD* gene can result in three disorders; XP, trichothiodystrophy (TTD) and CS with XP (Winkler et al., 2000, Lehmann, 2008). XPB is absolutely required for recruitment of TFIIH to damage sites in chromatin (Riedl et al., 2003, Oksenyshyn et al., 2009b).

TFIIH activity result in an opened DNA structure that leads to the recruitment of XPA, RPA and XPG (Tapias et al., 2004) and the formation of the stable pre-incision complex. Once localised to a damage site, TFIIH subsequently functions to separate the dsDNA surrounding a lesion (Evans et al., 1997b, Evans et al., 1997a). This strand separation by TFIIH requires ATP hydrolysis and involved the two helicases, namely XPB and XPD (Tapias et al., 2004). XPB may separate DNA using an ATPase activity alone, whilst XPD functions to translocate TFIIH along DNA and separate the strands as helicase activity of XPD is essential for NER. An XPB devoid of helicase function protein but retaining its ATPase activity is sufficient for separation (Sugasawa et al., 2009, Coin et al., 2007). Whilst XPD translocation is in a 5' → 3' direction, experiments that analyse either strand separation or cleavage of DNA relative to a lesion, suggest the bubble of separated DNA is positioned toward the 5' of the damage (Tapias et al., 2004, Matsunaga et al., 1995).

TFIIH has been previously suggested to verify the presence of a lesion. This bipartite damage recognition mechanism was originally proposed based upon the observation that lesions which fail to significantly alter DNA structure, are only efficiently repaired by NER if combined with a mismatch loop (Hess et al., 1997, Sugasawa et al., 2001). Studies on mammalian NER find a co-localization of TFIIH in NER and subsequent loss of the CAK complex, affects transcription activation (Coin et al., 2008). This suggests TFIIH is a dynamic complex in NER and CAK was statically engaged with TFIIH both during repair and transcription (Araujo et al., 2001, Mu et al., 1996a).

RPA and XPA

After the DNA strands are separated by TFIIH, recruitment of XPA, RPA and XPG functions to further separate the DNA around a lesion and this completes the formation of the PIC (Tapias et al., 2004). XPA is a small (36kDa) Zn-binding protein that is able to form a heterodimer in solution (Yang et al., 2002). However, according to fluorescence microscopy data, after UV irradiation the protein migrates to the DNA lesion as a monomer (Rademakers et al., 2003). XPA was shown to be able to interact with other repair factors: RPA, ERCC1, and TFIIH (Li et al., 1995a, Li et al., 1994). RPA is a stable heterotrimer consisting of 70, 32, and 14kDa subunits (RPA1, RPA2, and RPA3, correspondingly). The main function of RPA is the stabilization of single stranded DNA. This is one of the most abundant human proteins binding single stranded DNA. RPA is known to participate in all basic DNA metabolic processes: replication, repair, and homologous recombination (Wold, 1997, Pestryakov and Lavrik, 2008). RPA in NER probably takes part in all major stages of the process: damage recognition, preincision complex assembly, and the subsequent repair synthesis.

Both proteins, XPA and RPA, have increased affinity for disruptions of the DNA helix strand such as noncanonical base pairs, “bubbles”, and small loops (Missura et al., 2001). RPA supposedly participates in NER together with XPA. Indeed the presence of RPA enhance XPA binding and the proper positioning of XPA, RPA and TFIIH in the pre-incision complex. It also ensures the correct placement of the endonucleases near the junction of single-stranded and duplex DNA and also on the damaged strand (Fagbemi et al., 2011, Friedberg et al., 2005). The affinity of the XPA–RPA complex to damaged DNA is higher than that of RPA alone and by more than an order of magnitude (Schweizer et al., 1999). However, the affinity of the XPA–RPA complex to DNA damage is an order of magnitude lower than that of XPC–hHR23B (Hey et al., 2002). Although originally these proteins are hypothesized to be the primary damage recognition factor, XPA has a high affinity for kinked DNA rather than damaged DNA (Camenisch et al., 2006).

RPA has a high affinity for ssDNA and stable interaction of the complex with ssDNA occludes a region of ~30 nucleotides, however RPA may also bind shorter DNA fragments with a lower affinity (Kim et al., 1994, Kim et al., 1992). Interestingly, the 30 nucleotide DNA binding mode of RPA matches the DNA strand separation size during NER (Evans et al., 1997a, Riedl et al., 2003). RPA is also known to have a high preference for binding pyrimidines and UV induced DNA lesions such as (6-4)PPs (Kim et al., 1992, Wakasugi and Sancar, 1999). DNA binding is conferred by oligonucleotide binding (OB) domains; RPA1 contains 4 OB domains, whilst RPA2 and RPA3 each have one, and all three subunits contribute to DNA binding (Bochkarev et al., 1997, Salas et al., 2009). DNA binding by RPA occurs with a strict polarity and in different ways with the formation of complexes of different types depending on the length of the single stranded DNA region. For all DNA, high affinity DNA binding occurs at the 5' of ssDNA where the RPA1 OB domain DBDA is initially located, whilst the weaker DNA interactions that occur toward the 3' (by subsequent OB domains in RPA1 and 2) are only required for binding with longer nucleotide sequences (>12nt) (de Laat et al., 1998a, Bastin-Shanower and Brill, 2001). During NER, binding of RPA to the separated DNA strands is thought to both stabilise the ssDNA intermediates whilst co-ordinating PIC formation through specific protein-protein interactions (de Laat et al., 1998a). RPA appears to be bound to the undamaged strand and its binding can enhance the activity of the endonuclease ERCC1-XPF on the opposite strand (de Laat et al., 1998a). RPA also has roles in positioning and regulating the activities of XPG and XPF-ERCC1. RPA physically interacts with and stimulates the DNA incision activity of both endonucleases (Matsunaga et al., 1996, He et al., 1995). RPA only functions to recruit both endonucleases to their specific DNA junctions in one DNA binding orientation (de Laat et al., 1998a). After the damage excision RPA stays bound to DNA unlike the majority of the other repair factors, probably stabilizing the single stranded gap and attracting replication factors RFC and PCNA for single strand gap filling.

XPA was shown to prefer artificially created DNA structures containing crossed DNA

duplexes (Missura et al., 2001, Camenisch et al., 2006) and to have increased affinity for DNA structures containing transitions from single to double stranded DNA including Y-structures (Yang et al., 2006) and DNA with 3' or 5' overhanging single strand ends (Maltseva et al., 2006, Yang et al., 2006). XPA is no longer considered to play this primordial role due to the absolute requirement of XPC for damage localisation of XPA *in vivo* (Volker et al., 2001), and the ability of RPA to detect and stabilize DNA intermediates containing single strand regions. This provides XPA-RPA with a highly sensitive method for molecular verification of the early NER PIC (Missura et al., 2001). XPA has direct contact not only with RPA but also with ERCC1 protein (Saijo et al., 1996), one of the subunits of the ERCC1-XPF heterodimer-structure specific endonuclease cleaving damaged DNA strand in the 5' direction from the lesion. It was shown that these contacts are specifically important for NER but not for other repair pathways (Orelli et al., 2010). Research has further identified XPA as a potential pivotal intermediate protein between the core NER reaction and DNA damage responsive checkpoint proteins. Post UV, ATR functions to phosphorylate XPA and this improves CPD repair and survival (Wu et al., 2006). Acetylation and deacetylation of XPA is necessary for proficient CPD repair (Fan and Luo, 2010) and suggest that post-translational modifications of XPA may modulate NER activity.

1.3.1.5 Dual Incision

The formation of the preincision complex (PIC) is completed by the binding of XPG and then ERCC1-XPF to enable dual incision and oligonucleotide extrusion (Constantinou et al., 1999, Evans et al., 1997a, Evans et al., 1997b, Mu et al., 1997, Riedl et al., 2003). ERCC1-XPF is engaged to perform the incision 5' to the damage (Mu et al., 1997, Tapias et al., 2004, Tsodikov et al., 2007), whereas XPG cleaves 3' to the lesion (O'Donovan et al., 1994). An oligonucleotide of 24–32 nucleotides in length containing the lesion is then released (Ogi and Lehmann, 2006). The 5' incision is made 15-24 nucleotides from the lesion whilst the 3' incision occurs 2-8

nucleotides away, releasing an oligonucleotide of ~27 nucleotides (Huang et al., 1992, Matsunaga et al., 1995, Moggs et al., 1996).

In vitro, XPG is absolutely required for the recruitment of ERCC1-XPF suggesting that these factors are the last components to join prior to DNA incision (Riedl et al., 2003). XPG is a structure-specific endonuclease, its preference lies at the single-strand to double-strand junction, more accurate at open arms and bubble structures within the 5' extending ssDNA (Mu et al., 1996b, O'Donovan et al., 1994). This incision occurs within one nucleotide of the ds/ss junction depending upon the structure of the substrate (Hohl et al., 2003). The interaction between XPG and TFIIH is important for the stable recruitment of XPG to damage *in vivo*, and for functional repair (Araujo et al., 2001, Dunand-Sauthier et al., 2005, Ito et al., 2007). Lack of this leads to a dissociation of XPD and the CAK complex from TFIIH, adding weight to the view that XPG also has a structural role alongside its endonuclease function (Friedberg et al., 2005). Using catalytically inactive forms of XPG, the result suggest that the presence of XPG, but not its catalytic activity, is required for the generation of the 5' incision by ERCC1-XPF (Constantinou et al., 1999). Another study showed that the efficient 3' incision by XPG required the presence and catalytic activity of ERCC1-XPF (Tapias et al., 2004).

XPF and ERCC1 form a heterodimer and the two proteins are unstable in the absence of each other, this heterodimer functions to incise DNA structures with an exact opposite polarity to that by XPG (Sijbers et al., 1996a, van Vuuren et al., 1993). The heterodimer interacts at the C-terminal of both proteins, and the interaction is essential for NER (de Laat et al., 1998b, Sijbers et al., 1996b). XPF contains the endonuclease activity in the complex with the active site being at amino acids 670 to 740 (Friedberg et al., 2005). ERCC1-XPF is recruited to the NER PIC by TFIIH (Guzder et al., 1996, Tsodikov et al., 2007, Godon et al., 2012), and the interaction of XPF-ERCC1 with XPA is necessary for functional NER (Li et al., 1994, Li et al., 1995b).

The order of recruitment for the two endonucleases is well documented, but there is

controversy over the order in which the two incise DNA during NER. Results from utilising catalytically inactive forms of XPG and XPF suggests that the 5' cut by XPF comes first, as efficient XPG incision requires both the presence and catalytic activity of ERCC1-XPF (Tapias et al., 2004). Furthermore, it has been demonstrated *in vivo* that the incision by ERCC1/XPF was sufficient to initiate downstream DNA synthesis, in the absence of the XPG incision (Staresincic et al., 2009). This 'cut-patch-cut-patch' mechanism indicates that XPF carries out the 5' incision, which is followed by the initiation of repair synthesis, and then the second incision at the 3' end via XPG takes place allowing the completion of repair synthesis (Staresincic et al., 2009, Tapias et al., 2004). On the other hand, evidence has also been presented that on a variety of substrates the 3' incision by XPG takes place in the absence of XPF-ERCC1, suggesting XPF-ERCC1 should be the first incision (Evans et al., 1997a, Evans et al., 1997b). Although this seemingly controversial question has not yet been resolved, the incision events are believed to be an ordered and not simultaneous (Fagbemi et al., 2011). These studies have only been performed upon naked DNA templates and *in vivo* results will be fundamentally important to understand the order of dual incision.

1.3.1.6 Re-synthesis and ligation

Following dual incision of the damaged oligonucleotide, there is a 25-30 nt length gap that has to be filled to restore the native structure. *In vitro*, reconstitution of NER DNA resynthesis can be achieved through the addition of RPA, PCNA, RFC, polymerases delta (Pol δ) or epsilon (Pol ϵ) and DNA ligase I (Aroussekhra et al., 1995, Mocquet et al., 2008). Human Pol δ is comprised of 4 sub-units including the 125 kDa catalytic sub-unit POLD1, and 3 smaller sub-units of 50, 66 and 12-kDa. The 66-kDa mediates interactions with PCNA (Friedberg et al., 2005). PCNA co-localises to UV damage *in vivo* and complexes with RPA in a UV dependent manner (Essers et al., 2005, Green and Almouzni, 2003, Gilljam et al., 2012). As shown for PCNA, mammalian pol δ also colocalises with UV damage and complexes with RPA (Moser et al., 2007, Mocquet et al., 2008). Mammalian DNA ligase I also localises to UV

damage in a cell-cycle regulated manner (Moser et al., 2007). This pathway with respect to NER is poorly characterised and thus the molecular mechanism is extrapolated from supposed steps in DNA replication (Gillet and Scharer, 2006). RFC is a pentameric complex which functions to load the trimeric ring structure of PCNA proximal to the 3' primer DNA (Overmeer et al., 2010). PCNA then interacts with a DNA polymerase (Pol ϵ and Pol δ) and the complex resynthesise DNA, filling the oligonucleotide gap. DNA ligase subsequently restores the missing phosphodiester bond between the final nucleotide incorporated and the dsDNA molecule.

More recent research on mammalian NER has also implicated another DNA polymerase, polk, and ligase, XRCC1-DNA ligase III α (DNA ligase III), to be important for resynthesis (Ogi and Lehmann, 2006, Moser et al., 2007). Pol δ and polk apparently function within the same pathway, and depleting all three polymerases is sufficient to prohibit DNA resynthesis *in vivo* (Ogi et al., 2010). DNA ligase III localises to UV damage *in vivo* and apparently is the predominant ligase in mammalian NER (Moser et al., 2007).

1.3.2 NER in *Saccharomyces cerevisiae*

Nucleotide excision repair was first discovered in bacteria in the mid-1960s by Philip Hanawalt and David Pettijohn with the observation of non-semiconservative DNA synthesis during the excision of CPDs (Pettijohn and Hanawalt, 1964). Not long afterwards, excision repair of UV-induced DNA damage was also observed in mammalian cells (Rasmussen and Painter, 1964). The NER process in *Escherichia coli* is relatively well understood and requires only six proteins, whereas the NER process in eukaryotes displays a much higher degree of genetic complexity, requiring more than 30 proteins to reconstitute the reaction *in vitro* (Aboussekhra et al., 1995, Guzder et al., 1995). Genetic and biochemical studies in the yeast *Saccharomyces cerevisiae* have made major contributions for elucidating the mechanism of dual incision of damaged eukaryotic DNA, and they have yielded important insights into the functions of a multitude of NER proteins (Prakash and Prakash, 2000). Many

cellular processes such as replication, repair, cell division, and recombination are highly conserved from lower to higher eukaryotes, and most NER factors are conserved proteins, having orthologs in humans and yeast.

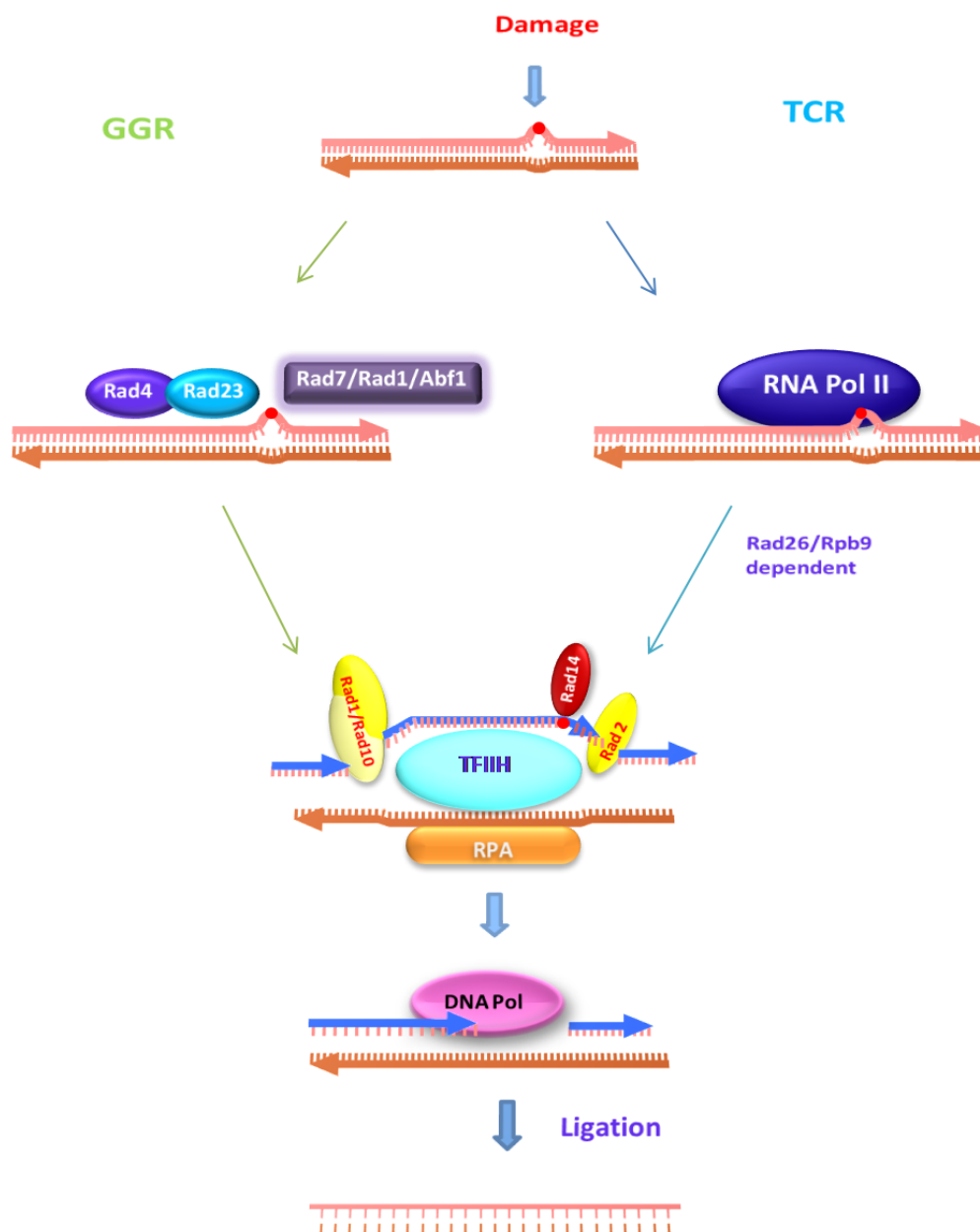


Figure 1.4 Molecular mechanism of two NER pathways in *S. cerevisiae*

(See the following text and Table 1.1 for a description)

Yeast genes with roles in NER are listed in Table 1.1 and their mode of action described in Figure 1.4. Just as in human nucleotide excision repair, yeast NER also consist of two sub-pathways: global genomic repair (GG-NER) and transcription coupled repair (TC-NER). GG-NER is responsible for damage in transcriptionally

silent regions and in the nontranscribed strand (NTS) of active genes, while TC-NER is dedicated to repairing lesions in the transcribed strand (TS) of active genes.

Table 1.1

Step	<i>S. cerevisiae</i>	<i>Human</i>	Function
Damage detection	RAD4	XPC	DNA damage recognition
	RAD23	HR23B	recruitment of other NER factors
	RAD33	CEN2	
	?	DDB1	DNA damage recognition and chromatin remodelling
	?	DDB2	
GG-NER specific	ABF1	?	DNA binding protein
	RAD7	?	SOCS box E3 ligase component
	RAD16	?	SnF2 family ATPase, RING finger Gen5 recruitment, H3 acetylation
TC-NER specific	RAD28	CSA	WD40 repeat E3 ligase component
	RAD26	CSB	SnF2 family ATPase
Pre-incision complex	RAD3	XPD	5' → 3' DNA helicase
	RAD25	XPB	3' → 5' DNA helicase
	SSL1	GTF2H2	Core TFIIH subunit p44
	TFB1	GTF2H1	Core TFIIH subunit p62
	TFB2	GTF2H4	Core TFIIH subunit p52
	TFB4	GTF2H3	Core TFIIH subunit p34
	TFB5	TTDA	Stabilise TFIIH
	TFB3	MAT1	CAK/TFIK
	CCL1	Cyclin H	CAK/TFIK
		RAD14	XPA
	RFA	RPA	ssDNA binding protein
Dual Incision	RAD1	XPF	Endonuclease incision ssDNA at 5'
	RAD10	ERCC1	
	RAD2	XPG	Endonuclease incision ssDNA at 3'

1.3.2.1 Damage recognition

Damage recognition is possibly the least well understood step of NER in eukaryotes, including *S.cerevisiae*. This step is expected to be the rate limiting aspect since lesions have to be located within a large background of undamaged DNA. Similarly to in humans, the two major pathways of NER only differ in the initial steps of DNA damage recognition. After lesion recognition and verification, the general steps in GG-NER and TC-NER are the same.

1.3.2.1.1 Damage recognition during yeast TC-NER

TC-NER was first discovered in the 1980s. It was shown to function in *E. coli* (Mellon et al., 1987), *S. cerevisiae* (Smerdon and Thoma 1990), and mammalian cells (Mellon et al., 1987). Lesions are repaired by TC-NER about 5-10 times faster in the transcribed strand when compared to lesions in non-transcribed regions (Hanawalt, 1994). In GG-NER, dedicated proteins directly recognize a lesion, and complexes containing Rad7, Rad16 and ABF1 are unique to this sub-pathway (Yu et al., 2004). By contrast, TC-NER is initiated when a lesion on the transcribed strand blocks RNA polymerase; unique to TC-NER are Rad26 and the Rpb9 subunit of RNA Pol II (Li et al., 2006c). Based on sequence homology to the encoded proteins, of the *CSA* and *CSB* genes, yeast homologs were identified as *RAD28* and *RAD26*, respectively (van Gool et al., 1994, Bhatia et al., 1996).

Rad 26

CSB and Rad26 share strong sequence homology, which includes the seven conserved motifs of DNA/RNA helicases in the SNF2 subfamily. Both proteins exhibit DNA-dependent ATPase activity but have no detectable helicase activity (Guzder et al., 1996). Although a *rad26* Δ single mutant is not sensitive to UV, CPD repair of the TS in a transcriptional active gene is significantly delayed in *rad26* Δ mutants (van Gool et al., 1994). While a *rad16* Δ *rad26* Δ double mutant shows higher UV sensitivity than a *rad16* Δ single mutant (Bhatia et al., 1996), it is still less UV sensitive than a completely NER-deficient strain such as *rad14* Δ , suggesting a Rad26-independent

TC-NER subpathway (Verhage et al., 1996). Rad26 may be also associated with RNA Pol II during transcriptional elongation; its “recruitment” to the site of the lesion would thus result from the stalling of RNA Pol II in an elongation mode (Malik et al., 2010). Furthermore, Rad26 is subject to Mec1-dependent phosphorylation, which enhances the rate of TC-NER of UV-induced damage *in vivo* (Taschner et al., 2010). Rad26 copurifies with Def1, which is a factor that is involved in the ubiquitination of RNA Pol II and leads to its degradation by the proteasome. This indicate Rad26 functions as an inhibitor of RNAP II degradation, when lesions are not accessible to the TC-NER factors, hence Def1 promotes the ubiquitination and subsequent degradation of the stalled RNAP II to allow repair to take place by other pathways (Woudstra et al., 2002).

Rad 28

Rad28, like its human homolog CSA, is also a WD40 repeat E3 ligase component protein with no identified catalytic activity and it is probably involved in protein interactions (Henning et al., 1995, Bhatia et al., 1996). As mentioned previously in humans, CSA is known to be exclusively required for TC-NER. Surprisingly, mutation of the yeast homologue *RAD28* does not seem to affect DNA repair kinetics (Bhatia et al., 1996, Venema et al., 1990). Although both Rad26 and Rad28 are involved in TC-NER, they do not form a stable complex with each other. This result was also observed for the human homologues of Rad26 and Rad28, CSB and CSA (Svejstrup, 2002).

Rpb 9

In yeast there are two apparent sub-pathways of TC-NER; the first is dependent upon Rad26, whilst the second is dependent upon a non-essential subunit of RNAPII, Rpb9 (Li and Smerdon, 2002a). Thus Rad26 is not essential for all TC-NER in yeast (Li and Smerdon, 2002a, Li and Smerdon, 2004). Rpb9 TC-NER strictly depends upon the active transcription of a gene, whereas Rad26-mediated TC-NER is unaffected by inhibition of transcription (Li et al., 2006b, Li et al., 2006d). While inactivation of Rad26 will lead to a delay in messenger RNA (mRNA) synthesis, data suggest

that Rad26 can promote elongation through endogenous DNA damages such as 8-oxoG, 3-MeA, and AP sites (Lee et al., 2001, Yu et al., 2003). In the absence of Rad26/CSB, permanent stalling of RNA Pol II at endogenous DNA lesions would significantly impair RNA synthesis and might generate a signal for apoptosis and cell death (Hanawalt and Spivak, 2008). At strongly blocking lesions, RNA Pol II permanently stalls without the possibility of bypass. Here, Rad26 initiates chromatin remodeling to attract additional NER factors to process TC-NER to repair damage such as CPDs (Hanawalt and Spivak, 2008). As *rpb9Δ rad26Δ* double mutants are completely defective in TC-NER, the *rad16Δ rad26Δ rpb9Δ* triple-mutant shows a similar UV sensitivity to a *rad1Δ* strain, and in this triple mutant removal of CPDs in both the TS and the NTS is abolished (Li and Smerdon, 2002c). These data suggest a direct or indirect recruitment of NER factors by Rpb9, similar to that described for Rad26-dependent TC-NER. Although little is known about the biochemical mechanism of Rpb9-mediated TC-NER, Rpb9's function is related to transcription elongation and this may be involved in TC-NER (Li et al., 2006b). In addition, Rpb9 plays a role in the Rpb1 ubiquitination and degradation that occurs in response to UV but this appears to be independent to NER (Chen et al., 2007). The Rad26-independent Rpb9-mediated pathway was shown to have different efficiencies and function in different areas of a gene (Li and Smerdon, 2002c). Interestingly, in some repressed regions Rad26 was required for Rad16-independent repair (Bhatia et al., 1996, Teng and Waters, 2000).

1.3.2.1.2 Damage recognition during yeast GG-NER

The GG-NER pathway repairs lesions independently of transcriptional status. It is initiated by a Rad4-Rad23-Rad33 trimeric complex which senses distortion of the DNA helix and then locates itself to DNA damage. This may be facilitated by interactions between Rad4 and chromatin remodeling complexes such as Ino80 (Sarkar et al., 2010) and the SWI/SNF complex (Gong et al., 2006). Similar to its human analog XPC-HR23B-Centrin2, yeast Rad4-Rad23-Rad33 also promotes

the opening of a region around the lesion (Tapias et al., 2004). The Rad7/Rad16/ABF1 complex is mandatory for GG-NER *in vivo*. This complex may associate with alternative factors to promote recruitment of Rad4 through its high affinity for DNA damage and its E3 ubiquitin (Ub) ligase activity (Sugasawa et al., 2005). Interestingly *in vitro* studies of yeast GG-NER demonstrate extrusion of the oligonucleotide is an active process requiring superhelical torsion produced by a Rad7/Rad16/Abf1 complex termed the GG-NER complex (Yu et al., 2004). This observation is reminiscent of the role of UvrD for oligonucleotide extrusion in prokaryotes, although in contrast to UvrD, the GG-NER complex is not a DNA helicase (Orren et al., 1992, Yu et al., 2009).

Rad4-Rad23-Rad33

S.cerevisiae contains Rad4 and Rad23 respectively which are homologues of human XPC and HR23, they form a stable heterodimeric complex (Guzder et al., 1998a, Wang et al., 1997). In addition, a functional homologue of human centrin 2 has also been found, Rad33. This is an additional NER factor that physically binds directly to Rad4 (den Dulk et al., 2008). In contrast to mammalian NER, unlike human XPC which is absolutely required for GG-NER but dispensable for TC-NER, yeast Rad4 is essential for both TC-NER and GG-NER (Prakash and Prakash, 2000). Whilst loss of either Rad23 or Rad33 only reduces repair, the simultaneous deletion of the genes for both these two proteins prohibits efficient GG-NER and TC-NER (den Dulk et al., 2006, Mueller and Smerdon, 1996).

The Rad4 structure consists of a 310-residue N-terminal α/β domain, followed by three 50–90-residues structurally related α/β domains characterized by a long β -hairpin (hereafter, BHD1, BHD2 and BHD3, for beta-hairpin domain). The N-terminal domain contains the ~45 residue core TGD (trans-glutaminase-homology domain), and lacks a Cys-His-Asp catalytic site so it does not have a structure-stabilizing role (Min and Pavletich, 2007). *RAD23* encodes a protein of 42-kDa and its expression is up-regulated up to 5-fold after UV radiation (Madura and Prakash, 1990, Friedberg et al., 2005). Like its mammalian homologue HR23B,

Rad23 has four domains; an N-terminal ubiquitin-like domain (Ubl), two ubiquitin associated domains (UBAs) and a Rad4-binding domain. The UBA1 domain is located centrally and the UBA2 domain is in the C-terminal. The Rad4-binding domain is located between the two UBA domains (Dantuma et al., 2009). Rad4-Rad23 shows high affinity binding for lesions including (6-4)PPs and N-acetyl-2-aminofluorene adducts, but it poorly recognises CPDs (Guzder et al., 1998a, Jansen et al., 1998, Xie et al., 2004). It is also required for dual incision in a reconstituted NER system (Guzder et al., 1995). The crystal structure of a Rad4-Rad23-DNA-CPD complex reveals that Rad4 inserts a β -hairpin through the DNA duplex, causing the two damaged base pairs to flip out of the helix. In this way the, damaged nucleotides are exposed while the undamaged ones contact Rad4. These structural data suggest that Rad4 recognizes damage by sensing thermodynamically unstable base pairs (Min and Pavletich, 2007). In the complex, Rad23 is unable to bind damaged DNA by itself, but it stimulates Rad4-binding activity and prevents its degradation by the proteasome (Xie et al., 2004).

A stabilizing effect of Rad23 on Rad4 has been observed following UV (Xie et al., 2004), and Human XPC also is stabilized by HR23A and HR23B, two homologs of Rad23 (Ng et al., 2003). Rad4 protein is stabilized in proteasome-deficient cells (Lommel et al., 2002) and CPD removal is enhanced in these cells (Lommel et al., 2000). This indicate that cellular Rad4 is actively degraded by the 26S proteasome and its quick turnover is protected by Rad23 protein (Gillette et al., 2006). *S.cerevisiae rad23 Δ* mutants are known to have a modest UV sensitivity unlike cells with mutation in mutants of essential NER genes such as rad4 and rad14 (Prakash and Prakash, 2000, He et al., 1996). Interestingly, Rad4 protein is lower in *rad23*-deleted cells due to a reduced Rad4 transcript level, and not due to the increased proteolytic degradation of Rad4 (Gillette et al., 2006). Expression of the Rad4 binding domain functions to stabilise Rad4 alone, and over expressing Rad4 in the absence of Rad23, is not sufficient to restore wild type UV survival. This demonstrate that Rad23 plays a role beyond stabilising Rad4 in NER (Xie et al., 2004, Ortolan et al., 2004).

Rad23 was the first Ubl-containing protein to be identified in yeast (Watkins et al., 1993). It is known to interact with the 26S proteasome and function to target this to the various cellular pathways and the UBL domain is required for this interaction (Schauber et al., 1998). The 26S proteasome, consisting of a 20S core particle and two copies of a 19S regulatory complex, and is a large protein complex involved in the degradation of proteins targeted by the ubiquitin pathway (Coux et al., 1996). It was further shown that the 19S regulatory complex negatively modulates NER in yeast cells (Lommel et al., 2000, Gillette et al., 2001). The ubiquitin-proteasome pathway (UPP) is responsible for the targeted degradation of proteins. The Ubl domain of Rad23 is important for NER and cell survival after exposure to UV. Deletion of the Ubl domain of Rad23 protein results in a UV survival intermediate between WT and a *rad23Δ* survival (Russell et al., 1999, Watkins et al., 1993). The Ubl domain of Rad23 is known to bind the Rpn1 subunit of the 19S base subcomplex (Elsasser et al., 2002, Saeki et al., 2002). This functions to recruit Rad23 to the proteasome but it does not result in its rapid degradation (Schauber et al., 1998, Watkins et al., 1993). Inhibition of protein degradation by the proteasome had no measurable effect on NER activity *in vitro* and suggests that the proteolytic activity of the proteasome is not required for NER (Russell et al., 1999). Indeed, the UBA2 domain of Rad23 has been demonstrated to protect the protein from proteolytic degradation (Heessen et al., 2005). UBA domains predominantly bind to ubiquitylated proteins rather than free ubiquitin chains (Chen and Madura, 2002). The simultaneous binding of UBA domains to ubiquitylated substrates and the Ubl domain to the proteasome has founded the hypothesis that Rad23 is important for the recruitment of ubiquitylated proteins to the proteasome (Elsasser et al., 2004, Verma et al., 2004). Furthermore, Rad23 also binds the E4 ubiquitin chain elongation factor Ufd2 via its Ubl domain, so suggesting it may couple ubiquitylation to subsequent degradation (Kim et al., 2004). However, the Rad23 UBA domains have also been shown to suppress polyubiquitin chain polymerisation *in vitro* (Ortolan et al., 2000, Chen et al., 2001).

These observations suggest Rad23 could also stabilise protein substrates by regulating polyubiquitylation, and overexpressing Rad23 has been shown to increase the half life of some UPP targets (Chen and Madura, 2002, Ortolan et al., 2000). An alternative proteasome interaction module can suppress the UV sensitivity of the UBL mutant. Rad23 likely has a primary role to accommodate an interaction with the proteasome (Dantuma et al., 2009). Whilst Rad4, Rad23 and the proteasome have been co-purified suggesting a role for the UPP pathway in NER, the proteasome may have a role independent of proteolysis as only mutations in the 19S of the proteasome affect NER (Russell et al., 1999, Schaubert et al., 1998). The 19S has been demonstrated to negatively regulate the rate of lesion removal *in vivo*. However, this activity is modulated through an interaction with the UbL domain of Rad23 which functions to suppress this (Gillette et al., 2001). The Rad7-containing E3 ligase complex can mono-ubiquitinate Rad4 *in vitro* (Gillette et al., 2006). In response to UV damage ubiquitination serves to regulate the steady state level of Rad4 (Gillette et al., 2006). Mutation of the Rad7 SOCS box will inhibits its E3 ligase function, and prohibits Rad4 UV-dependent ubiquitination. As altering the stability of Rad4 protein level in response to UV does not affect UV survival and UV induced Rad4 protein ubiquitination via Rad7-containing E3 ligase affects UV survival, so Rad4 ubiquitination but not the rad4 level regulates NER (Gillette et al., 2006). Collectively, these observations indicate that there are two components to the NER response to UV damage: pathway I operate via the Rad23-mediated nonproteolytic activity of the 19S preteasome complex and this occurs independently of *de novo* protein synthesis. Pathway II is dependent on *de novo* protein synthesis and involves the Rad7-containing E3 ligase ubiquitination of Rad4, and this may be part of a transcriptional response that operates following UV radiation (Gillette et al., 2006). As stated earlier, Rad33 is found in a complex with both Rad4 and Rad23 Rad33 (Krogan et al., 2006). It is an NER factor that binds directly to Rad4 (den Dulk et al., 2008, den Dulk et al., 2006). Rad4 interacts with Rad23 and Rad33 through independent sites in its C-terminal region, and the roles of these proteins are

presumably to modulate Rad4 activity and integrity (den Dulk et al., 2006). The Rad34 protein is a yeast protein that has sequence homology to Rad4. Like Rad4, it interacts with Rad23. Rad34 may have a role during NER that occurs uniquely in the repair of RNA Pol I-transcribed ribosomal DNA genes (Tremblay et al., 2008).

Rad4 protein steady state levels are reduced in cells lacking Rad33, and the reduced level is relatively stable when compared to in *rad23* cells (den Dulk et al., 2008). UV induced modification of Rad4 is strongly increased in *rad33* cells (den Dulk et al., 2008). The deletion of *RAD33* does cause moderate UV sensitivity, but a *rad23rad33* double mutant is as sensitive as completely NER deficient cells. In *RAD33* cells, repair of the transcribed strand is severely reduced while repair of the non-transcribed strand is absent (den Dulk et al., 2006). This result demonstrates that GG-NER completely requires Rad33 protein. Rad33 also appears to be required for TC-NER of RNAP II transcribed genes as its presence increases the efficiency of TC-NER, but it is not essential (den Dulk et al., 2006). In both yeast and human mutants when Rad4-Rad33 and XPC-Centrin 2 interaction is disrupted, GG-NER appears to be defective and the protein levels of both Rad4 and XPC are lower compared to in wild type cells. This observation, combined with the predicted structural resemblance and the fact that Rad33 and Centrin 2 bind to Rad4 or XPC via the same conserved motif (den Dulk et al., 2008), might suggest that the role of Rad33 in the Rad4-Rad23 complex is similar to that of Centrin 2 in the human XPC-HHR23B complex.

The GG-NER complex

Yeast *rad7 Δ* and *rad16 Δ* mutants respectively display a moderate UV-sensitivity which is not as severe as seen in mutants of other indispensable NER factors (Friedberg et al., 2005, Prakash et al., 1993). The single mutants and the double mutant have the same repair phenotype, indicating that the RAD7 and RAD16 gene products likely operate in the same nucleotide excision repair sub-pathway (Verhage et al., 1994). Rad7 and Rad16 are required for CPD removal for repair of UV-induced damage located in nearly all non-transcribed DNA and the non-transcribed strand (NTS) of transcriptionally active genes (Verhage et al. 1994), so indicating a specific

Rad16 dependent GG-NER sub-pathway (Hanawalt and Spivak 2008). In *S.cerevisiae*, although there is no direct homolog of human UV-DDB (Rad7 and Rad16 do not share much structural similarity with the UV-DDB complex), there are some striking functional similarities that have been observed between Rad7-Rad16 and DDB1-DDB2 (XPE) complexes (Reed, 2005). Mutations of these genes in both yeast and human cells result in defective GG-NER. They all have the ability to bind damaged DNA and form components of a class of cullin based E3 ubiquitin ligase whose substrate includes Rad4 and XPC respectively, and these two are homologues of the same repair factor in yeast and humans (Boiteux and Jinks-Robertson, 2013).

The RAD7 encoded protein contains 565 amino acids and is highly structured, with 50% of the charged residues clustered in the amino-terminal region (Perozzi and Prakash, 1986). Rad16 shares homology with Snf2, the catalytic subunit of the SWI/SNF chromatin-remodeling complex (Bang et al., 1992). However the complex does not have detectable DNA helicase activity. Snf2 also contains conserved motifs which have been found in a superfamily of ATPases thought to be involved in chromatin remodeling activities. The Rad7-Rad16 complex also displays a DNA-dependent ATPase activity, but this ATPase activity is inhibited when the complex comes across DNA damage (Guzder et al., 1998b). Rad16 facilitates histone H3 acetylation after UV irradiation (Teng et al., 2008a), and also functions to modulate histone H3 methylation during NER at silenced loci (Chaudhuri et al., 2009). With respect to histone H3 acetylation, Rad16 actually enhanced the occupancy of the histone acetyl transferase Gcn5 on chromatin in response to UV damage (Yu et al., 2011).

Rad7 and Rad16 form a stable complex in an ATP-dependent manner and binds UV-damaged DNA *in vitro* (Guzder et al. 1997). This damage binding is ATP dependent and possibly functions by two zinc fingers of the DNA binding domains on Rad16, yet it is independent of Rad7 (Bang et al., 1992). Rad4-Rad23 and Rad7-Rad16 synergistically enhance binding to a UV-damaged DNA (Guzder et al. 1999) indicating a role for the Rad7-Rad16 complex in damage recognition (Prakash

and Prakash, 2000). The physical interaction between Rad4 and Rad7 was found to favor the formation of a large lesion-recognition complex (Guzder et al. 1999). As mentioned before, the ATPase activity of the Rad7-Rad16 complex is inhibited when it comes across DNA damage. This suggested that the Rad7-Rad16 complex may act as an ATP-dependent motor that translocates along the DNA in search of damage. After the Rad7–Rad16 complex encounters a lesion in nontranscribed regions of the genome, the complex stalls and promotes remodeling open damaged chromatin and the recruitment of other NER factors to accomplish repair (Guzder et al. 1998). Apart from a role for Rad7-Rad16 in DNA damage recognition during GG- NER, studies also suggest an additional role for Rad7-Rad16 in post-incision events (Reed et al., 1998). The excision of the damage containing oligonucleotide was seen to require Rad16. This may relate to Rad16 creating torsion in the DNA so as the dually incision fragment is excised (Yu et al., 2004).

Co-purification of the Rad7-Rad16 in a complex identified the essential protein autonomously replicating sequence binding factor 1 (Abf1) as the third component of a trimeric Rad7-Rad16-Abf1 complex (Reed et al., 1999). Abf1 was originally identified for its ability to bind DNA at a variety of origins of DNA replication, as well as the silencing loci *HML* and *HMR* (Diffley, 1992). It is well established as an abundant, essential, global site-specific DNA binding protein which has roles in DNA replication, transcriptional activation, silencing and NER (Yarragudi and Morse, 2006). The protein binds the DNA consensus sequence 5'-CGTnnnnnnTGAT-3, which is predicted to be found at thousands of sites throughout the genome (Yu et al., 2009, Mukherjee et al., 2004). Abf1 may out-compete histones for accessibility to binding sites which will contribute to chromatin structure over a large proportion of the yeast genome (Ganapathi et al., 2011). Abf1 conditional mutants are defective in the removal of UV damage and exhibit sensitivity to UV radiation (Reed et al., 1999). As a complex Rad7-Rad16-Abf1 can generate superhelical torsion in DNA *in vitro*. This torsion depends on the Rad16 subunit and is necessary for the excision step in GG-NER (Yu et al., 2004). These evidences suggest that the GG-NER-complex binds

to ABF1 recognition sites in DNA. After UV irradiation, the complex can translocate on DNA in an ATP dependent manner, torsion is generated and eventually the complex stalls at damaged sites to recruit Rad4/Rad23 (Yu et al., 2009).

In addition to forming a complex with Abf1, Rad16 contains a RING-type *zinc* finger domain called a RING-H2 finger. This means that Rad7-Rad16 can interact with Elc1-Cul3 to form a cullin-based E3 Ub ligase that promotes UV-dependent ubiquitination of Rad4 and other chromatin-associated proteins (Ramsey et al., 2004, Gillette et al., 2006). Yeast Elc1 is a homolog of mammalian elongin C which forms a heterotrimeric complex with elongins A and B (Bradsher et al., 1993). Deletion of *ELC1* in a *rad16Δ* mutant did not increase UV-sensitivity. Conversely deletion of *ELC1* in a *rad26Δ* mutant did increase UV sensitivity, so suggesting a role in GG-NER but not TC-NER (Lejeune et al., 2009). A nucleotide level study of NER shows *elc1Δ* cells have no detectable repair of CPDs in the NTS of the constitutively expressed *RPB2* gene, but it has no role in TC-NER (Lejeune et al., 2009). As Elc1 is a component of a ubiquitin ligase (E3) that contains Rad7 and Rad16, Elc1 may play a role in NER by regulating the ubiquitin level of Rad4 in response to UV damage (Gillette et al., 2006).

Hence the Rad7/Rad16/Abf1 complex has multiple roles in lesion recognition for GG-NER that include binding to DNA damage, interacting with Rad4-Rad23-Rad33, driving conformational changes in DNA, and remodeling chromatin through acetylation and ubiquitination.

1.3.2.2 Open complex formation

After the respective GG-NER and TC-NER subpathway-specific damage recognition events, the next step of the two subpathways will utilise the same NER factors to assemble a pre-incision complex and form an open DNA bubble (Friedberg et al., 2005). However in GG-NER, after recognition, the DNA structure generated by Rad4-Rad23-Rad33 allows the recruitment and positioning of the TFIIH transcription factor, which extends opening of the helix using the ATPase/helicase

activities of Rad3 and Rad25. Then the Rad4-Rad23-Rad33 recognition complex is released, and Rad14 and RPA are recruited to stabilize the pre-incision complex. In the case of TC-NER, TFIIH is already positioned at the lesion (Boiteux and Jinks-Robertson, 2013).

TFIIH

TFIIH was initially identified as an essential factor required for the initiation of transcription at RNA Pol II promoters in different species (Feaver et al., 1991, Conaway and Conaway, 1989) and then it was found to have an important role in NER independent from that in transcription (reviewed in Friedberg et al., 2005). TFIIH consists of 10 subunits that can be divided into two parts. The first is a core TFIIH sub-complex with 7 subunits (Rad25, Rad3, Tfb1, Tfb2, Ssl1, Tfb4, and Tfb5) and the second is a 3-subunit CDK-activating kinase module (CAK) (Kin28, Ccl1, and Tfb3) (Egly and Coin, 2011). At least 6 of these subunits are required for NER but not all of them (Frit et al., 1999, Svejstrup et al., 1996). In yeast Rad3, Rad25, Ssl1, Tfb1, Tfb2 and Tfb4 are absolutely required for NER while the other sub-units Tfb3, Kin28 and Ccl1 constitute the protein kinase activity (reviewed in Friedberg et al., 2005) and Tfb5 acts as an architectural stabilizer giving structural rigidity to the core TFIIH so that the complex is maintained in its functional structure (Zhou et al., 2007). Yeast mutants with a temperature-sensitive *kin28* allele still have the ability to remove CPDs in non-transcribed DNA, suggesting that the kinase activity is not essential for NER (Tijsterman et al., 1998).

Rad3 is a DNA-dependent ATPase with 5' to 3' DNA helicase activity and belongs to Superfamily 2 (SF2) (Gorbalenya and Koonin, 1993, Harosh et al., 1989). While Rad25 is also a DNA-dependent ATPase with 3' to 5' DNA helicase activity (Guzder et al., 1994, Sung and Demple, 2006), the ATPase activity of Rad3 is essential for NER, but not for transcription (Feaver et al., 1993). Conversely, the helicase activity of Rad25 is essential for not only NER but also transcription. The Rad3 DNA helicase function requires single-stranded regions to start unwinding duplex DNA and purified

Rad3 can unwind long regions of duplex DNA, up to 850 bp (Sung et al., 1987, Harosh et al., 1989).

Unlike other subunits of the core TFIIH which are required for both GG-NER and TC-NER, Tfb5 has been shown to be essential for GG-NER but not absolutely required for TC-NER, as no apparent repair can be detected in the NTS, but a certain extent of repair can be seen in the TS of either the *RPB2* or *GAL1* genes (Ding et al., 2007). Lack of Tfb5 results in poor growth, enhanced UV sensitivity, and a greatly reduced NER activity *in vitro* (Zhou et al., 2007).

The human homolog of yeast Tfb5 is TTD-A. This has been shown to stabilize other subunits of TFIIH while Tfb5 does not seem to affect the stability of other TFIIH components (Vermeulen et al., 2000). However, yeast Tfb5 interacts with Tfb2 and acts as an architectural stabilizer giving structural rigidity to the core TFIIH so that the complex is maintained in its functional architecture (Zhou et al., 2007). Hence the roles of Tfb1, Ssl1, Tfb2, Tfb4 in NER are probably to stabilize the TFIIH core complex via protein-protein interactions. In addition, TFIIH interacts with Rad4, Rad23, and RPA (Bardwell et al., 1994). To conclude, TFIIH has a role in NER via its intrinsic helicase activities and its interactions with other essential NER components.

Rad14

Rad14 is known as a DNA damage recognition factor in nucleotide excision repair. It contains a zinc-finger domain which has high affinity for UV-damaged DNA (Guzder et al., 1993). Rad14 plays a crucial role in targeting the Rad1-Rad10 nuclease to the DNA (Guzder et al., 1996) which forms a tight complex with the damage recognition protein Rad14 and the complex of Rad1-Rad10-Rad14 can be purified intact from yeast cells (Guzder et al., 2006). The targeting of Rad1-Rad10 to the lesion by Rad14 is mediated via physical interaction of Rad14 with Rad1 but not Rad10 (Guzder et al., 1996). In contrast, TFIIH promotes the targeting of Rad2 nuclease (Habraken et al., 1996). Rad14 is highly conserved from yeast to humans and its human homolog is XPA (Rademakers et al., 2003).

RPA

RPA is the eukaryotic counterpart of the *E. coli* single-strand binding protein (SSB) and it is composed of three subunits encoded by the *RFA1*, *RFA2*, and *RFA3* genes. It binds with high affinity to single-strand DNA and is indispensable during NER (Guzder et al., 1995). RPA interacts with several NER factors including Rad14 and is a component of the pre-incision complex (reviewed in Friedberg et al., 2005) and is only partially required for TC-NER but is absolutely needed for GG-NER at certain yeast genes (Teng et al., 1998).

After damage recognition, a “verification step” was mediated by TFIIH, RPA, and Rad14. RPA binds the undamaged strand, whereas Rad14 binds to the DNA lesion (de Laat W.L et al., 1999). In the absence of lesion verification, the NER reaction aborts before dual incision occurs (Sugasawa et al., 2001).

1.3.2.3 Dual incision

After damaged DNA forms a favorable structure for dual incision, the Rad2 and Rad1-Rad10 structure-dependent endonucleases are positioned with TFIIH, RPA, and Rad14. Rad2 is the yeast homologue of human XPG protein and possess an identical structural specificity, and activity in NER (Habraken et al., 1995). Rad2 is an endonuclease responsible for an incision 2–8 nt from the lesion on the 3' side (Evans et al., 1997a). The yeast orthologue, Rad1-Rad10 of the human ERCC1-XPF complex, functions in NER in an identical manner although the protein interaction domains between the two complexes are non-homologous (de Laat et al., 1998b, Bailly et al., 1992). As does its human orthologue, Rad1-Rad10 makes an incision 15–24 nt from the lesion on the 5' side (Evans et al., 1997a). Neither Rad2 nor Rad1-Rad10 have specificity for damaged DNA; Rad2 interacts with TFIIH via Tfb1 (Lafrance-Vanasse et al., 2013), while Rad1-Rad10 forms a complex with Rad14 (Guzder et al., 1996). After dual incision, the oligonucleotide which contain the lesion is released together with other NER factors. There is controversy over the order of these two incisions during NER. In contrast to reconstituted NER in

S.cerevisiae, under certain conditions both uncoupled 5' and 3' incisions have been observed in mammalian NER (Matsunaga et al., 1995, Evans et al., 1997a). However, as stated earlier, another study in human cells suggests that 5' incision precedes 3' incision (Staresincic et al., 2009).

Rad1-Rad10 complex

The RAD1 and RAD10 genes encode polypeptides with predicted molecular weights of 126-200kDa and 24-300kDa, respectively (Reynolds et al., 1985). Rad1 forms a stable complex with Rad10 even in the absence of UV, with a half life of ca.15h (Bardwell et al., 1992), and it degrades circular single-strand DNA (Bailly et al., 1992) and nicks supercoiled DNA (Tomkinson et al., 1994). The Rad1-Rad10 complex as a duplex-3' single-strand junction-specific endonuclease cooperates with Rad2 to recognise the junctions between single-stranded and duplex DNA (reviewed in Friedberg et al., 2005). It specifically removes unpaired 3' tails by nicking within duplex DNA at a position 2–5 nt from the junction (Bardwell et al., 1994). The bimodal asymmetrical incision catalysed by Rad1-Rad10 and Rad2 results in oligonucleotide fragments 24 to 32 nt in length (reviewed in Friedberg et al., 2005). In NER reactions reconstituted from purified proteins, Rad1-Rad10 is essential for the incision of UV-damaged DNA (Guzder et al., 1996). However, Rad1-Rad10 has roles apart from NER. This complex is also important for removing 3' dirty ends generated during BER and nonhomologous 3' tails that arise during homologous recombination (Lyndaker and Alani, 2009). Rad1-Rad10 endonuclease products contain 3'-OH groups which are a required substrate for extension by polymerase (Bardwell et al., 1994), and in humans a 5' incision by ERCC1-XPF is required to generate a free 3'-OH group (Staresincic et al., 2009).

Rad2

Rad2, like Rad1-Rad10, is a junction-specific endonuclease with an endonuclease activity that degrades circular, single-strand DNA and a 5' to 3' exonuclease activity that digests single- or double-strand DNA (Habraken et al., 1995). Rad2 likely

displaces Rad4 from the pre-incision complex by competing for common binding sites on the various subunits of TFIID. This displacement ensures that TFIID is stabilized on the DNA and available for repair as otherwise it will lead to alternative functions such as those in transcription. It helps to establish the correct orientation of Rad2 on the DNA lesion (Lafrance-Vanasse et al., 2013). Rad2 removes 5'-overhanging tails and processes bubble structures by nicking duplex DNA 1 nt from a single- to double-strand junction (Habraken et al., 1995).

1.3.2.4 Re-synthesis and ligation

After the incision step, the size of the resulting gap is about 30 nucleotides (Tanaka and Wood, 1994). The synthesis step will fill the gap around the site of damage and then the DNA is restored by DNA ligase (Budd and Campbell, 1995). Although poorly documented in yeast, data suggest that either Pol δ or Pol ϵ can carry out repair synthesis (Budd and Campbell, 1995). In yeast DNA polymerase δ consists of three sub-units. The largest is the 125-kDa catalytic sub-unit encoded by the *CDC2 (POL3)* gene which has a 3'-5' exonuclease activity associated with it. The other two components are a 58-kDa subunit encoded by *POL31* and a 55-kDa sub-unit encoded by *POL32* (Hubscher et al., 2002, MacNeill et al., 2001). DNA Pol ϵ consists of a 256-kDa catalytic sub-unit POL2,80-kDa DPB2,24-kDa DPB3 and a 29-kDa DPB4. This polymerase has a 3'-5' exonuclease activity and *POL2* has a important role for DNA replication (Morrison et al., 1990). The final ligation reaction is performed by DNA ligase 1, the product of the *CDC9* gene (Budd and Campbell, 1995).

1.4.Chromatin structure during DNA repair

1.4.1 Chromatin structure

DNA does not exist naked in the nucleus of the eukaryotic cell, instead it associates with histone proteins to form a highly condensed complex termed chromatin that fits in to the nucleus. DNA in the nucleus is divided between a set of different

chromosomes. In human cells, approximately 2 meters of fully extended linear DNA will be packed into a nucleus of roughly 10 μm diameter. It is approximately 3.2×10^9 bp long and contains 20,000–25,000 distinct genes distributed over 24 different chromosomes. The yeast genome containing 12,800 kb of DNA with about 6000 genes distributed over 16 chromosomes. Structurally the basic sub-unit of chromatin is the nucleosome core particle (NCP). The NCP consists of 145–147 bp of DNA wrapped about 1.7 times around a histone octamer which is composed of two copies of each histone H2A, H2B, H3 and H4 (Davey et al., 2002, Luger et al., 1997). Nucleosomes are linked together by linker DNA. Linker DNA segments between nucleosome core particles are usually 20-60 bp in length and form a 11nm fibre to resemble a “beads-on-a-string” structure. The N-terminal domains of each histones are in contact with the DNA backbone on the surface and neighbouring histones. Each histone has an unstructured, flexible and positively charged N-terminal domain (histone tail) (Luger and Richmond, 1998, Davey et al., 2002). Histone amino-terminal tails are known to be the most frequent targets for post-translational modification including acetylation, methylation, phosphorylation and ubiquitination (Choi and Howe, 2009). These modifications affect the nucleosome-nucleosome or DNA-nucleosome interactions through the addition of physical entities, or by changing histone charges, or they represent a docking site for the recruitment of specific proteins which have different cellular functions. Reports have raised the possibility that all of these modifications are combinatorial and interdependent, therefore different combinations of modifications may result in distinct and consistent cellular outcomes, so forming a “histone code” (Jenuwein and Allis, 2001, Strahl and Allis, 2000).

In general, chromatin compaction occurs by the following steps. First, DNA wraps around histone proteins forming nucleosomes and intervening "linker" DNA to form a 10-nm-fiber, described as the "beads on a string" structure. Then arrangements resulting from short-range interactions between neighbouring nucleosomes giving rise to secondary structures to form chromatin fibres forming 30nm fibres leading to

α -helices and β -sheets (Tremethick, 2007). Following this, long-range interactions between distant nucleosomes could potentially lead to formation of 100 to 400nm fibre structures (Choi and Howe, 2009). After that, higher-level DNA packaging into the metaphase chromosome occurs during mitosis and meiosis. There are two forms of chromatin which can be distinguished cytologically by how intensely they stain, Euchromatin is less intense more accessible and is associated with transcriptionally active regions, whilst heterochromatin stains intensely and is more inaccessible (Grewal and Jia, 2007).

In the context of chromatin, “higher-order structure” may be defined as any assemblage of nucleosomes that assumes a reproducible conformation in 3D space (Woodcock and Dimitrov, 2001). The most obvious chromatin higher-order structure is the mitotic/meiotic chromosome in which the DNA is compacted some 10,000 to 20,000 fold. Metaphase chromosomes have characteristic shapes, banding patterns, and locations of specific genes.

1.4.2 Chromatin formation change following UV

In UV-treated mouse microglia cells, UV-induced apoptotic cells showed condensed chromatin accumulating at the nuclear periphery. Instead of undergoing fragmentation, chromatin translocated to the cytoplasm (Zierler et al., 2006). This suggests that UV-induced chromatin degradation is not only restricted to the nucleus, but similar results have not been found in other cell models (Farrell et al., 2011).

DNase I footprinting and Micrococcal nuclease (MNase) mapping of UV irradiated and unirradiated reconstituted nucleosomes revealed irradiation of nucleosomal DNA with UV light does not destabilize nucleosomes or change the rotational state (Ura et al., 2001, Schieferstein and Thoma, 1996). UV-irradiation of a 5S rDNA fragment reduced the efficiency of nucleosome reconstitution *in vitro* indicating that the induction of UV damage in a DNA sequence can alter the ability and characteristics of the DNA sequence to associate with histones (Liu et al., 2000). The rotational setting of chromatin was altered when DNA extracted from UV-irradiated

nucleosomes was used again for a second reconstitution (Schieferstein and Thoma, 1996). Similarly, CPDs are facing outwards when UV-irradiated DNA is reconstituted into nucleosomes as a preferential rotational setting (Suquet and Smerdon, 1993).

1.4.3 NER in a chromatin environment

Biochemical reconstitution studies have characterized how NER managed to repair helical distorting DNA lesions in naked DNA. However, knowledge of how NER occurs in the complex chromatin environment of the nucleus is limited.

Evidence indicates the presence of nucleosomes on damage DNA severely inhibits the repair capability of NER. Damage in reconstituted nucleosomes and in SV40 minichromosomes is much less efficiently repaired by NER compared to naked DNA (Liu and Smerdon, 2000, Sugasawa et al., 1993). Several *in vivo* studies also show a direct modulation of nucleosome positioning on NER. In the centre of nucleosomes repair is often slower, whereas the repair in the nucleosome-free DNA is faster (Wellinger and Thoma, 1997, Powell et al., 2003). Furthermore, there is also a trend that the repair becomes faster at the end of the nucleosome. Presumably, the DNA sequence in the centre of nucleosomes is less accessible for repair proteins compared with histone free regions. The correlation between nucleosome positioning and repair rate is observed only in the nontranscribed strand (NTS) of active genes and both strands of inactive genes, whereas the repair in the transcribed strand (TS) of active genes is rather homogenous due to TC-NER. However, caution should be applied as all of these studies have involved only a few genes and the trends observed may not apply throughout the genome.

Several lines of studies have found NER is associated with an alteration of chromatin structure by a localized decondensation of chromatin similar to that seen with transcription (Meijer and Smerdon, 1999, Ura and Hayes, 2002, Thoma, 1999). Furthermore, increasing the global histone acetylation level by using sodium butyrate to inhibit histone deacetylation was reported to enhance repair synthesis during NER (Smerdon et al., 1982).

These results suggest chromatin modifications and remodeling have a role in NER.

1.4.3.1 Chromatin remodeling in NER

In transcription and replication, changes in the chromatin structure are required in order to allow binding of the factors involved (Li et al., 2007, Groth et al., 2007).

There is increasing evidence that this is also happened for DNA repair.

Space was required in the excision step of NER as 25-30 bp of DNA are unwound in the open complex during NER (Evans et al., 1997b), and the human excision complex needs about 100 bp of DNA *in vitro* (Huang and Sancar, 1994). Compared with the structure of the nucleosome, the excision complex needs more space, and the linker DNA between nucleosomes is too short to accommodate a repair complex (Thoma, 1999). These results indicate alterations of chromatin are needed *in vivo* to improve the accessibility of proteins to DNA and facilitate damage recognition and repair.

Studies have demonstrated that chromatin remodeling enzymes such as the SWI/SNF superfamily play an important role in modulation the accessibility of the NER machinery to nucleosomal DNA (Osley et al., 2007). The GG-NER pathway of NER is modulated by chromatin structure. Snf6 and Snf5, two subunits of the SWI/SNF complex in yeast are found to co-immunoprecipitate with the Rad4-Rad23 heterodimer *in vivo*, and this is stimulated by UV irradiation (Gong et al., 2006). As the Rad4-Rad23 complex was required for GG-NER, this result shows SWI/SNF facilitates chromatin remodeling and has a role in facilitating GG-NER. No association was found between Snf6 and Rad16 (Gong et al., 2006).

The study of another chromatin remodeler, the Ino80 chromatin remodeling complex shows it also interacts with the early damage recognition complex of Rad4-Rad23 and has a UV-dependent affinity for Rad4. Lack of Ino80 will lead to defects in the recruitment of repair factors to the damage site and the restoration of the nucleosome structure after repair (Sarkar et al., 2010). The role of Ino80 in NER is conserved in eukaryotic cells as without components of the mammalian Ino80 complex (INO80 and ARP5) a significantly reduced cellular removal of UV-induced photolesions occurs and this is not due to the reduced transcription of NER factors (Jiang et al.,

2010). These results suggest Ino80 is recruited to sites of UV DNA damage by interaction with the NER machinery and it is also needed to restore the chromatin structure after repair.

Studies on Rad26 and CSB (human homolog of Rad26) also imply chromatin remodeling activities likely play a role in damage recognition during TC-NER (Zhang et al., 2009, Sarker et al., 2005, Newman et al., 2006).

1.4.3.2 Histone acetylation and NER in chromatin

In addition to chromatin remodelers, histone post-modifications have been implicated in various mechanisms of DNA repair. As mentioned in the last section, histones are constant targets for post-translational modifications including acetylation, methylation, phosphorylation, sumoylation, and ubiquitination (Kouzarides, 2007). Some of these modifications are related to NER (Waters et al., 2008). Acetylation is one of the abundant histone post-modifications and it has roles in transcription regulation, replication, histone deposition and DNA repair. Histone acetyltransferases (HATs) are a group of enzymes which catalyse and transfer acetyl groups from acetyl CoA to the ϵ -amine of lysine residues in the N-terminal tails of histone proteins whereas histone deacetylase (HDAC) have the reverse role of HATs. In combination HATs and HDACs regulate histone acetylation levels (Peng et al., 2008).

After UV irradiation, hyperacetylated histones were found as a response and in hyperacetylated nucleosomes regions, this facilitated more efficient NER (Ramanathan and Smerdon, 1986, Ramanathan and Smerdon, 1989). Our group extended these studies and showed a direct correlation between acetylation and repair. We demonstrated slower CPD removal in yeast cells lacking the histone acetyltransferase (HAT) Gcn5 and that UV irradiation induced an increase in the acetylation of H3K9 and H3K14 throughout the genome (Teng et al., 2008a, Yu et al., 2005a). In strains that lack one or the other of the damage recognition factors Rad4 or Rad14, hyperacetylated histone H3 was still found. This indicated that this acetylation is induced before NER, and that this induction is not reliant on the NER process.

Conversely the return of this hyperacetylation to pre-damage levels was dependent on NER (Yu et al., 2005a). UV-induced hyperacetylation of H3K9 and K14 was shown to be mediated by the GG-NER-specific factor Rad16 and pre-hyperacetylated regions exhibit efficient CPD removal by GG-NER even without Rad16 (Teng et al., 2008a). These results suggest that changes in chromatin structure induced by acetylation make the DNA more accessible not only to transcription factors but also for NER. The acetylation step changes the original positively charged lysine ammonium group to an uncharged state and reduces the affinity for adjacent histones and DNA, so making the DNA more accessible to DNA-binding proteins (Stryer et al., 2006, Kouzarides, 2007). This acetylation is conserved in mammalian cells. For example, the E2F1 transcriptional factor in human cells associates with GCN5 to acetylate H3K9 at the damaged site (Guo et al., 2011).

There are two predominant families that HATs can be categorized into based on their catalytic domain; the MYST (MOZ-Ybf2/Sas3-Sas2-Tip60) family and the GNAT (Gcn5 related N-acetyltransferases) family. In addition there is also the p300/CBP family which are the general transcription factor HATs. This includes the TFIID sub-unit TAF250 and the nuclear hormone-related HATs SRC1 and ACTR (Berndsen and Denu, 2008, Carrozza et al., 2003). Acetylated lysines can be recognised and react with a structural motif called a bromodomain which has been found in many DNA-interacting proteins, including chromatin remodellers, complexes that post-translationally modify histones including HATs and the transcription factor TFIID (Yang, 2004).

Histone hyperacetylation could regulate NER either by directly generating a suitable binding environment for repair proteins to reside or by indirectly through altering the compaction of nucleosomes (Irizar et al., 2010).

In yeast, Gcn5 hyperacetylates H3 (at K9 and K14) at the repressed *MFA2* promoter upon UV irradiation (Yu et al., 2005a). Histone H3 acetylation by Gcn5 is implicated in regulating ~5% of the yeast genome gene expression including at *MFA2*, but does not function at the *RPB2* promoter. This promoter does not require Gcn5 for histone

acetylation, and also it does not require Gcn5 for more efficient damage removal (Teng et al., 2002). In yeast, the Rad16/Rad7 complex which is essential for yeast GG-NER (Verhage et al., 1994, Yu et al., 2004) is associated with UV-induced histone acetylation (Teng et al., 2008b).

1.5 *MFA2* as a model gene

The *S.cerevisiae MFA2* gene was selected as a model gene for some of the experiments presented in this thesis. It is a mating-type specific gene. *MFA2* is a yeast mating-type gene which has been used extensively by the Waters group as a region to study nucleosome positioning, CPD repair at single-nucleotide resolution and UV-induced chromatin remodelling events. *S. cerevisiae* can stably exist as either a diploid or a haploid. Haploid cells of the yeast *S. cerevisiae* exhibit two distinct cellular phenotypes called a and α . These cell types are specialized for mating and produce different cell-type specific proteins respectively as listed in Table 1.2. Some of these proteins permit a and α cells to signal their presence to the opposite mating type and prepare the cells for mating. The response of haploid cells only to the mating pheromones of the opposite mating type allows mating between a and α cells, but not between cells of the same mating type (Nasmyth, 1982).

Table 1.2

MAT α haploid cells	MAT a haploid cells
Transcription factors, alpha-1 and alpha-2	Transcription factor a1
Mcm1 binds with alpha-1 to activate alpha-specific genes	a1 protein does not have transcription role
Mcm1 binds with alpha-2 to represses a-specific genes	Mcm1 by itself activates a-specific genes and haploid-specific genes
Mcm1 activate haploid-specific genes	α -specific genes are silent

The mating type of a haploid yeast cell is determined by the allele present at the mating type locus, *MAT*, near the centromere of chromosome III. Mating type switching occurs as the central Y region of a specific *MAT* allele is replaced by another copy carrying the opposite mating information located in the storage loci, *HMR* or *HML* (Haber et al., 1984). In these two Mating types, some of the activation and transcription of genes differ due to two different mating proteins having a different regulatory role. For example, the *MFA2* gene is repressed in *MAT* α cells but it is expressed in *MAT* a cells (Hartig et al., 1986). *MFA2* was chosen as a model gene because it was possible to look at events in either the repressed or transcriptionally active state, and because its small size meant that a comprehensive picture of NER can easily be obtained on a single sequencing gel.

MFA2 locates to the left arm of chromosome XIV, and encodes the a factor precursor consisting of 38 amino acids (Michaelis and Herskowitz, 1988). The transcriptional regulation of *MFA2* is well understood in mating type a cells (Keleher et al., 1992). In alpha cells, the repression of a specific genes is mediated by the cooperative binding of Mcm1 which is a protein of the MADS box family, and alpha2 factor (Mead et al., 2002). In addition to alpha 2 and Mcm1, in α cells the *MFA2* expression is repressed by the Tup1-Ssn6 complex, and full repression of *MFA2* and requires the presence of the Ssn6-Tup1 general repressor, because deletion of *TUP1* results in the depression of *MFA2* in a cells (Teng et al., 2008b).

The *MFA2* gene is relatively well characterized. A HaeIII restriction fragment contains the coding sequence of *MFA2* and 517bp of its upstream promoter region and the 83bp downstream transcription termination region. The Mcm1 binding site and the putative TATA box are located in the upstream region- 221 to -251 and -119 to -125 respectively. MNase mapping indicated two nucleosomes were positioned in the promoter and two in the transcribed region of this gene in alpha cells where the gene is repressed (Teng et al., 2001), whereas in a cells fixed nucleosomes are undetectable when *MFA2* is transcriptionally active. Thus it provides an ideal model

for the study of the relationships between DNA repair, transcription and chromatin structure.

1.6. The role of Histone modifications and variants in repair

1.6.1 Histone modifications

Histones are the chief protein components of the eukaryotic chromatin which bond with DNA to generate nucleosomes. They consist of linker histone H1A and core histone H2A, H2B, H3, H4. A nucleosome contains 2 molecules, each of H2A, H2B, H3, H4. Each of the core histones has a related globular domain that mediates histone–histone interactions within the octamer, and that organizes the two wraps of nucleosomal DNA (Luger et al., 1997). Each histone also harbours an amino terminal 20–35 residue segment that is rich in basic amino acids and extends from the surface of the nucleosome. These histones consist of a C-terminal domain and an unstructured N terminal tail. Although a variety of modifications occur throughout the histone proteins, they occur primarily on the N-terminal tail (Kouzarides, 2007, Bhaumik et al., 2007). Histone H2A is unique in having an additional ~37 amino acid carboxy-terminal domain that protrudes from the nucleosome (Rippe et al., 2008). These histone ‘tails’ do not contribute significantly to the structure of individual nucleosomes nor to their stability, but they do play an essential role in controlling the folding of nucleosomal arrays into higher order structures (Peterson and Laniel, 2004). Studies were first carried out by Allfrey in the early 1960s (Allfrey et al., 1964). Since then we know there are a number of different histone post-translational modifications (PTMs) which can be subject to at least 9 types of post-translational modifications: acetylation, lysine methylation, arginine methylation, phosphorylation, ubiquitination, sumoylation, ADP ribosylation, deimination and proline isomerisation (Bannister and Kouzarides, 2011). High-resolution X-ray experiments indicate that these modifications affect inter-nucleosomal interactions (Luger et al., 1997). More importantly, they affect recruitment of other proteins and complexes such as

remodelling enzymes. In this way, they can influence not only transcription but also DNA repair, replication and recombination (Bannister and Kouzarides, 2011).

1.6.1.1 Histone Acetylation

As stated earlier, histone acetylation has roles in replication, histone deposition, transcription regulation and DNA repair. Histones are acetylated by a group of enzymes known as histone acetyltransferases (HATs) which catalyse the transfer of acetyl groups from acetyl CoA to the ϵ -amine of lysine residues in the N-terminal tails of histone proteins (Stryer et al., 2006). Acetylation is a dynamic and reversible process thus the level of acetylation at a particular K residue is a result of the balance of HAT and histone deacetylase (HDAC) activities (Peng et al., 2008). Our group has already found a correlation between Gcn5 mediated histone H3 acetylation and efficient NER (Yu et al., 2005a).

Gcn5

Gcn5 (General Control Nonderepressible 5) was originally identified as a transcriptional co-activator/adaptor and the role of this protein in facilitating transcription has been reported (Kuo et al., 2000). It is also a HAT (histone acetyltransferase) that acetylate lysine residues on the N-terminal domain on histones H3 and H2B. The *GCN5* gene contains a highly conserved region at amino acids 170 to 253 which has been shown to be the minimal sequence for the catalytic HAT domain with 88% similarity from yeast to humans. In addition Gcn5 also has a region required for interaction with Ada2 (between amino acids 253 and 350) and a bromodomain (between aa 350 and 440) (Candau et al., 1997). It is a sub-unit of several multi-protein complexes, including SAGA, SLIK and ADA in yeast (Grant et al., 1997) and STAGA, TFTC and PCAF in humans (Brand et al., 1999, Martinez et al., 1998, Ogryzko et al., 1998). In yeast, a *GCN5* deletion mutant is viable indicating that it is not an essential gene (Zhang et al., 1998). However, absence of Gcn5 alters 10% of the yeast gene expression compared to WT (Huisinga and Pugh, 2004). These genes include many chromatin modifying enzymes and imply data that Gcn5 has a

role beyond transcription (Brand et al., 2001, Martinez et al., 2001, Teng et al., 2002, Yu et al., 2005b).

For its role in transcription, Gcn5 primarily has been shown to control the expression of inducible genes (Holstege et al., 1998). The transcription of Gcn5 regulated genes is dependent on the HAT activity of Gcn5, as catalytic function mutations of Gcn5 lead to a significant decrease in its ability to activate transcription (Kuo et al., 1997). The transcription heat shock protein *hsp70* was reported to be modulated by Gcn5, coupled with Elp3 through altering histone H3 acetylation (Han et al., 2008). Gcn5 is targeted to specific promoters by transcription activators, such as Gcn4 (Kuo et al., 2000). *GCN5* deletion result in a genomewide H3 acetylation level decrease, indicating that there may be a more global role for Gcn5 in histone acetylation that is not only restricted to its promoter specific roles (Kuo et al., 2000). In the yeast *Schizosaccharomyces pombe*, Gcn5 is preferentially located in the coding region of highly expressed genes and it is required for efficient transcription elongation, in addition to its previously characterized roles in transcription initiation (Johnsson et al., 2009). In *S.cerevisiae*, higher H3 acetylation was found in the promoters and peaking after the ATG start codon. Gcn5 is responsible for mediating acetylation in the promoter and 5' regions (Roh et al., 2004).

Bromodomains are acetyl lysine binding modules found in many complexes that regulate gene transcription. Gcn5 contains a bromodomain which recognises acetylated lysines by both the bromodomain directly interacting with amino acids that flank the acetylated lysine residue in specific proteins and the spatial arrangement of the bromodomain in the larger complexes (Li and Shogren-Knaak, 2009). The Gcn5 bromodomain has functional relevance, it plays a part in nucleosome acetylation in several ways and it is required for cooperative nucleosome acetylation, while other components of the SAGA complex may also be needed. After one of the histone H3 tails is already acetylated, the bromodomain promotes the acetylation of the other H3 N-terminal domain as there are two copies of histone H3 in one nucleosome (Li and Shogren-Knaak, 2009).

As an acetyltransferase, Gcn5 acetylates histone H3 at lysine 14 predominantly, but also at lysines 9, 18 and 23 (Li and Shogren-Knaak, 2009, Zhang et al., 1998). Acetylation of K9 and K14 peaks at transcription start sites of active genes and this correlates with Gcn5 localization and the transcription rate genome wide (Pokholok et al., 2005a). Gcn5 also acetylates several non-histone substrates including Rsc4, Cdc6 and the Snf2 sub-unit of the SWI/SNF complex (Paolinelli et al., 2009, VanDemark et al., 2007, Kim et al., 2010).

Although Gcn5 catalyses a covalent modification, the Gcn5 protein itself can also be covalently modified and it is the substrate for sumoylation (Sterner et al., 2006). The sumoylation of Gcn5 may negatively regulate the transcription of certain genes, however it has no detectable effect on the HAT activity of Gcn5 (Sterner et al., 2006).

Esa1

Esa1 is the only essential HAT in yeast, it is a member of the conserved MYST family of HATs. Esa1 is comprised of 445 amino acids and contains an N-terminal chromodomain and a C-terminal MYST domain. Primarily Esa1 is responsible for the majority of H4 acetylation. However it has also been shown to catalyse the acetylation of H2A and acetylation of the histone variant Htz1-K14 *in vivo* (Keogh et al., 2006). Esa1 cooperates with the H3 HAT in SAGA, Gcn5 to stimulate transcription elongation by mediating nucleosome acetylation *in vivo* (Ginsburg et al., 2009). Similar to the other HATs, Esa1 is part of two multi-subunit HAT complexes which is the catalytic subunit of the NuA4 and Pico NuA4 (picNuA4) complexes (Pillus, 2008). NuA4 is the larger complex made up of at least 13 polypeptides, whereas picNuA4 is comprised of only 3 polypeptides: Esa1, Yng2 and Epl1 (Boudreault et al., 2003). Essential roles of NuA4 and picNuA4 are to regulate the catalytic activity of Esa1 for global and targeted histone H2A, H2A.Z (HTZ1), and H4 acetylation (Decker et al., 2008). Like Gcn5, Esa1 relates to gene activation by mediating histones acetylation at the promoters of a subset of yeast genes. NuA4 is believed to provide the targeted histone acetylation at specific genes, where picNuA4 is more involved in maintaining the global level of histone H4 acetylation (Boudreault et al., 2003). Esa1

catalysed H4 acetylation at K5, 8, 12 and 16 peaks over transcription start sites and correlates with rates of transcription. However, the association is not as strong as in the case of Gcn5. A small but positive correlation with transcription is found for Esa1 (Pokholok et al., 2005a). The acetylation of H4 by Esa1 at sites near a double stranded breaks is important as this modification recruits chromatin remodellers such as INO80, to modify chromatin structure near the break (Decker et al., 2008). As the histone H2A variant Htz1 is acetylated by NuA4 (Keogh et al., 2006). My research will involve examining the role of Esa1 in NER.

Histone deacetylation is catalysed by HDACs. The balance of histone acetylation is important to modulate specific cellular function. In yeast there are three classes which are class I HDACs (Rpd3, Hos2 and Hos1), class II HDACs (Hda1 and Hos3) and class III HDACs (Hst2, Hst3, Hst4 and Sir2) (Ekwall, 2005).

Rpd3

Rpd3 is a class I HDAC. The gene encodes the catalytic subunit present in two HDAC complexes, the larger Rpd3(L) complex and the smaller Rpd3(S) complex which share 3 subunits with each other (Yang and Seto, 2008). Rpd3(L) and Rpd3(S) appear to have different functions and both of them have histone deacetylase activity. Rpd3L is likely responsible for Rpd3's role at gene promoters, as Rpd3 is recruited to chromatin via the Rpd3L-specific subunit Ume6, which recognizes specific upstream promoter sequences and is responsible for Rpd3's role in silencing and regulation of replication initiation (Keogh et al., 2005, Carrozza et al., 2005). The Rpd3S complex is recruited to methylated H3K36 within coding sequences to deacetylate histones and prevent intragenic transcription initiation. This is mediated through the chromodomain of Eaf3, one of the sub-units that comprises the Rpd3S complex, interacting with methylated histone H3K36 (Carrozza et al., 2005, Joshi and Struhl, 2005, Keogh et al., 2005). Rpd3 is involved in strongly deacetylating the histones at *INO1* and *IME2*, with the exception of histone H4K16 (Suka et al., 2001). Rpd3 deacetylates large regions of the chromatin in a process termed global deacetylation. CHIP-seq work has demonstrated that the binding for HATs and HDACs positively correlates with gene

expression, RNAPII binding and acetylation levels (Wang et al., 2009). Inhibition of the HDAC activities showed that they function to remove acetyl groups at active genes to maintain an acetylation level which supports transcription elongation but not promiscuous initiation. In addition HDACs promote removal of acetyl groups added by transient HAT binding at inactive genes so as to prevent RNAPII binding by keeping acetylation levels low (Wang et al., 2009). Rpd3 is excluded from the telomeric and sub-telomeric regions and Sir3 is involved in the maintenance of hypoacetylated histones in heterochromatin regions. (Suka et al., 2001). Esa1 and Rpd3 have opposing enzymatic activities and deletion of *RPD3* restored global histone acetylation levels in the *esa1* mutant. Esa1 and Rpd3 were found to regulate the dynamic acetylation and deacetylation of H4K12 (Chang and Pillus, 2009). Gcn5-dependent histone H3 acetylation and Rpd3-dependent histone H4 deacetylation have been found to have opposing effects on *IME2* transcription (Burgess et al., 1999). Genetic interaction between Gcn5, Esa1 and Rpd3 was also found (Lin et al., 2008). These roles and interactions may influence transcriptional regulation and DNA repair.

1.6.1.2 Histone methylation

Histones are methylated on lysine residues, arginine residues or both (Kouzarides, 2007). Histone arginine methylation can occur in the mono- or dimethylated form at specific positions on histone H3 and histone H4 in higher eukaryotes but it has not yet been reported in *S. cerevisiae* (Kouzarides, 2007, Shilatifard, 2006). The coactivator arginine methyltransferase (CARM1) and the protein arginine methyltransferase (PRMT1) are essential for the methylation of specific arginine residues on histones H3 and H4 (Kouzarides, 2007, Shilatifard, 2006).

Histone lysines can be mono-, di-, or trimethylated on lysines 4, 9, 27, 36 and 79 of histone H3 and Lys20 of histone H4. The sites of histone methylation are, for the most part, highly conserved from yeast to human, and specific sites such as histones H3K9, H3K27 and H4K20, are unmethylated in *S. cerevisiae* (Kouzarides, 2007, Shilatifard, 2006). The SET domain contains the enzymatic activity responsible for lysine

methylation of histone tails. Dot1 does not contain a SET domain, but still specifically methylates lysine 79 of histone H3 in the core domain (Khorasanizadeh, 2004).

Histone methylation of lysine residues on histone proteins is a far more stable histone modification than other modifications. Two histone methylations occur in response to UV irradiation, H3K79me and H4K20me. In *S.cerevisiae* tri-methylation of histone H3K79 is enriched in the transcribed regions of genes (Pokholok et al., 2005a) and extremely low in heterochromatin (van Leeuwen et al., 2002). The loss of Dot1 or mutation of H3 K79 to glutamic acid in yeast caused these strains to become UV-sensitive compared to WT (Bostelman et al., 2007). Histone H3K79 methylation is required for CPD repair in silent regions and both the modification and Dot1 are important for GG-NER at the NTS of the *RPB2* gene (Chaudhuri et al., 2009, Tatum and Li, 2011).

1.6.1.3 Histone ubiquitination

The covalent attachment of a ubiquitin to specific lysine in histones plays an important role in regulating transcription either through proteasome dependent degradation of transcription factors or other mechanisms related to the recruitment of modification complexes. This transcription regulation is typically a positive control.

Ubiquitination includes a three step enzymatic reaction. This involves ubiquitin-activating (E1), ubiquitin-conjugating (E2) and ubiquitin-ligating (E3) enzymes that can add either one or several ubiquitins to the target protein, and is dependent on the E2 and E3 enzymes involved (Passmore and Barford, 2004). In response to several DNA damaging sources, including UV light, the Rad6/Bre1 E2/E2 complex can ubiquitinate histone H2B at K123 (Giannattasio et al., 2005). In higher eukaryotes, histone H2A is mostly monoubiquitinated at lysine 119, though polyubiquitination has been reported, but this residue is not modified in the budding yeast *Saccharomyces cerevisiae*. Histone H2B, in contrast, is found only in the monoubiquitinated form (human Lys120; yeast Lys123) (Thorne et al., 1987). The ubiquitination site on histone H3 has yet to be characterized (Bhaumik et al., 2007).

The ubiquitination of H2B K123 is required for the methylation of H3K4 and H3K79 by the Set1 and Dot1 DNA methyltransferases respectively (Santos-Rosa et al., 2004, van Leeuwen et al., 2002). H2BK123 ubiquitination, catalysed by Bre1, is required for di- and tri-methylation of H3K79 by Dot1, and *BRE1* deletion results in compromised GG-NER in the NTS of the *RPB2* gene (Tatum and Li, 2011).

1.6.2 Histone variants

In most eukaryotes, histones are the major structural components of chromatin, including 4 highly conserved canonical histones H2A, H2B, H3 and H4 (Luger et al., 1997). Canonical histones are encoded by multicopy genes which are intronless, while histone variants are encoded by single-copy genes that contain introns (Albig and Doenecke, 1997). Unlike canonical core histones which are exclusively expressed during S phase of the cell cycle, variants of canonical histones are expressed throughout the cell cycle (Henikoff et al., 2004). Canonical histone transcripts contain a conserved 3' stem loop which is responsible for their restricted expression at S phase (Harris et al., 1991). Different from the core histones, histone variants are transcribed into mRNAs that are polyadenylated and constitutively transcribed at all stage of the cell cycle (Kamakaka and Biggins, 2005). While canonical histones are deposited in a replication-dependent manner, histone variants are deposited in specific regions of the genome, normally in a replication-independent manner and these contribute to a distinct or unique nucleosomal architecture. This heterogeneity has been found to have roles in a wide range of nuclear functions (Banaszynski et al., 2010). Accumulating evidence illustrates that histone variants have distinct functions related to DNA repair, meiotic recombination, chromosome segregation, transcription initiation and termination, sex chromosome condensation and sperm chromatin packaging (Talbert and Henikoff, 2010). All four histone have variant counterparts.

1.6.2.1 Histone H1

The linker histone H1 has an important role in establishing and maintaining higher

order chromatin structures. It has numerous variants including seven somatic subtypes (from H1.1 to H1.5, H1.0, and H1X), three testis-specific variants (H1t, H1T2m and H1LS1), and one restricted to oocytes (H1oo) (Happel and Doenecke, 2009, Izzo et al., 2008). In higher eukaryotes all H1 variants have the same general structure, consisting of a central conserved globular domain, and differences between the major histone subtypes and the variants occur in the less conserved nonglobular N- and C-terminal tail domains of these proteins (Izzo et al., 2008). The portion of these variants fluctuates in different cell types during the cell cycle, differentiation, and development (Brown, 2003) and different distribution patterns were found throughout the mammalian genome (Parseghian et al., 2001). In mice, single or double H1 variant knock-outs do not have an effect on the phenotype because of the compensatory up-regulation of other subtypes (Fan et al., 2001). Based on this research, disruption of one or two H1 subtype genes is quantitatively compensated by an increased expression of other subtypes, which suggests a functional redundancy of H1 subtypes. However, depletion of single H1 subtypes by inducible RNA interference in breast cancer cells produced different phenotypic effects (Sancho et al., 2008). This suggested specific subtypes of H1 participate in particular systems have specific functions of gene regulation. Based on these results, it is not clear whether the different variants have specific roles or regulate specific promoters.

1.6.2.2 Histone H2A

Among the core histones, H2A has more variants than the others including HTZ1 (H2A.Z in mammals), MacroH2A, H2A-Bbd, H2AvD, and H2A.X (Fernandez-Capetillo et al., 2004, Ausio and Abbott, 2002). H2A.Z and H2A.X have been found in most eukaryotic lineages (Jackson et al., 1996), while others, such as MacroH2A (Pehrson and Fuji, 1998) and H2A-Bbd (Chadwick and Willard, 2001) are restricted to vertebrates or mammals. Among these variants, significant major sequence changes at both the N- and C-terminal ends of their molecules were found with a substantially larger predominance of those affecting the carboxy end. H2A.X

and H2A.Z are constitutively expressed and localize throughout the human genome, H2A.Z shows some enrichment in intergenic regions. MacroH2A localizes predominantly to the inactive X-chromosome (Costanzi and Pehrson, 1998), while H2A-Bbd localizes to the active X-chromosome and autosomes (Chadwick and Willard, 2001).

HTZ1 (H2A.Z in mammals)

H2A.Z is highly conserved throughout evolution. It has a single evolutionary origin and remains distinct from all other H2A variants. My research has focused on this H2A histone variant and details are provided in a later section.

H2A.X

H2A.X is present in nearly all eukaryotes, except nematodes (Malik and Henikoff, 2003). This histone variant has a histone fold domain that is similar to the canonical H2A, although it has a unique C-terminal motif termed SQ(E/D) Φ (Φ represents a hydrophobic residue). Studies have found that H2A.X has a role in DSB repair through the phosphorylation of H2A.X C-terminus serine residue at the γ -position (termed γ -H2A.X). This is induced by DSBs (Fernandez-Capetillo et al., 2004). Although the FACT protein complex can mediate the exchange of γ -H2A.X-H2B with unmodified H2A.X-H2B (Heo et al., 2008), no specific de novo deposition chaperone for H2A.X has been identified. As a result of overall sequence similarity between H2A.X and canonical H2A (Malik and Henikoff, 2003, Talbert and Henikoff, 2010), the major H2A proteins in *Saccharomyces cerevisiae* and *Schizosaccharomyces pombe* are more similar to the mammalian H2A.X variant than the mammalian major H2A (Malik and Henikoff, 2003). Studies have mapped the phosphorylated form of H2A, which can be equated to H2A.X (H2A.XS129/28ph), across the budding and fission yeast genomes. These results suggest the same assembly factor may mediate H2A.X and canonical H2A deposition. Apart from the function in DSB repair, H2A.X has also been implicated in meiosis, growth, tumor suppression and immune receptor rearrangements (Fernandez-Capetillo et al., 2004).

MacroH2A

MacroH2A contains a unique large (200 residue) C-terminal domain termed “the macro domain” which shares no sequence similarity with any other histone (Malik and Henikoff, 2003). This C-terminal macro domain of macroH2A interferes with the binding of transcription factors, and the N-terminal domain impedes chromatin remodeling via SWI/SNF to repress gene expression (Angelov et al., 2003). In mammals, macroH2A is enriched on the inactive X chromosomes in females and is thought to be an epigenetic marker of X inactivation and it may contribute to the maintenance of an inactive X chromosome (Costanzi and Pehrson, 1998). Furthermore, macroH2A also involve gene silencing by inhibiting the catalytic activity and substrate binding capacity of the gene activation related enzyme PARP1 (Nusinow et al., 2007).

H2A-Bbd (Barr body-deficient)

H2A.Bbd has a truncated C-terminal docking domain, has only 48% identity to canonical H2A and is excluded from the inactive X chromosome from where its name was derived (Chadwick and Willard, 2001). H2A.Bbd-containing chromosomes exhibit a relaxed conformation compared with the native H2A. This lower stability means it can be assembled and disassembled by the nucleosome assembly protein (NAP-I) more easily (Gautier et al., 2004). H2A. Bbd is suggested to be involved in gene activation.

1.6.2.3 Histone H2B

Histone H2B is markedly deficient in variants. Nevertheless, a few tissue-specific H2B isoforms have been reported, including sperm specific H2B variant (spH2B), testis specific H2B variants TH2B and H2BFWT (Gineitis et al., 2000). They have very specialized functions in chromatin compaction and transcription repression, particularly during gametogenesis. H2BFWT appears to be enriched at telomere interstitial blocks, and it has been proposed that H2BFWT may serve as an epigenetic marker of telomeric identity in testis (Churikov et al., 2004).

1.6.2.4 Histone H3

There are two major histone H3 variants called H3.3 and centromeric H3 (CenH3) (Malik and Henikoff, 2003). In humans, apart from these two H3 variants, there are six other histone H3 variants including two ubiquitously expressed H3 variants (H3.1, H3.2) and one specifically expressed in the testis, H3 isoform H3T(H3.4). These are two primate-specific H3 variants, H3.X and H3.Y (Wiedemann et al., 2010) and a hominid-specific variant H3.5 (Schenk et al., 2011). H3.1 is the major canonical histone H3 in humans. However, in frog, chicken, and fly, H3.2 is the canonical histone H3, and H3.1 is absent in these species. Yeast has one non-centromeric H3, which is similar to H3.3 in higher eukaryotes (Malik and Henikoff, 2003).

CenH3

All eukaryotes have a conserved essential protein that binds to centromere H3 (CenH3), which has highly divergent N-terminal tails (Henikoff and Ahmad, 2005). This variant is named CENP-A in mammals and Cse4 in yeast. CENP-A shares only 50% identity in the histone fold domain with the canonical H3 histones (Malik and Henikoff, 2003). Although, the DNA structure in the CENP-A nucleosome is different from that of the H3 nucleosomes, the overall structure of the histone octamer is not altered. Biochemical studies suggested DNA in a CENP-A containing nucleosome is more accessible than in a canonical H3 nucleosome (Conde e Silva et al., 2007, Sekulic et al., 2010); a yeast Cse4 nucleosome also revealed this (Dechassa et al., 2011). CenH3 may be playing an essential role in defining the formation of the centromeric chromatin (Palmer et al., 1990).

H3.3

Histone H3.3 is a homomorphous variation with 96% identity to canonical histone H3. In humans, only four amino acids are different in the composition of this histone when compared with the major canonical H3.1. In H3.3, S31 replaces A31 within the N-terminal domain and A87, G90, S96 replace S87, M90, C96 within the $\alpha 2$ helix of the histone-fold domain (Malik and Henikoff, 2003). Biochemical research in HeLa cells showed that the canonical H3 histones are deposited by the CAF-1 complex in a

replication-dependent manner, while the HIRA complex deposited H3.3 histones in a replication-independent manner (Tagami et al., 2004). Compared with the canonical H3 histone, H3.3 histones are enriched in post-translational modifications that correlate with gene expression, such as H3K4 and H3K36 methylation, as well as H3K9, H3K18, and H3K23 acetylation (Benson et al., 2006). Furthermore, H3.3 is expressed throughout the cell cycle and incorporated predominantly at transcriptionally active regions. As both H3.3 deposition and active histone modifications are independently correlated with transcriptional activity, this suggests its role is in gene activation (Ahmad and Henikoff, 2002). H3 proteins in yeast are more similar to mammalian H3.3 than H3 (Malik and Henikoff, 2003). H3.3 histones are also reported to be critical for the formation of pericentromeric heterochromatin (Santenard et al., 2010) and the maintenance of the telomeres (Ahmad and Henikoff, 2002, Wong et al., 2010).

1.6.2.5 Histone H4

Although, there appear to be no known sequence variants of histone H4, there are H4 genes that are constitutively expressed throughout the cell cycle that encode for proteins that are identical in sequence to the major H4 in *Drosophila* (Akhmanova et al., 1996).

1.7 H2A histone variant Htz1(H2A.Z)

Histone variants not only alter the interactions of nucleosomes with other factors but they also affect their stability and DNA accessibility. One such variant, H2A.Z (Htz1 in yeast), is an evolutionary conserved histone with 90% sequence identity across species (Iouzalén et al., 1996), but only about 60% sequence identity to canonical H2A (Thatcher and Gorovsky, 1994, Jackson and Gorovsky, 2000). It is likely that the nonconserved residues are responsible for Htz1-specific functions with roles in transcription, silencing, genome integrity and cell cycle progression (Jackson and Gorovsky, 2000).

In many organisms, H2A.Z is essential for viability and its absence cause lethality; for example in *Tetrahymena thermophila* (Liu et al., 1996), *Drosophila melanogaster* (Clarkson et al., 1999), *Xenopus leavis* (Ridgway et al., 2004), and *Mus musculus* (mouse) (Faast et al., 2001). In the yeast *Saccharomyces cerevisiae*, deletion of H2A.Z (HTZ1) is tolerated, but results in growth defects (Jackson and Gorovsky, 2000) with a greatly affected transcription level and an increase of chromosome loss (Svotelis et al., 2009).

1.7.1 H2A.Z Structure

H2A.Z as a major histone H2A variant was first found by West and Bonner (1980) as approximately 4% of the total H2A in mouse L1210 cells (West and Bonner, 1980). The crystal structure revealed a difference in the residues 81–119 in H2A in the (H3–H4)₂ tetramer docking domain between the H2A subunits in the C-terminus and in the L1 loop. Specifically, the substitution of Gly106 in H2A.Z was originally Glu104 in H2A, this results in the loss of three hydrogen bonds (Suto et al., 2000). At least three features of H2A.Z/Htz1 can be distinguish from H2A: (1) a unique C-terminal tail important for specifying H2A.Z/Htz1 deposition (Adam et al., 2001), (2) an extended surface charge patch (α C helix) which may help regulate chromatin compaction (Fan et al., 2004), and (3) a small internal loop that helps ensure that nucleosomes contain either two H2A.Z molecules or two H2A molecules (Suto et al., 2000).

Although there are numerous amino acid differences between major H2A and H2A.Z, surprisingly the crystal structure of a nucleosome core particle containing the histone variant H2A.Z shows a similar overall structure to that containing major histone proteins (Suto et al., 2000). These similarities lead to the interaction between the histone folds of H2A.Z and H2B being virtually unchanged. However, sequence differences do lead to localized changes in the interaction of the H2A.Z–H2B dimer with the (H3–H4)₂ tetramer, and between the two copies of H2A.Z–H2B dimers in the same nucleosome (Suto et al., 2000).

Like canonical histone, N-terminal lysine residues are a postsynthetic modification target, including acetylation. Human H2A.Z contains five acetylable lysine residues: K4, K7, K11, K13, and K15 (Dryhurst et al., 2004). In yeast, four acetylable residues: K3, K8, K10, and K14 (most abundant *in vivo*) have been identified in the N terminus through mass spectrometric analysis (Millar et al., 2006). NuA4 is the only essential HAT in yeast and it is responsible for these Htz1 acetylations, more specifically by its functional subunit Esa1 (Keogh et al., 2006). In addition, C-terminal lysines K120 and K121 of H2A.Z were reported to be monoubiquitylated in mammalian cells (Sarcinella et al., 2007).

1.7.2 Htz1 deposition and genome dynamics

Specific Htz1 deposition required Swr1 which is a subunit of the SWR-complex. This is unique in efficiently replacing the H2A-H2B dimer with Htz1-H2B in yeast and H2A.Z-H2B in humans, in an ATP-dependent manner (Mizuguchi et al., 2004). Studies have indicated that Nap1 and Chz1 histone chaperones also take part in this exchange step. Nap1 mediates the nuclear import of cytosolic H2A.Z-H2B, whereas final deposition needs Chz1 to present the H2A.Z-H2B dimers to the SWR1 complex (Luk et al., 2007, Straube et al., 2010). Another ATP-dependent chromatin remodeling complex, the INO80 complex was reported to be involved in the replacement of H2A.Z with canonical H2A at transcription start sites in yeast (Papamichos-Chronakis et al., 2011).

Genome-wide distribution of Htz1 is well studied in yeast (Guillemette et al., 2005, Millar et al., 2006, Zhang et al., 2005). Htz1 occupies very small regions across the whole genome rather than large chromosomal domains (Guillemette et al., 2005). Htz1 generally occupies promoters. 75% of all Htz1 is within promoter regions whereas about 37% of promoter regions do not contain Htz1, and are mainly the promoters of highly active genes (Guillemette et al., 2005). Studies show that Htz1 significantly overlaps with transcription factors including Abf1, Fkh1, Reb1 and Pho4 and this represents a stronger negative correlation to transcription rate than does

histone H2A (Zhang et al., 2005). Htz1 occupancy correlates with relative acetylation levels at particular histone residues at intergenic regions (Kurdistani et al., 2004). A strong positive correlation with Histone H3 lysine 14 acetylation (H3K14ac) was observed, but Htz1 localization does not require this modification. Loss of Gcn5 or Sas3 which is responsible for this modification will reduce genome-wide Htz1 occupancy levels (Zhang et al., 2005). Apart from H3K14ac, Htz1 also has a strong negative correlation with H3K27ac, but a positive correlation with H2AK7ac and H4K8ac and negative correlation with H3K9ac levels (Zhang et al., 2005). Although Htz1 generally resides on repressed promoters, Htz1 K14 acetylation and Htz1 deposition takes place mainly at active promoters (Millar et al., 2006).

1.7.3 Functions of H2A.Z

1.7.3.1 Effect on Stability

Despite significant sequence divergence, nucleosomes containing H2A.Z overall reveal a high similarity to the H2A containing nucleosome (Luger et al., 1997). Other histone variants such as histone H2A variant H2ABbd and histone H3 variant H3.3 have been found to lower nucleosome stability (Gautier et al., 2004, Jin and Felsenfeld, 2007). Controversial results exist about whether H2A.Z causes destabilization of the interaction between the H2A.Z/H2B dimer and the H3/H4 tetramer compared to H2A.

H2A.Z from different organisms and different experimental set-ups and different sources of chromatin has been used to address this question. Some studies found stabilization (Thambirajah et al., 2006, Li et al., 1993, Park et al., 2004), whereas some found destabilization of the nucleosome (Suto et al., 2000, Abbott et al., 2001, Zhang et al., 2005). Some predict stabilization roles. For example salt-dependent dissociation of H2A.Z from hydroxyapatite adsorbed chromatin requires much higher salt concentrations than the canonical H2A (Li et al., 1993), characterization of the salt-dependent stability by Fluorescence Resonance Energy Transfer (FRET) also

indicated that H2A.Z stabilizes the histone octamer within the NCP (Park et al., 2004). Decreased sedimentation coefficient of NCPs containing native chicken erythrocyte H2A.Z reflect a destabilization compared with H2A, and also a subtle stabilization of the particle that is dependent on core histone acetylation (Thambirajah et al., 2006). Conversely, a crystal structural study found differences between H2A and H2A.Z that result in a subtle destabilization of the interface between the H2A.Z-H2B dimer and the (H3-H4)₂ tetramer (Suto et al., 2000). Chicken erythrocyte nucleosomes with recombinant H2A.Z/H2B dimers exhibited ionic-strength dependent, reduced stability in the analytical ultracentrifuge (Abbott et al., 2001). In yeast, chromatin salt-washed with increasing ionic strength suggested that Htz1 is less stable than either H2A or H3 (Zhang et al., 2005). Thus the overall stability of nucleosomes contain H2A.Z still remains controversial and is unclear.

1.7.3.2 The role in transcription

Observations with *Tetrahymena* indicated a positive role for H2A.Z in transcription, as *Tetrahymena* hv1 is only found in transcriptionally active macronuclei, but it is not detected in transcriptionally inactive micronuclei (Allis et al., 1980). Studies indicate that H2A.Z can have both an activating and a repressive influence on transcription.

It has an activating role, possibly in conjunction with chromatin modifiers such as SAGA and Swi/Snf in yeast. When genes were activated, a loss of H2A.Z was seen at active promoters (Santisteban et al., 2000). Comparing wild-type and htz1Δ yeast strains, 214 genes were significantly activated and 107 genes were repressed by H2A.Z (Meneghini et al., 2003). This shows its dual role in transcription. In early bovine embryos, a strong positive correlation between expression of p53 and H2A.Z was reported (Rodriguez et al., 2007). A genome-wide study reported a negative correlation between the promoter enrichment of H2A.Z and transcriptional activity (Guillemette et al., 2005), and this correlation extended occasionally to coding regions (Millar et al., 2006). Furthermore, although Htz1 is often localized in the promoters of repressed genes genome-wide, its acetylated counterpart Htz1K14ac accumulated in

promoters of active genes, indicating H2A.Z deposition may be regulated by its acetylation (Millar et al., 2006). These results indicate H2A.Z may act as transcriptional activator (or repressor), acting merely by structural alterations and deposition by its acetylation.

1.7.3.3 H2A.Z maintain genome integrity

After transcriptional induction, the yeast genes *INO1* and *GAL1* which localize to the nuclear periphery are rapidly reactivated after a short-time of transcriptional repression (Brickner et al., 2007). Htz1 is needed for this and suggests that H2A.Z mediates the epigenetic memory of the previous transcriptional state mediated by localization of recently repressed genes at the nuclear periphery (Brickner et al., 2007).

In mice, H2A.Z depletion caused genome instability and disruption of HP1 α localization at the pericentromeric regions. This suggests that HP1 α function and pericentromeric heterochromatin identity are regulated by H2A.Z during early embryonic development (Rangasamy et al., 2004).

In yeast, Htz1 is enriched in euchromatic regions and acts synergistically with a boundary element that prevent Sir2 and Sir3 from spreading into flanking euchromatic regions, so producing changes in histone H4 acetylation and H3 4-methylation that are indicative of ectopic heterochromatin formation (Meneghini et al., 2003).

A recent study reported histone H2A.Z regulates a chromatin remodeling step required for DNA DSBs repair in humans. Exchange of H2A.Z by p400 decreases the stability of the histone-histone and histone-DNA interactions within nucleosomes at the DSB. Tip60 mediated H4 acetylation and RNF8 regulated ubiquitination occurs prior to loading of the brca1 complex at DSBs (Xu et al., 2012). These histone modification required the p400-mediated exchange of H2A.Z onto nucleosomes at DSBs. Ku70/Ku80 loading required H2A.Z while Ku70/Ku80 binding is absolutely required for both HR and NHEJ-mediated DSB repair. These evidences suggest that

the p400 motor ATPase subunit of NuA4 catalyzes the rapid exchange of H2A.Z at DSBs. This alters histone-histone interactions both within and between adjacent nucleosomes, creating open, relaxed chromatin domains. This alteration of nucleosomes accommodates Tip60 to acetylate the N terminus of histone H4 and reveals cryptic ubiquitination sites for RNF8 mediated ubiquitination (Doil et al., 2009; Huen et al., 2007). As a consequence, H2A.Z exchange and DNA damage-induced histone modification then promotes transition to an open, relaxed chromatin conformation at the site of damage for Ku70/Ku80 promoting following repair (Xu et al., 2012).

In this thesis, I examined UV survival and repair of a range of mutants related to the presence of Htz1 in chromatin and Htz1 affects repair at specific genomic locations. I also extended these studies to a genome wide level through microarray analysis. My studies show that Htz1 enhances the occupancy of the histone acetyltransferase Gcn5 on chromatin to promote histone H3 acetylation following UV irradiation. Consequently, this results in an increased binding of a NER protein, Rad14, to damaged DNA with a concomitant increase in NER.

Chapter 2 Material and Methods

This chapter describes the molecular biological techniques employed in this study. The majority of solutions are described within the text, whereas some solutions have been named and these details can be found in Appendix I.

2.1 Strains, growth and storage

For the short term storage of strains, cell culture was streaked upon either YPD/synthetic drop out media agar plates and incubated at the appropriate temperature (30 °C unless otherwise stated) in a LEEC compact incubator until colonies had formed (typically 2-3 days). Plates were stored at 4 °C (weeks). For long term storage, cell cultures were grown to exponential phase, glycerol was added to a final concentration of 30% and cells were frozen at -80 °C.

Large amounts of cells for DNA and chromatin preparation were generated from large volumes of liquid media which were inoculated from a pre-culture. This pre-culture was made by picking a single colony from a plate, and inoculating it in fresh liquid media (about 10ml) and grown to exponential phase with a 2×10^7 cells/ml. Then liquid cultures were incubated at the appropriate temperature (30 °C unless otherwise stated) at 180rpm (normally over-night depend on cell growth). Cell cultures taken from - 80 °C stocks were first streaked either onto plates or in a small portion of culture media. This allowed cells to recover before proceeding with the above protocol.

For nearly all experimental purposes cell culture was grown to a density of 2×10^7 cells/ml (log phase). This density was calculated in two ways. Firstly, 1ml of cell culture was measured at 595nm with a Jenway 6300 Spectrophotometer, blanked against liquid media without cell culture. Cells were grown to a typical OD value of 0.6. Secondly, cell density was counted using an improved cell counting chamber (Hawksley).

2.2 UV damage

Yeast cells were collected by centrifugation and resuspended in chilled PBS (4 °C) to a density of 2×10^7 cells/ml. These cells were kept on ice and stored in dark to avoid additional visible light. 50ml of resuspended culture was poured into a 15cm diameter Pyrex dish and exposed to UV light at 254nm from a germicidal lamp at a fluence of $10\text{J}/(\text{m}^2 \cdot \text{sec})$ (the UV lamp was switched on at least 10 min before to ensure the irradiation gave a stable emission) . Cells were irradiated 50ml at a time until all of the culture had received the required dose of UV light ($100\text{J}/\text{m}^2$ will generate about 1CPD/kb). Yeast cells were subsequently pelleted by centrifugation and sampled or resuspended in liquid media for the required repair time.

The details of the UV irradiation procedure is as follows:

1. Cells from the overnight culture at a density of $2 \sim 4 \times 10^7$ cells/ml were collected by centrifugation at 4000rpm for 5min using a Beckman Avanti J-20XP centrifuge.
2. Cells were washed and then resuspended in PBS then put into 50ml 15cm diameter Pyrex dishes to treat with UV.
3. Cells were collected by centrifugation, followed by resuspension in YPD for repair or resuspended in liquid media for all downstream applications including crosslinking by formaldehyde. All unirradiated cultures were also resuspended in PBS in an identical manner to that of UV treated cells.

2.3 DNA manipulations

2.3.1 Preparation of yeast genomic DNA

This protocol is suitable for the extraction of genomic DNA from as many as 1×10^{10} cells per sample. From a 250ml cell suspension at a cell density of 2×10^7 cell/ml, 500-600ug of genomic DNA could normally be obtained. The details of the procedure are:

1. Cells from each sample above were collected by centrifugation at 4000 rpm for 5 min as above. Following removal of the supernatant, the cells were resuspended in

5ml of sorbitol solution.

2. 0.5ml of zymolyase 20T(10mg/ml in sorbitol TE solution) and 0.5ml of 0.28M beta-mercaptoethanol was added to each sample, and mixed well by shaking. Cells were incubated either at 37°C one hour on a shaking incubator, or at 4°C overnight on a shaking platform in the dark. The production of spheroplasts was monitored under a light microscope.

3. Spheroplasts were gently centrifuged at 3000rpm for 5 min and resuspended in lysis buffer/PBS 1:1(v/v) solution containing 150-200ul of RNase A at 37°C for 1 hour with occasional shaking. Following RNase A treatment, 0.5ml of proteinase K(5mg/ml in TE) was added. The samples were first incubated at 37°C for 1 hour and then at 65°C for another hour with shaking at regular intervals.

4. An equal volume (6ml) of phenol:chloroform:isoamylalcohol (25:24:1 in volume) was added. The tubes were shaken vigorously and then centrifuged at 10000rpm for 10 min. The aqueous upper phase containing DNA was then transferred to a fresh 24ml disposable polypropylene tube using a 3ml plastic Pasteur pipette. Care was taken to avoid disturbing the interface and the phenol/chloroform phase.

5. To ensure complete deproteinization, a second extraction with phenol/chloroform/isoamyl alcohol was performed as above, followed by a third extraction with chloroform: isoamyl alcohol (24:1). No protein precipitate at the interface was the sign of complete deproteinization. Finally, the aqueous phase was transferred to a fresh tube.

6. 2 volumes (12ml) of pre-chilled 100% ethanol were added to precipitate the DNA. The samples were kept at -20°C overnight after being mixed gently by inversion.

7. DNA pellets were collected by centrifugation at 4000rpm for 15min. The pellets were allowed to air dry, and then dissolved in 0.5-1 ml of TE. After being completely dissolved, the DNA was reprecipitated by addition of an equal amount of re-chilled iso propanol. The samples were left at room temperature for 20 min. The DNA pellets were carefully removed with pipette tips into new eppendorfs. After being dried thoroughly, the DNA was resuspended in 600-800ul of TE.

8. The quality of the DNA samples was checked by both non-denaturing agarose gel electrophoresis and UV spectrophotometry. Samples with clean DNA should give a sharp bright band on an EtBr stained agarose gel upon a UV transilluminator and a ratio of optical absorbance at 260nm to that at 280nm of around 1.8.
9. The DNA samples were stored at -20°C until further required.

2.3.2 DNA gel electrophoresis

Gel electrophoresis of DNA was routinely used for multiple applications including inspecting the success of PCR reactions or plasmid preparations, resolving restriction digestions, observing the uniformity of sonicated DNA samples, and the separation and isolation of DNA fragments for downstream cloning applications.

1. Various agarose concentrations were prepared depending on the downstream application. Typically, if DNA was to be purified from the gel, 0.7% agarose was used, otherwise a 1.0% agarose gel was prepared. Agarose was added to TAE buffer (40mM Tris-Acetate, 1mM ethylenediamine tetraacetic acid (EDTA), pH8.0) and heated in a microwave to dissolve.
2. The agarose solution was cooled to ~50 °C. To 100ml of agarose solution, 1 µl of 10mg/ml ethidium bromide was added and mixed well. Gels were either cast in a Horizon 58 (Life Technologies) or a Mini-Sub cell GT (Bio-Rad) and left to cool for one hour at room temperature.
3. 50-200ng of DNA was mixed with water to a total of 10 µl, to which 2 µl of 6x MassRuler loading dye (Fermentas) was added. To DNA samples with a large volume more loading dye was added. Gel tanks were filled with TAE buffer and samples were loaded into the wells. To one well a DNA ladder was loaded; either GeneRuler 1kb DNA ladder or FastRuler low range DNA ladder (Fermentas). Gels were run at 75V on a power-pac 200 (BioRad) at room temperature.
4. Following electrophoresis DNA was visualised using a BioDoc-It Imaging system (UVP) at 302nm. If DNA was to be purified following electrophoresis then it was visualised at 365nm to minimise UV damage, and excised from the gel with a scalpel.

DNA was purified from excised gel samples using the PureLink quick gel extraction kit (Invitrogen) according to the manufacturer's protocol. DNA was purified into 30 μl of water.

2.3.3 Polymerase Chain Reaction (PCR)

Unless otherwise stated all PCR reactions were performed using the Expand High fidelity PCR system (Roche). Typically PCR was performed in a total reaction volume of 50 μl . If larger quantities of DNA were required multiple 50 μl reactions were performed and pooled together during purification.

1. To a 0.2ml PCR tube on ice, the following were added:

10x buffer with magnesium chloride (Roche)MgCl ₂	10 μl
dNTP mix 10mM (Fermentas)	1 μl
Forward primer (10 μM)	0.8 μl
Reverse primer (10 μM)	0.8 μl
25mM Magnesium chloride (Roche) MgCl ₂	2 μl
DNA template	1-10ng plasmid, 100-500ng genomic DNA
Water	Up to a total volume of 49.3 μl

2. To this 0.7 μl of polymerase enzyme (Roche) was added and the tube was immediately vortex mixed, spun down and run on a PTC-200 PCR machine (MJ Research) with the following conditions:

1. 95.0 $^{\circ}\text{C}$ for 4:00 minutes
2. 94.0 $^{\circ}\text{C}$ for 0:30 minutes
3. AT $^{\circ}\text{C}$ for 0:30 minutes
4. 72.0 $^{\circ}\text{C}$ for ET minutes
5. Go to 2. x30 times
6. 72.0 $^{\circ}\text{C}$ for 10:00 minutes
7. End

AT (the annealing temperature) was calculated as five degrees Celsius lower than the

lowest primer T_m . ET (extension time) was calculated as 1:00 minute per kb of DNA to be amplified.

3. Fusion PCR: For fusion PCR the above protocol was also used with a single modification. DNA fragments to be fused were added to the reaction in equimolar concentrations to a total of 50-100ng of DNA.

4. All PCR products were purified into water using the QIAquick PCR purification kit (Qiagen) according to the manufacturer's instructions.

2.3.4 Cloning

Extensive DNA manipulations were performed for a wide variety of cloning purposes presented in subsequent chapters. Such manipulations included DNA restriction and DNA ligation. In these circumstances all enzymes used to perform these manipulations were from New England Biolabs. The following account outlines the common strategies employed for the production of a novel plasmid.

1. All DNA used for recombinant manipulations was purified into either water or 10mM Tris-HCl pH8.0 and quantified using a Nanodrop 1000 spectrophotometer (Thermo Scientific) according to the manufacturer's instructions.

2. For DNA restrictions: All restriction digestions were performed in a total volume of 40 μ l. 1500ng of DNA was combined with water to a total volume of 34 μ l for single enzyme digests, or 32 μ l for double enzyme digests. To this 4 μ l of enzyme buffer was added. 1 μ l of each enzyme (at a starting concentration of 10,000 or 20,000 units/ml) to be used was added to this and the reaction was incubated at 37 $^{\circ}$ C for 90 minutes. The reaction was briefly spun to collect condensation and a further 1 μ l of each restriction enzyme was added. This was incubated at 37 $^{\circ}$ C for a further 90 minutes. DNA was either directly purified with the QIAquick PCR purification kit (Qiagen) to

30 μ l water or purified following gel electrophoresis as described above.

3. DNA ligation and cloning in *E.coli*: DNA samples were combined with water to total a volume of 18 μ l consisting of ~200ng of DNA. Typically a single insert: vector ratio of 3:1 was used. For three fragment ligations insert: insert: vector ratios were altered according to size, where smaller fragments were added in a larger molar ratio. For example a 1kb:3kb:5kb (vector) ligation would typically have a 5:3:1 molar ratio respectively. To the DNA solution 2 μ l of 10x T4 DNA ligase reaction buffer and 1 μ l of T4 DNA ligase (400,000 cohesive end units/ml; NEB) was added. Reactions were incubated at 16 $^{\circ}$ C for 2-3 hours or at 4 $^{\circ}$ C overnight. 100 μ l of Library efficient DH5 α chemically competent cells (Invitrogen) were subsequently transformed with 10 μ l of the ligation reaction according to the manufacturer's protocol. All plasmids in the current study used ampicillin as a selection marker. Treated cells were plated onto LB plates supplemented with 100 μ g/ml ampicillin and left overnight to grow at 37 $^{\circ}$ C.

Single *E. coli* colonies were tested for the transformation of the correct plasmid by colony PCR (see below). Positive colonies were subsequently picked and grown overnight in LB supplemented with 100 μ g/ml ampicillin at 37 $^{\circ}$ C, at 225 rpm in a Multitron standard incubation shaker (Infors AG). For mini-preps, 5ml of culture was purified to 50 μ l of EB buffer with the QIAprep spin miniprep kit (Qiagen). For midi-preps 50ml of culture was purified to 1ml of elution buffer with the GenElute HP plasmid midiprep kit (Sigma Aldrich). Plasmid preparations were analysed by restriction digestion using half of the reaction volume to that stated above (20 μ l in total) and incubated at 37 $^{\circ}$ C for one hour. Following this 3 μ l of 6x MassRuler loading dye (Fermentas) was added and the samples were run on a 1% agarose TAE gel. Positive plasmid preparations were finally selected for sequencing to confirm the correct clone had been isolated.

2.4 Yeast transformation

This protocol was regularly used for the transformation of plasmids and stable

integration of DNA via recombination.

1. In order to amplify plasmid DNA, 50ml of competent *E.coli* cell culture was grown to an OD600 of 0.6-0.8.
2. Cells were collected by spinning at 3600 rpm for 5 minutes in an Eppendorf centrifuge 5810R at room temperature. The pelleted cells were washed once in 20ml of water and collected as before.
3. Cells were resuspended in 15ml of lithium acetate solution (100mM lithium acetate, 10mM Tris base, 1mM EDTA, pH7.5) and left at room temperature for one hour.
4. Once permeabilised, cells were collected as before and resuspended in 500 μ l lithium acetate solution. For each transformation the following was added to a 1.5ml polypropylene tube:

50% Polyethylene glycol 3800, 100mM lithium acetate, 10mM Tris base, 1mM EDTA, pH7.5	300 μ l
Cells in lithium acetate solution	50-100 μ l
Denatured UltraPure salmon sperm DNA solution 10mg/ml (Invitrogen)	15 μ l
DNA to be transformed (plasmid ~30ng, integrating DNA ~1-10 μ g)	1-5 μ l

5. Solutions were incubated on a Mini Labroller rotator (Labnet) at room temperature for 30 minutes and then transferred into a water bath set at 42 °C for 15 minutes. After 15 minutes the cells were placed on ice for 3 minutes.
6. To precipitate the cells 1ml of water was added to each tube, the solution was spun at 3600 rpm for 5minutes in an Eppendorf centrifuge 5414D and the supernatant discarded. Cells were resuspended in 100 μ l of water and plated on selective media

plates as undiluted, 1:10 diluted and 1:100 diluted cell solutions. Occasionally, to increase the efficiency of transformation, cells were resuspended in YPD and incubated for one hour in a Multitron standard incubation shaker (Infors AG) prior to plating.

7. Plates were incubated at a 30 °C until visible colonies had formed. Transformation of the correct DNA was initially confirmed by colony PCR, and ultimately by DNA sequencing and/or confirmation of protein expression by western blot.

2.5 Colony PCR

Colony PCR was performed to check the correct integration of exogenous DNA into both *E. coli* and *S. cerevisiae* cells.

1. Cell colonies were numbered on the plate as a reference. A P10 pipette tip was used to touch each colony on the plate. Each tip was then placed into 11.5 µl of water within a 0.2ml PCR tube. Tips were left for 5 minutes to allow cells to transit into solution, removed and the PCR tubes were closed and micro-waved at full power (800W) for 2 minutes. To each tube, 0.5 µl of a forward and reverse primer (at a starting concentration of 10 µM) were added, followed by 12.5 µl of 2x ReddyMix PCR master Mix (ThermoScientific).

2. PCR reactions were vortex mixed, spun down and run on a PTC-200 PCR machine (MJ Research) with the following conditions:

1. 95.0 °C for 4:00 minutes
2. 94.0 °C for 0:40 minutes
3. 55.0 °C for 0:50 minutes
4. 72.0 °C for 1:00 minutes
5. Go to 2. +3 sec/cycle x30 times
6. 72.0 °C for 10:00 minutes

7. End

3. For each sample 7 μ l of the PCR mix was loaded onto a 1% agarose TAE gel with a ladder to check for production of the correct product.

2.6 Protein analysis

2.6.1 Yeast whole protein lysates

The following protocol was performed for the isolation of the soluble protein fraction from yeast cell lysates.

1. 50ml of cell culture was grown to an OD600 of 0.6-0.8.
2. Cells were collected by spinning at 3600 rpm for 5 minutes in an Eppendorf centrifuge 5810R at room temperature.
3. Pelleted cells were resuspended in 500 μ l of cold yeast dialysis buffer (20mM HEPES-KOH pH7.6, 10mM magnesium sulphate, 10mM ethylene glycol tetraacetic acid, 20% glycerol) supplemented with 5 μ l of 100x proteinase inhibitors (1mg/ml pepstatin, 1mg/ml leupeptin, 1mg/ml chymostatin, 1mg/ml antipain, 250mM benzamide, 100mM phenylmethylsulfonyl fluoride in ethanol) and transferred to a 1.5ml polypropylene tube.
4. 500 μ l of acid washed glass beads (Sigma Aldrich) were added to each sample. Cells were lysed by vortexing on a Vortex Genie 2 (Scientific Industries) at the highest setting. Tubes were vortexed for 2 minutes at 4 $^{\circ}$ C and then transferred to ice for 1 minute. This was repeated four times in total.
5. Lysed cells were spun for 15 minutes at 13000 rpm in a Beckman Coulter

Microfuge 22R at 4 °C to collect cell debris. The supernatant was transferred to a new 1.5ml tube. Protein lysates were quantified using the Bradford assay (see below), aliquoted, frozen in liquid nitrogen and stored at -80 °C.

2.6.2 Western blotting

All western blots were performed using the Bio-Rad Mini-PROTEAN 3. Gel electrophoresis and protein transfers were performed as described in the Mini-PROTEAN 3 instruction manual (Bio-Rad). The following account does not reiterate the entire protocol but instead includes details necessary for an exact reproduction of the work.

All electrophoresis gels performed were 1.5mm thick. All stacking gels were set using the 1.5mm 10 slot combs (Bio-Rad).

Recipes for resolving and stacking gels:

20ml Resolving gel – 7.5% acrylamide	20ml Resolving gel – 5% acrylamide
3.75ml 40% acrylamide/bisacrylamide 19:1 (Bio-Rad)	2.5ml 40% acrylamide/bisacrylamide 19:1 (Bio-Rad)
5.00ml 1.5M Tris-Hcl (pH8.8)	5.00ml 1.5M Tris-HCl (pH8.8)
10.90ml H ₂ O	12.15ml H ₂ O
200µl 10% sodium dodecyl sulphate	200µl 10% sodium dodecyl sulphate
100µl 10% APS	100µl 10% APS
16µl TEMED (Sigma Aldrich)	16µl TEMED (Sigma Aldrich)
8ml Stacking gel – 4% acrylamide	
800µl 40% acrylamide/bisacrylamide 19:1 (Bio-Rad)	
5.00ml 1M Tris-Hcl (pH6.8)	
6.1ml H ₂ O	
80µl 10% sodium dodecyl sulphate	
40µl 10% APS	
8µl TEMED	

1. Two western gels were always prepared at one time using the reagents listed below in table 2.1. Gel solutions were not degassed under vacuum. Ammonium persulphate (APS) and N,N,N',N'-Tetramethylethylenediamine (TEMED) were added last to prevent polymerisation prior to pouring the gel solutions. 1ml of water was added to the surface of the resolving gel prior to its polymerisation.
2. 15 μ g of protein from yeast whole protein lysates was combined with water to a total of 10 μ l. To this 10 μ l of 2x SDS loading buffer (100mM Tris base, 4% sodium dodecyl sulphate (SDS), 0.2% bromophenol blue, 20% glycerol, 20mM dithiothreitol, pH6.8) was added. Protein samples were subsequently heated to 95 $^{\circ}$ C for 10 minutes.
3. Each 20 μ l sample was subsequently loaded to the polyacrylamide gel. Each gel included one lane loaded with 10 μ l of Kaleidoscope Precision Plus protein standards (Bio-Rad).
4. Polyacrylamide gels were run using 1x SDS-PAGE running buffer (25mM Tris base, 250mM glycine, 0.1% SDS, pH8.3) at 100V on a power-pac 300 (Bio-Rad) for 60 to 180 minutes at 4 $^{\circ}$ C.
5. Proteins were transferred from the gel to Immuno-Blot PVDF 0.2 μ m for protein blotting (Bio-Rad). PVDF membranes were cut to the same size as the gel, submerged in methanol and then water prior to loading to a cassette. Transfer was performed using Western transfer buffer (25mM Tris-base, 150mM glycine, 20% methanol, 0.015% SDS) at 4 $^{\circ}$ C, 100V for 90 minutes.
6. Following transfer membranes were air dried for 40 minutes, submerged in methanol, and then water and transferred to a plastic tank. Membranes were blocked in 2% ECL advance blocking reagent (GE Healthcare) TBST (150mM sodium chloride, 10mM Tris-HCl pH 8.0, 0.05% TWEEN 20 (Sigma Aldrich)) overnight at 4 $^{\circ}$ C. Membrane tanks were rocked at 20 rev/min on a Stuart Scientific platform shaker STR6.
7. In the morning membranes were prepared for chemiluminescent detection. The entire procedure was performed at room temperature on the platform shaker at 20 rev/min. Membranes were first washed in 20ml TBST for 5 minutes. A primary

antibody was diluted in 10ml 2% ECL advance blocking reagent TBST. Membranes were incubated with the primary antibody for one hour. Then three washes of 20ml TBST for 10 minutes were performed. A secondary antibody was diluted in 10ml 2% ECL advance blocking reagent TBST. Membranes were incubated with the secondary antibody for one hour. A final three washes of TBST for 10 minutes were performed.

8. Chemiluminescent antibodies bound to the membranes were detected using the ECL advance solution (GE Healthcare). Membranes were removed from TBST and blotted dry using tissue paper at the membrane edge. 1.5ml of development solution (solution A and B mixed) was applied to the membrane surface and left for 5 minutes. Membranes were subsequently blotted dry as before and applied to a plastic sheet for detection.

9. Chemiluminescence was detected with the AutoChemi BioImaging system (UVP) and images were captured using Labworks (Version 4.6.00.0, UVP). Typically images were exposed for 1 minutes 30 seconds, and re-exposed up to 9 times.

10. Reprobing membranes: Membranes were incubated with 100ml stripping buffer (62.5mM Tris-HCl pH6.7, 2% SDS, 100mM 2-mercaptoethanol) for 30 minutes at 50 °C with moderate shaking on a Hybaid Maxi 14 hybridization oven (ThermoScientific). Stripped membranes were washed for 5 minutes in TBST and blocked for one hour in 2% ECL advance blocking reagent TBST. The protocol was then resumed from step 7.

2.7 Chromatin immunoprecipitation (ChIP)

2.7.1 chromatin preparation

ChIP was performed in a similar manner to that previously detailed (Yu et al., 2009).

1. 100ml cell samples were grown either in YPD or selective media to a density 2×10^7 cells/ml or OD₆₀₀=0.6 to 1.0.

2. To crosslink cells, 3ml of 37% formaldehyde (Sigma) was added to 100ml of medium to make the final formaldehyde concentration 1%. Cell samples were left to crosslink for 10 to 40 minutes (depending on protein of interest) on a rotating

platform at 150rpm room temperature (cover with black plastic bag to exclude light).

3. After 10-40 minutes, 5.5ml of 2.5M glycine was added and left at room temperature for 5 minutes at 150rpm. Cells were pelleted by centrifugation at 4000rpm for 5 minutes at 4 °C using a Beckman Avanti J-20XP centrifuge.

4. Then cells were resuspended in 40ml of PBS in 50ml Falcon tubes at 4 °C and pelleted by centrifugation using an Eppendorf centrifuge 5810R. Pellets were resuspended in 1ml FA/SDS and transfer to 2ml eppendorf tubes, and pelleted by centrifugation using a Beckman Coulter Microfuge 22R centrifuge. Pellets were resuspended in 1ml FA/SDS (+PMSF) buffer centrifuged again using a Beckman Coulter Microfuge 22R centrifuge and the supernatant discarded. (If you are not using the cells immediately, snap-freeze them in liquid nitrogen and store at -80 °C).

5. Cells were resuspended in 500µl of FA/SDS(+PMSF) (-80 °C Cell pellets were first thawed on ice). 500µl of acid washed glass beads (Sigma) were added. Cells were lysed by vortexing the tubes on a Vortex genie 2 on the highest setting for 15 minutes at 4 °C.

6. The cell lysate was separated from the glass beads as shown in Fig. 2.1. A 25G needle was heated under a Bunsen burner and used to make a small hole in the base of the 1.5ml tube. These were subsequently placed into 2ml polypropylene tubes. Cell lysate was collected by a short centrifugation at 2000rpm, 4°C. 200µl lysis buffer/1x proteinase inhibitors was added to the glass beads to wash away the remaining lysate and it was collected as before.

7. The cell lysate was centrifuged at 13,000rpm for 15 minutes at 4 °C in a Beckman Coulter Microfuge 22R. The supernatant was decanted to remove the soluble protein fraction. Cell pellets were resuspended according to their mass; 100µl lysis buffer/1x proteinase inhibitors was added per 0.01g of cell pellet.

8. For sonication 0.5ml of cell lysate was pipetted into a 2ml eppendorf tube. Using a Bioruptor (Diagenode) three tubes at a time were sonicated with amplification poles for six cycles of 30 seconds on/ 30 seconds off at highest setting (200W), 4 °C water bath. This typically sheared DNA to an average length of 300-600bp.

9. To pellet cell debris, sonicated samples were transferred to a 1.5ml polypropylene tube and centrifuged at 13,000rpm for 20 minutes at 4 °C in an Eppendorf centrifuge 5810R. The supernatant was collected and flash frozen in liquid nitrogen.

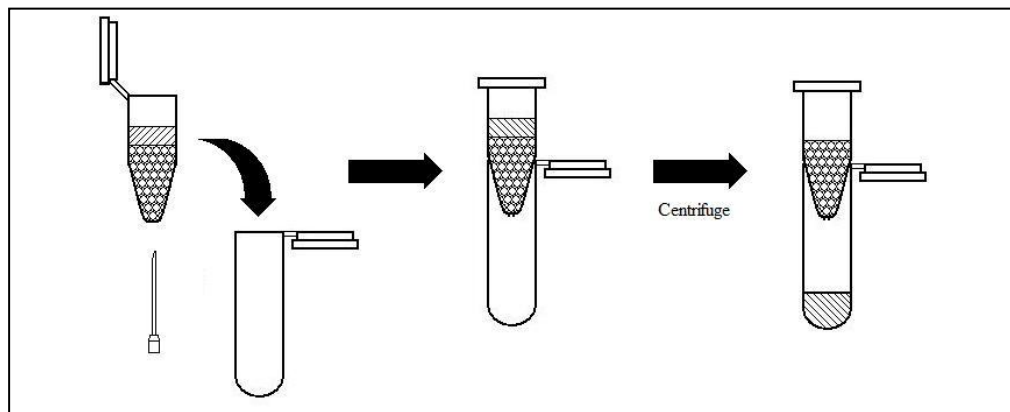


Figure 2.1 Separation of cell lysate from glass beads.

2.7.2 Immunoprecipitation (IP)

Step 1. Preparation of Dynabeads

1. Aliquot 50 μ l of Dynabeads (mouse or rabbit, depending on the antibody) for each sample to be immunoprecipitated into an eppendorf tube.
2. Put the tubes on the magnetic rack for 30sec and carefully remove the supernatant with a pipette and wash the beads 3 times with 500ul 1X PBS solution containing 1 mg/mL BSA.
3. Resuspend the beads in 50 μ l PBS/BSA (1mg/ml) per sample.
4. Add the optimised amount of antibody and incubate 30 ~60 min (depends on the antibody) at 30 °C in a Thermomixer at 1300 rpm (or overnight at 4 °C).
5. Put the tubes on the magnetic rack for 30sec and then carefully remove the supernatant with a pipette and add 1.0 ml 1X PBS solution containing 1mg/mL BSA, then put on a mini labroller for 5 minute. Remove the supernatant and wash twice with fresh 1.0 ml of PBS/BSA solution with a similar wash procedure.
6. Put the tubes on the magnetic rack for 30sec and then carefully remove the supernatant with a pipette and resuspend the beads in 50 μ l of PBS per sample.

Step 2. Chromatin Immunoprecipitation

1. Defrost the chromatin sample, transfer 100 μ l ~200 μ l of the chromatin sample into the washed beads as the IP sample, and 20~50 μ l of chromatin sample into a new tube for the input sample.
2. Add 30 μ l of 10x PBS/BSA (PBS containing 10mg/ml of BSA) into the IP sample and PBS to make up the total volume of 300 μ l. Incubate for 3hrs at 1300 rpm at 21 $^{\circ}$ C in a Thermomixer.
3. Put the tubes on the magnetic rack for 30sec discard the supernatant then add 500 μ l of FA/SDS. Put the tubes on a mini labroller for 10 minute, repeat 2 times with 500 μ l of FA/SDS + NaCl (adjust the NaCl concentration to 500mM).The final wash is in a Thermomixer for 10min, at 1300 rpm at 21 $^{\circ}$ C.
4. With the same wash procedure wash the beads with 500 μ l of IP buffer (LiCl solution) for 10min.
5. With the same wash procedure wash the beads with 500 μ l of TE for 5min.
6. Elute the DNA with 125 μ l of Pronase buffer at 65 $^{\circ}$ C at 900 rpm in an Eppendorf Thermomixer for 15~30min.
7. Transfer the supernatant into a new tube. Add 6.25 μ l of Pronase (20mg/ml), incubate at 37 $^{\circ}$ C for 1hr, then at 65 $^{\circ}$ C O.N.
8. At the same time as step 7, to the Input (IN) samples, add 25 μ l of 5 \times Pronase buffer and TE to make up a total volume of 125 μ l, add 6.25 μ l of Pronase, then continue with the same as step 7.
9. Add 1 μ l of 10mg/ml of RNase to IP and IN samples. Incubate at 37 $^{\circ}$ C for 1h.
10. Purify the samples using a PCR purification kit (Invitrogen).
11. Take 5 μ l IP samples and 1ul IN samples for RT-PCR checking.

Chapter 3 Investigating the role of histone Htz1 in the NER of genomic DNA

3.1 Introduction

Among all four core histone subunits, variants of H2A are particularly common. There are five major H2A-type histones (Thatcher and Gorovsky, 1994). Canonical H2A is the most abundant form; its expression and deposition are coupled to replication. H2A.Z, which is sometimes referred to as H2A.Z/F, is the most conserved variant; it is found in organisms as diverse as the early branching eukaryote *Plasmodium falciparum* to humans.

Eukaryotic cells organize their DNA as chromatin, a nucleoprotein complex consisting of DNA, histones and non-histone proteins. The basic repeating unit of chromatin is nucleosome, which is a particle with 146 bp of DNA wrapped in a left-handed superhelix around an octamer of core histones, consisting of two copies of H2A, H2B, H3, and H4 (Arents and Moudrianakis, 1993). The wrapping of the DNA in the nucleosome and the formation of higher-order chromatin structures restrict the access of cellular machinery to DNA (Zlatanova and Thakar, 2008). During replication, transcription, repair, and recombination, the structure of chromatin will be dynamically and reversibly altered to provide access to the underlying DNA template. Apart from canonical histones, other histone variants are also incorporated into nucleosomes (Henikoff et al., 2004).

In *S. cerevisiae* Htz1 is the only histone H2A variant and is an ortholog of mammalian H2A.Z (Jackson et al., 1996). Htz1 is highly conserved during evolution: it is found in different organisms and has been studied in a range of organisms such as humans and the yeast *Saccharomyces cerevisiae*, with sequence conservation of ~90% (Iouzalén et al., 1996). However, its sequence identity to the major H2A is only ~60% (Jackson and Gorovsky, 2000) which suggests unique and important functions for Htz1 apart from canonical H2A.

SWR1-C was the first ATP-dependent histone deposition complex identified as

dedicated to the deposition of histone variants such as Htz1, and NuA4 is a histone acetyltransferase for histones H4, H2A, and Htz1 in *S. cerevisiae* (Kobor et al., 2004, Krogan et al., 2004, Mizuguchi et al., 2004). Biochemical purifications of SWR1-C indicates its connection to other chromatin-modifying complexes such as NuA4 and INO80 (Kobor et al., 2004, Mizuguchi et al., 2004, Krogan et al., 2004) which also acetylates H2A.Z to restrict the spreading of heterochromatin and to prevent chromosome missegregation (Babiarz et al., 2006, Keogh et al., 2006, Millar et al., 2006, Kobor et al., 2004). We focused on the SWR1-C and NuA4 (histone acetyltransferase), as both complexes are central to understanding Htz1 biology. Together the NuA4 and SWR1-C chromatin-modifying complexes alter the chromatin structure through 3 distinct modifications in yeast: post-translational addition of chemical groups, ATP-dependent chromatin remodelling, and histone variant incorporation. There is already an established correlation between Gcn5 mediated histone H3 acetylation and the efficiency of NER (Yu et al., 2005a), and genome wide studies revealed that Htz1 occupancy is related to H3 acetylation (Zhang et al., 2005). Htz1 differs from canonical H2A in the C-terminal sequence and two internal loops (Zlatanova and Thakar, 2008). The C-terminal sequence is involved in the interaction with the H3-H4 tetramer and the internal loops are for self interaction with another Htz1. Htz1 is incorporated into nucleosomes by the SWR complex in the form of a Htz1-H2B dimer to replace H2A-H2B (Krogan et al., 2003, Kobor et al., 2004, Mizuguchi et al., 2004). NuA4 and SWR1-C are two chromatin-modifying complexes with overlapping functions and components. These two complex share four subunits Act1 and Arp4, along with Swc4 and Yaf9 (Galarneau et al., 2000). One of the shared subunits, Yaf9, is important for the cellular response to spindle stress, proper DNA repair and metabolism, H2A.Z chromatin deposition and acetylation, and histone H4 acetylation occur at telomere-proximal genes (Keogh et al., 2006, Le Masson et al., 2003, Wu et al., 2005, Zhang et al., 2004, Schulze et al., 2009). Yaf9 contains an evolutionarily conserved YEATS domain which is found in proteins associated with multiple chromatin-modifying enzymes and transcription complexes across

eukaryotes (Schulze et al., 2009). *yaf9Δ* strains and *htz1Δ* strains show significant overlap in phenotypes, but are not identical. For example, *yaf9Δ* strains are more sensitive to MMS, suggesting that Yaf9 has roles not only restricted to SWR1, but also a potential role in the functions of NuA4 as it is a stable member of NuA4, and NuA4 mutants are very sensitive to DNA-damaging agents such as MMS. *yaf9Δ* strains and *htz1Δ* strains show significant overlap in both affected genes and affected telomeres (Meneghini et al., 2003), whereas *yaf9Δ* strains show dramatic reductions in Htz1 deposition at telomeres. These results indicate that Yaf9 plays a functional role in the SWR1 complex in Htz1 deposition (Zhang et al., 2004). Experiments with an Esa1 functional mutant (*esa1-L254P*), found that there was an overlap of genes down regulated in *htz1Δ* strains and down regulated in *yaf9Δ* strains. This was even more extensive when considering the subset of affected genes within 20 kb of the telomere and where the overlap approached 50% (Zhang et al., 2004). This results suggest that Yaf9 assists not only SWR1/Htz1 but also NuA4 complexes in telomere-proximal gene expression. The exchange of H2A for Htz1 also requires acetylated histone H3 and H4 which generate a platform for the binding of the SWR complex (Zhang et al., 2005, Shia et al., 2006). Htz1 occupancy shows a significant reliance on Gcn5 and on Bdf1, suggesting that these factors participate in the acetylation and acetyl-recognition of promoter targets for Htz1 replacement (Zhang et al., 2005). In addition, Bdf1 and Htz1 occupy a largely overlapping set of promoters, with a clear bias toward TATA-less promoters (Zhang et al., 2005).

There is a growing realization that not only does Htz1 present a different structural feature in chromatin but that it also provides a discrimination required for gene expression (Santisteban et al., 2000, Zhang et al., 2005, Eirin-Lopez and Ausio, 2007), DNA repair (Mizuguchi et al., 2004), cell cycle progression (Dhillon et al., 2006) and chromosome segregation (Krogan et al., 2004). Genome-wide mapping of Htz1 occupancy revealed that Htz1 preferentially resides in nucleosomes in the promoter of inactive genes and also in the euchromatin/heterochromatin boundaries (Li et al., 2005, Raisner et al., 2005, Zhang et al., 2005, Albert et al., 2007). Although

preferentially residing at the repressed promoters, Htz1 does not contribute to the repression of the relevant genes. Instead, it is required for the subsequent activation of these genes during induction (Santisteban et al., 2000, Li et al., 2005, Zhang et al., 2005). Deletion of *HTZ1* reduces the recruitment of TATA binding protein (TBP) to Htz1-containing nucleosomes during transcriptional activation (Wan et al., 2009). In the euchromatin/heterochromatin boundaries, Htz1 is required to prevent the spreading of heterochromatin (Meneghini et al., 2003). In both cases, Htz1 needs to be acetylated by the NuA4 complex, most notably at K14 (Babiarz et al., 2006, Keogh et al., 2006, Millar et al., 2006).

Nucleotide excision repair (NER) is a major repair pathway that the cell utilizes to remove a broad range of DNA damages. Previously we have found that in the repressed *MFA2* promoter histone H3 acetylation and chromatin remodelling are activated following UV treatment (Yu et al., 2005a). Both of these events are necessary for the efficient NER of CPDs in this locus. As the central role for the histone H2A variant Htz1 is the formation of a boundary that prevents the spreading of heterochromatin proteins. Htz1 is present at certain telomeres and at the silent locus HMR and the loss of Htz1 results in the spreading of Sir proteins at HMR and at a subset of telomeres (Dhillon and Kamakaka, 2000, Krogan et al., 2003, Meneghini et al., 2003). This modulation of chromatin structure may have an effect on the local NER efficiency; lack of the histone variant to replace the canonical histone in some specific regions, many influence NER at specific regions or genome wide.

The UV survival of yeast has long been used to test and compare UV resistance between different mutant strains (Cox and Parry, 1968). Different wavelengths of UV radiation produce a wide range of lesions in DNA and other cellular responses. As mentioned in the general introduction UV at 260nm induces CPDs.

The *Micrococcus luteus* (ML) endonuclease has an exclusively function in cleaving the 5'-bond in these dimerized pyrimidines and contains an AP lyase activity (Shiota and Nakayama, 1997, Haseltine et al., 1980, Krokan et al., 1997). The purification of the *M. luteus* UV endonuclease and the cloning of its corresponding gene (pdg) has

revealed a 31-32kDa protein with significant identity to the Endo III family of DNA glycosylases but it does not overlap in substrate and function. This *M. luteus* UV endonuclease exclusively cleaves the *cis-syn* thymine dimer but not *trans-syn* or 6-4 products. T4 Endo V endonuclease has a similar function to *M. luteus* UV endonuclease but also can function at *trans-syn* thymine dimers with a cut activity of about 1% of that for the *cis-syn* dimer (Krokan et al., 1997). The ML endonuclease was employed in this study to measure CPD incidence.

Here I investigated both the UV survival of a range of mutants related to the presence of Htz1 in chromatin and the incidence of CPDs after UV in total DNA of these strains at various times after UV.

3.2 Materials and Methods

Table 1. Yeast strains

Strains	genotype	source
WT, BY4742	<i>MATα his3Δ1 leu2Δ0 lys2Δ0 ura3Δ0</i>	Euroscarf
<i>htz1Δ</i>	<i>MATα his3Δ1 leu2Δ0 lys2Δ0 ura3Δ0 htz1:: KanMX4</i>	Euroscarf
<i>swr1Δ</i>	<i>MATα his3Δ1 leu2Δ0 lys2Δ0 ura3Δ0 swr1:: KanMX4</i>	Euroscarf
<i>yaf9Δ</i>	<i>MATα his3Δ1 leu2Δ0 lys2Δ0 ura3Δ0 yaf9:: KanMX4</i>	Euroscarf
<i>bdf1Δ</i>	<i>MATα his3Δ1 leu2Δ0 lys2Δ0 ura3Δ0 bdf1:: KanMX4</i>	Euroscarf
<i>gcn5Δ</i>	<i>MATα his3Δ1 leu2Δ0 lys2Δ0 ura3Δ0 gcn5:: KanMX4</i>	Euroscarf
pCM302	CEN6-ARS4 URA3 HTZ1	This study
pCM544	CEN6-ARS4 URA3 <i>htz1K3,8,10,14R</i>	This study
pCM566	CEN6-ARS4 URA3 <i>htz1K3,8,10,14Q</i>	This study
WT,BY4742,	<i>MATα his3Δ1 leu2Δ0 lys2Δ0 ura3Δ0</i>	This study

<i>RAD14-Myc</i>	<i>RAD14-13Myc-KanMX4</i>	
<i>htz1Δ</i> ,	<i>MATα his3Δ1 leu2Δ0 lys2Δ0 ura3Δ0</i>	This study
<i>RAD14-Myc</i>	<i>RAD14-13Myc-KanMX4 htz1:: NAT1</i>	
BLY1	<i>MATα his3-Δ200 lys2-801 ura3-52</i>	(Clarke et al., 1999)
BLY457	<i>MATα his3-Δ200 lys2-801 ura3-52</i> <i>esa1-Δ414</i>	(Clarke et al., 1999)
<i>W303-1B</i>	<i>MATα ade2-1 can1-100 his3-11,15 leu2-3,112</i> <i>trp1-1 ura3-1</i>	(Decker et al., 2008)
<i>MSY2890</i>	<i>W303-1B esa1-C304STK.1.URA3</i>	(Decker et al., 2008)
<i>MSY3141</i>	<i>W303-1B esa1-E338QTK.1.URA3</i>	(Decker et al., 2008)

3.2.1 The analysis of UV sensitivity-Cell survival

UV-induced DNA damage is normally repaired by various repair pathways in the cell. However, if a mutation is present which affects such processes, a particular yeast strain may show higher, or lower, sensitivity to UV light. The UV sensitivities of the strains used in this study were compared by exposing cells to various doses of UV light and monitoring their survival by counting the number of colonies after 3 days of growth. For ease and accuracy, the cultures were diluted appropriately, using existing survival curves as a guide, to achieve about 200 colonies per plate. The details of the procedure were as follows:

(1) YPD agar plate (or other SD plate) were prepared and labelled in advance. 10 ml of cell cultures were grown overnight to give a density of $2-4 \times 10^7$ cells/ml. Serial dilutions were prepared according to the strain and UV dose. For example, samples to be irradiated at the higher UV dose were diluted just 10 or 100 fold, whereas those exposed to lower UV doses diluted up to 10000 fold.

(2) The diluted cell suspensions were mixed well using a vortex before pipetting

100ul onto the agar plates. Triplicates of each sample were prepared. autoclaved glass beads (diameter 3mm) were added to the plates and shaken laterally to spread the cells evenly across the surface of the plates.

(3) The UV lamp (245mm) was switched on 10 min in advance and calibrated before use. One plate at a time was placed centrally under the UV lamp and treated at a dose rate of $10\text{J}/\text{m}^2\text{s}$. Usually, times of 0, 2, 4, 8, 12 and 16 seconds were applied.

(4) Following irradiation, the plates were immediately placed in darkness to avoid repair by photoreactivation and were incubated at $30\text{ }^\circ\text{C}$ for three days. The number of colonies on each plate was then counted and survival curves created to determine UV sensitivity.

3.2.2 Detection of repair in genomic DNA overall-immunological slot blot assay

I also used a slot blot assay to directly examine the *in vivo* removal of DNA damage from the yeast genome following exposure to UV. A specific monoclonal antibody raised against CPDs was used to bind to this damage. The amount of DNA loaded from different samples was equalized according to the DNA concentration in each sample by a nanodrop detector and confirmed by DNA gel electrophoresis.

(1) A slot-blot transfer apparatus (Bio-Dot SF Microfiltration Apparatus, Bio-Rad) was thoroughly cleansed with water, 70% ethanol, dried and assembled before use. A vacuum pump (Pharmacia Biotech, UK) was attached. Two layers of filter paper were placed on the blot machine as a base, followed by a piece of GeneScreenPlus nylon membrane (Life Science Products) on top, which was previously soaked in a 0.4mol NaOH solution. The lid was positioned and screwed tightly. The vacuum pump was started and allowed a pressure of 40-50 mbar.

(2) 100ng of DNA from each sample in 200ul of TE containing 0.4mol NaOH was loaded in to each well. After all the solution have been vacuumed and gone through the membrane, a final rinse with 200ul of 0.4mol NaOH was undertaken.

(3) The membrane was removed from the apparatus, washed once with 1x TBST and then immersed in blocking solution (3% milk powder in 1x TBST) overnight to saturate non-specific binding.

(4) The membrane was incubated with 2 μ g of monoclonal mouse CPD-specific antibody in 10ml of 3% blocking solution and kept on the shaking platform for 1 hour, followed by three washes with 1x TBST.

(5) 5 μ l of an alkaline phosphatase-linked anti-mouse antibody (ECF Western Blotting Reagent Pack, Amersham) was diluted in 10ml of blocking solution and then incubated with the membrane for another 1 hour. Excessive secondary antibody was washed off with an extensive rinse with 1x TBST solution.

(6) 2ml of ECF detection solution (36mg of ECF substrate in 60ml of ECF dilution buffer, ECF Western Blotting Reagent Pack, Amersham) was pipetted onto a clean clingfilm. The membrane was placed on top of the solution with the side with DNA samples facing the detection solution and incubated for 2 minutes, making sure that the detection solution interacts with all of the membrane and no air bubbles existed. The fluorescent emission from individual samples on the membrane was scanned using a Typhon scanner. Quantification was carried out using imageQuant software.

3.2.3 Denaturing gel electrophoresis to detect genome-wide DNA repair level

100 μ l DNA (50 μ g) samples were treated with 10 μ l of damage specific ML endonuclease (*Micrococcus luteus* endonuclease) and incubated at 37 °C for one hour. The enzyme was removed by a phenol/chloroform extraction and DNA precipitated in 75% ethanol, finally 100 μ l of TE was added to re-dissolve the precipitated DNA pellets.

Application of a damage specific ML endonuclease to the DNA samples result in

single strand nicks at damage sites. In order to fractionate these single stranded DNAs, gel electrophoresis under denaturing condition has to be applied. The concentration of the agarose (ranging from 1 to 1.5%) was adjusted depending on the size of the DNA fragments to be resolved. The larger the full-length restriction fragment of interest, the less the concentration of agarose and vice versa.

The gel was prepared by boiling appropriate amount of agarose in a 250ml solution (247ml H₂O, 2.5ml 5M NaCl, 500ul 0.5M EDTA, Ph8.0) in a microwave oven. The molten agarose was swirled well and left for a while to allow air bubbles to disperse before pouring into the gel tray. After pouring, a comb for 20 samples to be loaded was employed. The gel was allowed to set and then submerged in 1L running buffer (986ml H₂O, 12ml 3M NaOH, 2ml 0.5M EDTA, pH8.0). For at least 30 minutes before loading the samples. After removing the comb, the DNA samples were carefully loaded onto the gel. Electrophoresis was normally carried out with an electric field of 1.0V/cm overnight for 16 hours. After running, the gel was neutralized by being soaked in neutralize solution (1M Tris-HCl, 1.5M NaCl, pH7.5) for 30 minutes (neutralize the gel because EtBr is an intercalating agent, and in alkaline condition it won't bind to DNA properly as DNA is single stranded), and then the gel was stained with an EtBr solution for a few hours. The gel was rinsed in water before taking a image. The gel image was quantified and analyzed by ImageQuant software.

3.2.4 Preparation of yeast chromatin, a non-chromatin fraction and different concentration salt washed extracts

(1) Cells from 200ml YPD (2×10^{10}) were pelleted by centrifugation at 4000rpm in a Beckman centrifuge for 5 min, washed in cold water and 1 M sorbitol.

(2) The cell pellets were resuspended in 5ml lysis solution (1M sorbitol ,5mM 2-mercaptoethanol) containing 5mg of zymolyase-20T per 1g of cells. Incubation was carried out with slight agitation at 30°C for 20min.

(3) The spheroplasts were collected by centrifugation at 3000 rpm for 5 min, washed once in cold 1 M sorbitol and lysed in 3ml Ficoll solution (18% w/v Ficoll, 20mM KH_2PO_4 PH 6.8, 1mM MgCl_2 , 0.25mM EGTA and 0.25mM EDTA) per 1g of centrifuged cells by one stroke with a syringe.

(4) The nuclear fraction was pelleted by centrifugation at 17000rpm in a Beckman Microfuge at 4°C for 30 min. The white top layer was removed and the supernatant was taken off. The nuclear pellets were resuspended in 500ul LS buffer. The supernatant has the non-chromatin nuclear fraction.

(5) The nuclear pellet was extracted consecutively with increasing concentrations (0.3,0.5,2.0mol/L) of NaCl in LS buffer (10 mM Tris-HCl pH7.4 ,0.2mM MgCl_2) to result in supernatant fractions , respectively designated as 0.3,0.5,2.0. The nuclear residue comprising of DNA and nuclear matrix was dissolved by sonication in LS buffer. Each protein fraction corresponding to an equivalent cell number, was loaded for SDS-PAGE and analyzed by immunoblotting with the indicated antibodies.

3.3 Results

3.3.1 Deletion of *HTZ1* and genes encoding components of the SWR complex results in increased UV sensitivity

To examine the potential role of the histone H2A variant Htz1 in NER, several mutants lacking Htz1 or SWR complex subunits were employed to test their UV survival. These were all derived from the *S. cerevisiae* strain BY4742 (EUROSCARF). Hence I employed isogenic strains, so allowing data derived from different experiments to be cross compared without the influence of genetic variation. The complete library of viable gene knockouts is also available from EUROSCARF. As seen in Figure 3.1, the *htz1* Δ strain is more sensitive to UV radiation when

compared with the wild-type strain. This result is consistent with the previous finding that a *htz1* mutant is sensitive to caffeine and MMS, and moderately sensitive to UV (Mizuguchi et al., 2004) and suggests a role in DNA damage repair or tolerance.

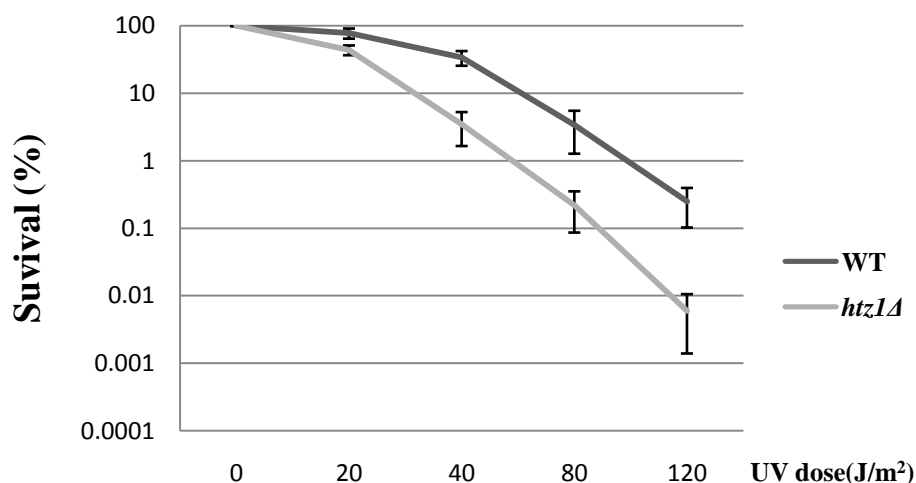


Figure 3.1 The UV sensitivity of the BY4742 wild-type and the *htz1Δ* strain

Cells were grown to log phase resuspended in PBS at a cell density of 2×10^7 cells/ml and processed as in materials and methods. Error bars represent the standard deviation of three independent experiments.

The SWR complex was the first complex identified as dedicated to the deposition of histone variants in *S. cerevisiae* (Kobor et al., 2004, Krogan et al., 2004, Mizuguchi et al., 2004). Swr1 is a function component of SWR complex, *Swr1Δ* abolishes chromatin binding of Htz1 *in vivo* (Mizuguchi et al., 2004). The UV survival of all 5 mutants related to Htz1 deposition show an increased UV sensitivity when compared to the wild-type strain shown in Figure 3.2. The *swr1Δ*, *yaf9Δ*, *bdf1Δ* and *gcn5Δ* mutants are all more sensitive to UV when compared to the wild type, and all to a very similar extent when compared to the *htz1Δ* mutant strain. This survival experiment shows that Htz1 in chromatin has a positive role in the response to the lethal effects of UV. However, the UV sensitivity could be due to a number of aspects and may be unrelated to NER.

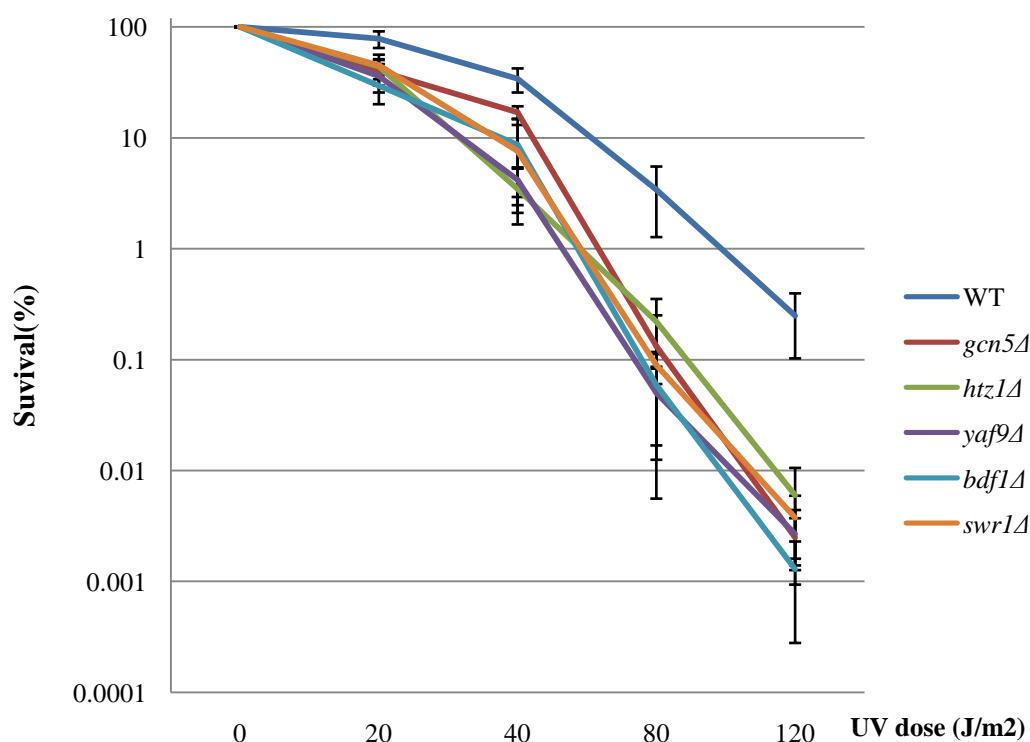


Figure 3.2 The UV sensitivity of BY4742 wild-type and *htz1Δ*, *swr1Δ*, *yaf9Δ*, *bdf1Δ* and *gcn5Δ* mutants strains. Cells were grown to log phase resuspended in PBS at a cell density of 2×10^7 cells/ml and processed as in materials and methods. Error bars represent the standard deviation of three independent experiments.

3.3.2 Deletion of *HTZ1* and *SWR* genes results in slower removal of CPDs from the overall genome.

I next decided to determine whether the increased UV sensitivity in these mutants reflects a less efficient NER of CPDs. To address and compare genomic DNA repair, denaturing gels were employed to examine DNA untreated or treated with a CPD specific endonuclease that introduces a strand break at a CPD. Genomic DNA from samples collected before and after UV at various time points was treated with the CPD specific ML endonuclease and subjected to agarose gel electrophoresis under denaturing conditions (see materials and methods). This enzyme efficiently recognises and cuts at CPD sites in genomic DNA and generates different length single stranded

DNA fragments. The removal of CPDs from DNA by NER restores DNA to longer fragments.

A typical denature Gel image

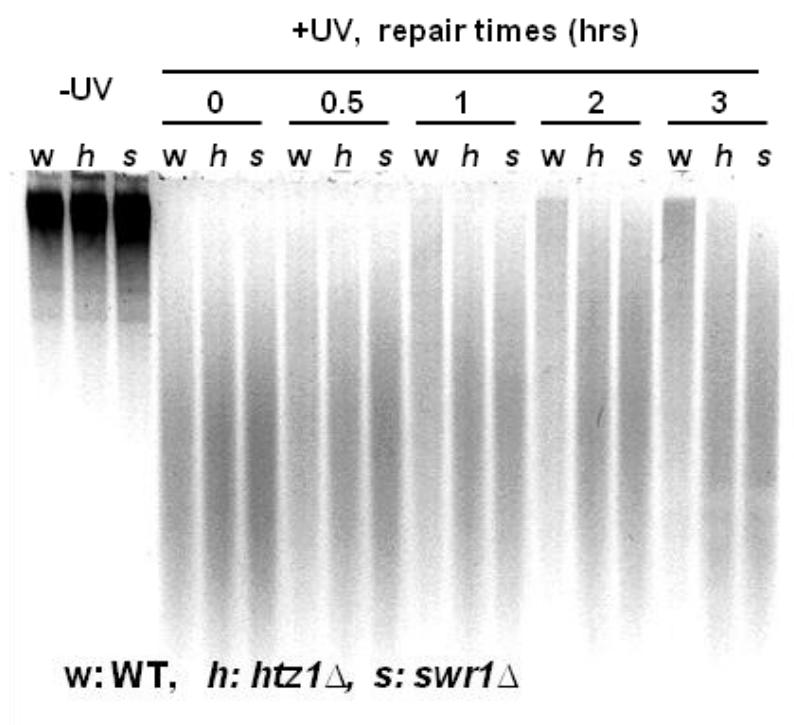


Figure 3.3 Repair of CPDs in BY4742 wild-type, *htz1*Δ and *swr1*Δ from the genome. DNA from samples taken before and after UV ($100\text{J}/\text{m}^2$) was treated with a CPD specific endonuclease. The digestion products were then separated by gel electrophoresis under denaturing conditions and visualized with EtBr. 0, 0.5, 1, 2, and 3 indicate repair times (hrs). The gel was scanned using a Typhoon Trio (GE Healthcare Life Sciences).

The results in Figure 3.4 show that the CPDs in the *htz1*Δ and *swr1*Δ mutants are repaired more slowly than in the wild type. The data shows that about 30% less CPDs have been repaired by *htz1*Δ and *swr1*Δ when compared with wild-type cells after 3 hours of repair. As this experiment is a direct measurement of the CPD level, it could either reflect a general defect in NER in these mutants, such as by the transcription of NER genes being influenced by Htz1, or a more efficient repair of CPDs in specific regions of the genome where Htz1 resides. Irrespective of the mode whereby Htz1 functions to promote efficient NER, this experiment shows that Htz1 has a positive role in NER.

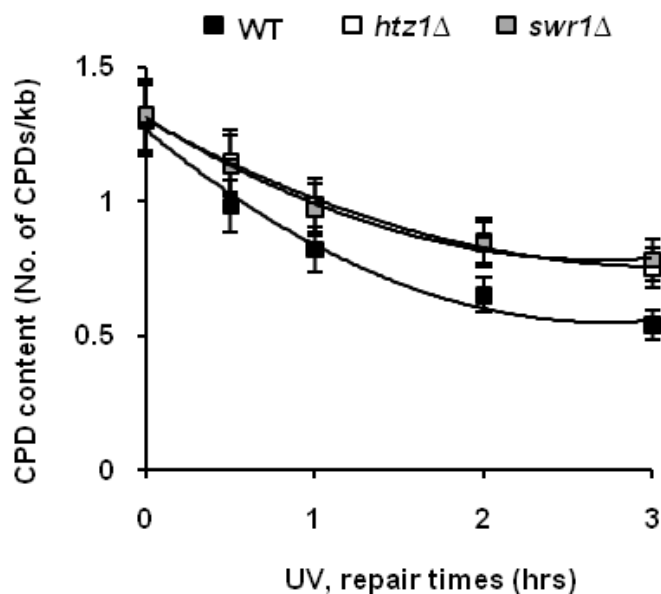


Figure 3.4 CPD frequency analysis. The gel quantified using ImageQuant 5.0 and the median migrating distances of the DNA smear were calculated. CPD content (CPDs/kb) was calculated as described by Sutherland and Bessalov (Sutherland and Shih, 1983, Bessalov et al., 2001). The data were fitted to a second-order polynomial. Values represent the mean \pm SD of three independent experiments

3.3.3 Does reduction of activity of Esa1 in the Nu4 complex increase UV sensitivity?

Following on from the above findings, I examined if the post-modification histone acetylation of Htz1 is related to this reduction of NER. The NuA4 complex have been reported to mediate acetylation on the Htz1 N-terminal tail at several lysine points. Esa1 is component of this complex and is required for its HAT activity. The BLY457 strain was generated by integrating the *Afl* II-digested plasmid, pLP0952 (Clarke et al., 1999) into the *ESAI* locus in its wild-type strain BLY1, followed by a loop-out of the wild-type *ESAI* sequence. In BLY457 (*esal-414*), deletion of a single nucleotide at position 1887 leads to a frameshift mutation in codon 414, altering 10 amino acids before terminating the ORF 22 amino acids prematurely. Among the mutant strains that they generated, BLY457 shows severe decreased levels of acetylation *in vivo* (Clarke et al., 1999). BLY1 and BLY457 are not in the same background as the strain that we normally use. The results shown in Figure 3.5 indicate an increased UV sensitivity in BLY457 compared with BLY1. Hence the reduced HAT activity does

affect the cells ability to survive after UV damage. However the reduction is less than that seen in the *htz1Δ* mutant.

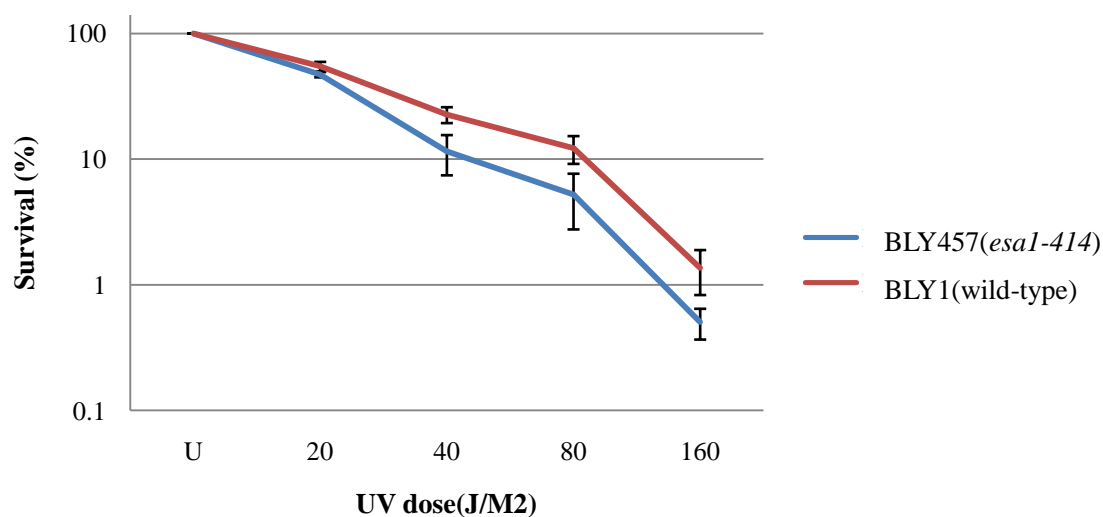


Figure 3.5 UV sensitivity of BLY1(wild-type) and BLY457(*esa1-414*) strains.

Cells were grown to log phase resuspended in PBS at a cell density of 2×10^7 cells/ml and processed as in materials and methods. Error bars represent the standard deviation of three independent experiments.

I also examined two *Esa1* functional mutants which were from a different genetic background (W303). The MSY2890 mutation has a single replacement of Cys304 with serine (C304S) and this mutant is report to be catalytically dead *in vitro* (Yan et al., 2002). The MSY3141 strain contain a *esa1*-E338Q (Glu338) allele created by site-directed mutagenesis. These two mutants retain acetylation of H4 <6% of wild-type levels by western blot (Decker et al., 2008). Hence these mutants dramatically reduce the HAT activity of *Esa1*. The UV survival is show in Figure 3.6.

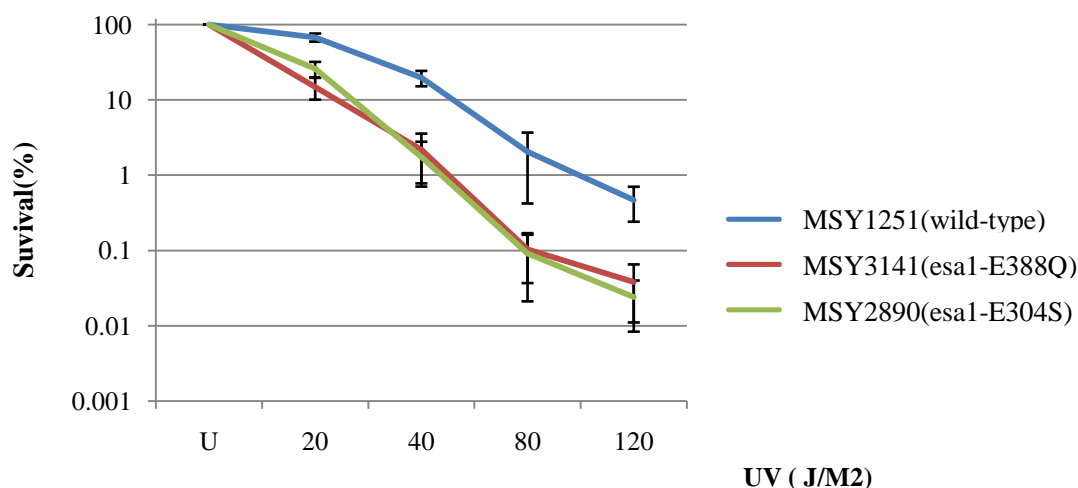


Figure 3.6 UV sensitivity of MSY1251(wild-type) and the MSY3141, MSY2890 strains. Cells were grown to log phase resuspended in PBS at a cell density of 2×10^7 cells/ml and processed as in materials and methods. Error bars represent the standard deviation of three independent experiments.

Result from Figure 3.6 show a greater UV sensitivity in the mutant strains when compared to the wild type. This finding is consistent with the report from Decker (Decker et al., 2008) who showed that these two strains are more UV sensitive using a drop test method. Furthermore, both *esa1-E338Q* (MSY3141) and *esa1-E304S* (MSY2890) have a similar UV sensitivity pattern which suggests that this increased UV sensitivity is caused by the lack of Esa1 HAT activity. However, as the NuA4 complex with Esa1 acetyl-transferases activity targets not only Htz1 but also H2A and H4, this greater UV sensitivity may result from Htz1 acetylation, or a combination with that of the other two histone acetylation, or just to H2A or H4 related events.

3.3.4 Acetylation of Htz1 at K3, 8, 10, 14 does not contribute to UV survival and CPD repair

Acetylation of Htz1 at one or more sites at K3, 8, 10, 14 plays an important role in transcription activation and *htz1* deposition during transcription activation and prevent the spreading of heterochromatin (Millar et al., 2006, Keogh et al., 2006). Htz1 needs to be acetylated by the NuA4 complex, most notably at K14 (Babiarz et al., 2006, Keogh et al., 2006, Millar et al., 2006). There is already an established

correlation between Gcn5 mediated histone H3 acetylation and efficient NER repair (Yu et al., 2005a). Thus there could be a role for the acetylation of histone Htz1 in NER. To explore whether Htz1 acetylation at these sites also has implications for cell survival and CPD repair after UV irradiation, three plasmids was transformed into the BY4742 *htz1Δ* strains to generate comparable histone lysine tail mutants. The transformed strains have all the four lysine residues of the endogenous Htz1 changed to arginine (R) or glutamine(Q). With the lysine site change for each strain, the lack of a lysine substrate, in these mutated Htz1 means that is excluded from being acetylated. UV survival was first examined. As indicated in Figure 3.7, both of the *htz1 K3, 8, 10, 14R* mutant arginine (R) or glutamine(Q) showed the same sensitivity to UV irradiation as the plasmid wild type.

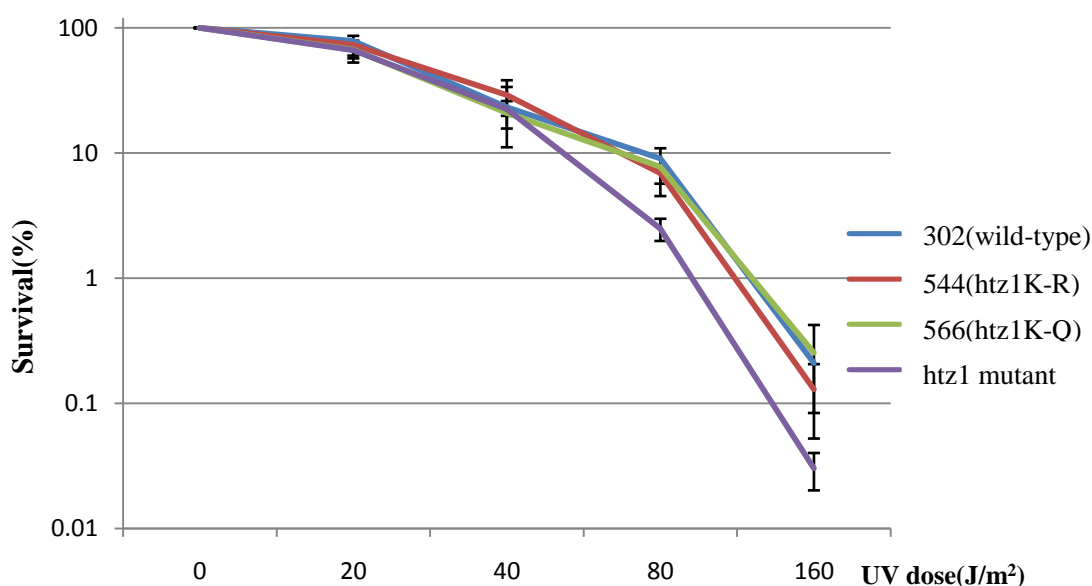


Figure 3.7 The UV sensitivity of the 302, 544 , 566 and *htz1Δ* strains

302 (wild-type), 544 (arginine (R) mutant), 566 (glutamine(Q) mutant) represent the different strains. Cells were grown to log phase resuspended in PBS at a cell density of 2×10^7 cells/ml and processed as in materials and methods. Error bars represent the standard deviation of three independent experiments.

To accurately monitor the incidence of CPDs I employed a slot blot assay with anti-CPD antibodies. Equal amounts of genomic DNA from different samples were purified from cells before UV and after UV at various time points. The DNA was processed for detection of CPDs using a specific antibody as described in materials

and methods. Figure 3.8 shows that there is a similar CPD repair from the genomic DNA in the arginine mutant and the wild type cells. These results indicate that the acetylation at these sites does not contribute to genomic CPD repair and cell survival after UV irradiation.

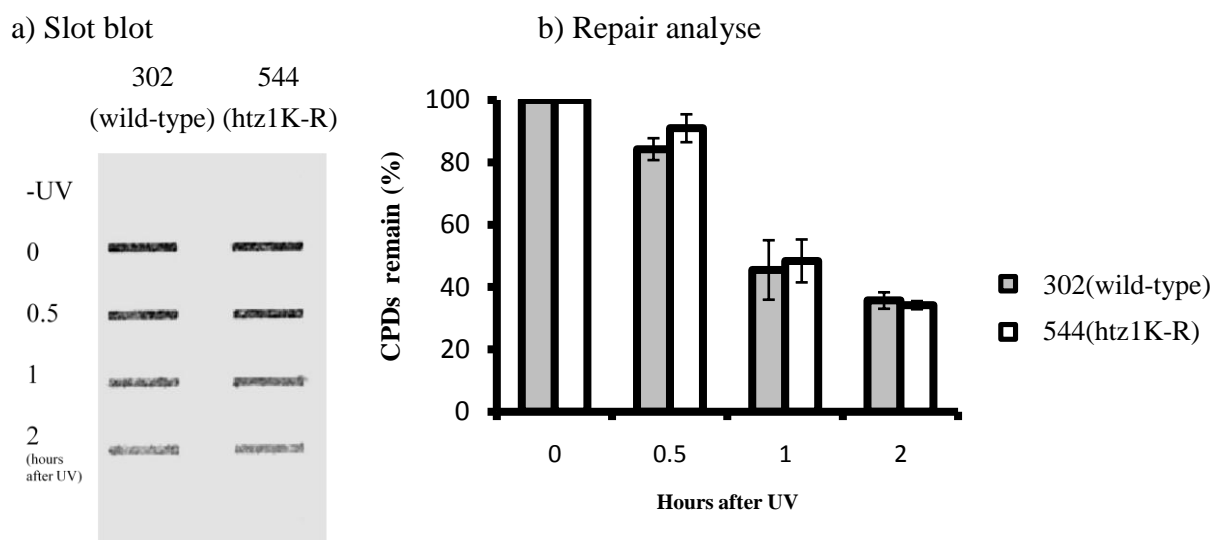


Figure 3.8 Genomic CPD incidence in 302 (wild-type), 544 (arginine (R) mutant), strains after UV irradiation. DNA was purified following the protocol in materials and methods. The extent of signal was quantified as in materials and methods. Values represent the mean \pm SD of three independent experiments.

3.3.5 Rad14 accumulates at CPDs after UV and binds more stably to chromatin

Rad14 is known to act as a DNA damage recognition factor in the early steps of NER, and its function in DNA repair has been almost exclusively assigned to NER (Guzder et al., 1993). I generated both wild-type and *htz1Δ* mutant Myc-tagged *RAD14* strains in a BY4742 background. Insertion of the epitope coding sequence was confirmed by PCR and sequencing. They showed the same sensitivity to UV when compared to the corresponding non-tagged strains, hence assuring that the tagging does not compromise the functionality of Rad14.

Yeast protein Rad14 is known to have binding activity to ultraviolet-damaged DNA (Guzder et al., 1993). To confirm that Rad14 is binding to CPDs, I sonicated chromatin fragments to around 500bp from UV irradiated cells before and after 30min

of repair. Chromatin containing Rad14 was selected with myc-antibody. The same amount of DNA for each sample was used in slot blot experiments. Figure 3.9 shows that Rad14 containing chromatin is enriched for CPDs after UV. This confirmed that Rad14 is associated with CPDs after UV irradiation.

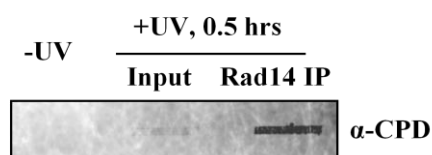


Figure 3.9 CPD level in genomic DNA and Rad14 IP samples.

Immunoprecipitation of Rad14 from chromatin fragment with anti-myc antibody followed by western blot with anti-CPD antibody. The gel image was generated by a UVP detector. Input refers to genome fragmented DNA whilst Rad14IP represent Rad14 contained DNA fragments.

Using whole cell extracts I tested the Rad14 expression levels in a wild type Myc-tagged RAD14 strain and a *htz1Δ* Myc-tagged RAD14 strain. The result revealed that lack of Htz1 does not change the expression level of Rad14 Figure 3.10. This result shows absence of Htz1 does not appear to alter the level of the NER Factor Rad14 in cells.

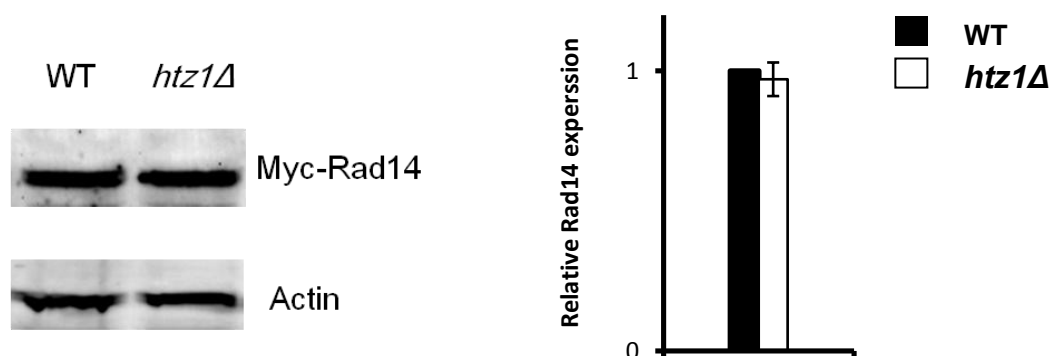


Figure 3.10 The level of Rad14 in wild-type and *htz1Δ*.

Whole genome extracts were used for western blots with anti-myc. The first western blot assay was stripped and a second western blot was carried out to detect actin with anti-actin antibody as a control. The data for Rad14 in wild-type and *htz1Δ* were normalized to the actin control data.

In order to investigate if UV irradiation will alter Rad14 levels, whole cell extracts

were collected before and after UV at various time points in the Myc-tagged RAD14 strain. Western blotting with anti-myc antibody reveals that before and after 0.5 hour, 1 hour and 3 hour post UV, Rad14 expression is consistent (Figure 3.11). This indicates that Rad14 does not have a change in its expression level in response to UV damage.

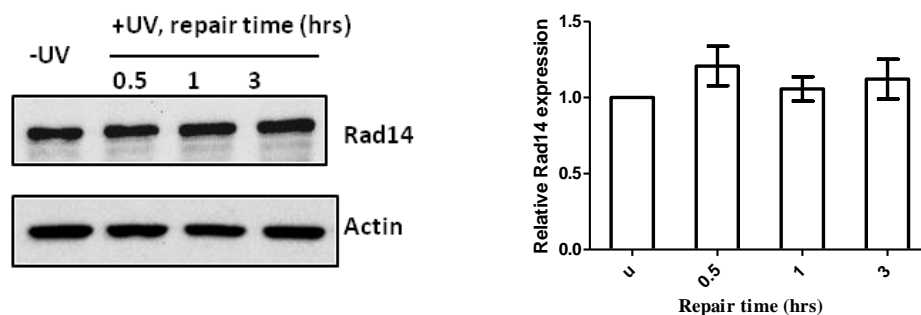


Figure 3.11 The cellular level of Rad14 before and after UV irradiation

Whole genome extracts were first used in western blots with anti-myc. Then the first western blot was stripped and a second western blot was carried out to detect actin with anti-actin antibody as a control. Expression data of Rad14 in wild-type were normalized to the actin control data. Data are the average of 3 biological experiments.

Quantitative Western blotting in Figure 3.11 showed that deletion of *HTZ1* does not change the cellular level of Rad14, and this level is unaffected by UV treatment. This raised the possibility that the expression of Rad14 is unchanged after UV, but that a translocation of Rad14 from the cytoplasm to nucleus might takes place. To examine this, I generated chromatin and non-chromatin extract from cells separately. The result from western blots show that following UV treatment, Rad14 protein relocates from the cytoplasm to chromatin.

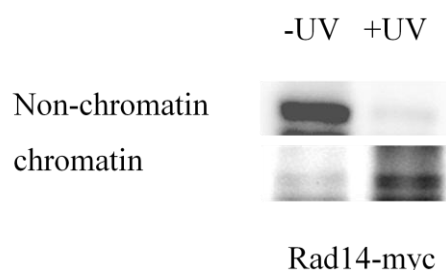


Figure 3.12 The cellular level of Rad14 before and after UV irradiation

Non-chromatin and chromatin extracts from a wild-type strain before and after UV were generated following the protocol in materials and methods. Western blots were

carried out to detect Rad14 with anti-myc antibody.

Rad14 has a relatively exclusive function in NER although one weak publication reports that it may have a role in transcription (Chaurasia et al., 2013). My data show that Rad14 translocates from a non-chromatin region (the cytoplasm) to chromatin. Although its human homologue is XPA, Rad14 also has a CPD binding ability similar to human DDB1. Human DDB1 protein exists as a non-chromatin bound and chromatin bound activity. After UV, it more firmly binds to chromatin when compared to before UV (Li et al., 2006a). To test if this also occurs for Rad14 in yeast, I adapted the approach of (Li et al., 2006a). Rad14-myc tagged cells were left unirradiated or treated with UV 150J/m² and allowed to repair for 30 min after UV. The nuclear pellet was extracted in LS buffer and consecutively with 10 mM Tris-HCl, pH 7.4, 0.2 mM MgCl₂ and increasing amounts (0.3,0.5,2.0mol/L) of NaCl. The nuclear residue comprising of DNA and nuclear matrix was dissolved by sonication in LS buffer. Each protein fraction, corresponding to an equivalent cell number, was loaded for SDS-PAGE and analyzed by immunoblotting with indicated anti-myc antibodies.

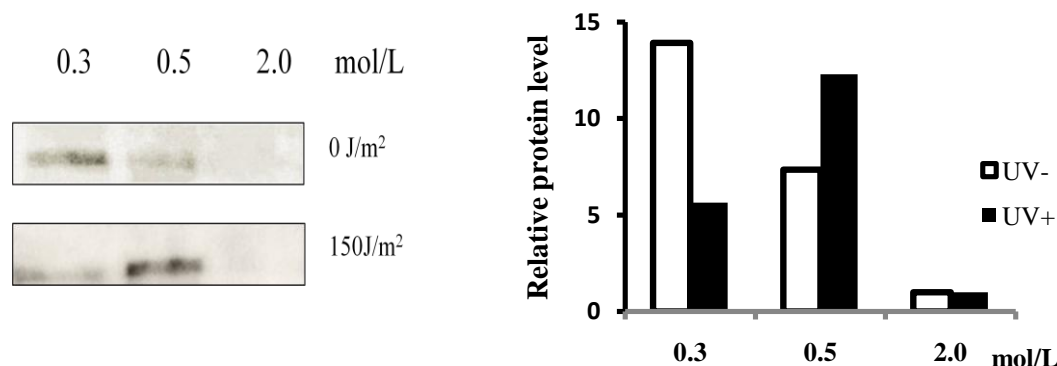


Figure 3.13 UV-induced more intense binding of Rad14 to damaged chromatin

The same amount of different extracts was loaded for western blots. Increasing amounts (0.3,0.5,2.0mol/L) of NaCl extracts results are shown in gel(A). Data were then quantify by imagequant software (B). Data from one experiment (more repeats are required to confirm)

The data from these experiments is show in Figure 3.13. Without UV, most of the Rad14 protein resides in the 0.3 mol/L fraction, indicating that Rad14 is loosely bound to chromatin. Following UV irradiation, there is a prominent shift in Rad14 chromatin association as most Rad14 translocates to the 0.5 mol/L fraction. This

implies a more firm binding of Rad14 after UV. Hence an originally weak Rad14 association with undamaged chromatin becomes stronger post UV.

3.3.6 Gcn5 levels in wild-type and the *htz1Δ* mutant

Gcn5 was tagged at the C-terminus by inserting 18 copies of the Myc epitope coding sequence into the normal chromosomal locus of *GCN5*. The plasmid p3747, a kind gift from Richard A Young, was used as a template to generate PCR products containing the Myc epitope coding sequence and a URA3 selectable marker flanked by homologous regions designed to recombine at the 3' end of *GCN5*. The PCR products were transformed into the BY4742 WT (by Shirong Yu) and by myself into *htz1Δ*. Clones were selected for growth on URA⁻ selective plates. Insertion of the epitope coding sequence was confirmed by PCR and sequencing, and the expression of the epitope-tagged protein was confirmed by Western blotting using an anti-Myc antibody. The same UV sensitivity was found between the tagged strains and non-tagged strains thus showing that the tagging does not compromise the functionality of Gcn5.

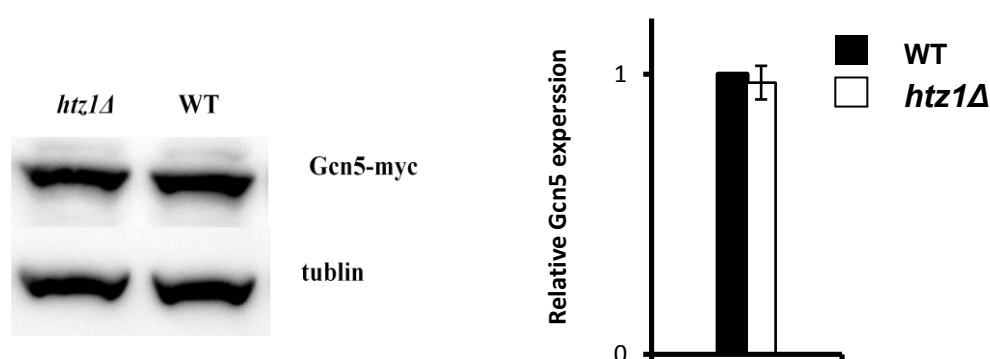


Figure 3.14 Cellular levels of Gcn5 before and after UV irradiation

Whole genome extract samples were first used in western blots with anti-myc. Then, after stripping out the first western blot assay, a second western blot were carried out to detect actin with anti-tublin antibody as a control. Expression data of Gcn5 in wild-type and *htz1Δ* were normalized to the tublin control data respectively. Values represent the mean \pm SD of three independent experiments

Using whole cell extracts to test the Gcn5 expression levels in the wild type GCN5

Myc-tagged strain and the *htz1Δ* GCN5 Myc-tagged strain, the data shows in Figure 3.14 revealed that lack of Htz1 does not change the cellular expression level of Gcn5.

3.4 Discussion

As the major component of chromatin, histones play a central role in how chromatin structure is formed and its diverse roles in cells. The wrapping of the DNA in the nucleosome and the formation of higher-order chromatin structures restricts the access of the cellular machinery to DNA (Zlatanova and Thakar, 2008). During replication, transcription, repair, and recombination, the structure of chromatin will be dynamically and reversibly altered to provide access to the underlying DNA template. The histone H2A variant H2A.Z has been found to be involved in DNA repair by its controlling how chromatin remodeling occurs for Double-Strand Break Repair (Yu et al., 2004). This report showed that H2A.Z along with H4 acetylation shifted chromatin to a favourable formation for this repair. Htz1 may work closely with a remodeling complex, including the SWR complex to create a favourable relaxed conformation for this repair. Based on this possibility, my research focused not on DSB repair, but on NER and where the Rad7/Rad16/Abf1 complex generates superhelical torsion in DNA for GG-NER (Yu et al., 2004).

The *htz1Δ* mutant was reported as sensitive to MMS (DNA-damaging agent), caffeine (elicits a stress response), and HU (an inhibitor of deoxynucleoside triphosphate synthesis). However, these experiments gave no indication in what DNA repair pathways Htz1 may play a role (Zhang et al., 2004, Mizuguchi et al., 2004). Here I have shown that not only is the *htz1Δ* sensitive to UV, but also the same sensitivity is exhibited in the *swr1Δ*, *yaf9Δ* and *bdf1Δ*, *gcn5Δ* mutants. The *swr1* complex is unique in its ability to efficiently replace H2A-H2B dimers with dimers bearing a histone H2A variant (Htz1 or H2A.Z) and a lack of Swr1 will cause a loss of Htz1 at loci where originally Htz1 resided (Mizuguchi et al., 2004). The *yaf9Δ* mutant was reported to be not only UV sensitive but also susceptible to a DNA damaging drug. This finding was suggested as being related to the role of Htz1 in preventing the

spreading of Sir proteins at yeast telomeres where Yaf9 was found to be required for H4 acetylation and Htz1 deposition at these location (Zhang et al., 2004). Bdf1 is a component of the SWR1 complex and has been reported to be well correlated with Htz1 occupancy as this relies on Bdf1 function at many loci. This could explain the similar UV sensitivities that were found here. The *gcn5Δ* mutant has already been reported as UV sensitive, and Gcn5 mediated histone modifications are needed for efficient NER (Yu et al., 2005a). Interestingly, similar UV sensitivities for the *htz1Δ* and *gcn5Δ* mutants are found in my study. Genome-wide Htz1 occupancy is partially reliant on Gcn5 and a positive correlation has been found between Htz1 occupancy and Gcn5 related H3 acetylation (Zhang et al., 2005). Hence it was possible that Htz1 and Gcn5 work together in this UV response. The relationship between these two will be discussed in Chapter 6.

The CPD removal efficiency from total DNA as measured by denaturing gels showed a slower repair in both the *htz1Δ* and *swr1Δ* mutants in an almost identical pattern at different time points after UV. The question remained as whether NER was influenced in region where Htz1 resides, or more globally.

We had found that the histone acetyl transferase Gcn5 mediated acetylation at lysines 9/14 of histone H3 is a major factor in enabling efficient NER (Yu et al., 2005a). The Histone H2A variant Htz1 has lysine residues in its N-terminal tail which are a target for different histone modifications including acetylation. Hence I investigated if this modification was also involved in NER. Yeast strains from three different genetics backgrounds were used in my experiments and they all show identical results. Esa1, a component of NuA4 complex is reported to be the only HAT activity carrier for Htz1. The mutant BLY457 in a S288c background has a reduced HAT activity and is slightly more UV sensitive when compared with the wide-type (BLY1). Two mutants (MSY3141- *esa1*-E338Q, MSY2890- *esa1*-C304S) from another background (w303) and where site-directed mutagenesis almost abolished its HAT activity also showed UV sensitivity when compared to their wide-type strain. These results implied that the HAT activity of Esa1 does have a role in the response to UV damage, although one

cannot conclude that this is NER related. Esa1 has distinct functions in acetylating the 4 N-terminal lysines (K3, K8, K10, K14) of Htz1, but it is also widely reported to acetylate histone H4 and histone H2A. Thus the increased UV sensitivity in the mutants may not be related to Htz1 acetylation, but to that of H2A acetylation or H4 acetylation, or to both.

To examine these relationships, I transformed plasmids into the BY4742 *htz1Δ* strain to generate comparable histone lysine tail mutants. In these mutants, all the four lysine residues of the endogenous Htz1 were changed to arginine (R) or glutamine (Q) and Htz1 was excluded from being acetylated. With these mutants I directly tested how the cells react to UV. Surprisingly, no UV sensitivity was observed between the lysine mutant strains when compared to a strain with an intact Htz1 gene. Genome-wide CPD removal after UV also showed an identical repair efficiency between these mutants and the wild-type Htz1 containing strain (I also examined NER at specific regions in Chapter 4). These results illustrate clearly that a lack of Htz1 acetylation does not render the cells UV sensitive nor does it slow down NER at the level of the whole genome. Thus acetylation of Htz1 at K3, 8, 10, 14 does not contribute to UV survival and CPD repair. Thus the increased UV sensitivity observed in the HAT activity mutant may result from Esa1 mediated H2A and H4 histone acetylation or another distinct function of Esa1.

In *Saccharomyces cerevisiae*, the NER DNA damage recognition step is mediated by a combination of Rad14p, Rad4p, Rad23p and RPA (replication protein A). To further examine how *htz1Δ* affects NER, I decided to examine the post UV presence of Rad14 in WT and *htz1Δ* strains. Rad14 has a damage-specific DNA binding activity that increases with greater UV doses, and in an ATP independent manner (Guzder et al., 1993). To confirm its UV damage binding activity, I employed ChIP experiments combined with slot blot assays. Here a high CPD level was detected in Rad14 IP fragments and very low CPD levels in all DNA fragments (input), whilst no detectable binding of Rad14 was seen in samples without UV. Quantitative western blots showed similar expression levels of myc-tagged Rad14 in our BY4742 background wild-type

and *htz1Δ* strains. This demonstrates that the reduced NER efficiency I observed in the *htz1Δ* strain is not caused by repressing the transcription of this NER factor. I also constructed WT and *htz1Δ* strains with myc-tagged GCN5. The western blots result revealed that a similar myc-tagged Gcn5 expression level in the wild-type and *htz1Δ* mutant. Gcn5 is involved in transcription regulation of at least 5% of genes in the yeast genome, and the lack of Gcn5 will reduce acetylation at 20% of all yeast genes. Gcn5 could have been related to NER either by influencing the transcription directly or indirectly of NER genes by controlling the acetylation balance via its HAT activity. However, studies on the repressed *MFA2* showed that lack of Gcn5 will result in slower NER at this gene, but not at *RPB2* (Yu et al., 2005a). This means the Gcn5p-mediated H3 hyperacetylation is required for efficient NER at some loci and that NER is not reduced at all regions of the genome. Gcn5-dependent chromatin modification governs the accessibility of DNA in chromatin to repair enzymes and consequently influence how the repair enzymes to function on chromatin templates (Teng et al., 2005). These results suggest that the reduced NER efficiency I observed in the *htz1Δ* strain is not caused by repressing the transcription of a NER factor such as Rad14.

I also found that a UV induced translocation of Rad14 occurs from a non-chromatin region to chromatin. This was similar to that seen for human DDB1 and they both have a UV induced damage binding activity. Increasing salt wash gave a raised relative binding intensity of Rad14 and chromatin. These findings imply Rad14 locates to damaged chromatin after UV and forms a more firm binding to UV-damaged sites in chromatin. Following this, likely Rad1-Rad10 and Rad2 nucleases will target these damaged sites. What drives this relocation remains to be determined. Hence Rad14 binding efficiency can change and it provides an indication of how any mutants could affect NER in a early age before the incision step.

In summary, there is a role for the histone H2A variant Htz1 in the UV damage response and also in efficient NER at the genome level. Lack of genes that regulate the Htz1 replacement step also render cells UV sensitive. Acetylation of Htz1 at K3, 8,

10, 14 does not contribute to UV sensitivity or CPD removal from total DNA. Following these findings, what now needs to be examined is whether these effects on NER occur in a genome wide fashion or whether they are restricted to regions where Htz1 resides. This is addressed in the next Chapter.

Chapter 4 The role of histone Htz1 in NER at selected genomic locations

4.1 Introduction

After found that a lack of Htz1 impaired the genomic extent of NER, I decided to examine how Htz1 contributes to the repair of UV-induced CPDs at a region containing Htz1-containing nucleosomes and compare this to a region where no Htz1 resided. Southern blotting allows the detection of lesions within specific restriction fragments by specific endonucleases and this method can investigate DNA damage and repair at the level of genes but it cannot show the details of DNA damage and repair at nucleotide resolution or in relation to regions where specific nucleosomes reside. Our laboratory had developed a method to examine DNA damage and repair at nucleotide resolution. This technique was first optimized using fragments containing the *MFA2* regulatory and coding sequences (Teng et al., 2009). The technology was also adapted to determine nucleosome position at specific genes (Teng et al., 2009). The technique has two main steps in the procedure: ligation mediated polymerase chain reaction and then the endlabelling of fragments, more information about this technique can be found in materials and methods.

Previously by using these methods, *MFA2* has been used as a model gene to study the effects of chromatin structure and transcription on DNA repair. It was found that enhanced repair of CPDs by NER occurred on the transcribed strand before the transcription start site. This was attributed to changes in chromatin structure associated with activation of the gene in that the promoter region becomes more accessible to repair enzymes (Teng et al., 1997).

MFA2 provides an excellent model for studying the relationships between transcription, chromatin structure and DNA repair in yeast (Teng et al., 1997, Teng et al., 1998). It is an α -specific gene. In α cells, the repression of *MFA2* is achieved through the binding of the Ssn6-Tup1 complex to α 2 protein on the α 2 operator accompanied with the assembly of a series of nucleosomes immediately

adjacent to the alpha2 operator (Teng et al., 2001). Four positioned nucleosomes have been mapped within the control and coding regions of *MFA2* in alpha mating type cells (Teng et al., 2001), and are referred to as -2,-1,+1 and +2. The -2 and -1 nucleosomes are situated in the control region approximately at positions of -412 to -272 and -207 to -62 relative to the start of the *MFA2* coding sequence, and the +1 and +2 nucleosomes at positions -58 to +88 and +122 to +254 respectively. However, in a mating type cells where *MFA2* is active, chromatin in this region becomes as sensitive to MNase as naked DNA. It suggested that these fixed nucleosomes are disrupted due to the activation of *MFA2* (Teng et al., 2001).

The silencing of the haploid mating-type loci is a critical requirement for the yeast life cycle (Haber, 2012). Mating types in the yeast *Saccharomyces cerevisiae* are defined by a set of genes expressed at the active *MAT* locus near the center of chromosome III. *MATa* and *MAT α* differ by approximately 750bp regions, designated *Ya* and *Y α* , respectively, which contain the promoters for genes encoding the master regulatory proteins that define the unique mating type of the cell. Strains with the *MATa* allele express the *a1* and *a2* genes, while strains with the *MAT α* allele express the *α 1* and *α 2* genes. In addition to the active *MAT* locus, two almost identical *HM* loci are located near the telomeres of chromosome III. *HML α* is near the left telomere, while *HMRa* resides near the right telomere. These loci are transcriptionally silent and make no direct contribution to mating type. Rather, they serve as donors during yeast mating-type interconversion or switching. With high-resolution micrococcal nuclease mapping, nucleosomes have been precisely positioned at the *HMLa* and *HMRa* loci (Weiss and Simpson, 1998, Ravindra et al., 1999). The entire chromatin domain at positions 11352 to 14553, is organized into 20 precisely defined nucleosomes in the the *HMLa* region while a highly organized domain consisting of 12 well-positioned nucleosomes spans a 1.94-kb region at *HMRa*. The *HMRa* region is carried in *MAT α* strains used in my study.

Chromatin dynamics have been widely reported to govern the regulation of transcription activation, but how NER operates in the chromatin environment is still

relatively unknown. Early studies concentrated on the physical hindrance of nucleosomes on NER and revealed that lesions in the linker DNA and towards the ends of positioned nucleosomes are repaired faster than those in the centre of the nucleosomes (Wellinger and Thoma, 1997, Li and Smerdon, 2002b, Powell et al., 2003, Teng et al., 2008b, Sarkar et al., 2010). Meanwhile, a hypothetical model of “access-repair-restore” was proposed, in an effort to rationalise the occurrence of chromatin remodelling during NER (Smerdon, 1991). More recently, direct evidence of roles for histone modifications and chromatin remodelling in NER has started to emerge. Our laboratory has previously found that histone H3 acetylation by Gcn5 is activated in the repressed *MFA2* promoter following UV irradiation in *S. cerevisiae* (Yu et al., 2005a). This UV-induced histone H3 hyperacetylation is necessary for the efficient repair of UV-induced CPDs in the *MFA2* promoter. Rad16 which is a SWI/SNF-like NER protein responsible for the repair of DNA damage in non-transcribed DNA, governs the occupancy of Gcn5 on chromatin to regulate histone H3 acetylation following DNA damage (Teng et al., 2008b, Yu et al., 2011). Others have shown that Dot1 gene mediated constitutive H3K79 methylation is required for the repair of CPDs in the *RPB2* and *HML* loci (Chaudhuri et al., 2009, Tatum and Li, 2011). In addition to histone modifications, chromatin remodelling by the SWI/SNF (Gong et al., 2006) and INO80 (Sarkar et al., 2010) ATP-dependent complexes was also found to be involved in the removal of CPDs from the transcriptionally silent *HML* locus by NER. Subunits of these chromatin remodelling complexes interact with Rad4-Rad23 in a UV dependent manner (Sarkar et al., 2010). The INO80 complex does not remodel the chromatin in the early stages following DNA damage. Instead, it is required for the restoration of chromatin after DNA damage is removed (Sarkar et al., 2010).

In the yeast *Saccharomyces cerevisiae*, Rad14 was reported to be essential to collaborate with Rad4-Rad23, RPA and TFIIH. Rad1-Rad10 and Rad2 mediate the dual incision of the damaged DNA strand, releasing a DNA fragment of about 30 nucleotide which contains the lesion (Guzder et al., 1995). In Chapter 3,

experiments showed Rad14 can be detected in DNA fragments containing CPDs but not in CPD free fragments. With its damage recognition ability, Rad14 is a component of NEF1 and provide for an efficient targeting of the Rad1-Rad10 nuclease to the lesion sites from the vast excess of undamaged DNA in yeast cells. Hence the level of Rad14 in chromatin could be used as a reference for the level of other NER factors, as Rad14 is NER specific.

The data presented in chapter 3 of this thesis demonstrated that Htz1 has a role in NER at the genomic level and this reduction in repair is not a result of repressing the level of transcription of Rad14, nor is it due to histone Htz1 acetylation itself. In this chapter, I will extend these studies to investigate how Htz1 affects repair at specific genomic locations. This will be modulated using the previously mentioned high resolution approaches to measure NER and nucleosome position.

4.2 Materials and methods

Yeast strains

Strains	genotype	source
WT, BY4742	<i>MATα his3Δ1 leu2Δ0 lys2Δ0 ura3Δ0</i>	Euroscarf
<i>htz1Δ</i>	<i>MATα his3Δ1 leu2Δ0 lys2Δ0 ura3Δ0 <i>htz1::KanMX4</i></i>	Euroscarf
<i>swr1Δ</i>	<i>MATα his3Δ1 leu2Δ0 lys2Δ0 ura3Δ0 <i>swr1::KanMX4</i></i>	Euroscarf
<i>yaf9Δ</i>	<i>MATα his3Δ1 leu2Δ0 lys2Δ0 ura3Δ0 <i>yaf9::KanMX4</i></i>	Euroscarf
<i>bdf1Δ</i>	<i>MATα his3Δ1 leu2Δ0 lys2Δ0 ura3Δ0 <i>bdf1::KanMX4</i></i>	Euroscarf
<i>gcn5Δ</i>	<i>MATα his3Δ1 leu2Δ0 lys2Δ0 ura3Δ0 <i>gcn5::KanMX4</i></i>	Euroscarf
WT, BY4742, <i>RAD14</i> -Myc	<i>MATα his3Δ1 leu2Δ0 lys2Δ0 ura3Δ0 <i>RAD14::13Myc--URA3</i></i>	This study
<i>htz1Δ</i> , <i>RAD14</i> -Myc	<i>MATα his3Δ1 leu2Δ0 lys2Δ0 ura3Δ0 <i>RAD14::13Myc-URA3</i></i>	This study
WT, BY4742, <i>GCN5</i> -Myc	<i>MATα his3Δ1 leu2Δ0 lys2Δ0 ura3Δ0 <i>GCN5::18Myc-URA3</i></i>	

<i>htz1Δ, GCN5-Myc</i>	<i>MATα his3Δ1 leu2Δ0 lys2Δ0 ura3Δ0</i>	This study
pCM302	<i>htz1Δ::kanMX4 GCN5::18Myc-URA3</i>	
pCM544	<i>CEN6-ARS4 URA3 HTZ1</i>	
	<i>CEN6-ARS4 URA3 htz1K3,8,10,14R</i>	This study

4.2.1 Use quantification PCR to study relative occupancy of protein-chromatin binding

This method is used in investigating Htz1 occupancy and H3 acetylation, Gcn5 and Rad14 measurement at specific regions.

Primer sequences for Quantitative PCR:

For nucleosome -2 of *MFA2*:

Forward: 5'- CGTTTATGGTATAAATTAGAAAAGTTAAAGC-3';

Reverse: 5'- GGCGTCCTATGCATGCACTTAA-3';

For nucleosome -1 of *MFA2*:

Forward: 5'- TGCATGTCAGAGGAAAAAGAACAAAG-3';

Reverse: 5'- CGGATGAACGACAGAAGAAGTGG-3';

For nucleosome 4 of *HMRa1*:

Forward: 5'- TTAGAAGAAAGCAAAGCCTT-3';

Reverse: 5'-GATTCTCATATTACATACCCAA-3';

For nucleosome 5 of *HMRa1*:

Forward: 5'-GATAGCCTTTGAATCAATTTAC-3';

Reverse: 5'-TGTGGTGGTATATTTCTAACCT-3'.

Preparation of DNA from immunoprecipitated and input samples

Input samples (IN): Input solution volume was made of 50ul chromatin sample with 25μl of 5× Pronase buffer (125mM Tris-HCl pH7.5, 25mM EDTA, 2.5% SDS) and 50μl of TE to make up total volume of 125 μl.

Immunoprecipitation samples (IP): Following aspiration of the TE wash, beads were resuspended into 125μl 1x pronase buffer (25mM Tris-Cl pH7.5, 5mM EDTA, 0.5% SDS) and heated at 65 °C on a Thermomixer comfort (Eppendorf) with shaking at 900rpm for 20 minutes to interrupt protein-protein interactions. Put the tubes on the

magnetic rack for 30sec and transfer the supernatant into a new tube.

For all samples: Add 6.25 μ l of pronase, and digest protein by incubating the solutions at 65 $^{\circ}$ C overnight. The next day, 1ul of 10mg/ml RNase A (Sigma) was added and left to incubate at 37 $^{\circ}$ C for 30 minutes.

Each sample of DNA was purified into 50 μ l Elution Buffer using the PCR purification kit (Invitrogen) according to the instructions.

To ensure that sonicated DNA samples were evenly sheared and to an appropriate length (~300-600bp), 10 μ l of each input DNA was run on a 1.5% TAE agarose gel alongside 5 μ l of FastRuler low range DNA ladder (Fermentas).

Quantification of DNA by qPCR

1. All DNA samples were quantified by quantitative PCR (qPCR) using SYBR green. Typically, one input sample was diluted into water to prepare a 10-fold dilution range from 10^{-1} down to 10^{-5} . This range was used as a reference for relative DNA quantification between samples. For quantification, all input samples were diluted 1000-fold in water and all immunoprecipitation samples were diluted 4-fold in water.
2. All qPCR reactions were performed in 96 well PCR plates (Type: LW2215, Alpha Laboratories) and each reaction was prepared with the reagents listed in the table below table. A mastermix of all reagents excluding the DNA sample to be quantified was prepared and 18 μ l aliquots were dispensed into wells using an Eppendorf multipipette stream.

Each qPCR well	μ l
2x iQ SYBR Green Supermix (Biorad)	9.8
Primer 1 (100 μ M)	0.1
Primer 2 (100 μ M)	0.1
IN sample DNA to be quantified	10 (1000X,10000X,100000X,1000000X dilution)
Total	20

Each qPCR well IP	μl
2x iQ SYBR Green Supermix (Biorad)	9.8
Primer 1 (100μM)	0.1
Primer 2 (100μM)	0.1
IP sample DNA to be quantified(diluted 5X with H ₂ O)	10
Total	20

3. All PCR reactions to be quantified were repeated in triplicate including the dilution range. Plates were film sealed and DNA was quantified using an icycler thermal cycler (Bio-Rad) coupled to a My iQ optics module (BioRad). qPCR reactions were performed under the following conditions:

1. 95 °C for 3 minutes
2. 95 °C for 0:15 minutes (heat denaturation)
3. 55 °C for 0:20 minutes(primer annealing)
 - Normally 1-2 °C lower than T_m (theoretical primer annealing temp)
4. 72 °C for 0:10 minutes (primer extention)
5. Go to 2. x44 times
6. 95 °C for 1:00 minutes
7. 72 °C for 0:30 minutes
8. Melt curve from 55 °C

Quantifying the relative occupancy of protein-chromatin binding

1. All qPCRs data were generated with the icycler thermal cycler (Bio-Rad) and analysed using the Bio-Rad iQ5 software. Prior to quantification of the data, the information which determines whether the reaction had suitably proceeded was checked. Firstly, any good qPCR reaction amplification efficiency should be between 90 and 110%. Secondly, any reaction that did not display a single uniform peak on a melt curve was disregarded (more than one peak means multiple products). Thirdly, all unknown DNA samples had to be quantified within the linear range created from the IN sample data. iQ5 graphically displays the Ct value of the standard dilution range combined with unknown samples. Only unknown samples in which the Ct value lay within the linear range of quantification were accepted. Lastly, each dataset was

triplicated, visually inspected to ensure that these three repeats gave a reproducible Ct value, and single abnormal errors were deleted.

2. All data was exported from iQ5 in excel format. The occupancy of immunoprecipitated DNA at a given genetic locus was calculated as follows:

$$\text{DNA relatively value} = \frac{\text{Starting quantity (SQ) mean of IP sample}}{\text{Starting quantity (SQ) mean of IN sample}}$$

4.2.2 Analysis of DNA repair at nucleotide resolution (High resolution method)

Primers for the high resolution approach:

For *MFA2*

Repair analysis focused on both strands of the *HaeIII* fragment (-517 to +83) in the *MFA2* promoter.

For the bottom strand of the *MFA2* promoter:

5'biotin-GATAGCTTTTTTCCCTCATCTATTTTCTCGGAAAACCTGGTG3'

For the top strand of the *MFA2* promoter:

5'biotin-GATAGCTTTTTTCCCTTGATTATATAGATTGTCTTTCTTTTCAGAGGA
T3';

For *HMRa1*

The top strand of the *RsaI-BglIII* fragment (+61 to +476) in the *HMRa1* locus was analysed.

For the top strand of *HMRa1*:

5'biotin- GTAAGCTTTTTTTCATACGTTTATTTATGAACTACAAATTGT3'.

We have a technique to determine the induction and repair of DNA damage at a particular nucleotide position (Teng et al., 1997). This technique involves the application of specifically designed probes and Dynabeads. First, restriction enzymes are used to digest genomic DNA to generate a DNA fragment of interest, followed by

specific damage recognition endonuclease incision. After DNA denaturation, the released single stranded DNA of different lengths due to the above enzymatic function is isolated via a biotinylated primer together with Dynabeads. Finally, each single strand DNA fragment is labelled at its 3' end with radioactive dATPs and separated by gel electrophoresis. The probe was specially designed so as to serve not only to isolate single stranded DNA fragments but also to act as a template for the subsequent labelling reaction. In addition to being complementary to the 3' end of a DNA sequence of interest, the probe has been biotinylated at its 5' end, and another short oligonucleotide is inserted between the complementary sequence and the 5' biotin end. The short oligonucleotide inserted consists of six dTs next to the complementary sequence and another six random nucleotides separating dTs and the 5' biotin end. The six dT overhang serves as a template to incorporate radioactive dATPs to the single stranded DNA which has been retrieved, and the six random nucleotides between dTs and the biotin end were added to eliminate any steric hindrance from Dynabeads while incorporation of radioactive dATPs is occurring. To indicate the precise position of each damage site within the DNA sequence investigated, a sequencing ladder is run alongside the DNA samples during electrophoresis. The sequencing ladder is synthesised using T7 sequenase Version 2.0 DNA sequencing kit (Amersham Pharmacia Biotech) based on the Sanger method according to the manufacturer's instructions. Due to the facts that the single stranded DNA fragments are purified with a probe complementary to their 3' end and DNA synthesis can only proceed from the 5' end to the 3' end, it is required here to load the sequencing ladder reflecting the sequence of the opposite strand to indicate the actual position of a DNA lesion in a specific DNA strand. The probe used to generate sequencing ladders is modified as well, but in a way different from that served to isolate single stranded DNA after damage incision. Six random nucleotides are added to the primer at the 5' end before the complementary sequence to compensate in the length of the ladder in the same way as the single stranded DNA samples are labelled with six radioactive dATPs. This allows a direct reference from the running positions of the sequencing ladder to that of

the DNA damage ladder.

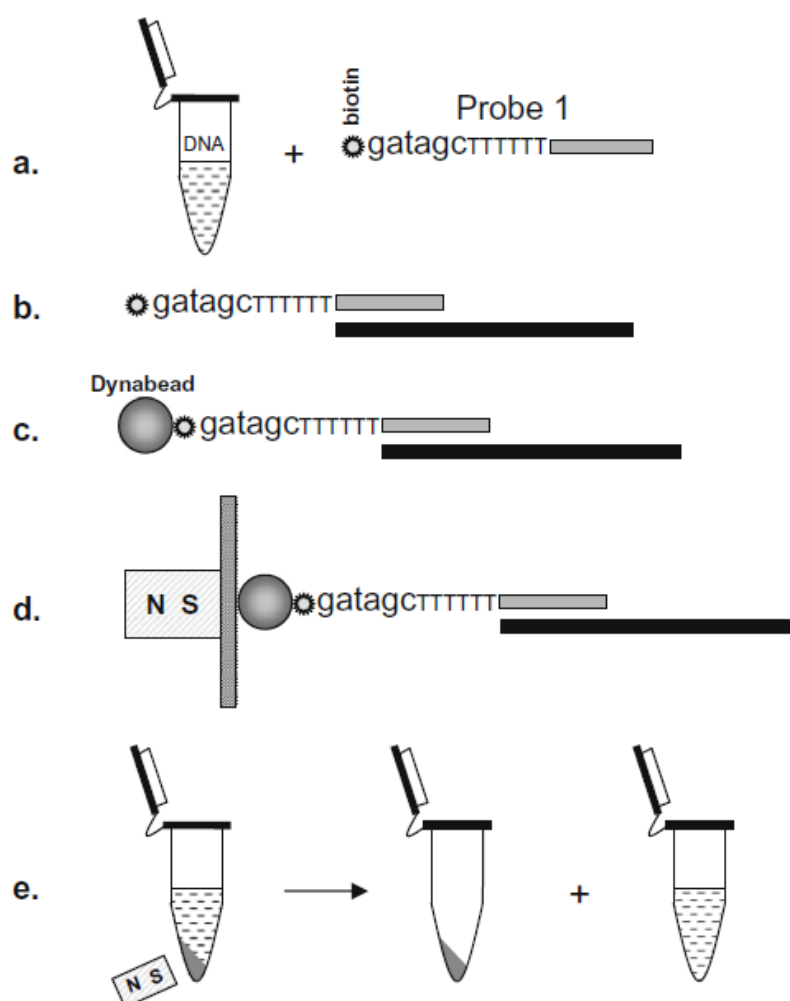


Figure 4.1 Purification of DNA fragments after enzymatic cleavage for CPD analysis

- Probe 1 is added to the restricted and CPD cut DNA.
- Probes anneal to the complementary sequences at 3' end.
- Dynabeads are added to bind the biotin at the 5' end of the probe.
- Dynabeads and the associated DNA fragments are immobilized on a magnetic rack and isolated
- The supernatant is transferred to a fresh tube for NTS purification. Dynabeads and the associated DNA fragments is added with polymerase and radioactive dAs which radioactively labelled at 3' end, after heat denatured, Dynabead associated strands are isolated, and supernatants saved for loading onto a sequencing gel.

(1) Restriction enzyme digestion and strand incision by the damage specific endonuclease

50ug of genomic DNA in 100ul TE buffer was restricted with 100 units (5ul enzyme) of appropriate endonucleases at 37 °C for 1 hour in a total reaction volume of 300ul

TE. DNA purification after enzymatic reaction was performed as depicted in the yeast genomic DNA extract (materials and methods section 2.3.1). Following re-dissolving in 100ul of TE, the DNA was incubated with a damage specific ML endonuclease at 37 °C for another hour, after which the enzyme was removed by a phenol/chloroform extraction and precipitated by 75% ethanol. Finally 100ul of TE was added to re-dissolve the precipitated DNA pellets.

(2) Purification of damage incised single stranded DNA

Following addition of 25ul of 5M NaCl to the above 100ul of DNA solution to make a final sodium concentration of 1M (optimal for binding of streptavidin coated beads to biotin), 1ul of biotinylated probe complementary to the 3' end of TS was added. The samples were denatured at 95 °C for 5 min and then incubated at the annealing temperature for 15 min to allow the probe to anneal to the fragments. 10ul of washed Dynabeads in 1xBW buffer was added, and thereafter single stranded DNA fragments were isolated using the magnetic dock. The supernatant was transferred to fresh tubes, and isolation of the NTS was carried out using a second probe. Upon completion of the above purification steps the beads were washed once with 1xBW buffer at the annealing temperature for 5 min, followed by two further washes with water at room temperature.

(3) End labelling DNA fragments with α -[³²P] dATPs

The washed beads were resuspended in 6ul of H₂O, 2ul of Sequenase buffer, 0.7ul of 0.1M DDT, 1ul (5uCi) of α -[³²P] dATP (6000Ci/mmol, Amersham) and 2ul of sequenase (diluted 1:30 in enzyme dilution buffer). The solution was incubated at room temperature for 10 min after mixing well with a pipette to allow complete labeling. Following the reaction the beads were collected using the magnetic rack and washed twice with TE buffer. The labeled DNA fragments were finally eluted from the beads by addition of 3ul of formamide loading buffer (95% formamide, 20mM EDTA, 0.05% Bromophenol Blue) and resolved by electrophoresis on a 6% denaturing polyacrylamide gel as described below.

(4) Denaturing polyacrylamide gel electrophoresis

A 0.4 mm thick denaturing polyacrylamide gel was used in this study to resolve single stranded DNA fragments. Two glass plates measuring 20cm by 60cm and 20cm by 62cm were used to construct the gel mould. The plates were thoroughly cleaned with detergent followed by plenty of water and absolute ethanol. The shorter plate was sprayed with Dimethyldichlorosilane solution (2% 1,1,1-trichloroethane) on the inner surface in order for an easy separation of the gel from the glass plates after electrophoresis. The two plates were separated with 0.4mm thick side spacers and firmly sealed with vinyl insulation tape. 75ml of 6% acrylamide EASI gel (acrylamide:bis-acrylamide=19:1, 7M urea, 1xTBE) was mixed with 800ul of 10% APS and 50ul of TEMED after being degassed under vacuum in a flask for 10 minutes. The gel mixture was then poured slowly into the gel mould. Care was taken to ensure no bubbles became trapped within the gel while pouring. A comb was inserted into the top of the gel immediately to generate the loading wells, and the gel was left to set for at least 1 hour. A GIBCO electrophoresis system and a Pharmacia powerpack (EPS 3500) were used to run each sequencing gel. Following pre-running of the gel in 1xTBE buffer for 30 minutes at 70 W output (it is designed so to achieve a gel temperature of around 50 °C during electrophoresis which is recommended for the separation of single stranded DNA), DNA samples were loaded carefully onto the gel. Electrophoresis was carried out for the required time at an output of 70W. After electrophoresis, the plates were separated carefully so that the gel was only stuck to one glass plate. A piece of Whatman filter paper was placed on top of the gel to allow a close attachment to it, after which the gel was cautiously peeled off from the glass plate. The paper merely acts as a support for the gel. Following covering the gel side with plastic cling film, the gel was placed on a Bio-Rad gel dryer for two hours under vacuum at 80 °C. Once dried, the gel was exposed to a phosphorimager screen in a cassette usually overnight. The phosphorimager screen was then scanned using a Typhoon scanner for image acquisition and quantification.

(5) Damage quantification and repair analysis

The image obtained was analysed using ImageQuant software version 5.0. The

intensity of each band, which reflects the frequency of DNA damage at a specific site, was measured as collective pixel values. To avoid a false judgement about repair resulting from a slightly varied loading of DNA samples in each lane, an adjustment was made as the total signal from individual lanes were multiplied by a factor to give equal values, and then the signal of each band was accordingly multiplied. The value from non-irradiated DNA was subtracted as a non-specific background. The damage remaining after particular repair times was presented as a percentile with respect to the initial damage (0 lane, 100% damage).

$$\text{Damage \%} = [\text{Damage}]_t / [\text{Damage}]_0 * 100$$

(Where t represents a particular repair time and 0 represents when the clock starts)

To generate repair curves, the data points representing % damage at defined sites at each repair time were fitted to an exponential curve. Finally the time, where 50% of the damage was removed ($T_{50\%}$ value), was calculated to compare repair rates of individual damages.

4.3 Results

4.3.1 Htz1 occupies the repressive *MFA2* promoter, but is not at the *HMRa1* locus

To investigate the role of Htz1 at the gene level, I chose specific regions in the genome to examine. The genomic localization of Htz1 has been reported by different researchers (Zhang et al., 2005, Li et al., 2005, Millar et al., 2006). I picked two different regions from these genome-wide studies. One with the Htz1 variant incorporated in its nucleosome and the other one which only contains H2A in its nucleosomes. In this way I could examine the role of Htz1 on NER at the gene level and see if htz1 functions influence NER in local nucleosome regions. The region selected in which Htz1 resides is at *MFA2* promoter (nucleosome -2 and -1, Teng *et al.*, 2001), and that where it does not was the inner sequence (nucleosome 4 and 5, Ravindra *et al.*, 1999) of the *HMRa1* locus. Both *MFA2* and *HMRa1* are repressed in my α mating type cells and these regions have defined nucleosomes (Teng et al., 2001). The low resolution mapping and high resolution mapping of nucleosomes on

MFA2 has established that in α mating type cells four nucleosomes reside in *Htz1* gene, 2 in the regulatory region and 2 in its coding sequence. There are also 12 well-positioned nucleosomes in the 1.94-kb region around the *HMRa1* gene (Ravindra et al., 1999). I designed two primers for each region. Specifically for the -2 and -1 nucleosomes of the *MFA2* promoter and the R5 and R4 nucleosomes of the *HMRa1* coding region. Chromatin from wild-type, *htz1Δ* and *swr1Δ* strains was purified from 2×10^9 cells (see materials and methods). My Q-PCR results in Figure 4.2 are consistent with the genome-wide data from Millar (Millar et al., 2006). The wild type strain has a Htz1 binding level more than 10 fold higher than the *htz1Δ* strain at the two *MFA2* promoter regions investigated. Similar, and low binding levels in both the wild-type and the *htz1Δ* strain were observed at the two *HMRa1* regions. These Q-PCR data clearly demonstrate Htz1 is not contained in every nucleosome, and that it occupies the repressive *MFA2* promoter but not the repressive *HMRa1* locus.

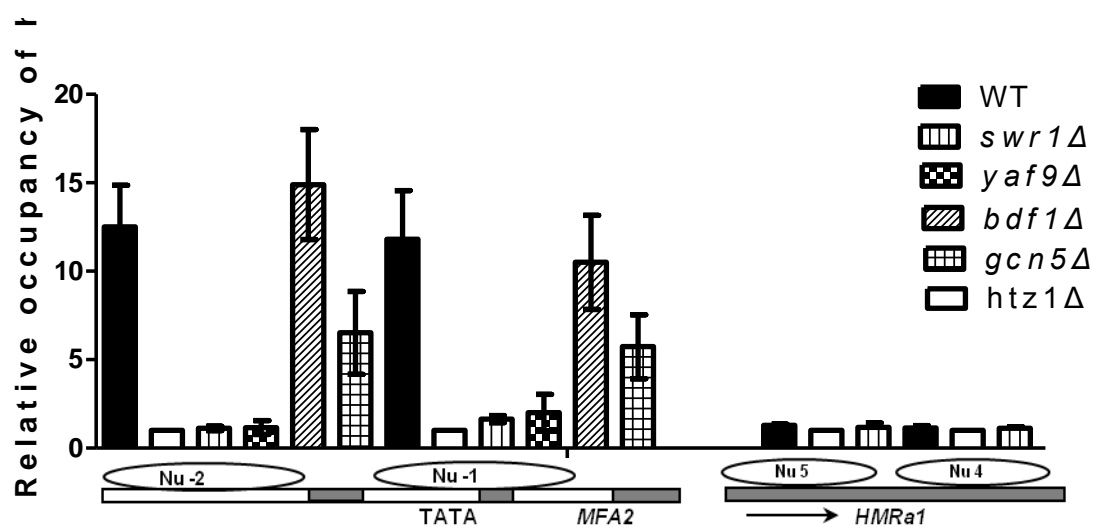


Figure 4.2 Htz1 level at *MFA2* promoter and *HMRa1* region in BY4742 wild-type and *htz1Δ*, *swr1Δ*, *yaf9Δ*, *bdf1Δ* and *gcn5Δ* mutants. Chromatin from different strains as generated from log phase cells. Immunoprecipitation was carried out with anti-Htz1 antibody (see materials and methods). Q-PCR with 4 different pairs of primers was used to generate the data above. Data are the average of at least two independent experiments \pm SD

Figure 4.2 clearly shows that Htz1 is present at the two nucleosomes in the *MFA2* promoter, but that it is absent from the *HMRa1* locus. Deletion of *SWR1*, *YAF9* and

GCN5 all reduce the presence of Htz1 in the *MFA2* promoter, although the reduction in the *gcn5Δ* mutant is less profound than in the *swr1Δ* and *yaf9Δ* mutants. This is consistent with Gcn5's role in Htz1 localization, which was not as necessary as Swr1 and Yaf9 (Zhang et al., 2005). The *bdf1Δ* mutant does not show a similar reduction of Htz1 in the *MFA2* promoter. This is not surprising as it was reported that Bdf1 and acetylated histones are only required for Htz1 loading at some loci, but not to all (Zhang et al., 2005). These data form a basis for the gene specific studies and I next decided to examine CPDs at nucleotide resolution in the WT, *htz1Δ* and *swr1Δ* strains.

4.3.2 Htz1 promotes repair of CPDs by NER in Htz1 nucleosomes in the repressed *MFA2* promoter

The results of the global repair analysis in Chapter 3 either indicate a general defect in the capability of the NER machinery or a defect in the repair of UV-induced CPDs following UV irradiation in some regions; for example the Htz1 bearing nucleosomes regions of the genome. I first investigated how deletion of *HTZ1* and *SWR1* affects the repair of CPDs following UV irradiation in the *MFA2* locus where Htz1 occupancy has been identified. This experiment was done in cooperation with Yu. Typical gels for the high resolution CPD repair analysis (Teng et al., 1997) in the *MFA2* promoter are shown in Figure 4.3. Repair efficiency is quantitatively presented in Figure 4.4 as the time needed to remove 50% of initial CPDs ($T_{50\%}$) at specific sites. The results show $T_{50\%}$ of CPDs repaired after UV to 3 hour after UV. Repair was analysed from -412 to -272 in nucleosome -2 and -61 to -207 in nucleosome -1 on both the bottom strand and the top strand. In the *MFA2* promoter. The repair of CPDs is significantly compromised at almost all sites in the two original Htz1 nucleosomes in the *htz1Δ* and *swr1Δ* mutant cells compared to that in the wild type cells (t-test, WT vs. *htz1Δ*, $P=2.39 \times 10^{-5}$, WT vs. *swr1Δ*, $P=8.44 \times 10^{-5}$). There is no apparent indication that the repair difference only occurs in certain regions within the two nucleosomes. Meanwhile, the repair of CPDs in these two nucleosomes in the *htz1Δ* and *swr1Δ* mutants are similar (t-test, $P=0.71$).

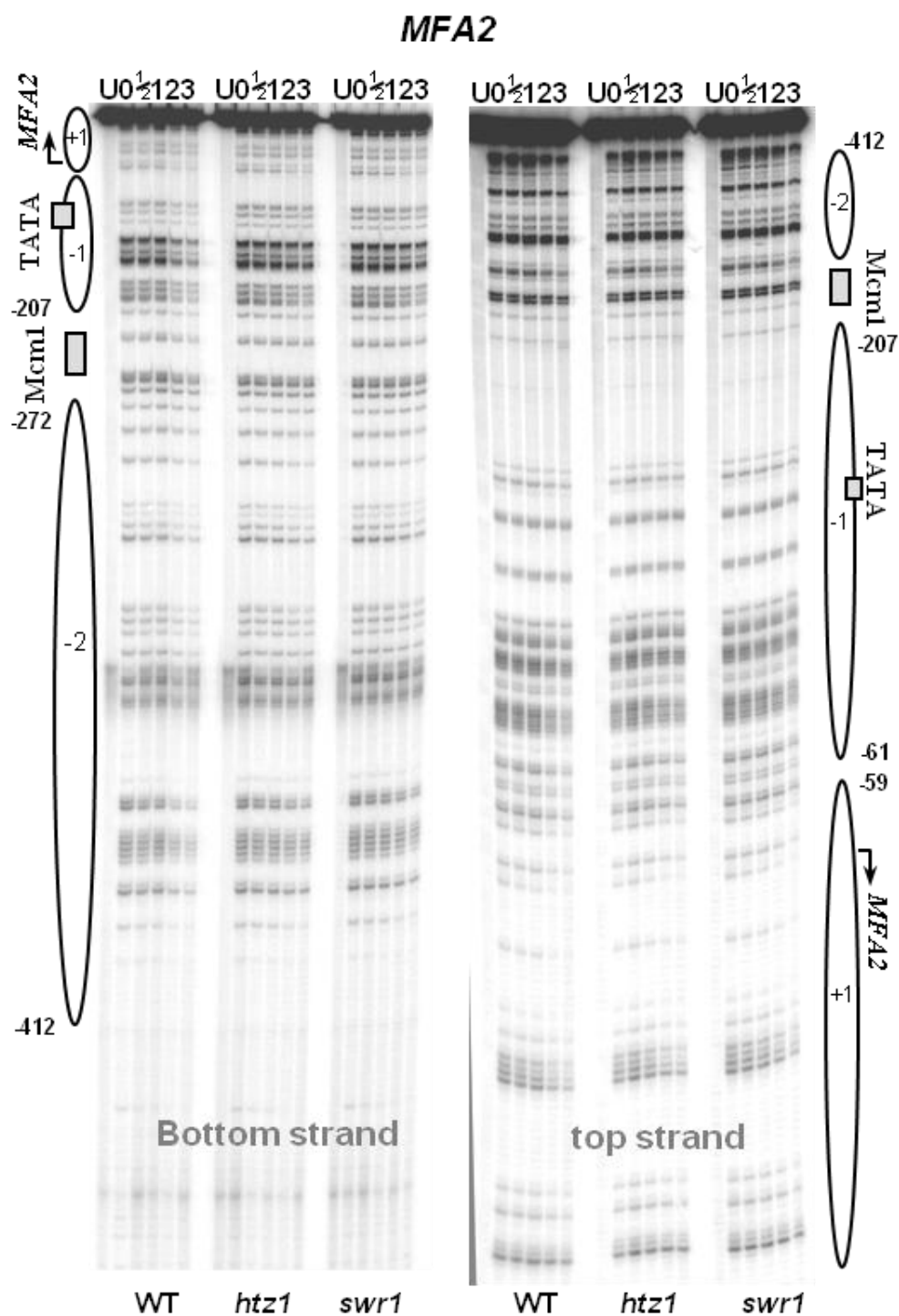


Figure 4.3 Repair of CPDs in the top strand and bottom strand of *MFA2* promoter region. Gel depicting CPDs in the top strand of the *Hae*III fragment (-517 to +83) in the *MFA2* promoter following a UV dose of 100 J/m². Lane U is DNA from mock irradiated cells while 0, 0.5, 1, 2 and 3 are DNA from irradiated cells following 0, 0.5, 1, 2 and 3 hour repair, respectively.

In the diagram Figure 4.4, different symbols reflect different strains. The distance from the centre line illustrates the time taken to repair half the CPDs at a given site,

the nearer to the line the higher the repair efficiency. The *htz1Δ,swr1Δ* mutants show slower repair at the *MFA2* promoter when compared to the wild type strain.

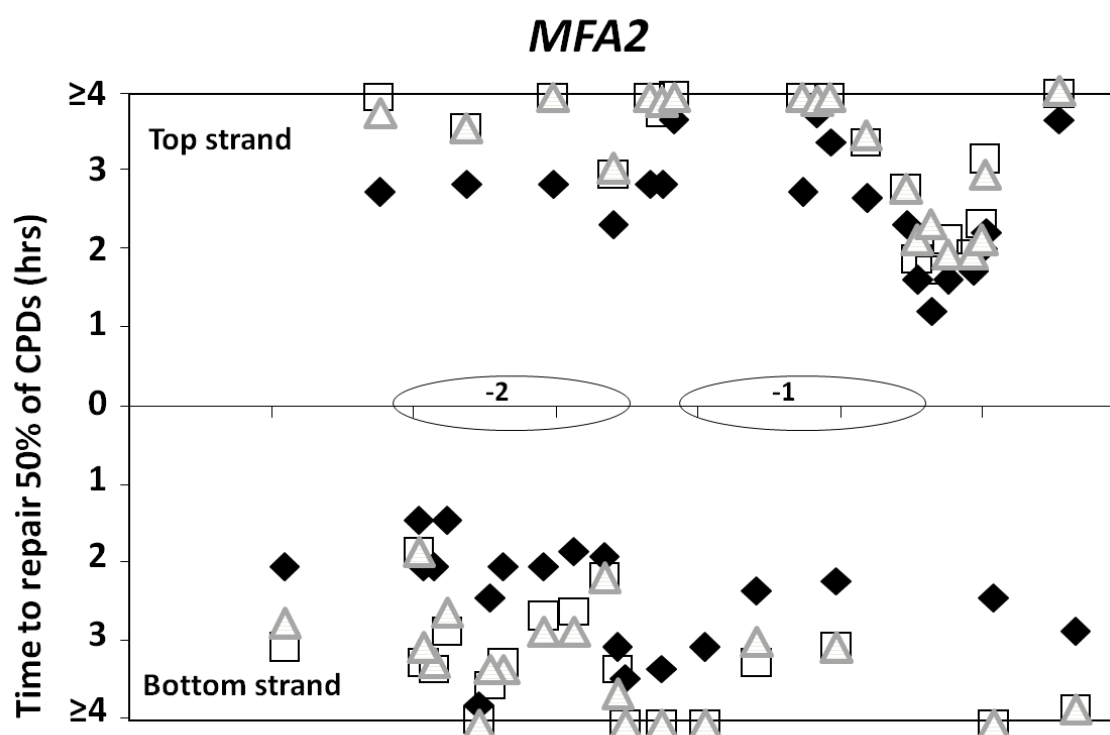


Figure 4.4 Repair of CPDs in BY4742 wild-type (◆) and *htz1Δ* (□), *swr1Δ* (△) of the *MFA2* promoter. Repair of CPDs is presented as the time needed to repair 50% of the initial CPDs at each detected site ($T_{50\%}$). The data were calculated from repair curves through Excel, and the formula and calculation are listed in materials and methods. Data represent the average of two independent experiments; tables of values can be found in the appendix. Data from the top strand and the bottom strand are listed respectively. Two nucleosome positions on the *MFA2* promoter are indicated as circles in the diagram. $T_{50\%}$ higher than 4 hours (slow repair or no repair) are shown at the same level on the 4 hr line.

4.3.3 The absence of Htz1 does not reduce NER at the repressed *HMRa1* locus.

I determined that the *HMRa1* coding region does not contain histone Htz1 in its nucleosomes. Hence I investigated how deletion of *HTZ1* and *SWR1* affects the repair of CPDs in the *HMRa1* locus. Typical gels for the high resolution CPD repair analysis in the *HMRa1* are shown in Figure 4.5. *RsaI*-*BglIII* restriction enzymes generated the fragment (+61 to +476) of the top strand of the *HMRa1* coding region.

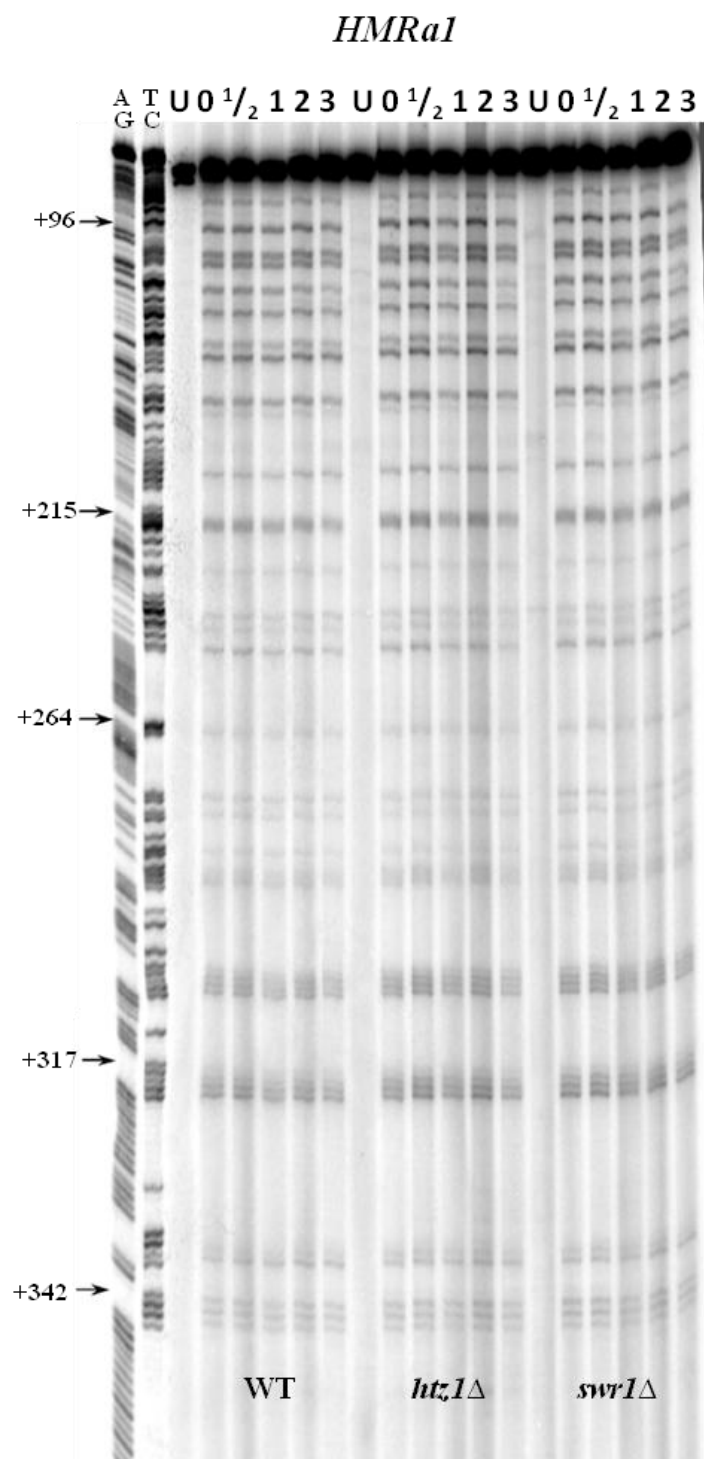


Figure 4.5 Repair of CPDs in the top strand of *HMRA1* coding region.

Gel depicting CPDs in the top strand of the *RsaI*-*Bgl*III fragment (+61 to +476) in the *HMRA1* sequence following a UV dose of 100 J/m². In the left of the gel are the sequences of the strand of interest, shown in combinations of A, G and C, T, respectively. Lane U is DNA from mock irradiated cells while 0, 0.5, 1, 2 and 3 are DNA from irradiated cells following 0, 0.5, 1, 2 and 3 hour repair, respectively.

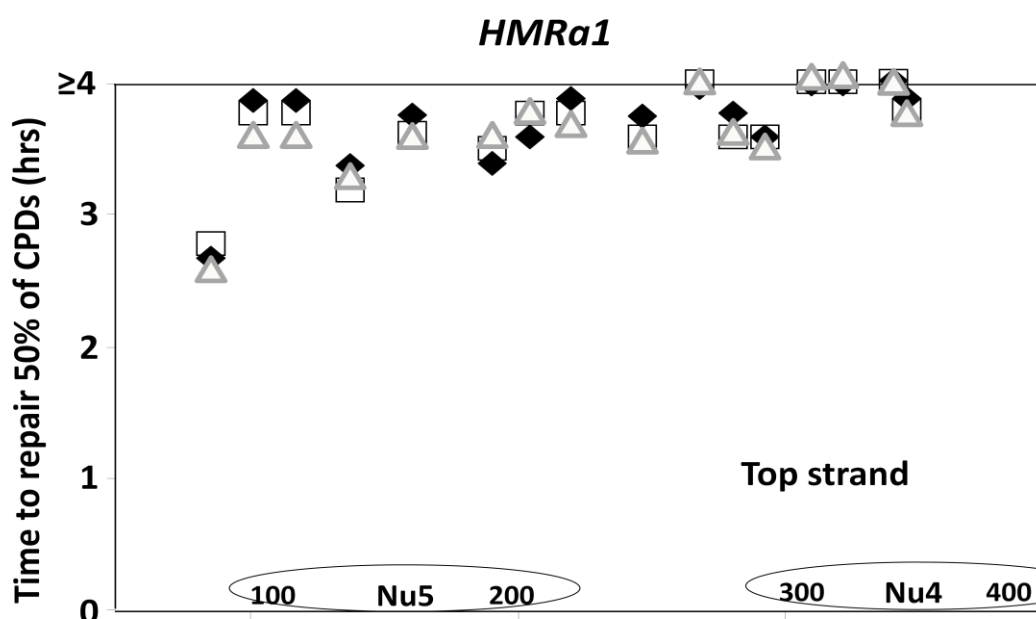


Figure 4.6 Repair of CPDs in BY4742 wild-type (◆) and *htz1Δ* (□), *swr1Δ* (△) on *HMRa1*. Repair of CPDs is presented as time needed to repair 50% of the initial CPDs at each detected site ($T_{50\%}$). These data were calculated from repair curves through Excel, the formula and calculation is listed in materials and methods. Data represents the average of two independent experiments, tables of values can be found in the appendix. Two nucleosome positions in the *HMRa1* region are shown as circles in the diagram. $T_{50\%}$ higher than 4 hours (slow repair or no repair) were shown at the same level on the top 4 hr line.

Repair of CPDs at individual dipyrimidine sites was calculated from these gels. Diagram Figure 4.6 depicts the data collected from the high resolution gels and shows a similar repair time ($T_{50\%}$) between BY4742 wild-type and the *htz1Δ*, *swr1Δ* strains at these individual sites of the *HMRa1* coding region. The repair of CPDs in these two nucleosomes in the *htz1Δ* and *swr1Δ* mutants are similar (t-test, $P=0.54$). This is different from what I found in the *MFA2* promoter, where the wild type strain showed a significantly faster repair than in the *htz1Δ*, *swr1Δ* strains. Both of these regions are transcriptionally silent, thus this difference results from the impact of histone Htz1 on

GG-NER. Hence, for the *MFA2* promoter, lack of Htz1 or the inability to place Htz1 in the local nucleosomes reduces the NER efficiency. Conversely, at the *HMRa1* region where no histone Htz1 resides, neither a lack of Htz1 itself nor the absence of Swr1 which is required to replace H2A-H2B with the Htz1-H2B dimer affects the NER efficiency.

4.3.4 Acetylation of Htz1 at K3, 8, 10, 14 does not contribute to CPD removal in the *MFA2* promoter

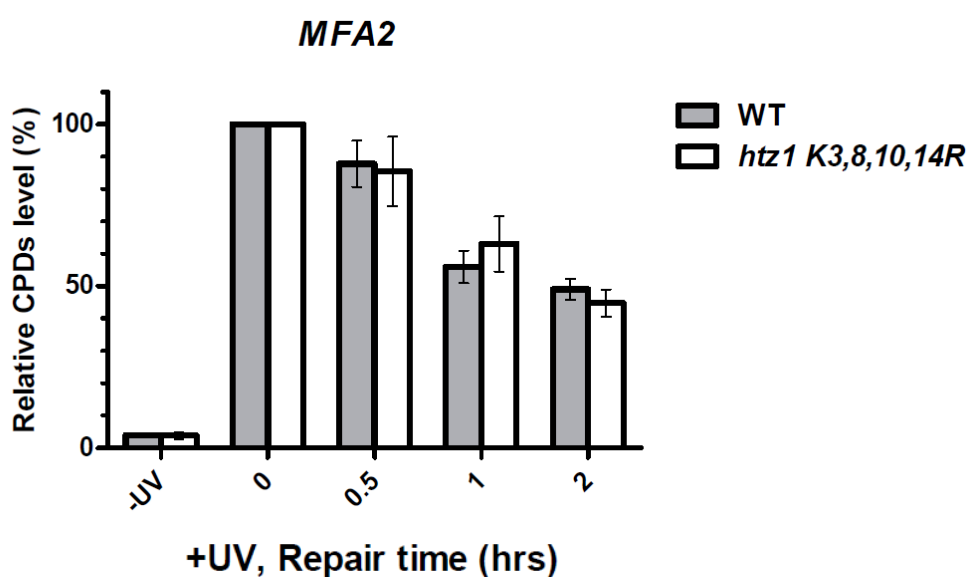


Figure 4.7 CPD removal from the *MFA2* promoter in the wild-type (302) and Htz1 acetylation mutant (544) after 100J/m² of UV. Genomic DNA was fragmented by sonication. Anti-CPD antibody was employed followed by Q-PCR with the *MFA2* promoter primers (see materials and methods). The data are the average of three biological repeat experiments.

Despite the fact that acetylation of Htz1 at K3,8,10,14 does not change the cells UV sensitivity when compared with that of wild type cells, and slot blots also showed that the CPD removal efficiency from total DNA does not alter without this lysine modification, I decided to examine gene specific NER to ensure that the local effects were not going undetected in the whole genome analysis. I had established that histone Htz1 occupied the *MFA2* promoter. Immunoprecipitation with CPD specific antibody was employed to examine NER uniquely at the *MFA2* in WT and a Htz1

acetylation mutant. This would determine if a local effect in the acetylation could influence NER. Primers were designed for the *MFA2* promoter (see materials and methods) and the CPD incidence was measured at this location.

The result in Figure 4.7 show a similar CPD repair rate in the wild type and in the mutant strain with the Htz1 lysines at K3, 8, 10, 14 mutated to arginine. CPD incidence immediately after UV treatment in Figure 4.7 is depicted as 0 hours and normalized to 100%. Data from different repair time points are normalized to the 0 hours data. No differences are found with and without these lysine residues. This result is consistent with the genome CPD removal data in the last chapter showing that Htz1 K3,8,10,14 lysine acetylation does not playing a role in NER.

4.3.5 After UV Htz1 promotes the binding of Rad14 to damaged DNA at the *MFA2* promoter

Since Htz1 nucleosomes in the repressed *MFA2* promoter display a unique feature of having higher levels of UV-induced histone H3 lysine 9 and 14 acetylation which was previously proven to be necessary for the efficient repair of CPDs, I investigated how deletion of *HTZ1* might influence the binding of a key NER factor, Rad14 to damaged DNA in chromatin after UV. Rad14 is believed to act as a DNA damage recognition factor in the early steps of NER, and its function is almost exclusively in NER (Guzder et al., 1993). Myc-tagged *RAD14* strains in both wild type and *htz1Δ* were employed for this experiment. In Chapter 3, Rad14 bound DNA showed enriched CPDs after UV treatment, confirming that Rad14 is preferentially associated with damaged DNA after UV. Quantitative Western blotting showed that deletion of *HTZ1* does not change the expression level of Rad14, and the expression of Rad14 is unaffected by UV treatment. Employing quantitative PCR at *MFA2*. A significantly reduction in Rad14 binding at the *MFA2* promoter in the *htz1Δ* cells compared to that in the wild type cells was observed, whilst the binding of Rad14 to the *HMRa1* locus was not affected (Figure 4.8). Specifically, Rad14 in the wild type strain shows a 3.69 ± 0.75 fold increase 15min after UV at the *MFA2* promoter while there is only a

1.93±0.13 fold increase in the *htz1Δ* strain. This reduction is not observed in the *HMRa1* region where similar relative binding levels of Rad14 are detected between the wild type and the *htz1Δ* strain. This result suggests a positive function for Htz1 in Htz1-containing nucleosomes to promote the binding of Rad14 to damaged DNA in chromatin following UV irradiation. It is important to note that Rad14 binds to both the *MFA2* promoter and the *HMRa1* inner sequence even before UV treatment and this binding was enhanced after UV. The binding of Rad14 to damaged DNA is very quick and a significant increase in Rad14 binding was observed between the no UV sample and the sample right after UV treatment. Rad14 binding did not reduce over the repair time up to 3 hours (Data not shown). As there is still DNA damage that needs to be repaired after 3 hours binding of Rad14 to DNA is still expected.

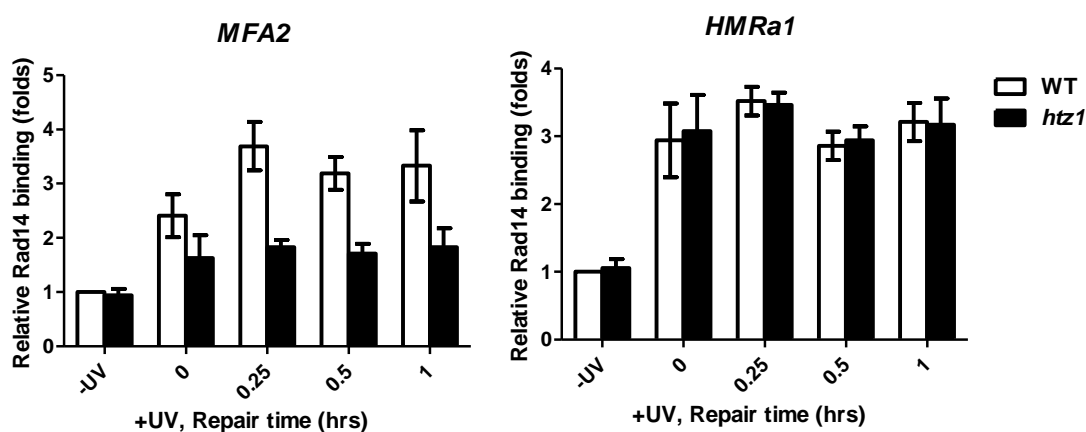


Figure 4.8 The binding of Rad14 to the *MFA2* promoter and the *HMRa1* inner sequence after UV (100J/m²). The level of Rad14 binding is presented as the relative level (fold) to those from the untagged strain. Quantitative data are the average of three independent experiments ±SD.

4.3.6 Htz1 promotes histone H3 hyperacetylation in Htz1 nucleosomes in the *MFA2* promoter after UV irradiation.

We had reported that UV irradiation activates histone hyperacetylation at H3 and H4. In particular, the elevated levels of acetylation at H3 lysine 9 and 14 are required for efficient repair of UV-induced CPDs in the *MFA2* promoter (Yu et al., 2005a). I examined and compared this response in the wild type and the *htz1Δ* mutant cells.

After UV, the *htz1Δ* mutant cells also failed to achieve similar levels of H3 acetylation at lysine 9, lysine 14 in the *MFA2* promoter when compared to wild type cells Figure 4.9. The *htz1Δ* mutant cells also exhibit a lower constitutive level of histone H3 lysine 9 and 14 acetylation in the promoter of *MFA2* before UV (0.65 ± 0.07 in *htz1Δ* vs. 1 in WT). The increase in the levels of H3 lysine 9 and 14 acetylation following UV irradiation in the *htz1Δ* mutant cells is significantly less than that in the wild type cells (e.g. 2.28 ± 0.17 fold increase in *htz1Δ* vs. 4.34 ± 0.22 fold increase in WT, 1 hr after UV). In the *HMRa1* locus where Htz1 is normally absent, similar increase in histone H3 lysine 9 and 14 acetylation following UV treatment was also observed in both the WT and *htz1Δ* strains. Hence that deletion of *HTZ1* has no influence on the extent of the increase at this locus. Although the UV induced H3 acetylation at *MFA2* is increases less in the *htz1Δ* strain when compared to the wild type, I still observed a gradually H3 acetylation increasing after UV (1.51 fold increase, 0.5 hour after UV, 2.28 fold increase, 1 hour after UV). Thus, histone H3 acetylation at lysine 9 and 14 is activated at both the *MFA2* and *HMRa1* loci following UV, and lack of Htz1 only reduced H3 acetylation at the Htz1 containing nucleosomes in *MFA2*.

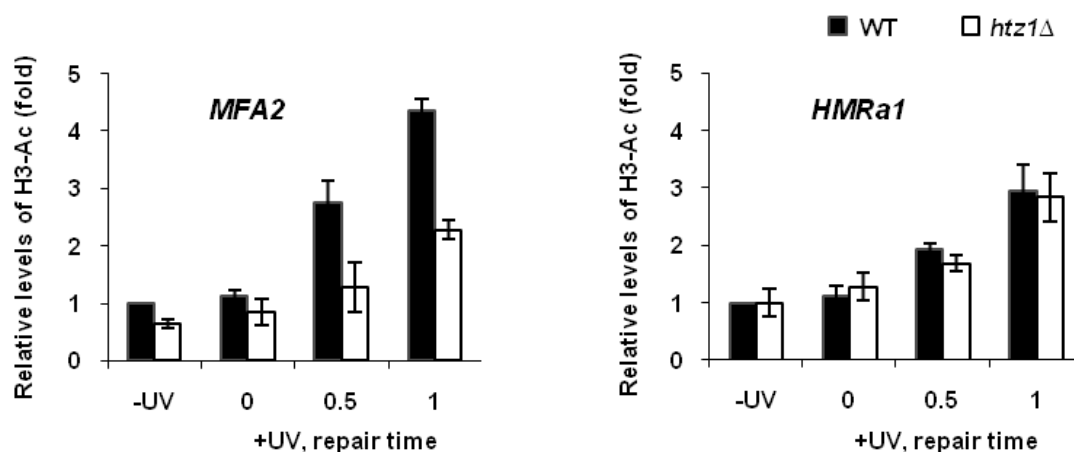


Figure 4.9 The level of H3 acetylation at the *MFA2* promoter and at the *HMRa1* inner sequence without UV or after UV (100J/m^2). ChIP analysis of Histone H3 acetylation (H3-Ac) was performed using Ac-H3 (K9, K14) antibodies. The H3 acetylation levels were first normalized against the H3 levels, and then presented as the fold change relative to the mock irradiated sample in wild type. -UV: mock irradiated samples; 0: cells received 100J/m^2 of UV without repair; 0.5 hr repair, or 1 hr repair. Cells were irradiated with UV and then were allowed to repair in YPD for the number of hours indicated. The primers and method were described in materials

and methods. Data are the average of three independent experiments \pm SD.

4.3.7 Htz1 promotes the occupancy of Gcn5 at Htz1 nucleosomes in the *MFA2* promoter after UV irradiation.

Previously I found that after UV Htz1 promotes histone H3 hyperacetylation in Htz1 nucleosomes in the *MFA2* promoter but not in the Htz1 free region *HMRa1*; this could be related to Gcn5. Gcn5 possesses a histone acetyltransferase activity with specificity for the Lys residues of H3 histone tails and we have reported Rad7 and Rad16 proteins mediate the increased occupancy of the histone acetyltransferase Gcn5 on the nucleosomes at the *MFA2* promoter following UV irradiation (Yu et al., 2011). This leads to histone hyperacetylation at H3 lysine 9 and 14 which is required for efficient repair of UV-induced CPDs. I thus suspected that Htz1 may affect H3 acetylation through this Gcn5 mediated acetylation process. In order to investigate how Htz1 influences the occupancy of Gcn5 on chromatin and histone H3 acetylation, this work employed a Gcn5 myc-tagged construct in both wild type and *htz1* Δ strains. In Chapter 3, a similar expression level of Gcn5 protein was observed in these two strains. Anti-myc antibody (cell signal) was used in this chromatin immunoprecipitation experiment. Quantitative PCR was undertaken and the data of Gcn5 occupancy at the two nucleosomes in the *MFA2* promoter were normalised against that in the *HMRa1* locus Figure 4.10. At *MFA2*, an increase in the occupancy of Gcn5 in the wild type cells following UV treatment was observed which is consistent with our previous findings (Yu et al., 2011). Deletion of *HTZ1* results in a reduction in the occupancy of Gcn5 at this locus, both before and after UV treatment. Although the levels of Gcn5 occupancy are slightly increased in the *htz1* Δ cells following UV treatment over time, they are still significantly lower than that seen in wild type at any time point (Figure 4.10). These data indicate Htz1 in the nucleosomes of the *MFA2* promoter promotes the occupancy of the histone acetyltransferase Gcn5 on chromatin and this results in increased histone H3 lysine 9 and 14 acetylation on these nucleosomes.

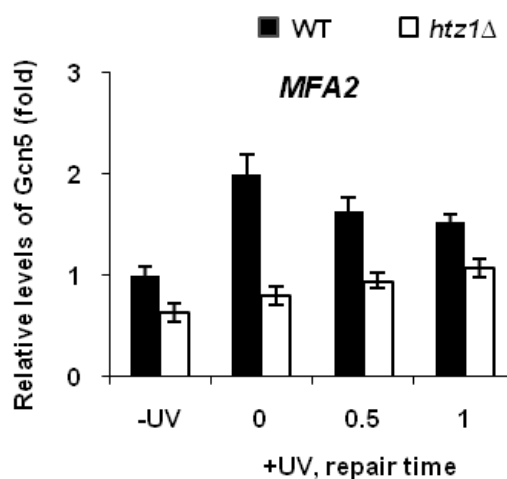


Figure 4.10 The occupancy of Gcn5 at the *MFA2* promoter without UV or after UV ($100\text{J}/\text{m}^2$). ChIP analysis of the occupancy of Gcn5 was performed with anti-Myc antibodies in *GCN5*-myc strains. The levels of Gcn5 binding at *MFA2* were normalised against those at the *HMRa1* locus (as they are unchanged in the *htz1Δ* compared to WT), and then presented as the fold change relative to the mock irradiated sample in wild type. The primers and method were as in materials and methods. Data are the average of three independent experiments \pm SD.

4. 4 Discussion

We previously mapped the nucleosome positions through a high resolution approach and found two nucleosomes at the *MFA2* promoter; nucleosome -2 is located upstream of the $\alpha 2$ operator approximately at positions -412 to -272 to the coding sequence, nucleosome -1 is located in the region between the Mcm1 binding site and the transcription start point approximately at positions -207 to -61 to the coding sequence and contains the TATA box in the middle of the nucleosomal DNA (Teng et al., 2001). Htz1 deposition requires Swr1 as absence of Swr1 will block this histone exchange. Lack of Yaf9 and will result a dramatic reduction of Htz1 genome-wide. This finding correlated with a *htz1Δ* mutant-like level of Htz1 occupancy in the promoter of *MFA2* in these *swr1Δ* and *yaf9Δ* mutants. Htz1 occupancy has also been found to be significantly reliant on Gcn5 and on Bdf1, and a lack of either results in a 10-15 percentile ranks loss of Htz1 (Zhang et al., 2005). The *bdf1Δ* and *gcn5Δ* mutants in my experiments showed a noticeable reduction of Htz1 at the *MFA2* promoter, but this was not as dramatic as in the *swr1Δ* and *yaf9Δ* mutants. The *HMRa1* data show that Htz1 does not reside in every nucleosome and a relatively

background level of Htz1 antibody binds at these locations in the WT and in all of the mutants examined. Thus these two regions, *MFA2* and *HMRA1* are a useful model to explore how this histone variant influences NER. *MFA2* and *HMRA1* are transcriptionally silent in *MAT α* cells, so this make them suitable for investigating GG-NER.

Faster repair was observed in wild type cells at the *MFA2* promoter when compared with the *htz1 Δ* and *swr1 Δ* strains while at the *HMRA1* similar repair rates were seen for these strains. Thus the slower repair I have found in genomic DNA is likely due reduced NER in regions like *MFA2* which originally contained histone Htz1 in their local nucleosomes. In other words, nucleosomes which do not have Htz1 have unchanged NER in the *htz1 Δ* and *swr1 Δ* strains. Thus Htz1 has a role in NER and it likely only affects repair at local nucleosomes containing Htz1.

My work investigated how this histone variant influenced NER. Evidences suggest that efficient repair of DNA damage in the chromatin environment requires histone modifications and chromatin remodelling (Czaja et al., 2012, Waters et al., 2012). Our previous studies, using the *S. cerevisiae MFA2* gene as an example, revealed that histone H3 acetylation and chromatin remodelling are activated following UV, and both events are required for NER to efficiently process UV-induced CPDs in chromatin (Yu et al., 2005a). These results raised the possibility that the placement of histone Htz1 could alter the chromatin structure and furthermore shift the nucleosome positions to favor repair steps after UV damage. Incorporation of Htz1 into the nucleosomes could potentially change their stability, and also their susceptibility to chromatin remodelling when required. Both the default chromatin structure and chromatin remodelling following UV have a significant influence on CPD repair in the *MFA2* promoter (Yu et al., 2005a, Yu et al., 2011). To address whether deletion of *HTZ1* results in any changes in chromatin accessibility in the *MFA2* promoter, and whether the deletion influences chromatin remodelling at this locus following UV treatment, Yu in our group employed a high-resolution nucleosome mapping approach (Teng et al., 2001) to examine the susceptibility of DNA in chromatin in the *MFA2*

promoter to micrococcal nuclease (MNase) digestion in wild type and the *htz1Δ* cells. This method is capable of assessing the sensitivity to MNase digestion of every site in a DNA sequence of interest in chromatin, and it has single nucleotide resolution. He scanned these gels to produce graphs of MNase sensitivity at individual cutting sites within the chromatin, and they are presented in Figure 4.11. These graphs reveal that MNase digestion in the *MFA2* promoter is almost identical between chromatin from wild type cells and the *htz1Δ* cells. Wild type and the *htz1Δ* cells have the same nucleosome positioning patterns in the *MFA2* promoter. Secondly, DNA within the two original Htz1 nucleosomes in the *MFA2* promoter is similarly sensitive to MNase in these two strains under normal growth condition. Thirdly, DNA within the two nucleosomes in these two strains has similar degrees of increased MNase sensitivity following UV irradiation (Figure 4.11). The same extra peaks and peak heights occur within the nucleosomes for the UV 1 hr and UV 2 hrs samples, irrespective of the presence of Htz1. Thus, deletion of *HTZ1* does not measurably change the accessibility of the nucleosomal DNA in the *MFA2* promoter, nor does it influence the kinetics of chromatin becoming more sensitive to MNase due to chromatin remodelling in this region following UV treatment. This MNase sensitivity and repair indicate that deletion of *HTZ1* reduces the efficiency in repair of CPDs in the Htz1-containing nucleosomes in the *MFA2* promoter without causing major detectable changes in chromatin accessibility both before and after UV treatment. This is similar to that in the *gcn5Δ* mutant that also exhibits reduced NER at the repressed *MFA2* gene (Yu et al., 2005a). In previous reports (Yu et al., 2011), Rad7 and Rad16 proteins were shown to mediate the increased occupancy of the histone acetyltransferase Gcn5 on the nucleosomes at the *MFA2* promoter following UV irradiation, and this leads to the histone hyperacetylation at H3 lysine 9 and 14 required for efficient repair of UV-induced CPDs (Yu et al., 2005a). This led me to suspect that if histone Htz1 affects repair, it could be related to histone acetylation which increases after UV. Acetylation of Htz1 at one or more sites at lysines 3, 8, 10, 14 is important for multiple functions of Htz1 (Mehta et al., 2010, Keogh et al., 2006, Millar et al., 2006).

However, my data in Chapter 3 indicate that acetylation at these sites plays no role in enabling more efficient NER genome-wide nor does it influence cell survival after UV. This finding is confirmed in this Chapter via analyses at the *MFA2* promoter. Others have also reported that point mutations at these sites do not recapitulate the sensitivity to the DNA damaging agent MMS that one sees with the *htz1Δ* mutant (Keogh et al., 2006). This indicates that when cells encounter DNA damaging agents, Htz1 has more functions in maintaining genome stability than those related to its N-terminal acetylation.

Interestingly, my ChIP results of H3 acetylation levels at *MFA2* and *HMRa1* indicate that Htz1 promotes histone H3 hyperacetylation in Htz1 nucleosomes in the *MFA2* promoter after UV irradiation. This finding coincides with a recent report which showed that H2A.Z nucleosomes in mammalian cells generally have higher histone acetylation levels on both H3 and H4 than H2A nucleosomes (Draker et al., 2012). This showed that Htz1 nucleosomes may inherently have a feature that can either promote or sustain higher levels of histone acetylation when needed. It should be noted that the *htz1Δ* mutant cells still managed a moderate increase in histone H3 acetylation level at the *MFA2* promoter following UV irradiation, unlike the *gcn5Δ* cells which only exhibit a minimal increase in histone H3 acetylation at this promoter (Yu et al., 2005a). This implies that Gcn5 is more important than is histone Htz1 in mediating this H3 acetylation. As Gcn5 is directly related with H3 acetylation via its transferases activity, Htz1 may have a more indirect correlation with H3 acetylation, or more specifically it may reduce but not negate Gcn5 occupancy.

The data provided in this thesis prove that these Htz1 nucleosomes display a unique feature in that Htz1 promotes the binding of Gcn5 to chromatin and consequently histone H3 hyperacetylation in these nucleosomes following UV, and this acetylation is required for efficient NER (Yu et al., 2005a). In order for NER to process DNA damage in repressive chromatin, for example, in the repressed *MFA2* promoter, NER proteins need to get access to DNA damage in chromatin. This may be facilitated by histone H3 acetylation and chromatin remodelling.

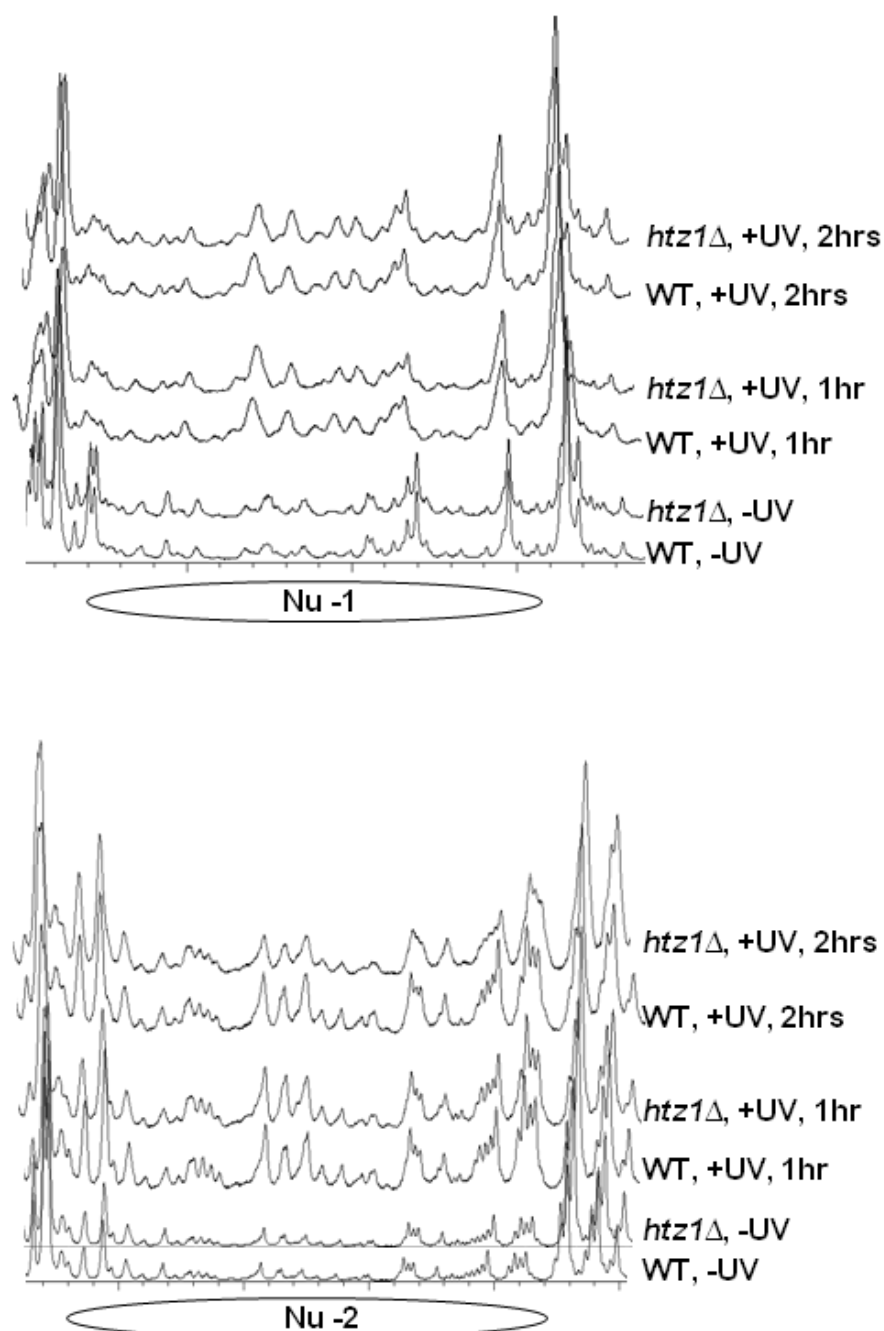


Figure 4.11 Deletion of *HTZ1* does not change the relative sensitivity of the nucleosomal DNA to MNase in the *MFA2* promoter. The graphs were obtained after scanning the lanes with 5 units of MNase in gels for the top and bottom strands of *MFA2*. The peaks indicate MNase sensitive sites, which increase in size and frequency after UV treatment but are not different between wild-type and the *htz1Δ* cells. This is a representative of at least three independent experiments (Yu et al., 2013).

My Rad14 binding data showed that deletion of *HTZ1* reduces the binding of Rad14 to damaged DNA by 50% following UV in the original Htz1 nucleosomes in the *MFA2* promoter, but not in the *HMRa1* locus where Htz1 is absent in wild type cells

with a functional *HTZ1* gene. This is an indication of a unique function of Htz1 in the nucleosomes in promoting the binding of an important repair protein, Rad14, to damaged DNA in the nucleosomes following UV. It directly coincides with the reduction in NER at *MFA2* in the absence of Htz1. Rad14 has a damaged DNA binding activity (Guzder et al., 1993), and there is no evidence so far indicating Rad14 interacts with histones. The presence of Htz1 may produce a favourable environment following UV. Histone Htz1 may render optimal level of histone H3 acetylation, to facilitate the enhanced binding of Rad14 to damaged DNA.

By performing the same analysis in the Htz1-containing nucleosomes at the *MFA2* promoter and the non-Htz1-containing nucleosomes in the *HMRA1* locus, my experiments revealed that this defect is directly related to the absence of Htz1 in the nucleosomes. This implicates intrinsic properties of Htz1 nucleosomes in facilitating more efficient NER in these nucleosomes in wild type cells. The positive functions of Htz1 nucleosomes influence NER in two ways. First, Htz1 promotes the occupancy of the histone acetyltransferase Gcn5 and therefore the UV-induced histone H3 acetylation in the Htz1-containing nucleosomes at *MFA2*. Second, Htz1 promotes the efficient binding of Rad14 to damaged DNA in the Htz1-bearing nucleosomes, thereby promoting NER following UV irradiation. These events are not mutually exclusive, and it is likely that the former enables the latter. Htz1 in the nucleosomes in this region promotes and maintains increased binding of Gcn5 to the nucleosomes, thus resulting in increased acetylation levels on histone H3 and enhance the recruitment of Rad14. This study has revealed an additional layer of information in chromatin at the *MFA2* promoter that cells use to regulate chromatin dynamics to ensure efficient DNA damage repair following UV irradiation.

In summary this chapter demonstrates that two regions, *MFA2* and *HMRA1* can be used as a model to explore how this histone variant influence NER. The next question is do these correlations pertain to other regions of the genome? To begin examining this in the next chapter I turned to microarray analyses of Htz1 occupancy before and after UV.

Chapter 5 The role of histone Htz1 in NER at genome-wide localization

5.1 Introduction

In Chapter 4, a positive role of the histone variant Htz1 in NER was observed when examining events at two yeast regions which respectively did or did not have Htz1 in the nucleosomes. In order to find out whether the results at *MFA2* and *HMRA1* also pertain to other regions in the yeast genome, I decided to embark upon a genome-wide study. Since the development of microarrays, second-generation sequencing and other high throughput technologies, genome-wide datasets are becoming more easily to achieve, and these datasets have raised genome-wide studies to new level. In this Chapter I employed a microarray approach to map the histone variant Htz1 throughout the entire yeast genome. This ChIP-on-chip technology is carried out by ChIP followed by hybridisation to microarrays. This has proven to be a technique for mapping the genome-wide localisation of a variety of features including protein-chromatin interactions (Venters et al., 2011), histones and histone modifications (Pokholok et al., 2005b) and direct DNA damage (Teng et al., 2010). There is also a wide variety of epitope tagged proteins available for genome-wide studies with *S. cerevisiae*, providing a database and a platform for correlative studies. My laboratory has already used this ChIP-on-chip technology to expand the histone H3 acetylation studies from those using *MFA2* as a model gene to a genome-wide scale. We also developed a genome-wide high resolution analysis of CPD induction and repair and employing the same microarrays (Waters et al., 2012, Teng et al., 2010). The ChIP-on-chip technology in this study allows one to investigate how the target protein bind throughout the entire genome. The concept and methodology of microarrays was first developed for antibody microarrays in 1983. This method is based on coated antibodies on a solid glass surface. After that the microarray studies moved to gene chip in the 1990's, and this technology of DNA microarrays has now become widely used. The first reported DNA microarray only contained 378 probes,

but with the development of technology, the resolution of DNA microarrays has increased significantly so as up to 2.1 million probes can be constructed on one array. Previously, ChIP on chip based experiments had generated genome-wide maps of nucleosome occupancy and histone modifications in yeast cells (Kurdistani and Grunstein, 2003, Pokholok et al., 2005a, Shivaswamy and Iyer, 2007). First, proteins are cross-linked to DNA in yeast cells, then cells are lysed and the crosslinked chromatin sonicated to fragments. Specific antibodies to the protein of interest are used to IP the sheared chromatin fragments. The cross-links between proteins and DNA are reversed and the DNA is purified and then amplified by PCR. In addition to the IP sample, for each experiment, an input DNA sample is taken from the sonicated chromatin before antibody immunoprecipitation and used as the reference sample. This Input DNA is purified and amplified as was the IP sample. The amplified IP and input samples are labelled respectively with different fluorescent dyes and hybridised to the microarrays.

Histone variant Htz1 is highly conserved during evolution and it has been implicated in many diverse biological processes, such as gene activation, chromosome segregation, heterochromatin silencing, and progression through the cell cycle. In order to understand how htz1 take part in these processes, several groups have investigated the genome-wide distribution of Htz1 in yeast (Zlatanova and Thakar, 2008).

From these studies, Htz1 has been found to resides within thousands of nucleosomes at different genomic loci throughout the yeast genome (Guillemette et al., 2005, Raisner et al., 2005, Zhang et al., 2005, Millar et al., 2006). A significant enrichment of Htz1 was found in promoter regions. More specifically, there is a Htz1 locus upstream of every ORF and intergenic regions that do not contain promoters are not enriched in Htz1. Intergenic regions between divergently transcribed genes contain two separable Htz1 loci. A very similar pattern was observed over a different region of the same chromosome. Guillemette estimated that about 75% of all Htz1 loci are within promoter regions of annotated genes. However, not all promoters are decorated

with Htz1: a significant portion of promoters (~37%) do not contain Htz1 (Guillemette et al., 2005). A similar distribution was also reported by another group (Raisner et al., 2005). These authors centered the genes represented in their data set on the nucleosome-free region (NFR) previously identified by genome-wide analysis of yeast promoters (Yuan et al., 2005). The NFR is a ~150 bp region without nucleosomes, it occurs at about 200 bp from the translation start site over relatively conserved nucleotide sequences that include transcription factor binding sites and multiple stretches of poly(A) or poly(T) (Yuan et al., 2005). RNA hybridization to the microarray revealed that 5' ends of transcripts coincided with NFR, identifying these regions as transcription start sites (TSSs). Raisner identified a profile in the chromatin regions surrounding the NFR and about two thirds of the genes had NRF the flanked by two nucleosomes that contain Htz1. The remainder of the genes appear either to have Htz1 present at only one nucleosome or lacked the variant altogether. The microarray data were precisely recapitulated by qPCR analysis of a specific region of Chromosome III. The genes that lacked Htz1 in their promoters correspond to genes in the HMLa silent cassette, genes near telomeres, uncertain ORFs, and euchromatin genes that may lie close to boundary elements. The Htz1-specific deposition complex SWR1 may be partly targeted to the promoter regions by acetylated histone tails (Kobor et al., 2004, Zhang et al., 2005). A more specific signal for Htz1 deposition may be provided by the NFR nucleotide sequence itself. In addition, no transcriptional activity is required for Htz1 enrichment. This suggest that Htz1 specifically marks promoter regions, independently of the transcriptional status of the linked gene. It should be mentioned that, despite the considerable attention to promoter enrichment, the transcribed genes also contain Htz1 nucleosomes (Zhang et al., 2005, Millar et al., 2006). The functional significance of these nucleosomes remains to be determined. A genome-wide study also found a relation between Htz1 K14ac and the location of Htz1. As Htz1 has shown a preferential association with promoters of repressed genes, its acetylated counterpart was enriched in promoters of active genes. The result suggest the Htz1 deposition may be regulated by its acetylation since the majority of

acetylation is seen at active promoters where nucleosomes are more relaxed (Millar et al., 2006).

Currently, Htz1 is mainly reported to have roles in transcription, double strand break repair and protecting euchromatin by prohibiting a heterochromatin spread at the boundary. The precise role of Htz1 in GGR is less well understood. I had previously found histone Htz1 to have a role in promoting efficient GGR at the *MFA2* promoter. I also found that the Htz1 level was reduced at the *MFA2* promoter region after UV irradiation. These observations on Htz1 occupancy pose a question as to whether Htz1 relocalises in response to UV, and is this reduction of Htz1 level related to promoting GG-NER?

In yeast an increase in histone H3 acetylation was observed after UV-irradiation at specific locations and also globally (Yu et al., 2005b). HATs catalyse the acetylation of histones and both HATs and HAT-containing complexes have been shown to have an involvement in NER to varying degrees (Brand et al., 2001, Guo et al., 2010, Martinez et al., 2001, Yu et al., 2005b). Furthermore, at the yeast repressed *MFA2* gene, UV-induced H3 acetylation was followed by chromatin remodelling (Yu et al., 2011, Yu et al., 2005b). Microarray analysis of H3 acetylation was undertaken by K. Evans in our group. The result revealed a positive role of H3 acetylation in GGR. The majority of the genome has higher H3 lysines 9 and 14 acetylation after UV. It has been previously found that the promoter regions are found to have a higher level of H3 lysine 9 and 14 acetylation than the ORF (K. Evans, PhD thesis 2011). The acetylation level was increased immediately after UV. This level reduces to the pre UV level as repair proceeds. Interestingly, although UV-treatment affects the level of histone H3 acetylation, the profile of H3 acetylation is similar in these datasets before and after UV irradiation. This indicates that the maintenance of an acetylation profile favourable for transcription events is important for the cell. The genome-wide mapping of H3 acetylation after UV suggests that histone H3 lysines 9 and 14 acetylation plays an important role in CPD repair.

The HAT Gcn5 has the ability to catalyse the acetylation of histone H3 lysines 9 and

14 and it has been implicated in facilitating efficient NER at *MFA2* (Yu et al., 2011, Yu et al., 2005b, Teng et al., 2002). Gcn5 can catalyse the acetylation of histone H3 at K9, K14, K18 and K23 and also at lysine residues on histone H2B and histone H4 (Suka et al., 2001, Zhang et al., 1998). Previous genome-wide studies showed that the acetylation of histone H3 K9 and K14 peaks at the transcription start sites of active genes and also correlates with the transcription rate genome wide. This suggest that there is a positive association between Gcn5, the K9 and K14 acetylation and transcription activity (Pokholok et al., 2005a). Deletion of *GCN5* significantly impaired but did not prevent the NER of CPDs at *MFA2* and in addition Gcn5 was responsible for catalysing the UV-induced H3 acetylation seen at this region (Yu et al., 2005b, Teng et al., 2002). Furthermore, the UV-induced H3 acetylation occurred independently of Rad14 and Rad4 but required the GG-NER proteins Rad7 and Rad16 (Teng et al., 2008a, Yu et al., 2011, Yu et al., 2005b). After UV-irradiation the occupancy of Gcn5 was found to increase at *MFA2* and again this increase in Gcn5 binding was found to depend on Rad16 (Yu et al., 2011). In response to UV, the DNA translocase and E3 ligase activities of Rad16 promote increased Gcn5 occupancy. This increase results in enhanced histone H3 acetylation and the subsequent chromatin remodelling observed at this region for efficient repair (Yu et al., 2011).

In this chapter I investigated the relationship between GGR and Htz1 DNA binding using the ChIP-on-chip method. The genome-wide localisation of histone Htz1 is mapped both before and after UV to investigate how changes in Htz1 binding may be related to promoting efficient GGR. In addition, both histone H3 lysines 9 and 14 acetylation and CPD repair are investigated at Htz1 occupancy peaks to see how CPD repair is organized in relation to Htz1 occupancy.

5.2 Materials and methods

Yeast strains

Strains	genotype	source
WT, BY4742	<i>MATα his3Δ1 leu2Δ0 lys2Δ0 ura3Δ0</i>	Euroscarf
<i>htz1Δ</i>	<i>MATα his3Δ1 leu2Δ0 lys2Δ0 ura3Δ0 <i>htz1:: KanMX4</i></i>	Euroscarf

For quantitative RT-PCR to validate microarray data:

Primer sequences

For nucleosome -1 of *MFA2*:

Forward: 5'- TGCATGTCAGAGGAAAAAGAACAAAG-3';

Reverse: 5'- CGGATGAACGACAGAAGAAGTGG-3';

For nucleosome 4 of *HMRa1*:

Forward: 5'- TTAGAAGAAAGCAAAGCCTT-3';

Reverse: 5'-GATTCTCATATTACATACCCAA-3';

Microarrays

In this study I used Agilent 4x44k Yeast Microarrays (G4493A) which have 60-mer (on average) oligonucleotides printed uniformly on them (Agilent 60-mer Sureprint technology). The features represent a part of the genome, with an average spatial resolution of a probe every ~290 nts. This offers a high resolution approach to analysing the entire yeast genome.

Other ChIP-on-chip datasets used in this study

The CPD repair and histone H3 lysine 9 and 14 acetylation and Gcn5 occupancy datasets used in this study were kindly provided by K. Evans and Y. Teng (K.Evans Phd thesis 2011, Teng et al., 2010).

5.2.1 ChIP-on-chip technology

ChIP samples were prepared for microarray analysis using a similar protocol to

that previously detailed (Chapter 4 materials and methods). This protocol consists of three main steps before scanning. First, IP chromatin containing DNA damage was repaired; second, DNA fragments were amplified using ligation mediated PCR; third, amplified input (IN) and immunoprecipitated (IP) DNA fragments are labelled by Cy5 and Cy3 dyes respectively and then combined for hybridising to microarrays.

1. ChIP experiments do not generate enough DNA for a microarray experiment. At least 1.5 μg of yeast genomic DNA is required for the labelling step. After ChIP the DNA yield is undetectable on an agarose gel and this is insufficient for the experiment. Therefore an amplification step is needed. A pair of IP DNA fragments and IN DNA fragments from one sample are needed for generating a single dataset. Following the ChIP protocol, 40 μl of IP sample or 1 μl of IN sample was diluted with water to a total volume of 40 μl . DNA damage within each sample was repaired using the PreCR repair mix (New England Biolabs). To each sample 10 μl of repair mix was added and this was incubated for 20 minutes at 37 $^{\circ}\text{C}$ in a water bath. Repaired DNA was purified into 50 μl Elution buffer by the QIAquick PCR purification kit (Qiagen).

Repair mix for one reaction:

dNTP (10mM)	0.5 μl
10xThermoPol buffer	5 μl
100xNAD ⁺	0.5 μl
PreCR repair mix	1 μl
Water	3 μl
Total	10 μl

2. To each sample 70 μl of blunt end mix was added and this was incubated for 20 minutes at 12 $^{\circ}\text{C}$ in a water bath. Following this incubation, 11.5 μl of 3M NaAc (pH5.2) and 0.5 μl glycogen (20mg/ml) were added and mixed by pipetting. Then 120 μl of phenol:chloroform:isoamyl alcohol 25:24:1 (10mM Tris, pH8.0, 1mM EDTA) was added and mixed on a vortex, and subsequently centrifuged at 13000 rpm

for 5 minutes in an Eppendorf centrifuge 5415D. The upper phase (approximately 120 μ l) of each sample was transferred to a new 1.5 μ l eppendorf tube and DNA was precipitated with 230 μ l of absolute ethanol following by centrifugation at 13000 rpm for 15 minutes at 4 °C in a Beckman Coulter Microfuge 22R. The supernatant was removed and the pellet was washed with 500 μ l of 75% ethanol and centrifuged as before for 5 minutes. Following this the wash was discarded and pellets were dried for 10 minutes in an ISS110 SpeedVac system (ThermoSavant) on the medium setting.

Blunt end mix for one reaction:

T4 DNA polymerase buffer	11 μ l
BSA (10mg/ml)	0.5 μ l
dNTP (10mM)	1 μ l
T4 DNA polymerase (NEB #M0203S)	0.2 μ l
Water	57.8 μ l
Total	70 μ l

3. Pellets were resuspended in 25 μ l of water to which 25 μ l of ligation mix was added and left overnight at 16 °C in a water bath.

Ligation mix for one reaction:

DNA ligase buffer	5 μ l
Linker hybrid DNA	6.7 μ l
T4 DNA ligase (NEB #M0202S)	0.5 μ l
Water	13 μ l
Total	25 μ l

4. In the morning 6 μ l of NaAC (3M) was added to each sample. Add 130 μ l of cold ethanol to each sample and to precipitate DNA put at -20⁰C for 1h. Samples were centrifuged at 13000 rpm for 15 min at 4⁰C to pellet the DNA. The DNA pellets are small and can hardly be seen by eye. Therefore the supernatant is carefully removed by pipetting from the other side to avoid touching the pellet. The pellet was washed

with 500 μ l of 75% ethanol and centrifuged in a microfuge for a further 5 min. After removing the supernatant, pellets were resuspended in 25 μ l of water and 15 μ l of PCR mix A was added and transferred to 0.5ml PCR tubes. Each sample was heated in a PCR block for 2 minutes at 55 $^{\circ}$ C (PTC-200 PCR machine (MJ Research)), after which 10 μ l of PCR mix B was added. PCR was performed with the conditions as shown below.

PCR mix A for one reaction:

5xHF Buffer (New England)	8 μ l
dNTP (10mM)	1.25 μ l
Oligo 102 (40 μ M)	1.25 μ l
Water	4.5 μ l
Total	15 μ l

PCR mix B for one reaction:

5xHF Buffer (New England)	2 μ l
Phusion DNA polymerase (New England M0530S)	1 μ l
Water	7 μ l
Total	10 μ l

PCR conditions:

1. 55.0 $^{\circ}$ C for 2:00 minutes
2. 72.0 $^{\circ}$ C for 3:00 minutes
3. 98.0 $^{\circ}$ C for 1:00 minutes
4. 55.0 $^{\circ}$ C for 0:30 minutes
5. 72.0 $^{\circ}$ C for 1:00 minutes
6. Go to 3. 15 times
7. 72.0 $^{\circ}$ C for 5:00 minutes
8. End

5. Following the PCR reaction, 450 μ l of water was added to each sample and it was checked with the Nanodrop 1000 spectrophotometer (ThermoScientific). A second

PCR amplification was performed with 5µl of the diluted DNA in combination with 45µl of PCR mix 2 and using the following PCR conditions.

PCR conditions:

1. 98.0 °C for 1:00 minutes
2. 55.0 °C for 0:30 minutes
3. 72.0 °C for 1:00 minutes
4. Go to 3. 25 times
5. 72.0 °C for 5:00 minutes
6. End

PCR mix 2 for one reaction:

5xHF Buffer (New England)	10 µl
NTP (10mM)	1.25 µl
Oligo 102 (40µM)	1.25 µl
Phusion DNA polymerase (New England M0530S)	0.5 µl
Water	32 µl
Total	45 µl

6. These PCR reactions were precipitated with the addition of 25 µl of Ammonium Acetate (7.5 M) and 225 µl of chilled ethanol to each sample and incubation at -20°C overnight. Alternatively, incubation can take place at -80°C for 20 min. After precipitation the DNA was pelleted with centrifugation for 15 min at 13000 rpm for 15 min. The DNA pellet was washed with 75% ethanol and re-suspended in 12 µl of water and the DNA concentration was quantified using a Nanodrop 1000 spectrophotometer (ThermoScientific). DNA concentrations were adjusted to 150ng/µl with water.

7. DNA was labelled using the BioPrime total genomic labelling system (Invitrogen) by combining the following:

Labelling reaction for one reaction:

DNA sample in water (150ng/μl)	10.5 μl
EDTA (5mM)	2.5 μl
Alexa Fluor Cy3 or Cy5 reaction mix	15 μl
Water	10 μl
Total	22 μl

Typically IP samples were labelled with Cy5 and input samples were labelled with Cy3. Reaction mixes were incubated at 95 °C for 5 minutes in a PCR block (PTC-200 PCR machine (MJ Research)). Each sample was subsequently put on ice for 5 minutes and 2μl of Exo-Klenow fragment was added. Samples were returned to the PCR block at 37 °C for 3 hours.

8. Labelled DNA was purified to 52μl buffer E1 using Invitrogen DNA purification kit columns according to the manufacturer's protocol. Purified DNA was measured using the Nanodrop 1000 spectrophotometer (ThermoScientific).

9. Corresponding IP and input samples were combined to give a total solution volume of 100μl. To the mixed solution add 12 μl of NaAc (3 M), 5 μl of Polyacrylamide (2.5 μg/ml) and 290 μl of chilled ethanol and put at -20⁰C overnight. The next day, the DNA was pelleted with centrifugation at 13000 rpm for 15 min at 4⁰C and washed once with 75% ethanol and dissolved in 39 μl of H₂O.

10. Pellets were dissolved in 39μl of water, and to each sample the following were added in order:

for one reaction:

Human Cot-1 DNA (1.0mg/ml) (Invitrogen)	5 μl
10x Blocking agent (Agilent)	11 μl
2x Hybridisation buffer (Agilent)	55 μl

11. Samples were mixed and heated at 95 °C for 3 minutes in a PCR block. Following

this, samples were immediately transferred to another PCR block at 37 °C and incubated for 30 minutes.

12. Each 110µl sample was loaded onto one of four arrays on a yeast whole genome ChIP-on-chip microarray 4x44K (Agilent, #G4493A). Slides were transferred to an Agilent Hybridization oven (G2545A) set at 65 °C and the maximal rotation speed (20) and left to incubate for ~24 hours.

13. Following hybridisation, the array was washed for 5 min in Washing buffer 1 (300 ml of 20 x SSPE, 250 µl of 20% Sarcosine and 700 ml of H₂O) , followed by a 5 min wash in pre heated Washing buffer 2 (3 ml of 20 x SSPE and 997 ml of H₂O) at 30 °C. After the wash, carefully take out the array from Washing buffer 2 with no drops remaining on the array. Now the array is ready for scanning.

14. The microarrays were scanned with an Agilent microarray scanner (G2505B, Agilent technologies) according to the manufacturer's instructions with the following settings:

Scan region	61 x 21.6 mm
Scan resolution	5µm
5µm scanning mode	Single pass
eXtended dynamic range	Selected
Dye channel	Red & Green
Green PMT	XDR Hi 100%, XDR Lo 10%
Red PMT	XDR Hi 100%, XDR Lo10%

This process creates a TIFF image file.

15. Features were extracted from the TIFF files of the scanned slides with Agilent's Feature Extraction software (version 10.10.1.1) and the protocol ChIP_1010_Sep10 according to the manufacturer's instructions. Data were exported as a tab delimited

text file (.tab). Data under the column titles 'Row', 'Col', 'ProbeUID', 'ControlType', 'ProbeName', 'GeneName', 'SystematicName', 'Description', 'rBGSubSignal' and 'gBGSubSignal' were extracted from the text files. 'gBGSubSignal' represents the quantification of Cy3 labelled DNA hybridisation, which is referred to as the 'Green channel' or G. 'rBGSubSignal' represents the quantification of Cy5 labelled DNA hybridisation, which is referred to as the 'Red channel' or R. Data were imported into the statistical open source software language 'R' (M. Bennett PhD thesis CU 2012) and all subsequent data analysis was performed in R using custom scripts written by Mark Bennett (PhD thesis CU 2012). The binding profile for ChIP-on-chip experiments was calculated as $\log_2(R/G)$.

5.3 Results

5.3.1 Normalisation of data

The microarray data of the Htz1 occupancy profile were calculated in 'R' by dividing the background subtracted red channel (IP) by the background subtracted green channel (input) data values. All data were extracted by the Agilent extraction software from the Tif image of the microarray. The microarray raw data cannot be used directly for analysis because of the experimental bias introduced by this particular technique between biological repeats, and the biological differences of the DNA samples. Data normalization aims to maintain biological differences of repeats and render different array datasets comparable.

My microarray datasets were normalised using a Mark Bennett normalization script. This normalization is carried out in three different steps.

(1) Redundant probes which including probes for mitochondrial DNA and deleted genes (markers) were removed from datasets prior to data analysis. This step is applied to every microarray dataset before going on to next step of normalization.

After this step all the datasets contain the same quantity values for probes.

(2) Quantile normalisation (M. Bennett PhD thesis CU 2012) was performed between biological replicates, but was not performed across datasets. Quantile normalisation

involves imposing the same distributions of intensities on each biological repeat and maintains biologically relevant changes between these. This corrects for non-linear systematic error which may be introduced from sources such as the differential PCR efficiency of DNA.

(3) Pseudo-modal shift was used to centre the estimated background region on zero. All datasets were shifted such that the modal value of enrichment was centred at 0. After this adjustment the pseudo-means for each dataset is shifted and lies on zero in the density plots. The estimated background subpopulation is then scaled to the standard normal distribution, so that it is the same across all datasets. This step equalise the background between different datasets, so as different datasets are comparable to each other .

The density plot in Figure 5.1 shows the result of normalising the three Htz1 occupancy datasets without UV. The raw data are Plotted in Figure 5.1 (A) and the normalised data is plotted in Figure 5.1 (B).

After normalisation, the scatter graphs (Figure 5.3) and snapshot of genome plots (Figure 5.2) show that the datasets of Htz1 were highly reproducible between biological replicates. The mean of these three biological replicates was used for further analysis and investigation. Data for the entire genome are provided in the disc in the appendix.

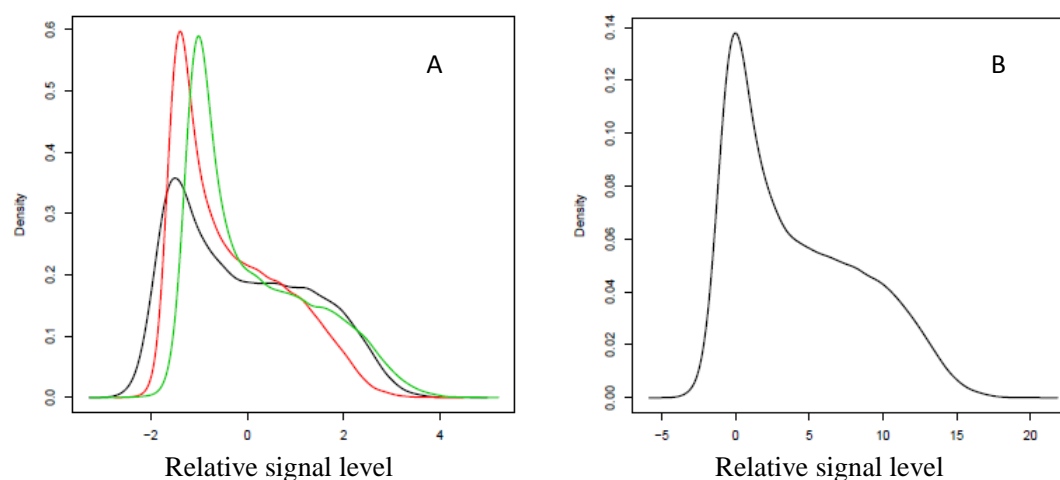


Figure 5.1 Raw data versus normalised data in density plots. (A) Different colours represent 3 different biological repeats (replicate 1, black, replicate 2, red, replicate 3, green). (B) after normalization, three biological repeats share the same density plot.

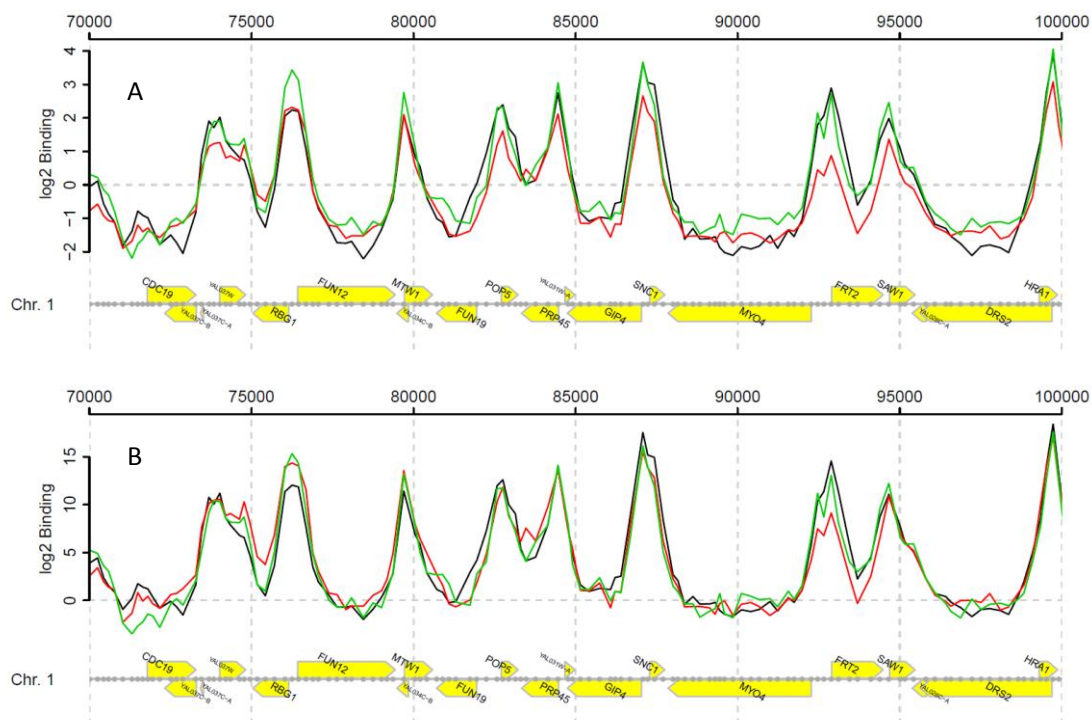


Figure 5.2 Raw data versus normalised data in genome plots-a snapshot of chromosome 1. Different colours represent 3 different biological repeats (replicate 1, black, replicate 2, red, replicate 3, green). A represents raw data while B represents data after normalization.

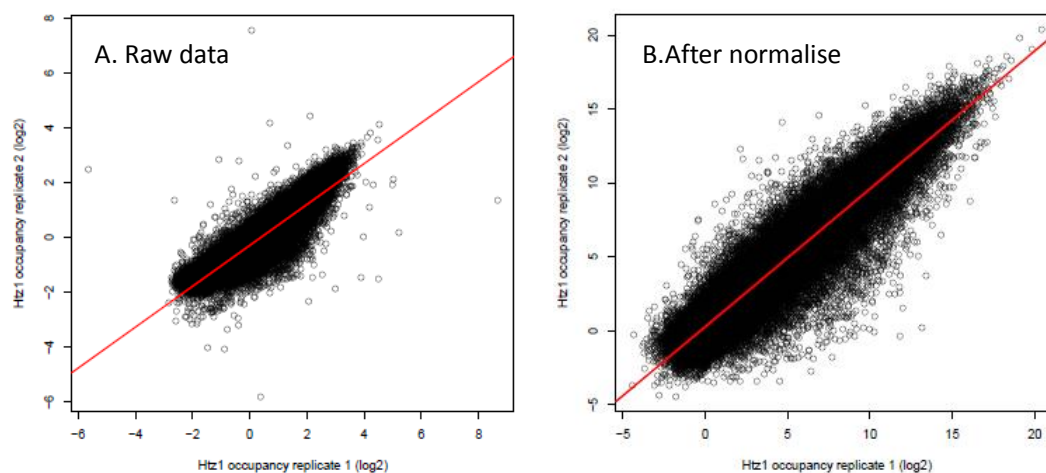


Figure 5.3 Raw data versus normalised data in scatter plots. Two biological replicates before (A) and after (B) normalisation.

5.3.2 The validation of the histone Htz1 occupancy microarray data

Before analysing the ChIP-on-chip results I decided to validate the microarray data. This validation was carried out in two ways. First I compared the Htz1 microarray dataset with the control datasets. Second, I compared the microarray data to the

quantitative PCR results of different loci.

In order to validate the Htz1 occupancy microarray data, I also analysed a sample extracted from *htz1Δ* cells as a control. The same chromatin preparation and chromatin immunoprecipitation steps were applied to this sample. In *htz1Δ* cells, no histone Htz1 could be detected as the *HTZ1* gene has been removed. A snapshot of the genome plot in Figure 5.4 have shows the differences between a normalised data of Htz1 occupancy without UV in wild type cells (black curve) and *htz1Δ* cells (red curve). The data from *htz1Δ* cells shows a background level of noise when compared to the data from wild type cells. Note that the y axis scale is log2 which means that the binding peak value of Htz1 in wild type cells is more than 1000-fold higher than the background level data from *htz1Δ* cells. This pattern is not restricted to this region, it is consistent and can be found throughout the whole genome plot. This result demonstrated that the ChIP-on-chip technology I employed has generated Htz1 binding peaks across the whole yeast genome, which reflect Htz1 location. The dataset for the entire genome can be found on the disc provided as part of the appendix.

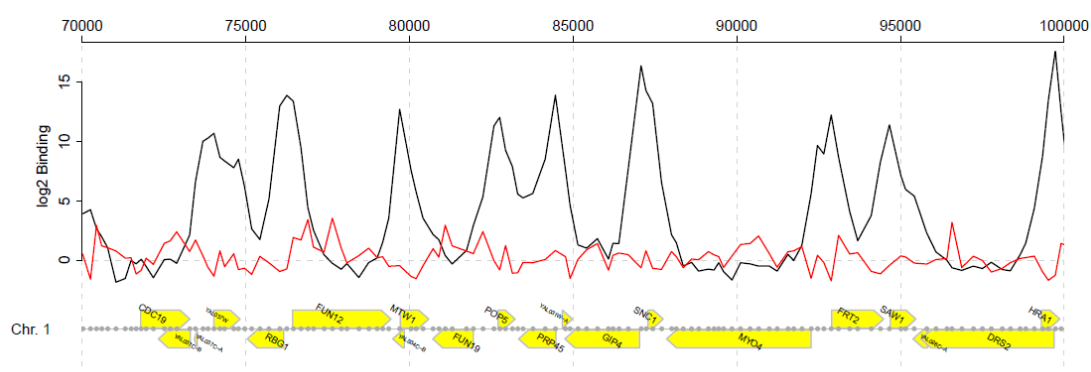


Figure 5.4 Htz1 occupancy in wild type versus in *htz1Δ* cells: a snapshot of chromosome 1. Wild type in black, *htz1Δ* in red.

I also employed the two regions that I had studied in Chapter 4, namely the *MFA2* promoter region where Htz1 resides and the *HMRa1* coding region where there is no Htz1 occupancy. The IP and input sample used in this quantitative PCR experiment were taken from the sample I put on the array. The protocol for chromatin sample preparation and the quantitative PCR methodology were described in Chapter 4

Materials and Methods. For the quantitative PCR data, the starting quantity of DNA was determined by use of a standard curve. For the microarray data, the values are determined by the relative fluorescence intensity value of each particular probe. To render the results in each experiment comparable, the value of IP divided by Input was calculated to generate a relative level for each experiment.

The results comparing the relative fold changes in unirradiated and UV treated cells by qRT-PCR and microarrays are shown side by side in Figure 5.5. Both the qPCR and microarray data indicate the same pattern of Htz1 occupancy. There is a loss of Htz1 occupancy after UV in the both quantitative PCR experiments and microarray analysis, and the patterns are the same in both circumstances.

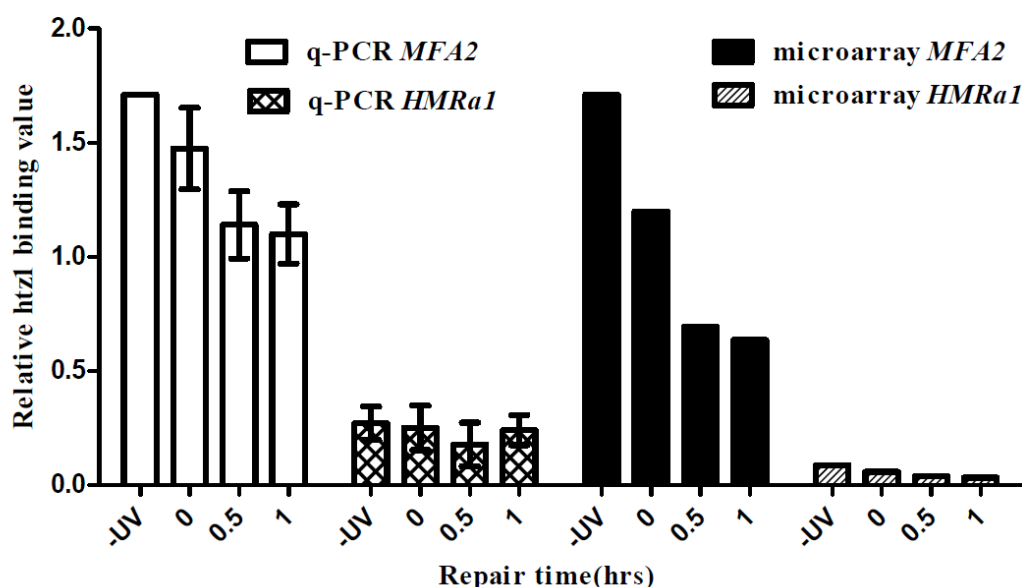


Figure 5.5 Htz1 occupancy data before and after UV at different regions: a q-PCR/microarray comparison. The microarray data were compared to quantitative PCR data at the *MFA2* promoter region and the *HMRA1* coding region. 4 different time points before and after UV are represented in this comparison. For quantitative PCR, each bar represents the average values \pm SD of three biological repeats. Data are the average of three independent experiments \pm SD. The microarray data are normalized from three repeats.

5.3.3 Investigating the histone Htz1 binding peaks without UV

As I described in the introduction, a former histone Htz1 microarray study had found that Htz1 is preferentially located in the promoter regions as opposed to the coding

regions. In Figure 5.6, I have plotted my genome-wide Htz1 occupancy data using this profile plot function. This plot basically shows the average Htz1 occupancy values along all of the genes. Clearly, the level of Htz1 is higher in the promoter and downstream regions and lower in the coding region throughout the whole genome. This result is consistent with the published Htz1 data (Zhang et al., 2005). As a control, the Htz1 binding level in *htz1Δ* cells shows the background binding level in the promoter, the coding and downstream regions.

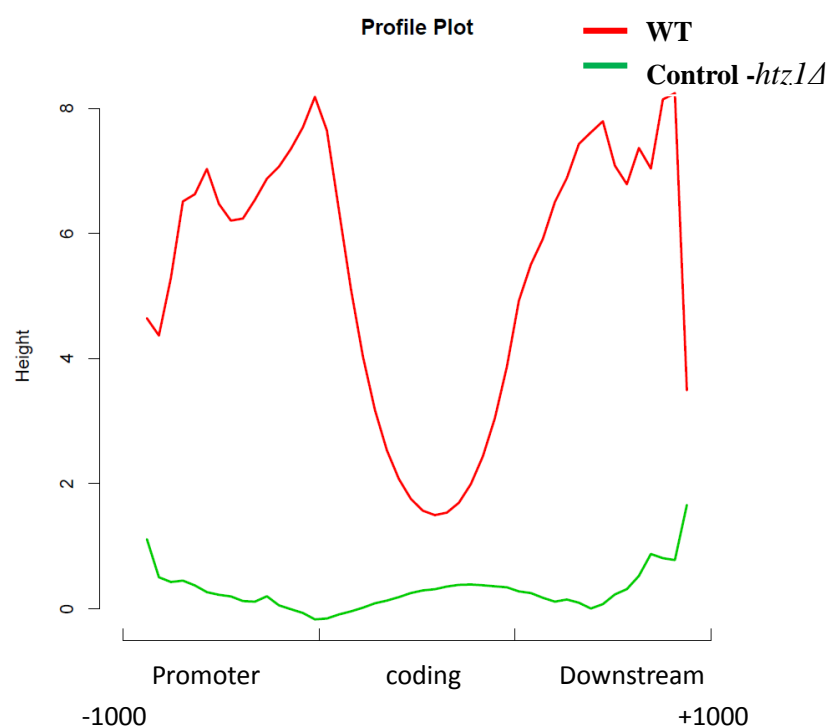


Figure 5.6 A gene profile plot of the histone Htz1: wild type versus *htz1Δ*

In this profile plot, Htz1 occupancy in the wild type strain (red) and *htz1Δ* cells (green) are plotted at all genes. Both trend lines represent the average Htz1 level at thousands of genes.

After validating the histone Htz1 microarray data, and in order to investigate genome-wide Htz1 occupancy I used the peak detection function in R software which was developed by Mark Bennett (PhD thesis CU 2012). This peak detection method can identify peaks from genome plots by scanning through the data on a constant window size (equivalent to the sheared chromatin size). All the probe values in each given window are calculated, and the highest value in each window is recognized as a

peak. After the data of all windows have been assigned, the average binding values of each window are analysed to validate real peaks. This peak detection is applied to other datasets I used in this chapter.

5363 statistically significant Htz1 binding peaks were identified in the Htz1 datasets without UV. The Htz1 peaks positions are listed in Table 5.1 below. For the histone Htz1 binding peaks 55.3% are found in the intergenic region and about 44.7% peaks are allocated to the intragenic regions. On the microarrays, there are more probes allocated in the intragenic regions than the intergenic regions. About 73% of the total probes evenly cover the intragenic regions within the whole genome. Considering this, Htz1 will be located more than three times more in the intergenic regions when compared to the intragenic regions.

Table 5.1

Location of Htz1 occupancy peaks

Htz1 peak position	Number of peaks	% of peaks	% of probes on arrays	Ratios
Intragenic	2396	44.7	73	0.61
Intergenic	2967	55.3	27	2.04
-Promoter	2095	39.1	14	2.79
-Downstream	872	16.3	5	3.25
-Divergent	1382	25.8	8	3.22
Total	5363	100	100	1

5.3.4 Investigating histone Htz1 binding peaks before and After UV irradiation

To investigate the genome-wide localization of Htz1 in response to UV damage, the same peak detection as described above was performed on datasets of cells sampled 2 hour after UV.

As for the no UV datasets, three biological repeats of data from cells 2-hour after UV were generated and normalized. Statistically significant Htz1 binding peaks were identified in the U and 2-hour datasets to give 5363 and 5944 peaks respectively. The position plots shown in Figure 5.7 indicate the distribution of all the peaks on each gene location. Clearly, the majority of the peaks were found adjacent to the intragenic regions, and were either at the promoter region or the downstream regions in both unirradiated (U) and the 2-hour post UV datasets. Density plots and the percentage of

peaks allocated to regions in both the U (no UV) and 2-hour datasets show a similar result.

This investigation shows that the binding pattern of histone Htz1 does not rapidly changed after UV irradiation, although that about 10% more peaks were detect in the 2-hour post UV samples when compared to the U datasets (Figure 5.8). This could be the result of increased histone Htz1 occupancy or it being relocalised to regions that are different from the peaks in the U datasets as a response to UV. On other hand, due to the high resolution of the microarrays, these peaks may also be the result of a single probe shifting off peak on the microarray or some redundant detections in low enrichment regions. In these circumstances, rather than representing a genuine re-localisation of Htz1 occupancy, these peaks just represent the error of the system. Further validation is needed to eliminate these errors.

The majority of these Htz1 binding peaks overlap between the no UV and the after UV datasets. I carefully examined the Htz1 occupancy for the whole genome and the chromosomal maps demonstrate that Htz1 does not relocalise after UV irradiation. Apart from the overlapping peaks, identical peaks still hold 22.8% and 30.34% of the total peaks of U and 2-hour datasets respectively (Table 5.2). Further investigation was undertaken to validate the discrepancy between these non-overlapping peaks.

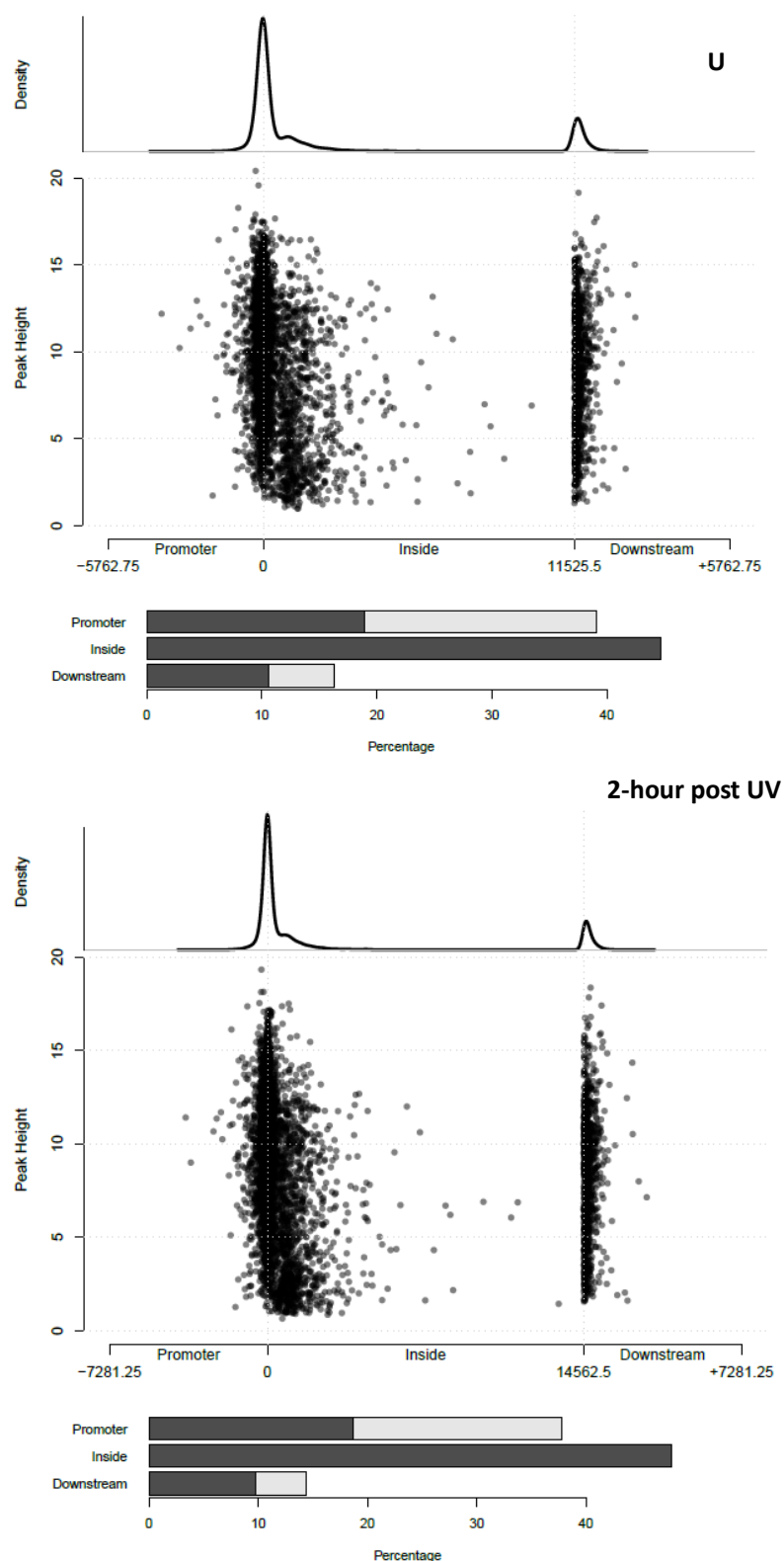


Figure 5.7 Position plot of peaks in unirradiated and 2-hour post UV datasets

Position plot showed the position of peaks on the each gene. The bar chart represent the percentage of peaks in different regions. Grey bars represent the portions of divergent promoter regions and divergent downstream regions.

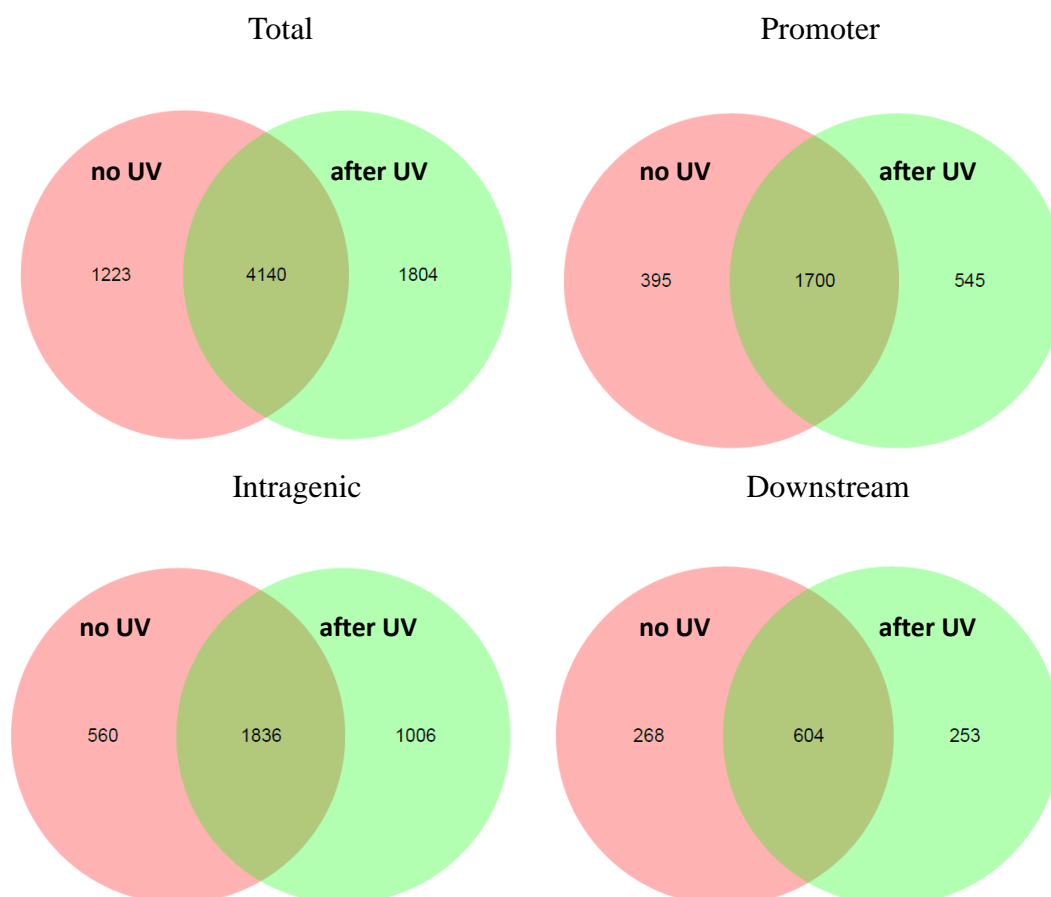


Figure 5.8 Venn diagrams of peak overlaps: no UV versus 2-hour after UV

These Venn diagrams show the result of comparing the Htz1 peaks detected without UV and 2 hours after UV. The diagram shows total peak overlap and the overlap in different regions between the two datasets.

Table 5.2

Htz1 peak position	U peaks	2-hour peaks	Overlap peaks	% of U peaks	% of 2-hour peaks
Total	5363	5944	4140	77.20	69.65
-Promoter	2095	2245	1700	81.15	75.72
-Inside	2396	2842	1836	76.63	64.60
-Downstream	872	857	604	69.27	70.48

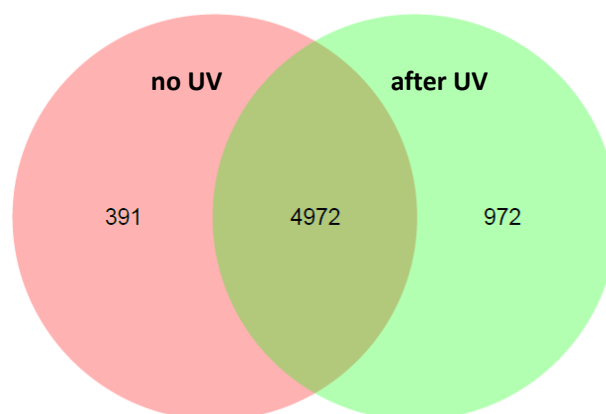


Figure 5.9 Venn diagrams of peak overlaps: no UV versus 2-hours after UV

These Venn diagrams show the result of comparing Htz1 peaks (excluding the shift by one probe issue) detected without UV and 2-hours after UV. The diagram shows total peak overlap.

Due to the high resolution of the microarrays, the shift between one probe in the peak position is likely to be within the error of the system. Those non-overlap probes which are within one probe distance in location is likely due to system error rather than representing a localisation of Htz1 binding. To exclude these false non-overlapping peaks, I filtering non-overlapping peaks by discounting those that had shifted by one probe. After that 832 more peaks were found to be actually overlapping which means 93.7% of the peaks pre UV were found after UV. As there are 391 peaks pre UV (972 peaks after UV) still not overlap (Figure 5.9). To investigate these non-overlapping peaks, I compared the value of these peaks with the value from the same place but from the other datasets (Figure 5.10). Results show that these peaks are either from quite low binding level area, or these peak values correlate quite well between datasets which means they are actual identical peaks. To confirm this, I carefully checked the whole genome plot which highlights these unique peak regions. Results shown in Figure 5.11 are a snap shot and clearly show that these peaks are identical. The same phenomenon can be found for all of these unique peaks throughout the genome (whole genome plot is provided in the appendix disc).

Therefore, the localisation of Htz1 binding is the same before and after UV irradiation.

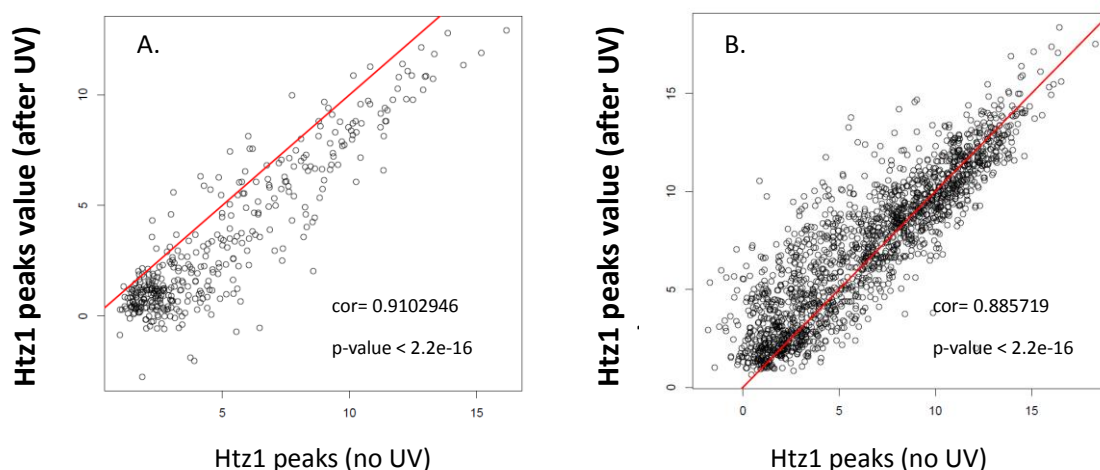


Figure 5.10 Non-overlapping peak value correlation in scatter plots

(A) 391 peaks unique in dataset before UV (B) 972 peaks unique in dataset after UV. Trend line in red. Pearson correlations were employed to investigate correlations.

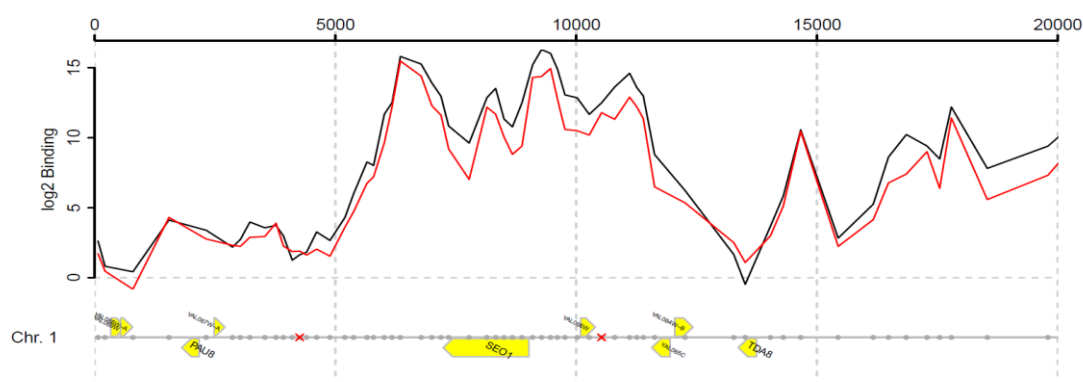


Figure 5.11 Htz1 occupancy in wild type versus in *htz1Δ* cells in genome plot with highlight peaks. Wild type in black, *htz1Δ* in red. Red cross represent the unique peaks location.

5.3.5 UV dependent changes in Htz1 occupancy

The analysis above illustrated that the majority of the Htz1 binding peaks are identical in unirradiated datasets and the post UV 2-hour datasets. This means that majority of Htz1 occupancy location is the same before and after UV irradiation. Histone Htz1 has already been reported to preferentially occupy the promoter to ORF regions. I observed that the Htz1 level peaks in the intergenic region and this peak is raised from the edges of the ORF boundary. This suggests Htz1 preferentially binds chromatin at intergenic regions. Upon analysis of the genome-wide chromosomal plots it was

apparent that a peak of Htz1 binding can be observed upstream of nearly every promoter region. However, statistically significant binding peaks are only identified at 39.1% of the yeast promoters in the no UV datasets. From unirradiated cells the peaks of Htz1 occupancy at low binding level regions could be missed by the peak detection function. Therefore I tested the profile plot of these lower htz1 binding data regions. The results showed that the Htz1 level also goes up slightly in the intergenic region. This confirmed that the Htz1 occupancy pattern still corresponds to the same preferential localisation as seen with statistically significant peaks of Htz1 binding. As the occupancy pattern of Htz1 is unchanged before and after UV, I moved on to investigate the Htz1 level changes before and after UV irradiation. First I used the gene profile plot function in Figure 5.12 which represents the actual average Htz1 occupancy value for all genes.

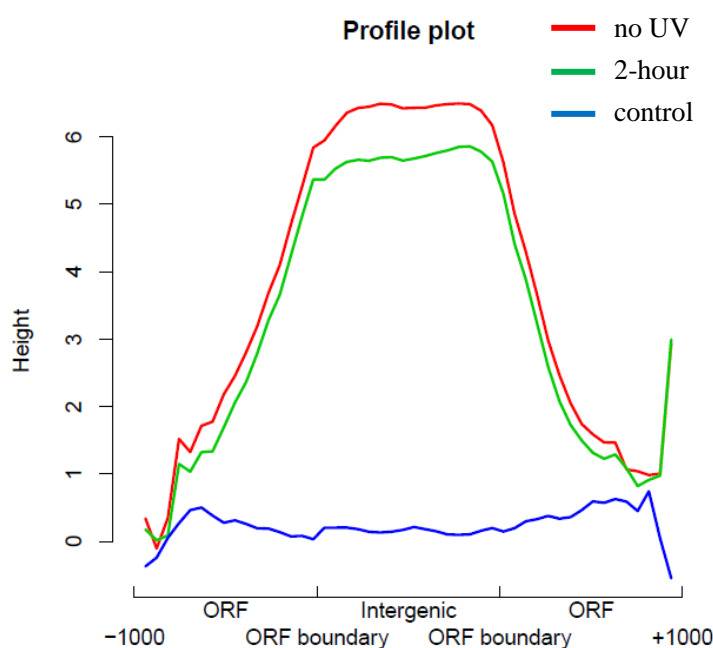


Figure 5.12. A gene profile plot of histone Htz1 occupancy before and after UV

In this profile plot, Htz1 occupancy without UV (red) and 2-hours after UV (green) and in *htz1Δ* cells (blue) are plotted together at all intergenic and ORF regions. These three trend lines represent the average Htz1 level at thousands of genes.

When comparing the Htz1 levels in the datasets from unirradiated cells with those from the post UV 2-hour datasets, the binding level of Htz1 is significantly reduced in the intergenic region but not in the ORF region. This result is consistent with the quantitative PCR data which I had previously provided for the *MFA2* promoter. As the scale in the microarray datasets is log₂, the gene profile plot shows that, in the intergenic regions, the average 2-hour binding level of Htz1 is reduced to about half that of the value in datasets from unirradiated cells. These data corresponded to my previous quantitative PCR results showing that about 50% of the pre-UV histone Htz1 level was observed at the *MFA2* promoter at the 2-hour post UV sample. For the ORF region, a distinguishable reduction of Htz1 level can also be constantly observed. This reduction is not as abundant as in the intergenic region.

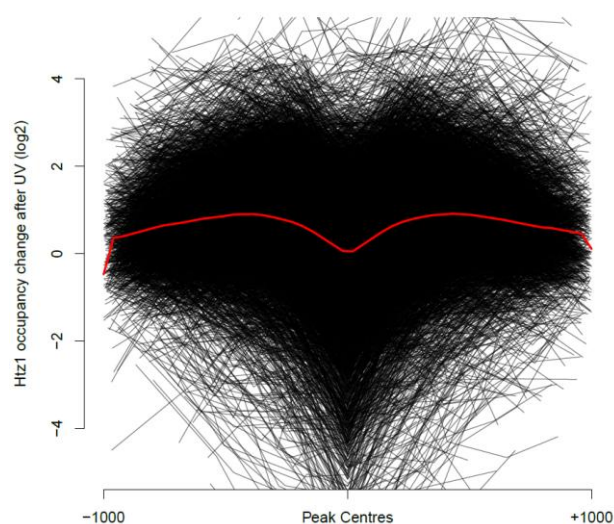


Figure 5.13 Histone Htz1 level changes after UV at Htz1 binding peaks in the profile plots. Taking regions of 2kb, here are plotted the changes after UV in Htz1 occupancy throughout the genome. The centre of this plot colocalises at Htz1 binding peaks defined in cells before UV. This plot is repeated and superimposed for each of the Htz1 binding peaks.

Interestingly, the plot (Figure 5.13) of the UV induced Htz1 occupancy level change at the Htz1 peaks show that the reduced Htz1 level is not right at the peak centres, but occurs at either side of the original Htz1 binding peaks. The trend line shows that the average binding value at peak centers is about 0. A similar result was seen when I

divided the datasets into promoter regions, open reading frame regions and downstream regions. This suggests that the peak height before and after UV remains at a similar value, and that after UV there is a reduced histone Htz1 occupancy either side of the original Htz1 peak sites.

5.3.6 Histone Htz1 occupancy and CPD repair

In Chapter 3 and 4, I found that the lack of histone Htz1 could affect efficient GGR in both total DNA and at specific regions. In order to investigate the relationship between histone Htz1 and GGR at a genome-wide scale I employed the datasets generated through a microarray based method which was developed by our laboratory to determine the relative CPD repair throughout the entire yeast genome. I used these data to investigate if there was any relationship between histone Htz1 and CPD repair. The high correlation between the predicted and experimentally established profile of CPD incidence demonstrates that this method provides accurate information of the presence of CPD damage and repair throughout the genome (Teng et al., 2010).

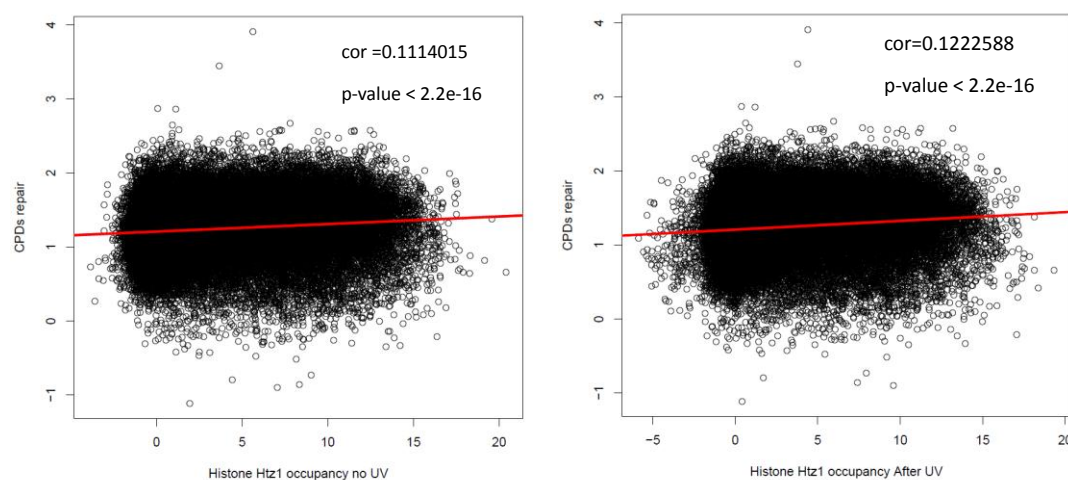


Figure 5.14 Histone Htz1 occupancy versus CPD repair in scatter plot

This Scatter plot show histone Htz1 (x-axis) versus 2-hour CPD repair (y-axis) of each 4*44k probe value. 41450 single spots are plotted on each diagram, after calculation the trend line (red) is plotted to represent the trend of all these spots. A Pearson correlation test is undertaken to calculate the correlation between each datasets.

Scatterplots of the histone Htz1 data versus the CPD repair show the comparative values of each probe between these two different datasets (Figure 5.14). Overall the correlation between histone Htz1 occupancy (no UV and and post UV 2hour) and CPD repair is about 0.1 (Pearson correlation), and a Pearson correlation analysis does not identify a correlation between Htz1 occupancy changes after UV and efficient CPD repair.

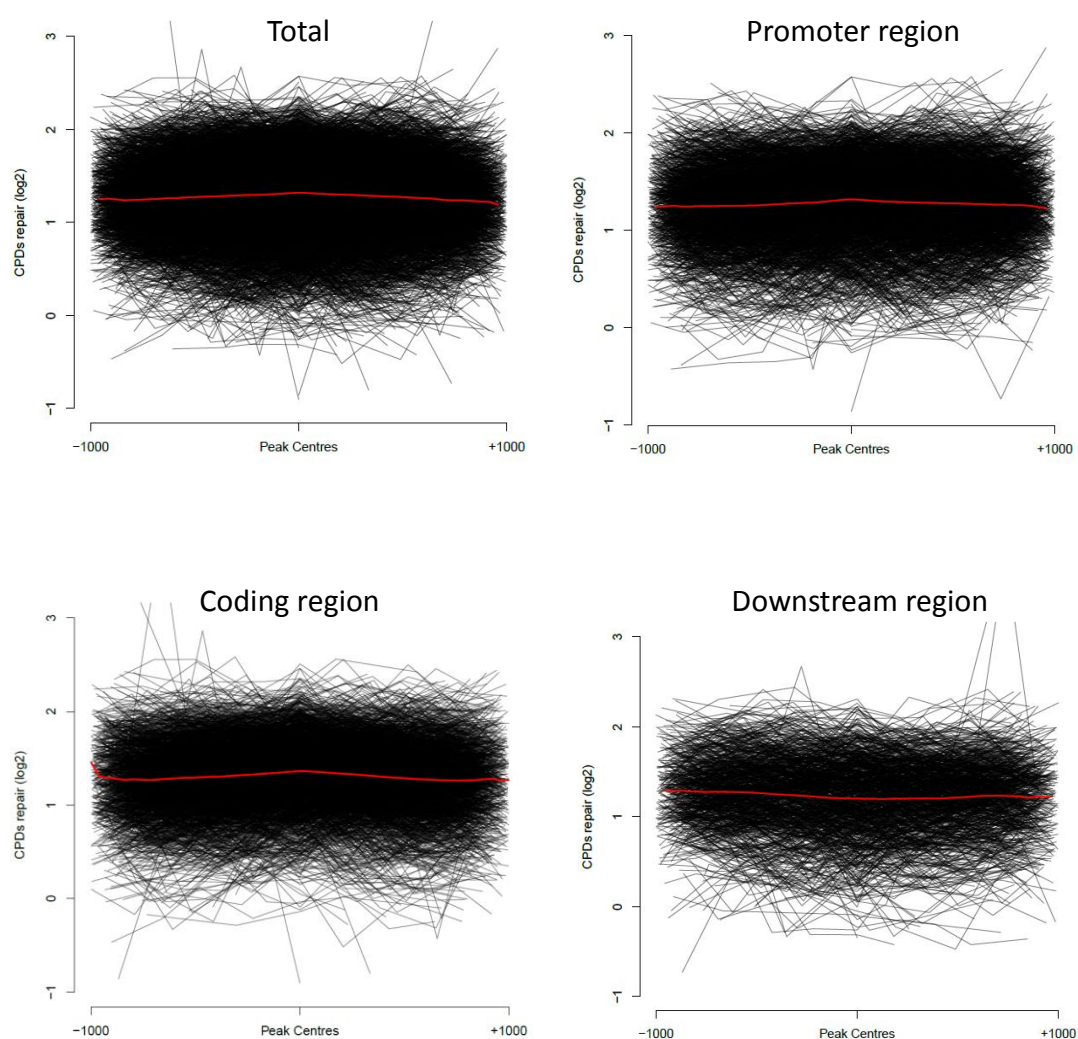


Figure 5.15 CPD repair data at Htz1 occupancy peaks in profile plots

Taking regions of 2kb, here are plotted the CPD repair after UV in Htz1 peaks throughout the genome. The centre of this plot colocalises at Htz1 binding peaks defined in cells before UV. This plot is repeated and superimposed for each of the 5636 Htz1 binding peaks.

After investigating the correlation of Htz1 occupancy to CPD repair, I expanded my

analysis to investigate how CPD repair relates to Htz1 binding sites. A plot function is used to generate the trend lines for the CPD repair at the 5636 Htz1 binding peaks. This plot (Figure 5.15) show a result consistent with the scatter plot I generated earlier in Figure 5.14; it shows that there is a very low but noticeable relationship between Htz1 occupancy and CPD repair. After dividing these data into different regions, this correlation can only be observed in the promoter regions and the coding regions, but not in the downstream regions. This result suggests that Htz1 occupancy correlates to CPD repair only in the promoter and coding regions.

5.3.7 Investigating histone H3 lysines 9 and 14 hyperacetylation at Htz1 binding peaks

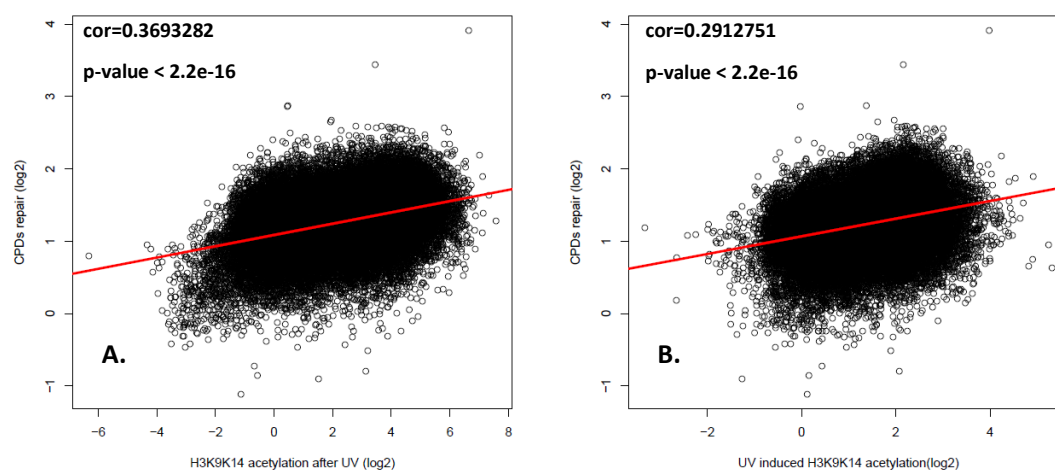


Figure 5.16 Scatter plots of CPD repair versus H3 lysines 9 and 14 acetylation

These diagrams plot histone H3 lysines 9 and 14 acetylation (x-axis) versus CPD induction or repair (y-axis) at each of the 4*44k probes. (A) represents total H3 lysines 9 and 14 acetylation after UV versus CPD repair. (B) represents UV induced H3 lysines 9 and 14 acetylation vs CPD repair.

We had previously reported that UV induced H3 hyperacetylation at lysines 9 and 14 enables efficient GGR at the repressed *MFA2* promoter (Yu et al., 2005a). Using microarray technology, we mapped the genome-wide UV response of histone H3 lysines 9 and 14 acetylation and CPDs induction and repair (K. Evans PhD thesis CU 2011, Y.Teng, unpublished data,). These results have thus expanded the investigation

of the relationship between H3 hyperacetylation and efficient GGR from specific gene regions such as *MFA2* to a genome-wide level. The scatter plot results in Figure 5.16 show no positive correlation between CPD induction and H3 lysines 9 and 14 acetylation before UV or to UV induced H3 lysines 9 and 14 acetylation. However a clear positive correlation was observed between CPD repair and both the acetylation after UV and UV induced H3 lysines 9 and 14 acetylation. These data suggest that the higher CPD repair can normally be found in the regions with pre UV higher H3 lysines 9 and 14 acetylation levels or higher UV induced acetylation levels. In Chapter 4 I described how the histone variant Htz1 has a positive role in promoting H3 lysines 9 and 14 acetylation at *MFA2* which contained histone Htz1 in its local chromatin environment. Here, I investigated if this finding applies to the entire genome.

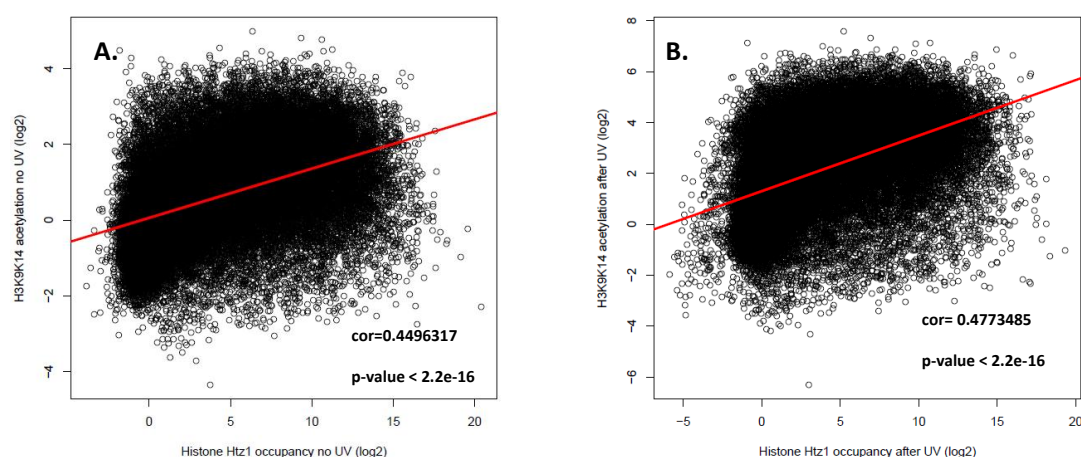
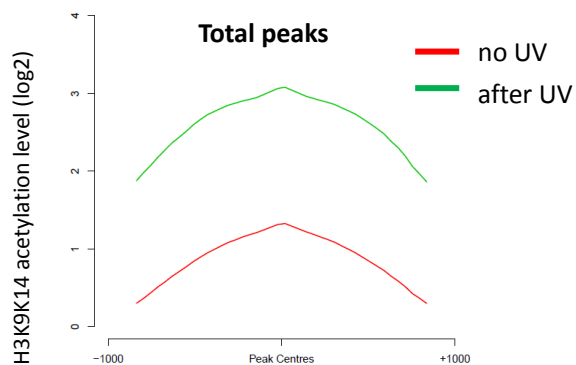


Figure 5.17. Scatter plots of histone Htz1 occupancy versus H3 lysines 9 and 14 acetylation. These diagrams plot histone Htz1 value (x-axis) versus H3 lysines 9 and 14 acetylation value (y-axis) at each of the 4*44k probes. (A) represents the datasets without UV (B) represents datasets after UV.

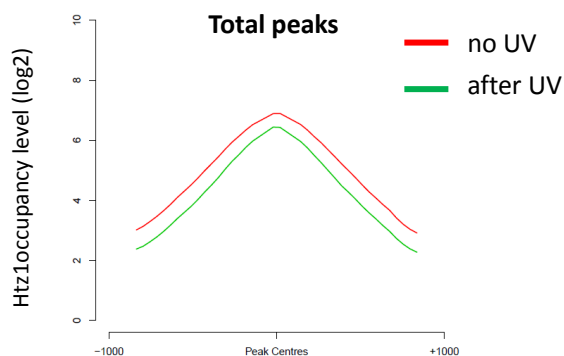
To address this question, I first plotted a comparison between the genome-wide Htz1 occupancy and H3 lysines 9 and 14 acetylation using a scatterplot function (Figure 5.17). A positive correlation between histone variant Htz1 occupancy and histone H3 lysines 9 and 14 acetylation was established both before and after UV. The Pearson correlation value of these before and after UV is 0.44 and 0.47 respectively. This

result shows that the co-localisation of H3 acetylation and histone Htz1 can be expanded from specific regions like the *MFA2* promoter to the whole- genome.

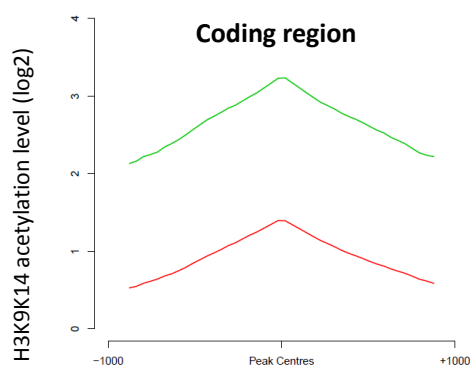
To further investigate how histone H3 lysines 9 and 14 acetylation is organised at Htz1 occupancy sites, profile plots of the acetylation data were plotted in relation to previously detected Htz1 binding peaks, both before and after UV irradiation. Conversely, Htz1 occupancy data were plotted in relation to the detected H3 lysines 9 and 14 acetylation peaks both before and after UV irradiation. From Figure 5.18, the trend line of H3 lysines 9 and 14 acetylation data plotted for all of the Htz1 occupancy peaks shows an increase at the Htz1 peak centre before and after UV. Further investigation revealed that this increase is primarily in coding and promoter regions, but less so in downstream regions. The coding regions contain the narrowest peak of the trend lines amongst the different regions, and this means that the acetylation peaks in these regions are the most likely to co-localize at the Htz1 peak sites. A significant increase of H3 lysines 9 and 14 levels has been observed after UV, and a similar increased level occurred for all the different regions. On the plots on the right hand side, the trend lines for before and after UV show a consistent Htz1 occupancy peak at the H3 lysines 9 and 14 acetylation peak centre, both in total peaks and in the different groups of peaks. This suggest that for every H3 lysines 9 and 14 acetylation peak in the genome there is Htz1 occupancy. However, this phenomenon does not exist for every Htz1 peak. This as a indicating that Htz1 has a role in the upstream regulation of this H3 lysines 9 and 14 acetylation. There is a slight reduction of Htz1 levels after UV irradiation, and this reduction is similar in all of the different groups of peaks, yet the trend line before and after UV retains the same pattern. The narrowest trend line peak of Htz1 occupancy is allocated to the promoter regions which are is also the most abundantly Htz1 occupied regions.



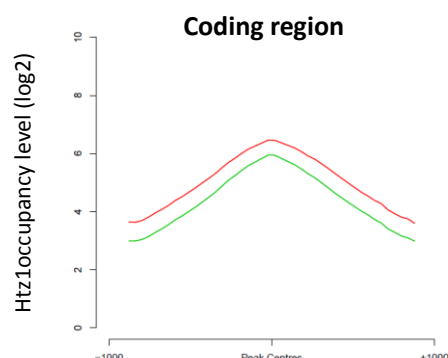
Distance from Htz1 peaks (nucleotides)



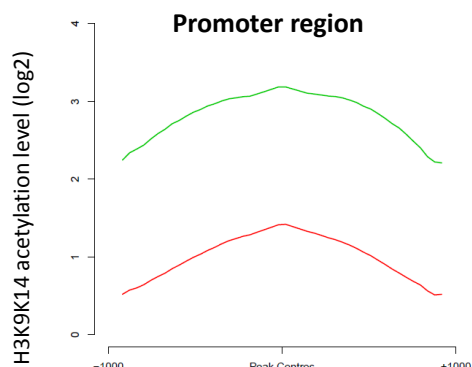
Distance from H3K9K14ac peaks (nucleotides)



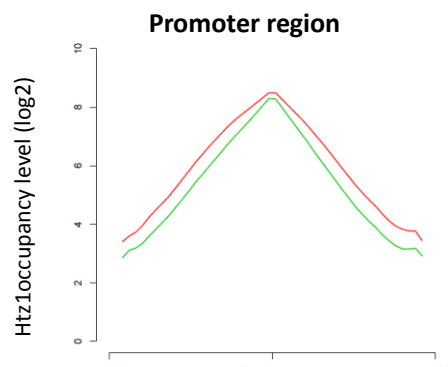
Distance from Htz1 peaks (nucleotides)



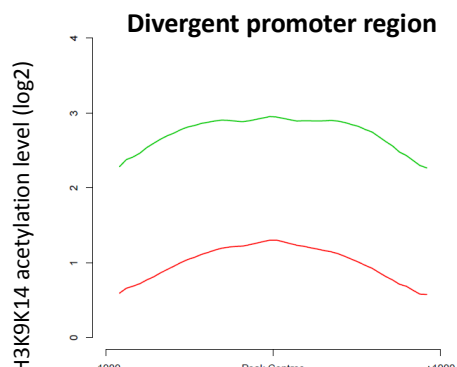
Distance from H3K9K14ac peaks (nucleotides)



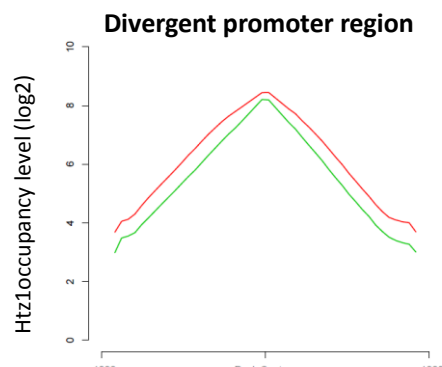
Distance from Htz1 peaks (nucleotides)



Distance from H3K9K14ac peaks (nucleotides)



Distance from Htz1 peaks (nucleotides)



Distance from H3K9K14ac peaks (nucleotides)

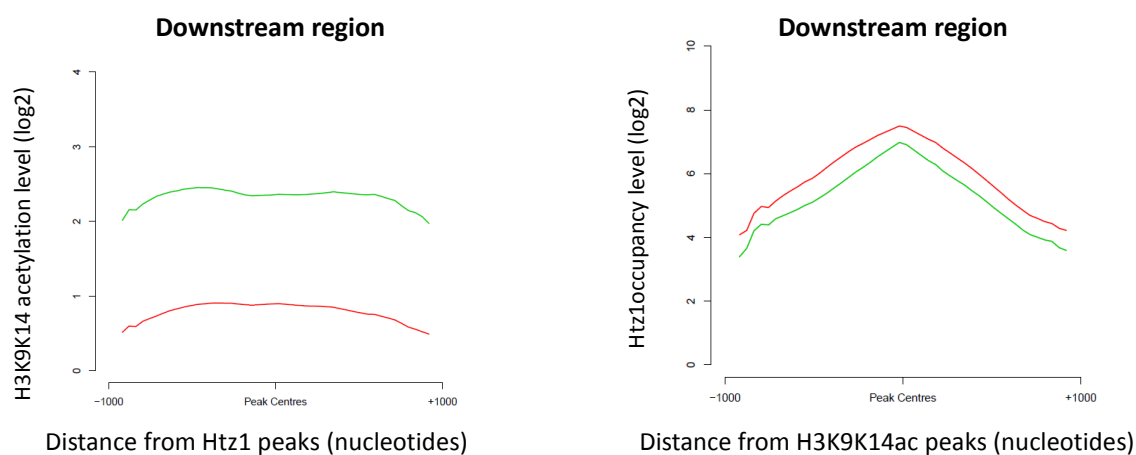
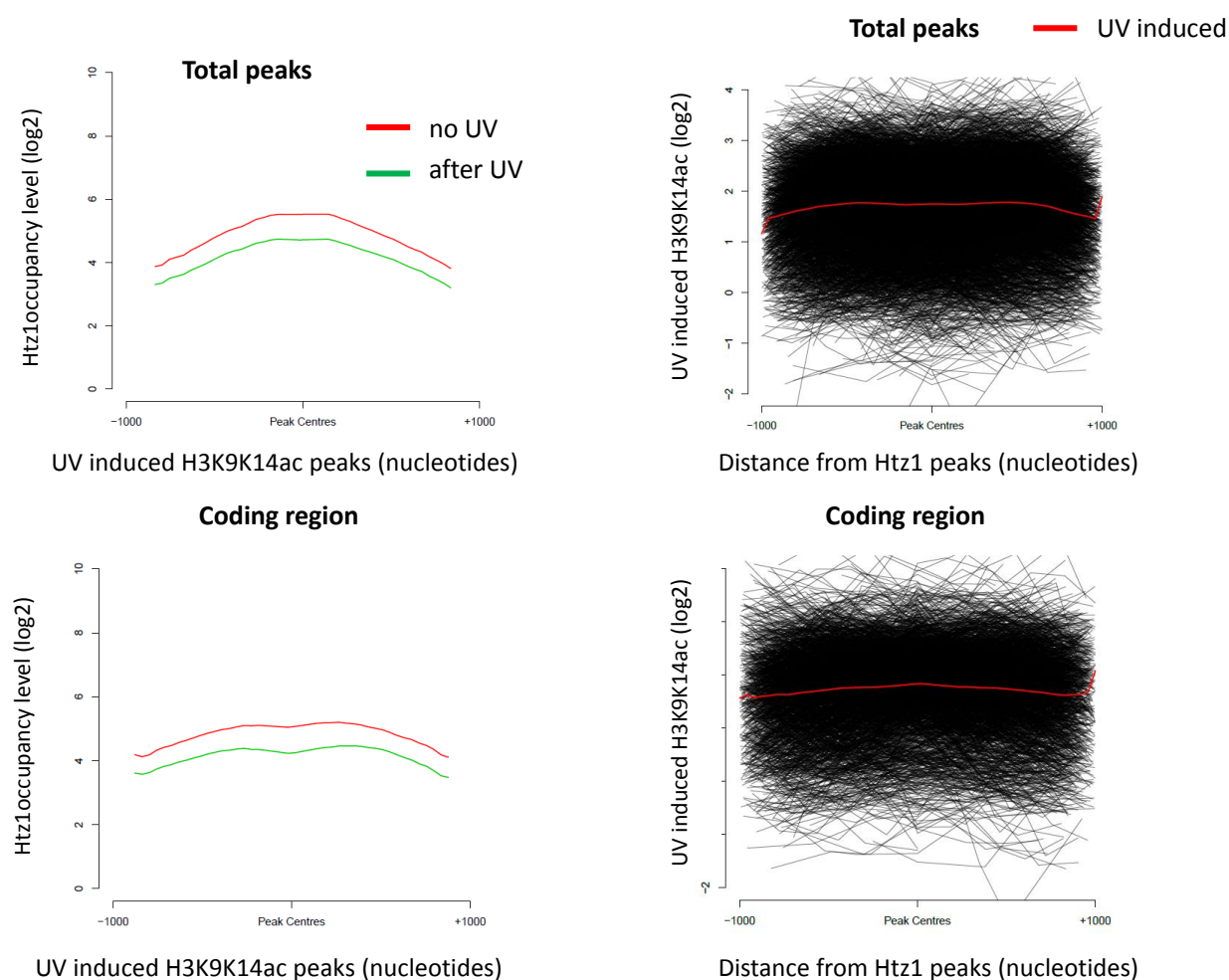


Figure 5.18 Profile plots of H3 lysines 9 and 14 acetylation and Htz1 occupancy at each other's peaks. Composite profiles of histone H3 lysines 9 and 14 acetylation data both before UV (red line) and after UV irradiation (green line) at Htz1 binding peaks are on the left. Composite profiles of Htz1 occupancy both before UV (red line) and after UV irradiation (green line) at H3 lysines 9 and 14 acetylation binding peaks are on the right. Only the trend line of each plot is shown.



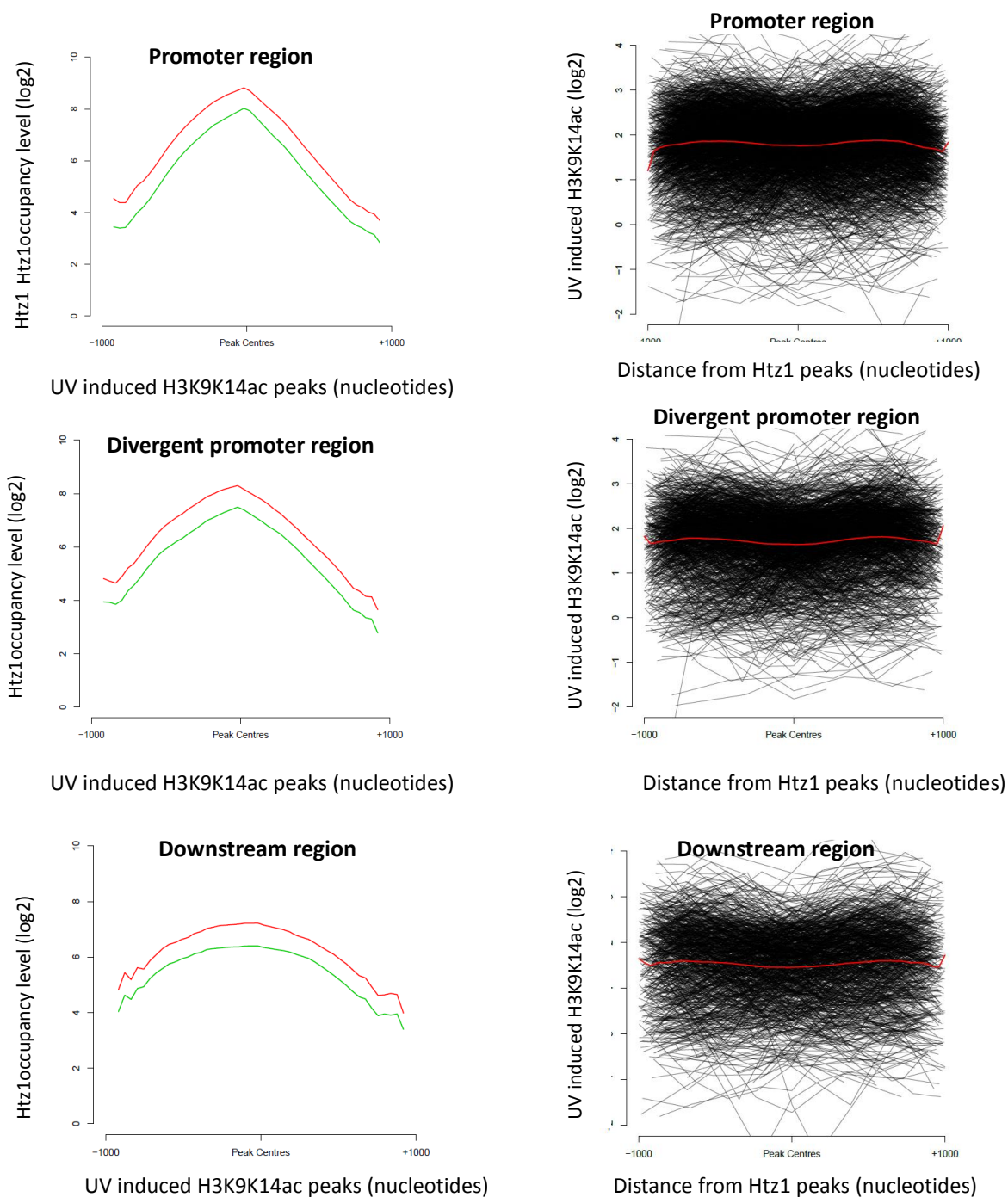


Figure 5.19 Profile plots of UV induced H3 lysines 9 and 14 acetylation and Htz1 occupancy at each other's peaks. Composite profiles of UV induced H3 lysines 9 and 14 acetylation data (red lines) at Htz1 binding peaks are on the right. Composite profiles of Htz1 occupancy both before UV (red lines) and after UV irradiation (green line) at H3 lysines 9 and 14 acetylation binding peaks are on the left. These data are first plotted for all the peaks, then plotted in 4 different groups of peaks for different types of regions. Only the trend line of each plot is shown.

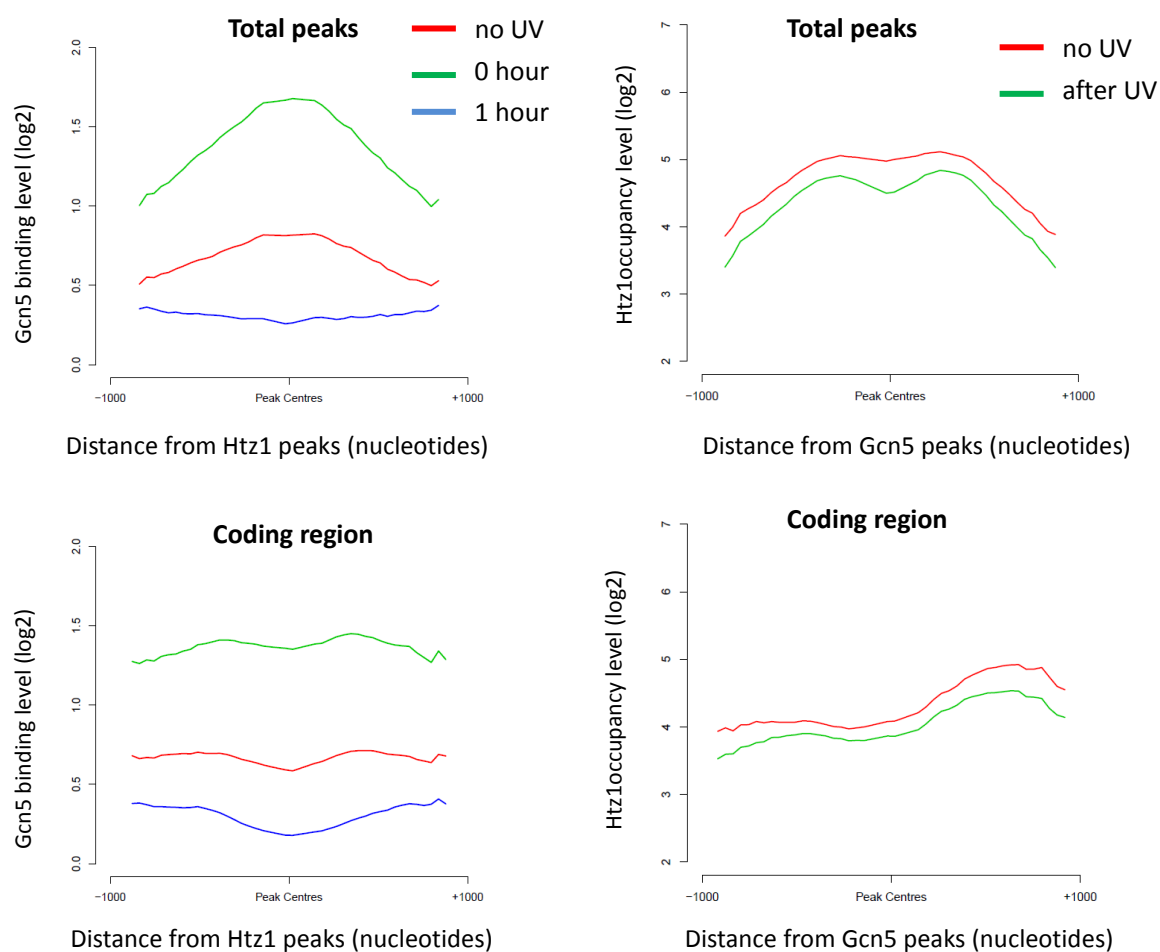
As the UV induced H3 lysines 9 and 14 acetylation has a positive correlation with CPD repair and this was observed all over the genome, I decided to investigate how this change related to Htz1 (Figure 5.19). These profile plots on the right show that UV induced H3 lysines 9 and 14 acetylation does not exhibit a significant increase at the Htz1 occupancy sites overall, or at different groups of peaks. However, Htz1 levels represent a relative increase at the UV induced H3 lysines 9 and 14 acetylation peaks and this increase is mainly in the promoter regions. This result suggests histone Htz1 has a positive role in regulating this UV induced H3 lysines 9 and 14 acetylation primarily at promoter regions.

5.3.8 Investigating Gcn5 at Htz1 binding peaks

After investigating the relationship between histone H3 lysines 9 and 14 acetylation and the histone variant Htz1, my study went on to study how Htz1 could impact on this acetylation. Previously, we had uncovered a role of the HAT Gcn5 in NER (Teng et al., 2002). This UV-induced H3 acetylation is widespread throughout the genome and the majority appears to be catalysed by Gcn5 (K. Evans PhD thesis CU 2011). Deletion of the *GCN5* gene results in almost no change in the H3 lysines 9 and 14 acetylation after UV-irradiation. Gcn5 appears to bind to discrete locations. Although Gcn5 binding has a general correlation with gene expression, the UV-induced Gcn5 binding observed in the genome are independent of gene expression changes. Therefore the UV induced changes are likely primarily related to repair events. Microarray studies on Gcn5 have revealed that Gcn5 moves away from its pre-UV binding locations immediately after UV in order to catalyse the UV-induced H3 acetylation. The majority of identified Gcn5 binding peaks are in the same location when CPDs remain regardless of the post UV repair time. The genome-wide Gcn5 level reaches its highest level at 0 hour post UV and is then reduced to a significantly lower levels during repair. This results in fewer peaks being identified in the 1 h repair samples compared to the earlier repair times (K. Evans PhD thesis CU 2011). In this study, I used the 0 hour Gcn5 peaks to represent the location of Gcn5 genome-wide.

Previously in Chapter 4, Gcn5 levels decreased at the *MFA2* promoter in *htz1Δ* cells before and after UV. Hence here, my study investigated the genome-wide data to determine the relationship between Htz1 occupancy and Gcn5 binding patterns before and after UV.

After employing a Pearson correlation function to test these data, no positive or negative Pearson correlations were found between Htz1 occupancy and Gcn5 occupancy both before and after UV irradiation.



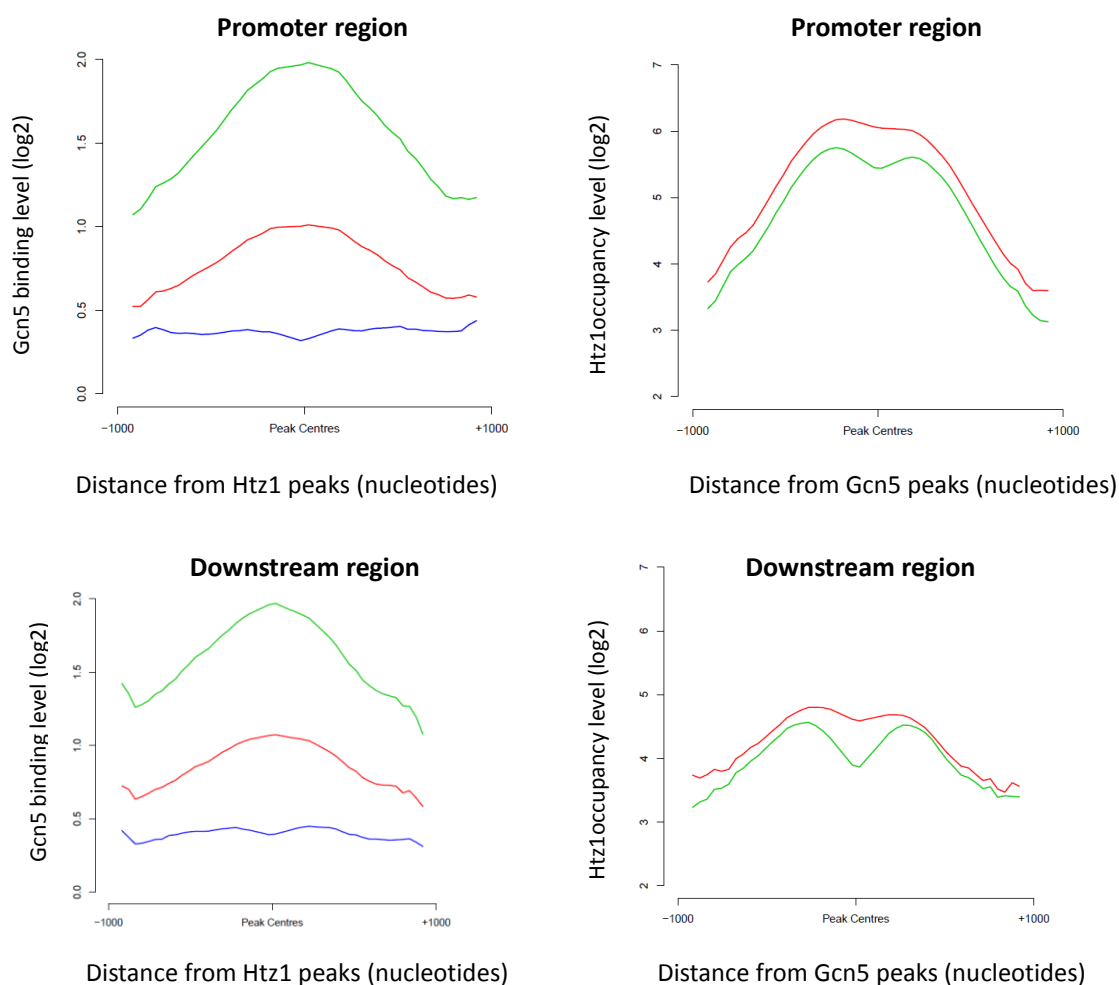


Figure 5.20 Profile plots of Gcn5 binding and Htz1 occupancy at each other's peaks. Composite profiles of Gcn5 data (no UV-red, UV 0 hour-green, UV 1 hour-blue) at Htz1 binding peaks are on the left. Composite profiles of Htz1 occupancy both before UV (red line) and after UV irradiation (green line) at Gcn5 binding peaks are on the right. Data were plotted as total Htz1 peaks in the first row. Data are divided into 3 different group by region are plotted below. Only the trend line of each plot is shown.

Although no Pearson correlation occurred, the composite profiles plots in Figure 5.20 show there is an association between Htz1 and Gcn5. In both the Htz1 and Gcn5 datasets, the genome plots show significant peaks and the majority of the peaks depicted in the datasets before and after UV are identical. This allowed me to perform composite profiles on each dataset and to see if they co-localized at the same genomic loci. The result show that these is a clear Gcn5 peak at Htz1 peaks and these peaks are consistent with the way genome-wide Gcn5 level changes in response to UV. These

Gcn5 peaks can only be observed in promoter and downstream regions but not in the coding regions. The Htz1 occupancy trend line also show peaks at Gcn5 peaks, these peaks are quite wide and suggests that Htz1 may occur proximal to the Gcn5 binding sites. Interestingly, these peaks are also only observed in promoter regions and downstream regions but not in the coding regions.

I also plotted the Htz1 data on UV induced Gcn5 peaks in Figure 5.21. This shows a peak at either side of the Gcn5 binding peak centre. This suggested that Htz1 can be found near the UV induced Gcn5 binding locations. As UV induced Gcn5 peaks are concomitant with the original Gcn5 peaks, this result confirmed that Htz1 occupancy and Gcn5 binding sites are related. These findings, along with the reduced Gcn5 binding in *htz1Δ* at Htz1 containing regions, suggest that lack of Htz1 affects the genome-wide Gcn5 levels and co-localization of Htz1 and Gcn5 occurs at regions apart from the intragenic ones. A reduced Gcn5 level will directly affect H3 lysines 9 and 14 acetylation efficiency and result in a slow repair at these regions genome-wide.

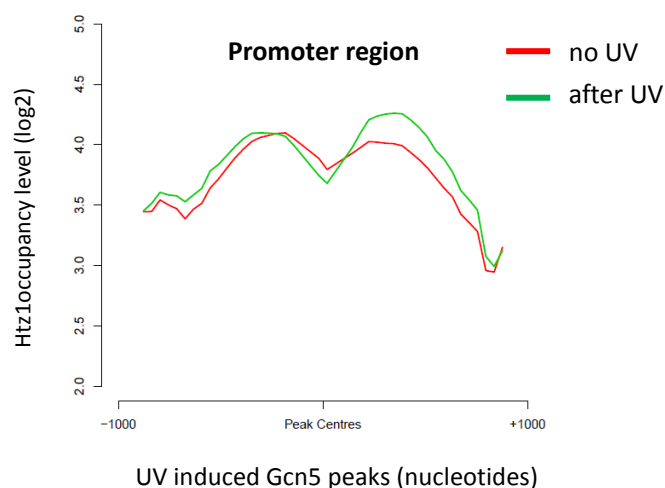


Figure 5.21 Htz1 occupancy at UV induced Gcn5 peaks in profile plot

Composite profiles of Htz1 occupancy both before (red line) and after UV irradiation (green line) at UV induced Gcn5 binding peaks. Only the trend line of each plot is shown.

5.4 Discussion

In this chapter I mapped the occupancy of Htz1 before and after UV irradiation throughout the yeast genome. I then employed our ChIP-on-chip method to

investigate how this related to genome-wide GG-NER. This built on the studies I undertook in Chapter 4, where histone Htz1 was found to be required for efficient GGR at the Htz1 containing region, namely the *MFA2* promoter. Htz1 occupancy has been previously studied with microarrays and its binding pattern was mainly at promoter regions. However, the genome-wide Htz1 occupancy in response to UV had not been studied. My ChIP-on-chip datasets illustrate Htz1 distribution after UV. Unlike most previous Htz1 genome-wide studies which were carried out in a Htz1 tagged strain, and which then employed a anti-tag antibody to pull down the Htz1 containing fragment in chromatin, my histone Htz1 genome-wide study used the wild type strain with a high affinity Htz1 antibody derived by Catherine B. Millar. This antibody was titrated (the antibody titration test can be found in the appendix) and it was compared with the commercial Htz1 antibody. Millar's antibody enhanced the microarray sensitivity and enabled me to use a wild strain and avoid any influence of the gene tag. The quantitative PCR results show a significantly reduced Htz1 level after UV irradiation at different sites and suggested a potential relocalisation of histone Htz1 as a UV damage response. However, the high-resolution nucleosome mapping result I described in Chapter 4 illustrated that there is no measurably change in the accessibility of the nucleosomal DNA in the *MFA2* promoter (as the chromatin did not become more sensitive to MNase due to chromatin remodelling in this region following UV). This result raised the possibility that a UV induced histone Htz1 relocalization may not occur as various reports have mentioned that the histone Htz1 containing chromatin displays a diverse accessibility when compared to Htz1 free chromatin.

The ChIP-on-chip datasets I generated illustrated a highly reproducible profile of Htz1 occupancy both before and after UV between biological repeats. Its accuracy was enhanced by employing quantitative PCR and a *htz1Δ* strain as a control. These pre-UV data profiles are consistent with data reported by other researchers (Zhang et al., 2005, Guillemette et al., 2005, Millar et al., 2006). Both in the presence and absence of UV damage, Htz1 occupancy can be observed throughout the whole

genome. From the profile plots, Htz1 is preferentially localized at the intergenic regions such as the promoter and downstream regions, with the highest occupancy occurring at the sequences adjacent to the boundary of intergenic region and intragenic regions. The Htz1 peak locations and their level before and after UV were analysed and compared. The results from genome-wide chromosome plots show that histone Htz1 occupancy levels in the presence and absence of UV are identical, with a 0.95 Pearson correlation. These peaks of the Htz1 occupancy can be easily distinguished from the background, and they give a more than a 1000 fold increase in signal intensity compared to the background in the *htz1Δ* strain. The Htz1 peaks in my experiments were sharper than these seen in the other datasets obtained using this technology. The reasons for this could be the antibody employed and the intensity of it associated with the chromatin fragments. As Htz1 is a core histone H2A variant in the nucleosome core, clear peaks would be expected. These sharp peaks and their reproducibility are undoubtedly due to histone Htz1 occupancy. A peak detection function identified 5363 and 5944 statistically significant Htz1 peaks in the unirradiated and 2-hour post UV datasets respectively. More than half of the total peaks are located in the intergenic regions and the peak position plots clearly illustrate that the most abundant peaks are located in the intergenic region and the coding region boundary, with slightly more peaks just at the promoter regions upstream of the coding regions. More than 88% of these Htz1 peaks overlap before and after UV. The peak detection function may pick up some peaks that sit in the background regions and which should not be taken into account. These datasets show that the localisation of Htz1 occupancy is the same both before and 2-hours after UV irradiation. UV induced relocalization of histone Htz1 is not observed and suggests that Htz1 occupies the same location as in the pre-UV situation, this presence of Htz1 occupancy may required to maintain other cellular processes (Dhillon et al., 2006) such as protecting euchromatic genes near telomeres from heterochromatic spreading as a boundary element (Meneghini et al., 2003). My data indicate that one role of Htz1 is in assisting efficient GG-NER. This function is not carried out through a direct UV induced Htz1

relocalization to alter the chromatin structure to promote efficient repair. Although the localization of histone Htz1 occupancy is unchanged, after UV it should be mentioned that there is some Htz1 loss after UV. This occurs in the intergenic regions where Htz1 is normally abundant. From the profile plots, the loss of Htz1 can be observed from the trend line with ~ 1 value loss at the intergenic regions. As a \log_2 scale was used in all of the microarray datasets, this loss means that Htz1 is reduced to almost half of its pre UV level. This finding is consistent with what I observed from the quantitative PCR study on the *MFA2* promoter. Histone variant Htz1 is deposited by the SWR1 chromatin remodeling complex which has a unique role in exchanging Histone H2A-H2B for a Htz1-H2B dimer (Mizuguchi et al., 2004). This stepwise and ATP-dependent process can exchange both of the H2A-H2B dimers in one nucleosome. A hybrid nucleosome with only one Htz1 could also be generated from an Htz1 free nucleosome by stepwise replacement with Htz1-H2B dimers. This replacement could occur in a replication-independent manner in all phases of the cell cycle, including the G1 phase. Hybrid nucleosomes could also appear as a consequence of disruption of the nucleosome contain two Htz1s and reassembly with a H2A contain histone dimer during DNA replication in S phase (Luk et al., 2010); this step required INO80 which has histone-exchange activity to replace nucleosomal Htz1-H2B with free H2A-H2B dimers (Papamichos-Chronakis et al., 2011). In my experiments, after UV the Htz1 level dropped to half of the pre UV level in intergenic region. This could indicate that pre UV, the nucleosomes containing Htz1 at the intergenic region has two Htz1 molecules and after UV, one of the two Htz1 molecules has been replaced by H2A. However, the profile plot at the Htz1 occupancy peaks reveals that this difference does not occur exactly at the peak sites, but is adjacent to the peak sites. This result means that the reduction of Htz1 is not simply a result of one of the two Htz1 containing dimers being lost from the original two Htz1 containing nucleosome. The reasons for these reductions are currently unknown, but the collective data suggests that the predominant loss of Htz1 occupancy correlates with DNA repair following UV damage. Correlations were not observed between

Htz1 level changes after UV and CPD repair rates. These results all could be due to UV induced repair replication changes affecting Htz1 levels. In order to address this, a future study could investigate Htz1 level change in a Rad14 mutant, as lack of Rad14 means that the repair process is abolished. If Htz1 loss is still observed, this Htz1 loss would be a pre-repair event and not occurring post CPD removal.

I have found that there is a weak Pearson correlation between Htz1 occupancy and CPDs repair throughout the entire genome. I examined if Htz1 showed a higher association to repair rates at different regions, as Htz1 has a preferential abundance occupancy in the intergenic regions. Here the repair data did not show any significant correlation to Htz1 occupancy. The peaks with higher Htz1 values do not appear to result in faster repair.

As Htz1 does not relocalize in response to UV and there is no direct relation between Htz1 occupancy and CPD repair, these result might implying that Htz1 not influence GG-NER in a direct manner. However, caution should be applied because it maybe that an as yet unidentified subset of these intergenic regions do have Htz1 playing a direct role. It is apparently unclear as to how the various roles of Htz1 in other processes might impinge on any potential role in GG-NER.

Htz1 occupancy has been reported to correlate with particular histone acetylation patterns. Htz1 has a strong positive correlation with acetylation at H3 lysine14, and a strong negative correlation with H3K27 acetylation, an apparent positive correlation with H2AK7ac and H4K8ac, and a negative correlation with H3K9ac levels. Interestingly, Htz1 deposition patterns are not dramatically altered in strains bearing amino acid replacement at these histone tails (Zhang et al., 2005). H3 lysine 56 hyperacetylation has been reported to rapidly alter the substrate specificity of the chromatin remodeling enzyme SWR-C to facilitate widespread decreases in Htz1 levels in yeast mutants, and this influences gene regulation (Watanabe et al., 2013) . As previously stated, histone H3 lysines 9 and 14 acetylation plays a role in NER, not only in a specific region (Yu et al., 2005b) but also throughout the entire genome (K. Evans PhD thesis CU 2011). Our group has examined the gene expression changes

after UV-irradiation in yeast. There is a pre-UV relationship between acetylation and expression, but no obvious relationship between the UV-induced gene expression changes and UV-induced H3 acetylation. There is a strong positive relationship between CPD repair and histone H3 acetylation, and regions with higher H3 acetylation or UV-induced H3 acetylation also tend to have faster CPD repair.

In Chapter 4 I described that in the strain lacking *HTZ1* there is a reduction of H3 lysines 9 and 14 acetylation level at the original Htz1 located site, but not at a locus which does not contain Htz1. As H3 lysines 9 and 14 acetylation levels have a positive relationship with CPD repair rates, I compared the Htz1 occupancy with H3 acetylation and also the UV induced H3 acetylation data to see if there were possible correlations. Interestingly, there is a significant correlation between Htz1 and H3 acetylation. The scatter-plot and Pearson correlation tests shared a positive relationship between this histone modification and the histone variant, with 0.44 and 0.47 correlations before and after UV. The UV induced acetylation also has a significant 0.33 Pearson correlation value. In order to see how this correlation pertained to different regions, I divided both the Htz1 peaks and acetylation peaks into different groups to further investigate. I used 1 hour H3 acetylation data to compare with Htz1; this was selected because the pre and post UV H3 acetylation profiles are mainly similar, but the peaks are clearer at 1 hour post UV. The results show that Htz1 peaks can be found co-localised with H3 lysines 9 and 14 peaks at different regions. H3 acetylation binding peaks are less significant at Htz1 binding peaks, especially the divergent promoter and downstream regions when compared to Htz1 at H3 acetylation peaks. These results suggest that H3 acetylation peaks are always accompanied by Htz1 binding, but not the other way around. This indicates that Htz1 could help regulate this H3 lysines 9 and 14 acetylation level. With the respect to UV induced acetylation, the results show that Htz1 binding peaks can be found at the intergenic regions, but not at the intragenic region at peaks, and no measurable UV induced H3 acetylation peaks can be detected at the Htz1 occupancy peaks. Along with the quantitative PCR results I described in Chapter 4, this could suggest that

Htz1 has an upstream regulatory role in maintaining the level of this H3 acetylation. Absence of Htz1 will not abolish this H3 lysines 9 and 14 acetylation but it will definitely alter the acetylation level.

The HAT Gcn5 has been identified as being responsible for catalysing acetylation of the H3 lysines 9 and 14 hyper-acetylation at the *MFA2* gene. In the *gcn5Δ*, a dramatic reduction of UV induced H3 lysines 9 and 14 acetylation was observed in some domains, such as *MFA2* (Yu et al., 2005a). Deletion of *GCN5* does not abolish all of the UV induced genome-wide hyper-acetylation (Yu et al., 2005a). There may be redundancy because two different HATs (Gcn5 and Sas3) can acetylate Histone H3 K14, and disruption of both of the *GCN5* and *SAS3* genes is synthetically lethal. The loss of one of these two HAT activities, may be partly compensated for the other (Howe et al., 2001). A genome-wide study has expanded the understanding of Gcn5's role. It appears to be required for most of the H3 lysines 9 and 14 acetylation in the promoters of genes both pre- and post-UV irradiation. Almost no change in the H3 lysines 9 and 14 acetylation can be found in *gcn5Δ* cells after UV-irradiation (K. Evans PhD CU 2011). In the results of Evans, Gcn5 was not found to exactly colocalize with H3 acetylation peaks, but was at both sides adjacent to the H3 acetylation site. As the Gcn5 binding was boosted immediately after UV, I used 0 hour and pre UV values to calculate the UV induced Gcn5 change. No significant Pearson correlation was found between Htz1 occupancy and Gcn5 binding before or after UV. This was not surprising because there are diverse roles of Gcn5 and Htz1 and these may affect the localization. For example movement of Gcn5 along the chromatin may not function to just catalyse histone H3 acetylation, but it also may be involved in the recruitment of chromatin remodellers such as SWI/SNF or NER factors (Kim et al., 2010).

The profile plot of Htz1 and Gcn5 data at each other's peaks produced a picture that shows after UV the Gcn5 level rises at Htz1 occupancy peaks around the genome, but not in the coding regions. A wide peak was observed of Htz1 occupancy at Gcn5 peaks in most of the regions except the coding regions. Thus the Htz1 occupancy

more likely resides around Gcn5 peaks and is not exactly at the same sites as Gcn5. It appears that more Htz1 often resides downstream of UV induced Gcn5 binding peaks before UV and more Htz1 is found upstream after UV. These results suggest that there is a relationship between Htz1 occupancy and Gcn5 localization and this correlation is connected with H3 acetylation. I previously found in chapter 4 that Gcn5 occupancy was reduced in *htz1Δ* cells. The genome-wide study described here could be expanded to examine if the occupancy of Htz1 and Gcn5 have a UV induced relationship which is linked through H3 acetylation.

In summary, this Chapter demonstrates that Htz1 occupancy can be observed through the whole genome at a high frequency. Consistent with previous studies, it is predominantly situated within promoter and downstream regions and boundary regions. In response to UV, Htz1 does not relocalise but the global occupancy of Htz1 occupancy is reduced at intergenic regions. A positive correlation has been found between Htz1 occupancy and H3 acetylation. Htz1 is believed to regulate the distribution of histone H3 lysines 9 and 14 acetylation at promoters both before and after UV. Some Htz1 could interact with Gcn5 genome-wide for catalysing the UV-induced H3 acetylation to promote a genome-wide faster GG-NER.

Chapter 6. General conclusions and future experiments

6.1 General discussion

In eukaryotic cells, two copies of each histone protein, H2A, H2B, H3 and H4 are assembled into an octamer with about 150 base pairs (bp) of DNA wrapped around it to form a nucleosome core. This highly conserved nucleoprotein complex occurs essentially throughout all genomes. In *Saccharomyces cerevisiae*, Htz1 is a histone H2A variant and it belongs to the highly conserved family of H2A.Z (Jackson et al., 1996). This conserved property of H2A.Z across species results from sequence similarity between each other more than with the canonical histone H2A from the same species. This suggests that H2A.Z may have specific functions that are different from those of canonical histone H2A (Zlatanova and Thakar, 2008). Htz1 is incorporated into the nucleosomes by the ATP-dependent SWR complex to replace H2A-H2B with a Htz1-H2B dimer, and the incorporation is independent of DNA replication (Krogan et al., 2003, Kobor et al., 2004, Mizuguchi et al., 2004, Luk et al., 2010). In my study, I found that there is a positive role for Htz1 in promoting nucleotide excision repair (GG-NER) in the Htz1-containing nucleosomes of *S. cerevisiae*. It does so by regulating UV-induced histone H3 acetylation and the binding of Rad14 to damaged DNA at a specific region. Deletion of *HTZ1* and genes encoding components of the SWR complex results in increased UV sensitivity. Deletion of these genes also impairs the removal of UV-induced CPDs in the two Htz1 containing nucleosomes at the *MFA2* promoter, but not in the *HMRa* locus where Htz1 is originally absent. This was not related to any detectable alteration in the accessibility of nucleosomal DNA in the Htz1 nucleosomes in the repressed *MFA2* promoter (MNase accessibility is not affected by *HTZ1* deletion). However, the UV-induced histone H3 hyperacetylation and the binding of Rad14 to damaged DNA were significantly compromised in this region without Htz1. Gcn5 occupancy, which catalysis H3 hyperacetylation was also reduced without UV at this region. My microarray study expanded these finding to the genome-wide level. These data also

suggest that Htz1 is related to promoting efficient GG-NER at other locations. The acetylation on four previously identified lysine sites (K3, 8, 10, 14) of Htz1 plays little role in GG-NER and cell survival after UV.

Although canonical histones are the major histones assembled into nucleosome, other histone variants are also incorporated into nucleosomes in some regions of the genome (Waters et al., 2009). Evidence has suggested that histone variants in nucleosomes may have an alternative role or co-operate with post-translational histone modifications to affect chromatin to influence different cell processes (Yuan and Zhu, 2012). As Htz1 is the sole histone H2A variant in *S. cerevisiae*, I investigated how this variant related to GG-NER. In Chapter 3, I found that not only is the *htz1Δ* sensitive to UV, but also a similar UV sensitivity is found in the *swr1Δ*, *yaf9Δ* and *bdf1Δ*, *gcn5Δ* mutants. These genes are known to be related to Htz1 occupancy. Swr1, Yaf9 and bdf1 have roles in the ATP-dependent Htz1 deposition, while Gcn5 has been correlated with Htz1 occupancy through its transferases ability to cause histone H3 hyperacetylation. CPD removal was impaired in total DNA from both *htz1Δ* and *swr1Δ* strains. Chapter 4 examined GG-NER at precise locations in the yeast genome. Here my data showed that this slower repair occurs in the Htz1 bearing region but not in the Htz1 free region. As canonical histones, the lysine end at the N-terminal of histone variant Htz1 are also potential targets for acetylation. To investigate if Htz1 acetylation was involved in GG-NER, three different sets of strains were employed. The results show that acetylation of Htz1 at K3, 8, 10, 14 does not contribute to UV survival or CPD repair. Htz1 acetylation is reported to occur after assembly into chromatin by NuA4 and the unacetyltable Htz1 lysine mutant showed a similar Htz1 express level and is efficiently assembled into chromatin (Keogh et al., 2006). Although Htz1 acetylation has been reported to be important to its deposition during nucleosome reassembly, this acetylation was not required for efficient CPD repair. A UV induced histone Htz1 relocalisation related to chromatin formation change was one of the possible pathway of how Htz1 could take part in this GG-NER, and how it participates was not clear prior to my study.

The NER factor Rad14 has a well established UV damage binding activity and this binding activity is ATP independent (Guzder et al., 1993). The recruitment of Rad 14 could be a good indicator as to how NER is operating in different mutants. I first confirmed the UV damage binding activity of Rad14 and high CPD levels were detected in the Rad14 IP'd chromatin from irradiated cells. I found that Rad14 locates to damaged chromatin after UV and forms a more firm binding to UV-damaged sites in chromatin. This result shows that Rad14 binding intensity can be changed. Thus Rad14 recruitment can be used as an indicator of how efficiently repairs progresses.

Rad14 and Gcn5 myc-tagged strains were generated and examined in wild type and *htz1Δ* cells. It appears that the study of Rad14 location and level changes could be a good indicator of how GG-NER factors accumulate at the damage site.

My study then moved from examining total DNA to investigating selected genomic locations. It was still unclear if the different repair efficiencies from all cellular DNA were related to Htz1 occupancy. Genome-wide studies have shown that Htz1 is dramatically enriched at the promoter-proximal nucleosomes of inactive genes and in the euchromatin/heterochromatin boundaries (Zhang et al., 2005, Li et al., 2005, Raisner et al., 2005, Albert et al., 2007). Although preferentially residing at these repressive promoters, Htz1 does not contribute to the repression of downstream genes. Instead, it is required for the subsequent activation of these genes when the induction signal strikes (Zhang et al., 2005, Li et al., 2005, Raisner et al., 2005, Santisteban et al., 2000, Jin and Felsenfeld, 2007, Halley et al., 2010). These results prompted me to select specific regions to study the role of Htz1 in GG-NER. Two different regions were investigated. Four positioned nucleosomes have been mapped within the control and coding regions of *MFA2* in alpha mating type cells (Teng et al., 2001) and 12 well-positioned nucleosomes span a 1.94-kb region at *HMRa* (Weiss and Simpson, 1998, Ravindra et al., 1999). I picked these regions (*MFA2* promoter and *HMRa1*) from the information available from genome-wide Htz1 occupancy data (Zhang et al., 2005). *MFA2* has nucleosomes bearing Htz1, whereas *HMRa1* does not. *MFA2* and *HMRa1* are transcriptionally silent in *MATα* cells and this makes them suitable for

investigating GG-NER. These different regions allowed me to investigate how repair processed at a Htz1 contain region and a Htz1 free region in the same cells. My data confirmed that these two regions were suitable for my study into how repair proceeds with and without a Htz1 containing nucleosome in its local chromatin environment. High resolution gels enabled me to examine the repair rates at these two different regions. Faster repair was observed in wild type cells at the *MFA2* promoter when compared with the *htz1Δ* and *swr1Δ* strains while at *HMRa1* similar repair rates occurred for the wild type strains and these mutants. This result clearly demonstrated that the slow repair I saw in the total DNA due to a lack of Htz1 is not the result of a genome-wide transcription level change or a genome-wide damage recognition delay for NER as if this were the case I would not have seen unchanged GG-NER at *HMRa1* in the Htz1 mutant. Thus this demonstrated that the reduced GG-NER efficiency I observed in the *htz1Δ* strain is not caused by repressing the transcription of GG-NER factors and that the slow genomic repair likely reflects reduced NER at regions like the *MFA2* promoter which normally contain Htz1 in its local nucleosomes. This result also confirmed that Htz1 has a role in promoting efficient GG-NER in sequences around its nucleosome.

The Htz1 containing nucleosome could govern a more suitable chromatin structure for GG-NER factors to operate directly or indirectly. For example, Htz1 could localise after UV and the nucleosome position might change. The Htz1 containing region could have had a higher accessibility to enzymes compared to the same region in *htz1Δ* strain. Surprisingly, our high resolution MNase assay which is capable of assessing the sensitivity of many sites in chromatin to MNase *in vivo* revealed that deletion of *HTZ1* reduces the efficiency in repair of CPDs in the Htz1-containing nucleosomes in the *MFA2* promoter without causing major detectable changes in chromatin accessibility both before and after UV treatment. No UV induced nucleosome position change was observed in these two nucleosomes at *MFA2* promoter in the wild type strain. These results indicate that Htz1 may not directly change the chromatin environment, and are consistent with other studies regarding the

effect of Htz1 on chromatin structure (Morillo-Huesca et al., 2010, Li et al., 2005). In addition, my data also revealed that, with or without Htz1, these nucleosomes at *MFA2* all become equally more sensitive to MNase in response to UV irradiation. This suggests that using this assay Htz1 has no influence on chromatin remodelling in this region following UV irradiation. Hence the positive function of Htz1 in GG-NER cannot be simply explained by the general stability of the nucleosomes. Rad7 and Rad16 proteins were found to mediate the increased occupancy of the histone acetyltransferase Gcn5 on the nucleosomes at the *MFA2* promoter following UV (Yu et al., 2011). This leads to histone hyperacetylation at H3K9K14 which is required for efficient repair of UV-induced CPDs (Yu et al., 2005a). Could it be that the histone variant Htz1 influences histone acetylation which increases after UV?

I had measured the total levels of Gcn5 protein in wild type cell and the *htz1Δ* mutant by quantitative western blotting. These data indicated that the levels of Gcn5 remain the same in these two strains. My ChIP results of H3 acetylation levels at *MFA2* and *HMRa1* indicate that Htz1 promotes histone H3 hyperacetylation in Htz1 nucleosomes in the *MFA2* promoter after UV irradiation. On the other hand, deletion of *HTZ1* results in a reduced occupancy of Gcn5 at this locus both before and after UV treatment when compared to that at the *HMRa1* locus. Although the levels of Gcn5 occupancy are slightly increased in *htz1Δ* cells following UV treatment, they are still significantly lower than that seen in wild type cells. These results indicate that Htz1 promotes the occupancy of the histone acetyltransferase Gcn5, and therefore the UV-induced histone H3 acetylation in the Htz1-containing nucleosomes at *MFA2*. This finding suggested that Htz1 promotes efficient GG-NER through generating a higher Gcn5 occupancy at its local nucleosome and this renders a significantly higher H3 acetylation to facilitate faster repair when compared to *htz1Δ* cells. Recently, two studies revealed a similar phenomenon in mammalian cells in processes other than GG-NER (Draker et al., 2012, Xu et al., 2012). Here, H2A.Z promotes histone H4 acetylation and in combination with H4 acetylation, Htz1 promotes the recruitment of downstream effector proteins to chromatin. These events occur during transcription

activation (Draker et al., 2012) and DNA double strand break repair (Xu et al., 2012). Taking all of these data together, it suggests that this function of Htz1 (H2A.Z) may be conserved from yeast to humans, and that it has roles in different processes.

In addition to the exciting H3 acetylation findings, I also found a relationship between Htz1 and the recruitment of the NER factor Rad14. Deletion of *HTZ1* does not change the expression levels of Rad14 yet there is a significant reduction in Rad14 binding to the original Htz1 nucleosomes at the *MFA2* promoter in the *htz1Δ* cells when compared to that in wild type cells. The binding of Rad14 at the *HMRa1* locus was not affected and was the same in both strains. This indicates that Htz1 promotes the efficient binding of Rad14 to damaged DNA in the Htz1-bearing nucleosomes, thereby promoting GG-NER following UV irradiation. Although Rad14 is a damaged DNA binding protein (Guzder et al., 1993), and there is no evidence to indicate that Rad14 interacts with histones, the presence of Htz1 may produce a favourable environment following UV. For example Htz1 can promote the occupancy of Gcn5 and induced histone H3 acetylation so enhancing the binding of Rad14 to damaged DNA.

These data let me to propose a model as to how Htz1 promotes GG-NER in Figure 6.1 Htz1 promotes the occupancy of the histone acetyltransferase Gcn5 and therefore the UV-induced histone H3 acetylation in the Htz1-containing nucleosomes at *MFA2*. This acetylation promotes the efficient binding of Rad14 to damaged DNA in the Htz1-bearing nucleosomes, and results in promoting GG-NER following UV irradiation. Thus this study revealed an additional layer of information in chromatin at the *MFA2* promoter that cells use to regulate chromatin dynamics to ensure efficient DNA damage repair following UV irradiation. As these data came from experiments at specific regions of the genome, a genome-wide microarray study was needed to examine the significance of these results for the entire yeast genome.

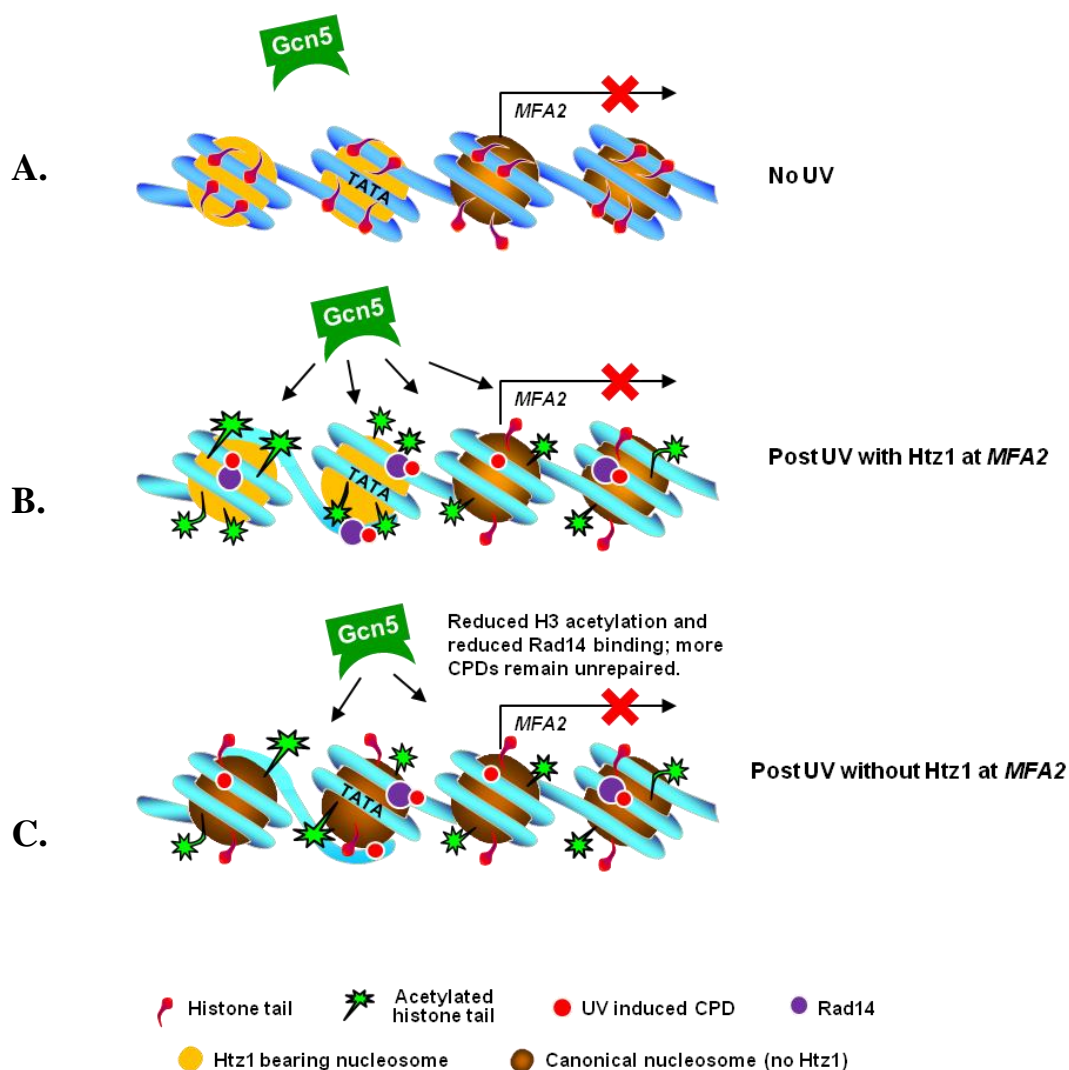


Figure 6.1 Model for chromatin remodelling at *MFA2* during GG-NER.

(A) In the absence of UV histone H3 tails remain unacetylated and chromatin remains repressive. (B) Following UV irradiation, the increased occupancy of Gcn5 that is mediated via the Rad7/Rad16 GG-NER complex is promoted by the presence of Htz1. This helps achieve hyperacetylation levels on histone H3 and enhance Rad14 to damaged DNA. This leads to efficient lesion removal. (C) Without Htz1 in these nucleosomes, the occupancy of Gcn5 and the acetylation levels on histone H3 are reduced. Therefore, the maximal binding of repair proteins to damaged DNA cannot be achieved and more CPDs remain unrepaired (Yu et al., 2013).

The specific region study established a possible pathway of how Htz1 promotes efficient GG-NER, I next use a ChIP on chip technology to extend these findings to a genome-wide level. ChIP on chip examined histone Htz1 occupancy before and after UV-irradiation.

The histone Htz1 genome-wide occupancy investigations before and after UV were

successful. I employed a Htz1 antibody directly as Htz1-tagged strains might be influenced by this protein being tagged. The normalisation process efficiently minimised the variations between each biological experiment. After normalization, the ChIP-on-chip datasets showed remarkably highly reproducible profiles for Htz1 both before and after UV, and between biological repeats. The microarray datasets were then compared to the quantitative PCR results for analysing the same regions. Although these two technologies are different with respect to the preparation and detection procedures, the normalised microarray data matched those from the quantitative PCR. Hence I concluded that the microarray data correctly represent Htz1 occupancy before and after UV. The Htz1 occupancy data show that it is located in the genome at thousands of sites, and is preferentially localised to promoter regions of the genome. This is consistent with the previous findings by other researchers (Millar et al., 2006, Zhang et al., 2005, Guillemette et al., 2005). As I mentioned in Chapter 4, the high resolution MNase map of nucleosomes revealed that no nucleosome position change occurred after UV in wild type or *htz1Δ* strains. This implies that Htz1 occupancy did not change. The peak detection results of Htz1 occupancy before and after UV also gave a clear answer to this question. More than 93% of the peaks overlap between before and after UV, suggesting that the nucleosome containing Htz1 pre-UV still have a Htz1 residue and that they have not relocated (within the resolution of the microarrays). This suggests that Htz1 does not undergo a UV induced relocation.

However the Htz1 level is reduced by about 50% at intergenic regions after UV. This microarray finding was matched with quantitative PCR data. I could not establish whether this is a result of nucleosomes containing two Htz1s having one replaced with H2A. The peaks of Htz1 occupancy pre UV and after UV are identical and this suggests that Htz1 is not completely lost from its occupancy sites. Hence this supports the idea that in the intergenic regions where Htz1 resides, one of the two Htz1s in a single nucleosome are replaced by H2A as a response to UV. The profile plots of Htz1 occupancy at the Htz1 peaks do not show a significantly greater reduction at

intergenic regions, so suggesting that there is an even Htz1 loss around the whole genome. The Htz1 loss after UV is gradual. Hence, the CPD repair data after 2 hours repair was used to compare with the Htz1 occupancy data. The repair results show a weak Pearson correlation with Htz1 occupancy before and after UV, but no significant correlation between repair was observed at Htz1 peaks in the different regions. Htz1 occupancy is unchanged after UV, and Htz1 has roles more than in GG-NER. It is possible that no direct correlation between total Htz1 occupancy and CPD repair might be detected in the analyses. Htz1 occupancy has been reported to correlate with particular histone acetylation patterns. Htz1 was reported to have a strong positive correlation with acetylation at H3 lysine 14, a strong negative correlation with H3 lysine 27 acetylation, an apparent positive correlation with H2A lysine 7 acetylation and H4 lysine 8 acetylation and a negative correlation with H3 lysine 9 acetylation levels (Zhang et al., 2005). As the H3 K9K14 acetylation level has a positive relationship with CPD repair, I compared the Htz1 occupancy with H3 acetylation, and the UV induced H3 acetylation to examine possible correlations. A very strong correlation was found between Htz1 and H3 acetylation. In addition, Htz1 occupancy peaks can be found at H3 K9K14 peaks at many regions, but H3 acetylation peaks are less significant at Htz1 peaks. Htz1 deposition patterns do not dramatically alter in strains bearing amino acid replacement at these histone tails (Zhang et al., 2005). This indicates that Htz1 could be an upstream regulator of this H3 K9K14 acetylation level. Recently, H3 lysine 56 hyperacetylation was reported to rapidly alter the substrate specificity of the chromatin remodeling enzyme SWR-C to create widespread decreases in H2A.Z levels in yeast mutants and influence gene regulation (Watanabe et al., 2013). Hence there could be more of a correlation between Htz1 occupancy and other H3 acetylations. The profile plot also shows that Htz1 and Gcn5 bind at each other's peaks sites. After UV, the Gcn5 level rises at the Htz1 occupancy peaks around the genome, but not for the intragenic regions. A wide peak was observed for Htz1 occupancy at Gcn5 peaks in regions other than the intragenic ones. Furthermore, the Htz1 data on UV induced Gcn5 peaks show a similar binding pattern and Htz1 resides

at both sides of these peaks before and after UV. This result suggest that there is a positive correlation between Htz1 occupancy and Gcn5 binding.

6.1 Conclusions

I have extended our understanding on how chromatin is modified to regulate efficient repair of UV-induced DNA damage. Following UV irradiation, Rad7 and Rad16 regulate the occupancy of Gcn5 at the *MFA2* promoter to acetylate histone H3. Htz1 in the nucleosomes in this region maintains increased binding of Gcn5 to the local nucleosome enviroment. Gcn5 promotes hyperacetylation levels on histone H3. The increased levels of H3 acetylation enhance the recruitment of Rad14, and possibly other GG-NER factors to the damage sites. This leads to more efficient lesion removal by NER.

Without Htz1 in the nucleosomes the higher acetylation levels on histone H3 cannot be achieved due to a reduced binding of Gcn5 to these nucleosomes. This results in reduced binding of Rad14 and, perhaps, other repair proteins to damaged DNA. Thereby, the rate of lesion removal is compromised. This function of Htz1 cannot be replaced by canonical histone H2A because GG-NER is compromised in both the *htz1* Δ strain and in the *swr1* Δ strain which cannot deposit Htz1 to replace H2A/H2B in these nucleosomes.

Htz1 genome-wide occupancy data were generated and more than 5000 Htz1 occupancy peaks were detected throughtout the genome. These genome-wide studies correlated well with quantitative PCR results. Htz1 genome-wide occupancy after UV irradiation was investigated. There is no relocalization after UV, and histone Htz1 still resides at the pre-UV sites, yet there is a reduction of Htz1 levels at intergenic regions. Although no direct correlation was found between Htz1 occupancy and repair, Htz1 occupancy is found to be an upstream regulator of H3 lysine 9 and 14 acetylation. A genome-wide colocalization was found between Htz1 and Gcn5. The relationship between Htz1 and H3 K9K14 acetylation is believed to be established through the interaction between Htz1 and Gcn5 via the model previously described. The lack of

correlation between Htz1 and repair genome-wide is likely the result of Htz1 only influencing NER at some location. This could be due to the various roles that Htz1 plays in the cell; some only being related to NER.

This is the first evidence that a histone variant impinges on GG-NER and links this histone variant to another important epigenetic event which is histone H3 acetylation.

6.2 Future experiments

At this stage, the microarray data are still limited, the next phase of these studies should include:

1. Investigating genome-wide CPD repair in a *htz1*Δ strain.
2. The genome-wide Gcn5 binding before and after UV in a *htz1*Δ strain.
3. The genome-wide Rad14 binding data in the wild type and *htz1*Δ strain

The CPD repair study will allow one to investigate how the repair varies at every Htz1 occupancy site. The Gcn5 study will show how Gcn5 changes at the Htz1 bearing nucleosomes genome-wide. The Rad14 study will show how Rad14 is recruited at every Htz1 occupancy site. The Rad14 microarray data will also be worth comparing with CPD repair data, as it has damage DNA binding ability and will relocate to damage sites after UV.

Appendix I - Liquid and solid media.

1.Growth media

YPD (1L)

10 g Bacto Yeast Extract

20 g Bacto Peptone

20 g Glucose

Made up to 1000 ml with H₂O

Autoclave at 125 °C for 15 minutes.

YPD plates were obtained with addition 20g Bacto Agar

Minimal media (1L)

6.6 g Yeast Nitrogen Base w/o Amino Acids

20 g Glucose

Made up to 1000 ml with H₂O

Autoclave at 125 °C for 15 minutes.

Minimal media plates were obtained with addition 20g Bacto Agar

LB Media with ampicillin (1L)

10g Bacto tryptone

5g Bacto yeast extract

5g NaCl

Fill to 1L with H₂O. Autoclave at 125 °C for 15 minutes. Allow to cool to 55 °C and add ampicillin to a final concentration of 100µg/ml.

Synthetic complete Amino Acids added medium

Adenine 40 µg/ml

Tryptophan 40 µg/ml

Leucine	60 µg/ml
Lysine	40 µg/ml
Uracil	20 µg/ml
Histidine	40 µg/ml

2. Stock Solutions

PBS (1 L)

NaCL	8 g
KCl	0.2 g
Na ₂ HPO ₄ ·2H ₂ O	1.8 g
KH ₂ PO ₄	0.24 g
H ₂ O	800 ml

Adjust the pH to 7.4. Add H₂O to 1 L.

Autoclave at 125 °C for 15 minutes.

0.5 M EDTA (pH 8.0)

EDTA · Na ₂ · 2H ₂ O	186.1 g
H ₂ O	800 ml

pH was adjusted with NaOH to pH 8.0.

Add about 100ml H₂O to make 1 L

Autoclave at 125 °C for 15 minutes.

1 M Tris

Tris base	121.1 g
H ₂ O	800 ml

Adjust the pH to the desired value (7.6 or 8.0) by adding concentrated HCl.

Add H₂O to make 1 L.

10 x TE Buffer (400 ml)

40 ml 1 M Tris-HCl, pH 7.5

8 ml 0.5 M EDTA, pH 8.0

352 ml of H₂O

3 M Sodium acetate (pH 5.2) (400 ml)

Sodium acetate · 3H₂O 163.24 g

H₂O 300 ml

Adjust the pH to 5.2 with acetic acid.

Add H₂O to make 400 ml

Use filter to sterilise.

5 M NaCl (400 ml)

Dissolve 116.9 g of NaCl in 350 ml of H₂O. Adjust the volume to 400 ml with H₂O.

Sterilise by autoclaving.

10% SDS (Sodium dodecyl sulfate) (1 L)

Dissolve 100g of SDS in 800 ml of distilled H₂O. Add distilled H₂O to make a total volume of 1 L.

20% SDS (Sodium dodecyl sulfate) (500 ml)

Dissolve 100 g of SDS in 350 ml of distilled H₂O. Add dissolved H₂O to make a total volume of 500 ml.

Sorbitol TE (1L) (Kept in cold room)

Sorbitol 165 g

Tris . HCl (pH8.0) 100 ml

EDTA 200 ml

Add 500 ml H₂O to dissolve the sorbitol. Adjust the final volume to 1L.

DNA Lysis Buffer (1 L)

Urea	240 g
NaCl	11.69 g
CDTA	5 g
n-Lauroyl Sarcosine	5 g
1 M Tris-HCl (pH 8.0)	100 ml

Add 700 ml of H₂O to dissolve the chemicals and then adjust the final volume to 1L.

3. Solutions for electrophoresis**50 x TAE (Tris-acetate) (1 L)**

Tris base	242 g
Sodium Acetate · 3 H ₂ O	136 g
0.5 M EDTA	200 ml
H ₂ O	500ml

Adjust to pH 7.2 with acetic acid.

Add H₂O to make 1 L.

10 x TBE (1 L)

Tris base	108 g
Boric acid	55 g
EDTA	8.3 g

Add H₂O to 1 L.

Non-denaturing loading buffer (10 ml)

Ficoll	10%	1 g
SDS	0.5%	0.5 ml of 10% solution
Bromophenol Blue	0.06%	6 mg

Made up in 1 x TAE solution.

1x Denaturing Running Buffer

NaOH	36mM
EDTA	1mM

Denaturing loading buffer (10ml)

NaOH	50mM	166ul of 3M stock
EDTA	1mM	20ul of 0.5M stock
Ficoll	2.5%	0.25g
Bromophenol Blue	0.025%	2.5mg

Add H₂O to make 1L.

Neutralising gel buffer for denature gel

Tris-HCL (pH7.5)	1M
NaCl	1.5M

3. Solutions for western blotting**10x TBST**

Tris-Base (1M,pH 8.0)	100ml
NaCl (5M)	300ml
Tween 20	5ml

Add H₂O to make 1L

2x SDS loading buffer

Tris base	100mM
sodium dodecyl sulphate (SDS)	4%
bromophenol blue	0.2%
glycerol	20%
dithiothreitol, pH6.8	20mM

10x SDS running buffer	1L
Tris base	30 g
glycine	144 g
SDS	10.0 g
H ₂ O	800ml

Adjust pH to 8.3.

Add H₂O to make 1L.

Western transfer buffer

Tris-base	25mM
glycine	150mM,
methanol	20%,
SDS	0.015% w/v

4. Solutions for chromatin immunoprecipitation

FA/SDS Buffer

HEPES KOH pH 7.5	50mM
NaCl	500mM
EDTA	1mM
Triton X 100	1%
Deoxycholate Na	0.1%
SDS	0.1%
PMSF	1Mm

PMSF (Phenylmethanesulfonyl fluoride) as the serine protease inhibitor is rapidly degraded in H₂O which need to add before use. The NaCl concentration can be

adjusted from 500mM to 1000mM to adapt to different protein-antibody binding intensity.

5 x Pronase Buffer (100 ml)

1 M Tris pH7.5	12.5 ml
0.5 M EDTA	5 ml
10% SDS	25 ml

Add H₂O to make 100 ml.

LiCl Buffer (500 ml)

1 M Tris pH 8.0	5 ml
5 M LiCl	25 ml
0.5 M EDTA	1 ml
NP40	2.5 ml
Deoxycholate Na	25 ml

Add H₂O to make 500 ml.

Appendix II - Raw data for experiment in Chapter 3

Cell UV survival data

BY4742 (wild-type)

Irradiation Time (seconds)	Dilution	Number of colonies			Mean Survival (%)	Standard Deviation (%)
		EXP.1	EXP.2	EXP.3		
0	10 ⁻⁴	186/195/174	203/194/225	234/205/201	100	0
2	10 ⁻⁴	155/147/121	184/161/182	173/145/161	78.6461	5.353
4	10 ⁻³	53/54/66	87/73/84	72/60/63	33.68	4.867
8	10 ⁻³	48/41/36	78/61/77	75/82/78	3.236	0.645
12	10 ⁻²	40/50/35	53/44/60	83/62/56	0.266	0.045

BY4742 (*htz1Δ*)

Irradiation Time (seconds)	Dilution	Number of colonies			Mean Survival (%)	Standard Deviation (%)
		EXP.1	EXP.2	EXP.3		
0	10 ⁻⁴	232/241/198	217/244/207	187/177/182	100	0
2	10 ⁻⁴	101/109/92	88/92/97	65/84/71	42.387	2.454
4	10 ⁻³	173/196/190	163/151/156	139/142/127	7.623	0.658
8	10 ⁻²	58/62/47	48/59/40	33/28/28	0.214	0.0437
12	10 ⁻¹	21/13/26	25/10/15	9/11/14	0.007	0.001

BY4742 (*gcn5Δ*)

Irradiation Time (seconds)	Dilution	Number of colonies			Mean Survival (%)	Standard Deviation (%)
		EXP.1	EXP.2	EXP.3		
0	10 ⁻⁴	245/240/225	178/197/190	184/212/220	100	0
2	10 ⁻⁴	98/104/109	69/74/81	101/77/74	41.618	4.4543
4	10 ⁻³	128/109/105	106/100/87	111/120/124	5.235	0.477
8	10 ⁻²	44/39/38	30/24/21	24/14/18	0.133	0.039
12	10 ⁻¹	17/20/12	8/5/7	11/9/16	0.005	0.001

BY4742 (*swr1Δ*)

Irradiation Time (seconds)	Dilution	Number of colonies			Mean Survival (%)	Standard Deviation (%)
		EXP.1	EXP.2	EXP.3		
0	10 ⁻⁴	147/153/146	184/169/171	224/204/198	100	0
2	10 ⁻⁴	63/55/55	100/94/91	80/93/79	44.486	4.805
4	10 ⁻³	134/123/131	155/140/157	163/161/190	8.489	0.272
8	10 ⁻²	12/11/9	14/18/26	25/19/31	0.103	0.025
12	10 ⁻¹	8/7/10	22/13/14	17/22/24	0.008	0.003

BY4742 (*yaf9*)

Irradiation Time (seconds)	Dilution	Number of colonies			Mean Survival (%)	Standard Deviation (%)
		EXP.1	EXP.2	EXP.3		
0	10 ⁻⁴	199/220/215	183/174/170	163/172/163	100	0
2	10 ⁻⁴	67/73/77	61/76/68	71/49/50	35.684	4.678
4	10 ⁻³	163/174/171	145/164/141	124/138/155	8.288	0.269
8	10 ⁻²	24/27/15	19/29/11	10/16/13	0.098	0.017
12	10 ⁻¹	24/31/20	17/23/16	17/18/18	0.011	0.001

BY4742 (*bdf1*)

Irradiation Time (seconds)	Dilution	Number of colonies			Mean Survival (%)	Standard Deviation (%)
		EXP.1	EXP.2	EXP.3		
0	10 ⁻⁴	134/153/155	162/153/166	235/253/240	100	0
2	10 ⁻⁴	89/93/80	92/105/101	139/128/148	59.055	2.477
4	10 ⁻³	137/103/112	107/114/119	126/117/127	6.432	1.471
8	10 ⁻²	11/12/7	8/9/10	11/17/15	0.605	0.014
12	10 ⁻¹	8/2/3	6/7/12	15/14/10	0.005	0.001

BLY457

Irradiation Time (seconds)	Dilution	Number of colonies			Mean Survival (%)	Standard Deviation (%)
		EXP.1	EXP.2	EXP.3		
0	10 ⁻⁴	309/296/290	282/288/265	204/219/198	100	0
2	10 ⁻⁴	141/134/149	130/128/133	93/65/73	44.492	5.723
4	10 ⁻³	296/282/283	231/225/237	135/117/127	8.222	1.776
8	10 ⁻³	31/39/33	22/18/26	19/17/10	0.915	0.022
12	10 ⁻²	21/17/24	12/13/17	16/14/10	0.061	0.011

BLY1

Irradiation Time (seconds)	Dilution	Number of colonies			Mean Survival (%)	Standard Deviation (%)
		EXP.1	EXP.2	EXP.3		
0	10 ⁻⁴	199/204/209	170/164/161	180/188/177	100	0
2	10 ⁻⁴	123/117/129	95/93/89	108/121/112	59.745	3.357
4	10 ⁻³	291/291/286	221/239/193	223/208/189	12.960	1.423
8	10 ⁻³	47/33/36	28/23/29	19/21/29	1.604	0.315
12	10 ⁻²	13/16/23	11/5/18	13/9/8	0.070	0.016

W303-1B (MSY-1251)

Irradiation Time (seconds)	Dilution	Number of colonies			Mean Survival (%)	Standard Deviation (%)
		EXP.1	EXP.2	EXP.3		
0	10 ⁻⁴	176/165/173	201/203/189	184/169/179	100	0
2	10 ⁻⁴	119/108/99	137/134/120	128/109/154	67.602	5.243
4	10 ⁻³	346/330/355	359/367/334	310/371/349	19.042	1.115
8	10 ⁻³	64/48/43	73/82/71	93/62/71	3.703	0.624
12	10 ⁻²	82/88/91	90/112/91	76/73/90	0.484	0.031

MSY-2890

Irradiation Time (seconds)	Dilution	Number of colonies			Mean Survival (%)	Standard Deviation (%)
		EXP.1	EXP.2	EXP.3		
0	10 ⁻⁴	158/163/155	181/195/177	201/217/186	100	0
2	10 ⁻⁴	31/35/30	44/51/39	53/21/65	22.596	2.085
4	10 ⁻³	57/42/60	90/101/93	83/101/85	4.360	0.906
8	10 ⁻³	10/13/10	21/46/24	23/29/35	1.292	0.050
12	10 ⁻²	39/33/46	80/98/63	73/60/79	0.349	0.095

MSY-3141

Irradiation Time (seconds)	Dilution	Number of colonies			Mean Survival (%)	Standard Deviation (%)
		EXP.1	EXP.2	EXP.3		
0	10 ⁻⁴	167/163/159	199/210/176	213/209/177	100	0
2	10 ⁻⁴	63/67/71	63/54/55	55/43/63	31.918	7.590
4	10 ⁻³	160/157/169	110/109/89	150/144/161	7.466	2.337
8	10 ⁻³	50/33/72	31/50/44	23/22/28	2.110	0.976
12	10 ⁻²	58/98/43	59/69/43	20/19/37	0.265	0.138

302

Irradiation Time (seconds)	Dilution	Number of colonies			Mean Survival (%)	Standard Deviation (%)
		EXP.1	EXP.2	EXP.3		
0	10 ⁻⁴	178/173/186	165/187/173	201/196/203	100	0
2	10 ⁻⁴	148/134/156	154/145/163	158/154/167	78.243	4.339
4	10 ⁻³	430/403/412	490/437/451	460/402/395	19.042	5.358
8	10 ⁻³	180/171/159	110/107/103	180/176/188	8.918	0.666
12	10 ⁻²	90/54/93	43/52/22	42/45/68	0.307	0.117

544

Irradiation Time (seconds)	Dilution	Number of colonies			Mean Survival (%)	Standard Deviation (%)
		EXP.1	EXP.2	EXP.3		
0	10 ⁻⁴	182/173/186	198/205/190	208/225/213	100	0
2	10 ⁻⁴	137/143/132	138/154/159	152/130/155	73.285	4.883
4	10 ⁻³	420/403/430	480/430/421	470/495/325	21.858	1.675
8	10 ⁻³	203/134/150	107/98/110	143/135/176	7.114	1.846
12	10 ⁻²	35/54/23	30/22/31	27/33/46	0.1704	0.034

566

Irradiation Time (seconds)	Dilution	Number of colonies			Mean Survival (%)	Standard Deviation (%)
		EXP.1	EXP.2	EXP.3		
0	10 ⁻⁴	191/183/173	186/173/187	157/145/163	100	0
2	10 ⁻⁴	137/143/130	119/143/102	105/99/97	68.784	5.430
4	10 ⁻³	464/410/457	277/234/298	327/349/311	20.125	4.852
8	10 ⁻³	173/153/153	132/124/128	121/119/109	7.765	0.890
12	10 ⁻²	79/44/67	31/34/55	40/48/21	0.267	0.069

htz1Δ strains

Irradiation Time (seconds)	Dilution	Number of colonies			Mean Survival (%)	Standard Deviation (%)
		EXP.1	EXP.2	EXP.3		
0	10 ⁻⁴	197/184/203	176/173/183	217/204/199	100	0
2	10 ⁻⁴	159/143/167	99/83/113	143/138/103	65.898	12.894
4	10 ⁻³	465/445/401	277/294/254	486/435/599	20.609	4.475
8	10 ⁻³	80/55/64	32/43/66	54/32/23	2.605	0.826
12	10 ⁻²	13/10/11	6/3/3	7/5/2	0.034	0.021

Genomic CPD incidence in 302 (wild-type), 544 (arginine (R) mutant)

	Timepoint				Averaged Datasets	
		Expt1 (%)	Expt2 (%)	Expt3 (%)	Average	SD
302	0	100.00	100.00	100.00	100.00	0.00
	0.5	80.92	87.38	84.46	84.25	3.23
	1	43.12	54.32	43.21	46.88	6.44
	2	33.48	36.81	32.19	34.16	2.38
544	0	100.00	100.00	100.00	100.00	0.00
	0.5	92.06	87.13	93.17	90.79	3.22
	1	48.13	52.98	44.66	48.59	4.18
	2	33.87	36.71	32.73	34.44	2.05

Genomic CPD frequency analysis (denature gel method) in WT, *htz1Δ* and *swr1Δ*

	Timepoint				Averaged Datasets	
		Expt1	Expt2	Expt3	Average	SD
WT	0	1.42	1.36	1.20	1.33	0.12
	0.5	0.97	0.94	1.08	1.00	0.07
	1	0.74	0.79	0.91	0.81	0.09
	2	0.54	0.65	0.79	0.66	0.12
	3	0.49	0.58	0.58	0.55	0.05
<i>htz1Δ</i>	0	1.37	1.41	1.31	1.36	0.05
	0.5	1.12	1.27	1.06	1.15	0.11
	1	0.91	0.97	1.07	0.98	0.08
	2	0.78	0.84	0.94	0.85	0.08
	3	0.76	0.77	0.82	0.78	0.03
<i>swr1Δ</i>	0	1.38	1.29	1.41	1.36	0.06
	0.5	1.09	1.17	1.28	1.18	0.09
	1	0.88	1.01	1.03	0.97	0.08
	2	0.83	0.90	0.82	0.85	0.04
	3	0.81	0.75	0.71	0.76	0.05

Appendix III - Raw data for experiment in Chapter 4

Quantitative PCR results

ChIP qRT-PCR data for *MFA2* Nucleosome -1

MFA2 Nu -2	strain	SQ mean			Fold change	Averaged Datasets	
		Input	IP	IP/Input		Average	SD
Expt 1	WT	9.77E-02	9.22E-02	9.44E-01	1.37E+01	1.18E+01	2.75E+00
	<i>htz1Δ</i>	7.59E-02	5.23E-03	6.89E-02	1.00E+00	1.00E+00	0.00E+00
	<i>swr1Δ</i>	9.30E-02	1.14E-02	1.23E-01	1.78E+00	1.64E+00	1.97E-01
	<i>yaf9Δ</i>	7.13E-02	1.35E-02	1.89E-01	2.74E+00	2.01E+00	1.03E+00
	<i>bdf1Δ</i>	5.92E-02	5.05E-02	8.52E-01	1.24E+01	1.05E+01	2.66E+00
	<i>gcn5Δ</i>	1.07E-01	5.17E-02	4.84E-01	7.02E+00	5.74E+00	1.81E+00
Expt 2	WT	1.51E-01	1.23E-01	8.11E-01	9.81E+00		
	<i>htz1Δ</i>	9.05E-02	7.48E-03	8.27E-02	1.00E+00		
	<i>swr1Δ</i>	9.59E-02	1.19E-02	1.24E-01	1.50E+00		
	<i>yaf9Δ</i>	1.38E-01	1.46E-02	1.06E-01	1.28E+00		
	<i>bdf1Δ</i>	1.33E-01	9.48E-02	7.13E-01	8.62E+00		
	<i>gcn5Δ</i>	1.09E-01	4.01E-02	3.69E-01	4.46E+00		

ChIP qRT-PCR data for *MFA2* Nucleosome -2

MFA2 primer 1	Strain	SQ mean			Fold change	Averaged Datasets	
		Input	IP	IP/Input		Average	SD
Expt 1	WT	1.03E-01	1.08E-01	1.05E+00	1.42E+01	1.25E+01	2.36E+00
	<i>htz1Δ</i>	9.12E-02	6.74E-03	7.39E-02	1.00E+00	1.00E+00	0.00E+00
	<i>swr1Δ</i>	7.17E-02	6.40E-03	8.92E-02	1.21E+00	1.12E+00	1.29E-01
	<i>yaf9Δ</i>	8.87E-02	9.40E-03	1.06E-01	1.43E+00	1.16E+00	3.92E-01
	<i>bdf1Δ</i>	8.21E-02	1.04E-01	1.27E+00	1.71E+01	1.49E+01	3.11E+00
	<i>gcn5Δ</i>	1.08E-01	6.53E-02	6.05E-01	8.18E+00	6.52E+00	2.34E+00
Expt 2	WT	1.32E-01	1.23E-01	9.29E-01	1.09E+01		
	<i>htz1Δ</i>	9.91E-02	8.48E-03	8.56E-02	1.00E+00		
	<i>swr1Δ</i>	1.02E-01	8.94E-03	8.77E-02	1.02E+00		
	<i>yaf9Δ</i>	1.25E-01	9.40E-03	7.52E-02	8.79E-01		
	<i>bdf1Δ</i>	1.71E-01	1.87E-01	1.09E+00	1.27E+01		
	<i>gcn5Δ</i>	1.09E-01	4.54E-02	4.17E-01	4.87E+00		

ChIP qRT-PCR data for *HMRa1* Nucleosome 4

HMRa1 Nu 4	Timepoint	SQ mean			Fold change	Averaged Datasets	
		Input	IP	IP/Input		Average	SD
Expt 1	WT	1.10E-01	4.93E-03	4.49E-02	1.26E+00	1.30E+00	5.70E-02
	<i>htz1Δ</i>	1.11E-01	3.93E-03	3.55E-02	1.00E+00	1.00E+00	0.00E+00
	<i>swr1Δ</i>	9.83E-02	4.71E-03	4.79E-02	1.35E+00	1.18E+00	2.39E-01
Expt 2	WT	1.06E-01	3.22E-03	3.04E-02	1.34E+00		
	<i>htz1Δ</i>	6.84E-02	1.55E-03	2.26E-02	1.00E+00		
	<i>swr1Δ</i>	9.58E-02	2.19E-03	2.28E-02	1.01E+00		

ChIP qRT-PCR data for *HMRa1* Nucleosome 5

HMRa1 Nu 5	Timepoint	SQ mean			Fold change	Averaged Datasets	
		Input	IP	IP/Input		Average	SD
Expt 1	WT	1.07E-01	5.48E-03	5.13E-02	1.24E+00	1.15E+00	1.28E-01
	<i>htz1Δ</i>	1.02E-01	4.23E-03	4.13E-02	1.00E+00	1.00E+00	0.00E+00
	<i>swr1Δ</i>	9.01E-02	4.00E-03	4.43E-02	1.07E+00	1.13E+00	8.40E-02
Expt 2	WT	9.98E-02	3.22E-03	3.23E-02	1.06E+00		
	<i>htz1Δ</i>	8.67E-02	2.64E-03	3.04E-02	1.00E+00		
	<i>swr1Δ</i>	1.19E-01	4.32E-03	3.63E-02	1.19E+00		

ChIP qRT-PCR data for *MFA2* CPDs in WT (302) and Htz1 K3,8,10,14R (544)

BY4742 (302)	Time (hrs)	SQ mean			Fold change	Averaged Datasets	
		Input	IP	IP/Input		Average	SD
Expt 1	no UV	8.96E-02	3.35E-02	3.74E-01	3.62E-02	3.62E-02	6.00E-03
	0	1.22E-01	1.26E+00	1.03E+01	1.00E+00	1.00E+00	0.00E+00
	0.5	9.19E-02	9.02E-01	9.83E+00	9.52E-01	9.12E-01	7.21E-02
	1	1.18E-01	7.27E-01	6.16E+00	5.97E-01	5.87E-01	4.99E-02
	2	1.38E-01	7.37E-01	5.33E+00	5.16E-01	5.09E-01	3.27E-02
Expt 2	no UV	1.03E-01	5.55E-02	5.39E-01	3.62E-02		
	0	9.44E-02	1.41E+00	1.49E+01	1.00E+00		
	0.5	1.17E-01	1.52E+00	1.30E+01	8.73E-01		
	1	1.18E-01	1.02E+00	8.60E+00	5.77E-01		
	2	1.27E-01	9.46E-01	7.47E+00	5.01E-01		
Expt 3	no UV	9.56E-02	6.24E-02	6.52E-01	4.66E-02		
	0	1.04E-01	1.45E+00	1.40E+01	1.00E+00		
	0.5	1.43E-01	1.61E+00	1.13E+01	8.08E-01		
	1	1.13E-01	7.94E-01	7.04E+00	5.02E-01		
	2	8.38E-02	5.32E-01	6.35E+00	4.53E-01		

BY4742 (544)	Time (hrs)	SQ mean			Fold change	Averaged Datasets	
		Input	IP	IP/Input		Average	SD
Expt 1	no UV	1.01E-01	5.05E-02	4.99E-01	3.87E-02	3.35E-02	1.04E-02
	0	9.82E-02	1.27E+00	1.29E+01	1.00E+00	1.00E+00	0.00E+00
	0.5	8.69E-02	1.09E+00	1.26E+01	9.75E-01	8.75E-01	1.07E-01
	1	9.35E-02	8.44E-01	9.03E+00	7.01E-01	6.19E-01	8.47E-02
	2	7.27E-02	4.58E-01	6.30E+00	4.89E-01	4.70E-01	4.21E-02
Expt 2	no UV	1.35E-01	7.14E-02	5.29E-01	2.82E-02		
	0	9.36E-02	1.75E+00	1.87E+01	1.00E+00		
	0.5	1.23E-01	1.78E+00	1.45E+01	7.74E-01		
	1	9.41E-02	9.46E-01	1.01E+01	5.36E-01		
	2	6.66E-02	5.63E-01	8.45E+00	4.51E-01		
Expt 3	no UV	1.11E-01	8.53E-02	7.71E-01	4.91E-02		
	0	1.20E-01	1.89E+00	1.57E+01	1.00E+00		
	0.5	1.09E-01	1.39E+00	1.28E+01	8.12E-01		
	1	1.13E-01	1.16E+00	1.03E+01	6.53E-01		
	2	1.36E-01	8.65E-01	6.36E+00	4.05E-01		

ChIP qRT-PCR data for *MFA2*, Rad14 in WT and *htz1Δ*

	Time (hrs)	SQ mean		IP/Input	Fold change	Averaged Datasets	
		Input	IP			Average	SD
<i>MFA2</i>							
BY4742 (WT)							
Expt 1	no UV	1.04E-01	9.62E-03	9.22E-02	1.00E+00	1.00E+00	0.00E+00
	0	7.66E-02	1.62E-02	2.12E-01	2.29E+00	2.41E+00	3.95E-01
	0.25	7.70E-02	2.54E-02	3.30E-01	3.57E+00	3.69E+00	7.52E-01
	0.5	5.21E-02	1.60E-02	3.08E-01	3.34E+00	3.19E+00	3.03E-01
	1	2.03E-01	6.54E-02	3.22E-01	3.50E+00	3.33E+00	6.57E-01
Expt 2	no UV	1.74E-01	1.49E-02	8.54E-02	1.00E+00		
	0	1.35E-01	2.40E-02	1.78E-01	2.08E+00		
	0.25	8.57E-02	3.29E-02	3.84E-01	4.49E+00		
	0.5	1.11E-01	3.20E-02	2.89E-01	3.38E+00		
	1	1.20E-01	4.00E-02	3.32E-01	3.88E+00		
Expt 3	no UV	1.09E-01	5.83E-03	5.33E-02	1.00E+00		
	0	1.13E-01	1.72E-02	1.52E-01	2.85E+00		
	0.25	1.36E-01	2.18E-02	1.60E-01	3.00E+00		
	0.5	1.39E-01	2.11E-02	1.51E-01	2.84E+00		
	1	1.32E-01	1.83E-02	1.39E-01	2.60E+00		
BY4742 <i>htz1Δ</i>							
Expt 1	no UV	9.86E-02	8.50E-03	8.62E-02	9.35E-01	9.45E-01	1.14E-01
	0	8.40E-02	8.91E-03	1.06E-01	1.15E+00	1.63E+00	4.18E-01
	0.25	7.04E-02	1.18E-02	1.67E-01	1.81E+00	1.83E+00	1.32E-01
	0.5	7.36E-02	1.02E-02	1.39E-01	1.51E+00	1.71E+00	1.81E-01
	1	9.86E-02	1.56E-02	1.58E-01	1.71E+00	1.83E+00	3.47E-01
Expt 2	no UV	9.86E-02	7.05E-03	7.15E-02	8.36E-01		
	0	8.40E-02	1.35E-02	1.60E-01	1.88E+00		
	0.25	7.04E-02	1.03E-02	1.46E-01	1.71E+00		
	0.5	7.36E-02	1.11E-02	1.51E-01	1.77E+00		
	1	9.86E-02	1.87E-02	1.90E-01	2.22E+00		
Expt 3	no UV	1.09E-01	6.20E-03	5.67E-02	1.06E+00		
	0	1.31E-01	1.31E-02	9.98E-02	1.87E+00		
	0.25	1.04E-01	1.09E-02	1.05E-01	1.97E+00		
	0.5	8.31E-02	8.23E-03	9.90E-02	1.86E+00		
	1	2.41E-01	2.00E-02	8.28E-02	1.55E+00		

ChIP qRT-PCR data for HMRa1, Rad14 in WT and *htz1Δ*

	Time (hrs)	SQ mean			Fold change	Averaged Datasets	
		Input	IP	IP/Input		Average	SD
<i>HMRa1</i>							
BY4742 (WT)							
Expt 1	no UV	1.09E-01	1.62E-03	1.48E-02	1.00E+00	1.00E+00	0.00E+00
	0	1.31E-01	5.82E-03	4.43E-02	2.99E+00	2.94E+00	5.44E-01
	0.25	1.04E-01	5.68E-03	5.48E-02	3.69E+00	3.52E+00	2.10E-01
	0.5	8.31E-02	3.82E-03	4.59E-02	3.09E+00	2.86E+00	2.07E-01
	1	9.62E-02	4.99E-03	5.18E-02	3.50E+00	3.21E+00	2.81E-01
Expt 2	no UV	2.41E-01	8.10E-03	3.36E-02	1.00E+00		
	0	2.62E-01	2.09E-02	7.98E-02	2.37E+00		
	0.25	2.15E-01	2.37E-02	1.10E-01	3.29E+00		
	0.5	1.19E-01	1.12E-02	9.36E-02	2.79E+00		
	1	6.73E-02	7.22E-03	1.07E-01	3.19E+00		
Expt 3	no UV	1.03E-01	9.62E-02	9.38E-01	1.00E+00		
	0	8.20E-02	2.66E-01	3.25E+00	3.46E+00		
	0.25	9.09E-02	3.05E-01	3.36E+00	3.58E+00		
	0.5	8.00E-02	2.03E-01	2.53E+00	2.70E+00		
	1	1.33E-01	3.65E-01	2.75E+00	2.93E+00		
BY4742 <i>htz1Δ</i>							
Expt 1	no UV	1.06E-01	1.63E-03	1.53E-02	1.03E+00	1.06E+00	1.29E-01
	0	9.87E-02	4.40E-03	4.46E-02	3.01E+00	3.08E+00	5.31E-01
	0.25	8.81E-02	4.78E-03	5.42E-02	3.66E+00	3.46E+00	1.83E-01
	0.5	8.08E-02	3.78E-03	4.68E-02	3.16E+00	2.94E+00	2.07E-01
	1	1.06E-01	5.49E-03	5.18E-02	3.49E+00	3.17E+00	3.90E-01
Expt 2	no UV	1.05E-01	3.30E-03	3.15E-02	9.38E-01		
	0	1.21E-01	1.05E-02	8.70E-02	2.59E+00		
	0.25	1.09E-01	1.25E-02	1.15E-01	3.41E+00		
	0.5	9.02E-02	8.31E-03	9.21E-02	2.74E+00		
	1	1.48E-01	1.64E-02	1.10E-01	3.29E+00		
Expt 3	no UV	1.87E-01	2.09E-01	1.12E+00	1.19E+00		
	0	1.17E-01	4.01E-01	3.42E+00	3.64E+00		
	0.25	1.20E-01	3.72E-01	3.10E+00	3.30E+00		
	0.5	2.15E-01	5.90E-01	2.75E+00	2.93E+00		
	1	1.19E-01	3.06E-01	2.57E+00	2.74E+00		

ChIP qRT-PCR data for MFA2, H3 lysine 9 and 14 acetylation in WT and *htz1Δ*

	Time (hrs)	SQ mean			Fold change	Averaged Datasets	
		Input	IP	IP/Input		Average	SD
<i>MFA2</i>							
BY4742 (WT)							
Expt 1	no UV	1.08E-01	1.92E-02	1.78E-01	1.00E+00	1.00E+00	0.00E+00
	0	8.97E-02	1.89E-02	2.11E-01	1.19E+00	1.18E+00	1.24E-01
	0.5	8.54E-02	3.76E-02	4.40E-01	2.47E+00	2.85E+00	3.32E-01
	1	8.39E-02	6.12E-02	7.30E-01	4.10E+00	4.34E+00	2.26E-01
Expt 2	no UV	8.51E-02	2.55E-02	2.99E-01	1.00E+00		
	0	6.84E-02	2.17E-02	3.17E-01	1.06E+00		
	0.5	9.77E-02	8.80E-02	9.01E-01	3.01E+00		
	1	8.82E-02	1.15E-01	1.30E+00	4.36E+00		
Expt 3	no UV	9.95E-02	2.79E-02	2.81E-01	1.00E+00		
	0	1.08E-01	3.95E-02	3.67E-01	1.31E+00		
	0.5	1.07E-01	9.20E-02	8.63E-01	3.07E+00		
	1	7.14E-02	9.13E-02	1.28E+00	4.56E+00		
BY4742 <i>htz1Δ</i>							
Expt 1	no UV	8.59E-02	9.63E-03	1.12E-01	6.30E-01	6.51E-01	7.48E-02
	0	7.07E-02	1.13E-02	1.60E-01	9.01E-01	8.65E-01	1.31E-01
	0.5	7.77E-02	2.45E-02	3.15E-01	1.77E+00	1.51E+00	2.33E-01
	1	1.18E-01	5.08E-02	4.30E-01	2.42E+00	2.28E+00	1.40E-01
Expt 2	no UV	1.00E-01	1.76E-02	1.76E-01	5.89E-01		
	0	1.36E-01	2.93E-02	2.15E-01	7.20E-01		
	0.5	8.96E-02	3.75E-02	4.18E-01	1.40E+00		
	1	9.36E-02	5.99E-02	6.40E-01	2.14E+00		
Expt 3	no UV	9.78E-02	2.02E-02	2.06E-01	7.34E-01		
	0	7.80E-02	2.13E-02	2.74E-01	9.74E-01		
	0.5	6.72E-02	2.54E-02	3.78E-01	1.35E+00		
	1	6.77E-02	4.35E-02	6.42E-01	2.29E+00		

ChIP qRT-PCR data for *HMRa1*, H3 lysine 9 and 14 acetylation in WT and *htz1Δ*

	Time (hrs)	SQ mean			Fold change	Averaged Datasets	
		Input	IP	IP/Input		Average	SD
<i>HMRa1</i>							
BY4742 (WT)							
Expt 1	no UV	1.04E-01	3.56E-02	3.44E-01	1.00E+00	1.00E+00	0.00E+00
	0	8.10E-02	2.81E-02	3.47E-01	1.01E+00	1.17E+00	1.71E-01
	0.5	7.64E-02	5.79E-02	7.58E-01	2.20E+00	2.53E+00	2.94E-01
	1	7.65E-02	6.35E-02	8.30E-01	2.41E+00	3.06E+00	5.65E-01
Expt 2	no UV	9.78E-02	2.51E-02	2.57E-01	1.00E+00		
	0	7.80E-02	2.33E-02	2.99E-01	1.16E+00		
	0.5	6.72E-02	4.49E-02	6.69E-01	2.61E+00		
	1	6.77E-02	5.73E-02	8.46E-01	3.29E+00		
Expt 3	no UV	1.03E-01	1.80E-02	1.75E-01	1.00E+00		
	0	1.02E-01	2.42E-02	2.36E-01	1.35E+00		
	0.5	5.99E-02	2.91E-02	4.86E-01	2.77E+00		
	1	4.90E-02	2.97E-02	6.06E-01	3.46E+00		
BY4742 <i>htz1Δ</i>							
Expt 1	no UV	9.95E-02	3.58E-02	3.60E-01	1.05E+00	1.11E+00	1.76E-01
	0	1.08E-01	3.91E-02	3.64E-01	1.06E+00	1.28E+00	2.29E-01
	0.5	1.07E-01	8.77E-02	8.22E-01	2.39E+00	2.50E+00	3.43E-01
	1	7.14E-02	6.23E-02	8.73E-01	2.54E+00	2.97E+00	5.02E-01
Expt 2	no UV	1.03E-01	3.46E-02	3.36E-01	1.31E+00		
	0	1.09E-01	3.53E-02	3.25E-01	1.27E+00		
	0.5	1.33E-01	7.63E-02	5.73E-01	2.23E+00		
	1	6.00E-02	5.43E-02	9.04E-01	3.52E+00		
Expt 3	no UV	9.99E-02	1.70E-02	1.70E-01	9.71E-01		
	0	1.32E-01	3.51E-02	2.65E-01	1.51E+00		
	0.5	9.88E-02	4.99E-02	5.05E-01	2.89E+00		
	1	8.12E-02	4.05E-02	4.98E-01	2.85E+00		

ChIP qRT-PCR data for MFA2, Gcn5 in WT and *htz1Δ*

	Time (hrs)	SQ mean			Fold change	Averaged Datasets	
		Input	IP	IP/Input		Average	SD
<i>MFA2</i>							
BY4742 (WT)							
Expt 1	no UV	1.04E-01	3.28E-02	3.16E-01	1.00E+00	1.00E+00	0.00E+00
	0	6.78E-02	4.42E-02	6.53E-01	2.06E+00	2.03E+00	2.39E-01
	0.5	9.02E-02	4.88E-02	5.41E-01	1.71E+00	1.71E+00	1.69E-01
	1	1.03E-01	5.37E-02	5.22E-01	1.65E+00	1.58E+00	8.27E-02
Expt 2	no UV	9.47E-02	4.39E-02	6.23E-01	1.00E+00		
	0	7.05E-02	1.07E-01	1.11E+00	1.77E+00		
	0.5	9.66E-02	9.34E-02	9.58E-01	1.54E+00		
	1	9.75E-02	9.02E-02	9.26E-01	1.49E+00		
Expt 3	no UV	1.06E-01	7.59E-02	7.18E-01	1.00E+00		
	0	6.35E-02	1.02E-01	1.61E+00	2.25E+00		
	0.5	8.11E-02	1.09E-01	1.35E+00	1.88E+00		
	1	9.82E-02	1.12E-01	1.14E+00	1.59E+00		
BY4742 <i>htz1Δ</i>							
Expt 1	no UV	1.24E-01	2.93E-02	2.36E-01	7.46E-01	7.28E-01	1.98E-02
	0	1.75E-01	4.32E-02	2.47E-01	7.81E-01	7.89E-01	1.59E-02
	0.5	1.60E-01	4.70E-02	2.93E-01	9.27E-01	8.51E-01	6.76E-02
	1	1.19E-01	3.95E-02	3.33E-01	1.05E+00	9.84E-01	7.13E-02
Expt 2	no UV	1.23E-01	5.41E-02	4.40E-01	7.07E-01		
	0	1.54E-01	7.48E-02	4.85E-01	7.78E-01		
	0.5	1.43E-01	7.13E-02	4.97E-01	7.98E-01		
	1	1.22E-01	7.51E-02	6.17E-01	9.90E-01		
Expt 3	no UV	1.20E-01	6.29E-02	5.24E-01	7.30E-01		
	0	1.64E-01	9.50E-02	5.79E-01	8.07E-01		
	0.5	1.45E-01	8.59E-02	5.94E-01	8.28E-01		
	1	1.15E-01	7.52E-02	6.53E-01	9.09E-01		

CPD repair data***MFA2* promoter region, *HaeIII* fragment CPD nucleotide position**

NTS	position	TS	postion	
	1	426	1	65
	2	364	2	2
	3	303	3	-103
	4	261	4	-159
	5	235	5	-196
	6	226	6	-226
	7	217	7	-251
	8	127	8	-258
	9	116	9	-266
	10	108	10	-288
	11	83	11	-309
	12	55	12	-320
	13	47	13	-337
	14	37	14	-347
	15	25	15	-355
	16	8	16	-377
	17	-1	17	-387
	18	1	18	-394
	19	53	19	-397
			20	-491

***HMRa1* coding region, *RsaI-BglII* fragment CPD nucleotide position**

NTS	position	
	1	82
	2	98
	3	114
	4	135
	5	158
	6	188
	7	202
	8	217
	9	244
	10	265
	11	278
	12	290
	13	307
	14	319
	15	338
	16	343

CPDs in the *MFA2* NTS in WT strain (*HaeIII* fragment)

(1) Band density values (peak areas)

	Experiment1				
Time (hr)	0	0.5	1	2	3
Top bands	115770217	108377492	114696335	122639815	111214930
1	10530660	9587285	10787994	8327838	3709872
2	3140296	2947838	3237209	2775440	1248968
3	10252185	9444781	10530854	9623018	5231673
4	3498285	3023772	3351963	2205351	942428
5	4383917	3960739	4347107	3793158	1843024
6	335223	274825	333029	253511	131926
7	202792	226149	227718	247250	112235
8	902345	801046	885995	642006	316355
9	1139280	1020275	1083236	1027644	634209
10	960611	811151	810862	748942	420646
11	12788755	11539429	11992029	9198259	4405366
12	3816561	3443789	3266806	2164940	1112841
13	864257	649219	614946	348972	209165
14	310833	233810	175086	85073	49246
15	3458969	2711408	2493049	1438147	672645
16	309109	252224	247680	135252	71564
17	470479	397166	456150	310196	139803
18	1996373	1807292	1936844	1467994	730311
19	608963	495930	498849	529292	344838
Total	175740111	162005619	171973740	167962102	133542048
Ratio	1.00	0.92	0.98	0.96	0.76

	Experiment2				
Time (hr)	0	0.5	1	2	3
Top bands	74190157	79451028	76501742	82593934	75269976
1	6726015	6121262	6890980	5313890	2353529
2	1988401	1865024	2050527	1754508	775958
3	6547499	6029909	6726140	6144169	3329084
4	2217890	1913702	2124090	1389051	579450
5	2785627	2514348	2762030	2406920	1156780
6	190200	151481	188793	137818	59875
7	105304	120277	121283	133804	47252
8	553755	488817	543274	386864	178104
9	705643	629354	669716	634078	381866
10	591107	495294	495110	455416	244960
11	8173574	7372690	7662831	5871876	2799377
12	2421922	2182955	2069500	1363145	688694
13	529338	391488	369517	199013	109390
14	174564	125188	87543	69840	36873
15	2192687	1713460	1573480	897233	406505
16	173459	136993	134080	62007	21180
17	276906	229908	267720	174156	64925
18	1255085	1133874	1216924	916366	443472
19	365681	293221	295092	314608	196363
Total	112164815	113360277	112750371	111218699	89143617
Ratio	1.00	1.01	1.01	0.99	0.79

(2) Band density after adjustment

	Experiment1				
Time (hr)	0	0.5	1	2	3
Top bands	115770217	117565506	117208283	128319035	146357830
1	10530660	10400074	11024260	8713484	4882158
2	3140296	3197749	3308107	2903966	1643630
3	10252185	10245489	10761488	10068642	6884834
4	3498285	3280121	3425373	2307477	1240227
5	4383917	4296522	4442312	3968812	2425403
6	335223	298124	340322	265251	173614
7	202792	245322	232705	258699	147700
8	902345	868957	905399	671736	416321
9	1139280	1106772	1106960	1075232	834614
10	960611	879918	828621	783624	553566
11	12788755	12517718	12254665	9624213	5797421
12	3816561	3735746	3338351	2265195	1464488
13	864257	704258	628414	365132	275259
14	310833	253632	178921	89012	64807
15	3458969	2941275	2547649	1504745	885195
16	309109	273607	253105	141515	94177
17	470479	430837	466140	324560	183979
18	1996373	1960510	1979262	1535975	961083
19	608963	537974	509774	553803	453803
Total	175740111	175740111	175740111	175740111	175740111

	Experiment2				
Time (hr)	0	0.5	1	2	3
Top bands	74190157	78613163	76104439	83296545	94708328
1	6726015	6056709	6855193	5359094	2961324
2	1988401	1845357	2039878	1769434	976348
3	6547499	5966320	6691208	6196437	4188815
4	2217890	1893521	2113059	1400867	729092
5	2785627	2487832	2747686	2427395	1455517
6	190200	149884	187812	138990	75338
7	105304	119009	120653	134942	59455
8	553755	483662	540452	390155	224100
9	705643	622717	666237	639472	480482
10	591107	490071	492538	459290	308221
11	8173574	7294940	7623035	5921827	3522312
12	2421922	2159934	2058752	1374742	866548
13	529338	387359	367598	200706	137639
14	174564	123868	87089	70434	46395
15	2192687	1695390	1565309	904865	511484
16	173459	135548	133384	62535	26650
17	276906	227484	266330	175637	81692
18	1255085	1121917	1210604	924162	557998
19	365681	290129	293560	317285	247074
Total	112164815	112164815	112164815	112164815	112164815

(3) Signal remain (%)

	Experiment1					Experiment2					T50% (hrs)
Time (hr)	0	0.5	1	2	3	0	0.5	1	2	3	
Top bands	100	102	101	111	126	100	106	103	112	128	
1	100	99	105	83	46	100	90	102	80	44	2.9
2	100	102	105	92	52	100	93	103	89	49	3.1
3	100	100	105	98	67	100	91	102	95	64	3.4
4	100	94	98	66	35	100	85	95	63	33	2.6
5	100	98	101	91	55	100	89	99	87	52	3.2
6	100	89	102	79	52	100	79	99	73	40	3
7	100	121	115	128	73	100	113	115	128	56	3.4
8	100	96	100	74	46	100	87	98	70	40	2.9
9	100	97	97	94	73	100	88	94	91	68	4
10	100	92	86	82	58	100	83	83	78	52	3.4
11	100	98	96	75	45	100	89	93	72	43	2.9
12	100	98	87	59	38	100	89	85	57	36	2.5
13	100	81	73	42	32	100	73	69	38	26	1.8
14	100	82	58	29	21	100	71	50	40	27	1.2
15	100	85	74	44	26	100	77	71	41	23	1.8
16	100	89	82	46	30	100	78	77	36	15	2.2
17	100	92	99	69	39	100	82	96	63	30	2.7
18	100	98	99	77	48	100	89	96	74	44	2.9
19	100	88	84	91	75	100	79	80	87	68	>4

CPDs in the *MFA2* NTS in *htz1Δ* strain (*HaeIII* fragment)

(1) Band density values (peak areas)

	Experiment1				
Time (hr)	0	0.5	1	2	3
Top bands	113683744	100644934	100414019	120615710	118506774
1	6099051	8745739	10747570	5654720	1548411
2	3252219	2973558	2826550	2496084	1819838
3	10487993	9565812	9302972	8743284	6836543
4	3355755	2883222	2762286	2372354	1413707
5	4638209	4285830	4064456	4142643	3055485
6	331217	282284	238215	218269	167529
7	214088	184804	222861	217009	155540
8	928017	870061	763082	661574	489478
9	1346468	1197401	1103221	1129067	996105
10	888931	717909	820479	808012	635638
11	13290626	12298363	10943368	9346923	6164204
12	3615309	3327879	3047569	2271103	1134218
13	1039606	787045	623027	473452	277275
14	356006	252415	213247	154635	81181
15	3513806	2980552	2534973	1746500	1080165
16	300832	242256	181582	128226	71850
17	476035	389433	345534	260351	153206
18	2077924	1836548	1577059	1331515	945775
19	816385	871841	683302	736862	649827
Total	170712221	155337887	153415374	163508293	146182751
Ratio	1.00	0.91	0.90	0.96	0.86

	Experiment2				
Time (hr)	0	0.5	1	2	3
Top bands	72852617	94994048	70346019	92296375	73944435
1	3885119	5581787	6865067	3600280	967917
2	2060149	1881512	1787272	1575426	1141917
3	6698664	6107497	5939003	5580213	4357891
4	2126521	1823602	1746076	1496109	881565
5	2948642	2722749	2580836	2630958	1934032
6	187632	156263	128012	115226	82699
7	112545	93773	118169	114418	75013
8	570212	533059	464480	399408	289085
9	838462	742901	682527	699096	613860
10	545155	435522	501274	493282	382782
11	8495300	7859207	6990584	5967178	3926886
12	2292909	2108651	1928958	1431201	702398
13	641747	479842	374697	278812	153052
14	203523	137115	112007	74433	27345
15	2227840	1885996	1600356	1094903	667747
16	168153	130603	91707	57504	21363
17	280468	224951	196810	142203	73517
18	1307364	1152628	986282	828875	581596
19	498650	534200	413337	447671	391878
Total	108941670	129585906	103853474	119323571	91216979
Ratio	1.00	1.19	0.95	1.10	0.84

(2) Band density after adjustment

	Experiment1				
Time (hr)	0	0.5	1	2	3
Top bands	113683744	110606116	111735217	125929855	138392214
1	6099051	9611336	11959307	5903859	1808234
2	3252219	3267861	3145230	2606057	2125207
3	10487993	10512574	10351838	9128500	7983715
4	3355755	3168584	3073720	2476876	1650927
5	4638209	4710014	4522704	4325162	3568195
6	331217	310223	265073	227885	195641
7	214088	203094	247987	226570	181639
8	928017	956174	849116	690722	571613
9	1346468	1315912	1227604	1178812	1163251
10	888931	788963	912984	843612	742298
11	13290626	13515575	12177180	9758734	7198557
12	3615309	3657251	3391168	2371164	1324540
13	1039606	864942	693270	494312	323801
14	356006	277397	237290	161448	94803
15	3513806	3275548	2820779	1823448	1261416
16	300832	266233	202054	133876	83906
17	476035	427977	384492	271822	178914
18	2077924	2018317	1754865	1390179	1104477
19	816385	958131	760341	769327	758869
Total	170712221	170712221	170712221	170712221	170712221

	Experiment2				
Time (hr)	0	0.5	1	2	3
Top bands	72852617	79860616	73792551	84266010	88312837
1	3885119	4692556	7201414	3287033	1155997
2	2060149	1581770	1874838	1438354	1363806
3	6698664	5134516	6229978	5094699	5204688
4	2126521	1533085	1831623	1365938	1052865
5	2948642	2288989	2707281	2402048	2309840
6	187632	131369	134284	105200	98769
7	112545	78834	123959	104463	89589
8	570212	448138	487236	364657	345258
9	838462	624550	715967	638270	733141
10	545155	366139	525834	450364	457161
11	8495300	6607162	7333080	5447996	4689932
12	2292909	1772723	2023465	1306678	838883
13	641747	403398	393055	254553	182792
14	203523	115271	117494	67957	32659
15	2227840	1585539	1678764	999640	797499
16	168153	109796	96201	52500	25514
17	280468	189114	206452	129830	87802
18	1307364	969004	1034604	756758	694608
19	498650	449097	433588	408721	468025
Total	108941670	108941670	108941670	108941670	108941670

(3) Signal remain (%)

	Experiment1					Experiment2					T50% (hrs)
Time (hr)	0	0.5	1	2	3	0	0.5	1	2	3	
Top bands	100	97	98	111	122	100	110	101	116	121	
1	100	158	196	97	30	100	121	185	85	30	2.8
2	100	100	97	80	65	100	77	91	70	66	3.6
3	100	100	99	87	76	100	77	93	76	78	>4
4	100	94	92	74	49	100	72	86	64	50	3
5	100	102	98	93	77	100	78	92	81	78	>4
6	100	94	80	69	59	100	70	72	56	53	3.6
7	100	95	116	106	85	100	70	110	93	80	>4
8	100	103	91	74	62	100	79	85	64	61	3.6
9	100	98	91	88	86	100	74	85	76	87	>4
10	100	89	103	95	84	100	67	96	83	84	>4
11	100	102	92	73	54	100	78	86	64	55	3.2
12	100	101	94	66	37	100	77	88	57	37	2.6
13	100	83	67	48	31	100	63	61	40	28	2
14	100	78	67	45	27	100	57	58	33	16	1.7
15	100	93	80	52	36	100	71	75	45	36	2.3
16	100	88	67	45	28	100	65	57	31	15	2.2
17	100	90	81	57	38	100	67	74	46	31	2.4
18	100	97	84	67	53	100	74	79	58	53	3.2
19	100	117	93	94	93	100	90	87	82	94	>4

CPDs in the *MFA2* NTS in *swr1Δ* strain (*HaeIII* fragment)

(1) Band density values (peak areas)

	Experiment1				
Time (hr)	0	0.5	1	2	3
Top bands	112356595	108803342	105520913	124502029	117771126
1	5948324	7665922	7792765	4670997	2580977
2	3282215	3227837	2728232	2222343	1736133
3	10464502	10274229	9193168	8170772	6594877
4	3382850	3230318	2717043	2143598	1298561
5	4558472	4384154	3877529	3451645	2774319
6	261112	251947	206401	157587	141678
7	294859	228205	197419	194470	182995
8	891569	934611	753739	706856	546301
9	1246906	1120122	1007910	969134	891502
10	835686	826669	732777	738275	636191
11	12885024	12477824	10592553	9008388	6616959
12	3781835	3602863	3114901	2320054	1577080
13	878139	779783	600004	409053	284238
14	254245	287085	186601	131159	94412
15	3344028	3143777	2415992	1525439	922849
16	281184	230390	200537	126682	92163
17	446674	431794	335542	211845	157899
18	1945474	1826425	1478558	1235989	862408
19	1514655	1400019	1267878	1257507	875718
Total	168854346	165127315	154920463	164153825	146638389
Ratio	1.00	0.98	0.92	0.97	0.87

	Experiment2				
Time (hr)	0	0.5	1	2	3
Top bands	72001844	73724020	65619809	84787712	74472845
1	3788495	4889567	4970879	2969661	1629847
2	2079378	2044518	1724245	1399943	1088257
3	6683605	6561630	5868612	5213202	4202970
4	2143890	2046109	1717073	1349464	807750
5	2897526	2785779	2461006	2187992	1753790
6	142690	136815	107618	76326	66127
7	164324	121595	101860	99969	92614
8	546847	574439	458490	428436	325512
9	774637	693361	621428	596570	546804
10	511023	505243	445053	448577	383136
11	8235288	7974251	6765693	5750159	4217126
12	2399661	2284930	1972121	1462582	986296
13	538238	475186	359938	237528	157515
14	138288	159341	94925	59384	35827
15	2119003	1990632	1524083	953191	566899
16	155558	122996	103859	56514	34385
17	261645	252107	190404	111108	76526
18	1222456	1146139	923138	767639	528153
19	946278	872791	788081	781433	536685
Total	107750674	109361449	96818315	109737391	92509067
Ratio	1.00	1.01	0.90	1.02	0.86

(2) Band density after adjustment

	Experiment 1				
Time (hr)	0	0.5	1	2	3
Top bands	112356595	111259104	115011694	128067127	135613644
1	5948324	7838947	8493663	4804750	2971999
2	3282215	3300691	2973615	2285979	1999160
3	10464502	10506125	10020021	8404741	7594012
4	3382850	3303228	2961420	2204980	1495295
5	4558472	4483107	4226282	3550483	3194633
6	261112	257634	224966	162100	163143
7	294859	233356	215175	200038	210719
8	891569	955706	821532	727097	629067
9	1246906	1145404	1098564	996885	1026566
10	835686	845328	798684	759415	732574
11	12885024	12759456	11545270	9266342	7619440
12	3781835	3684182	3395062	2386488	1816010
13	878139	797383	653970	420766	327300
14	254245	293565	203384	134915	108716
15	3344028	3214735	2633292	1569120	1062662
16	281184	235590	218574	130310	106126
17	446674	441540	365721	217911	181821
18	1945474	1867649	1611543	1271382	993064
19	1514655	1431619	1381914	1293516	1008391
Total	168854346	168854346	168854346	168854346	168854346

	Experiment 2				
Time (hr)	0	0.5	1	2	3
Top bands	72001844	72638145	73029350	83252691	86742840
1	3788495	4817549	5532172	2915897	1898377
2	2079378	2014405	1918941	1374598	1267556
3	6683605	6464984	6531274	5118821	4895443
4	2143890	2015972	1910958	1325033	940833
5	2897526	2744748	2738893	2148380	2042741
6	142690	134800	119770	74944	77022
7	164324	119804	113362	98159	107872
8	546847	565978	510261	420680	379143
9	774637	683149	691597	585770	636895
10	511023	497801	495306	440456	446260
11	8235288	7856799	7529649	5646056	4911931
12	2399661	2251276	2194805	1436103	1148796
13	538238	468187	400581	233228	183467
14	138288	156994	105643	58309	41730
15	2119003	1961312	1696177	935934	660300
16	155558	121184	115586	55491	40050
17	261645	248393	211903	109096	89134
18	1222456	1129258	1027375	753741	615170
19	946278	859935	877068	767285	625109
Total	107750674	107750674	107750674	107750674	107750674

(3) Signal remain (%)

	Experiment1					Experiment2					T50% (hrs)
Time (hr)	0	0.5	1	2	3	0	0.5	1	2	3	
Top bands	100	99	102	114	121	100	101	101	116	120	
1	100	132	143	81	50	100	127	146	77	50	3
2	100	101	91	70	61	100	97	92	66	61	3.6
3	100	100	96	80	73	100	97	98	77	73	>4
4	100	98	88	65	44	100	94	89	62	44	2.8
5	100	98	93	78	70	100	95	95	74	70	>4
6	100	99	86	62	62	100	94	84	53	54	3.5
7	100	79	73	68	71	100	73	69	60	66	>4
8	100	107	92	82	71	100	103	93	77	69	>4
9	100	92	88	80	82	100	88	89	76	82	>4
10	100	101	96	91	88	100	97	97	86	87	>4
11	100	99	90	72	59	100	95	91	69	60	3.4
12	100	97	90	63	48	100	94	91	60	48	2.8
13	100	91	74	48	37	100	87	74	43	34	2
14	100	115	80	53	43	100	114	76	42	30	2.5
15	100	96	79	47	32	100	93	80	44	31	2.2
16	100	84	78	46	38	100	78	74	36	26	2.2
17	100	99	82	49	41	100	95	81	42	34	2.4
18	100	96	83	65	51	100	92	84	62	50	3
19	100	95	91	85	67	100	91	93	81	66	>4

CPDs in the *MFA2* TS in WT strain (*HaeIII* fragment)

(1) Band density values (peak areas)

	Experiment1				
Time (hr)	0	0.5	1	2	3
Top bands	68595309	62461290	78333381	75299007	78936560
1	1005100	846872	1098873	601132	451923
2	1357833	1263458	1433515	796179	528399
3	10317954	9425946	9891996	5000619	3175394
4	3821355	3461616	3515550	1692373	1124360
5	441501	380532	439120	212645	151758
6	682601	710992	846904	469626	334788
7	3037887	2785710	3323889	2166413	1636099
8	369303	380660	445271	330857	235631
9	549909	477203	570258	335888	248082
10	531129	403335	455809	225188	152513
11	342619	227391	265197	145986	89152
12	1273574	1001725	1093986	558920	367501
13	1355226	1087676	1180593	585418	429070
14	527678	468895	550211	242312	216780
15	4236525	5097435	5923390	3480965	3941276
16	2055734	1459978	1442394	638472	377230
17	3497697	2828150	3226657	1631001	1028988
18	1318151	1017669	1063281	561513	355165
19	218955	139466	154673	56950	35751
20	944788	868581	814708	355310	239306
Total	106480828	96794581	116069656	95386776	94055728
Ratio	1.00	0.91	1.09	0.90	0.88

	Experiment2				
Time (hr)	0	0.5	1	2	3
Top bands	59738958	64396618	78220197	85577452	78745528
1	872195	734388	953865	520364	390413
2	1179403	1097208	1245317	690238	457018
3	8983096	8206215	8612114	4352037	2762382
4	3324973	3011663	3058636	1470766	976062
5	381336	328236	379262	182016	128988
6	591318	616045	734415	405831	288396
7	2642622	2422992	2891712	1883624	1421754
8	318456	328347	384619	284972	202036
9	475752	412430	493475	289353	212880
10	459396	348095	393797	192941	129645
11	295216	194859	227786	123961	74462
12	1106019	869255	949609	483600	316886
13	1177132	944113	1025038	506678	370509
14	456390	405194	476015	207855	185618
15	3686560	4436358	5155711	3028515	3429417
16	1787230	1268364	1253050	552885	325359
17	3043087	2459955	2807029	1417314	892999
18	1144842	883142	922866	485858	306143
19	187512	118283	131526	46416	27953
20	819666	753295	706375	306268	205236
Total	92671159	94235056	111022417	103008947	91849690
Ratio	1.00	1.02	1.20	1.11	0.99

(2) Band density after adjustment

	Experiment1				
Time (hr)	0	0.5	1	2	3
Top bands	68595309	68711800	71862049	84056732	89364363
1	1005100	931618	1008092	671047	511624
2	1357833	1389892	1315089	888779	598202
3	10317954	10369202	9074791	5582221	3594875
4	3821355	3808020	3225121	1889206	1272892
5	441501	418612	402844	237377	171806
6	682601	782141	776939	524247	379015
7	3037887	3064476	3049293	2418380	1852233
8	369303	418753	408486	369338	266759
9	549909	524957	523147	374954	280854
10	531129	443697	418153	251379	172660
11	342619	250146	243288	162965	100929
12	1273574	1101967	1003609	623926	416049
13	1355226	1196520	1083061	653505	485752
14	527678	515818	504757	270494	245418
15	4236525	5607536	5434042	3885822	4461933
16	2055734	1606078	1323234	712730	427063
17	3497697	3111163	2960094	1820696	1164921
18	1318151	1119508	975440	626820	402084
19	218955	153423	141895	63574	40474
20	944788	955500	747403	396634	270919
Total	106480828	106480828	106480828	106480828	106480828

	Experiment2				
Time (hr)	0	0.5	1	2	3
Top bands	59738958	63327912	65290926	76989056	79449799
1	872195	722200	796198	468141	393904
2	1179403	1078999	1039474	620967	461106
3	8983096	8070027	7188590	3915275	2787088
4	3324973	2961683	2553064	1323162	984792
5	381336	322788	316573	163750	130142
6	591318	605822	613022	365103	290975
7	2642622	2382781	2413731	1694587	1434470
8	318456	322898	321044	256373	203843
9	475752	405585	411907	260314	214784
10	459396	342319	328705	173578	130805
11	295216	191626	190135	111520	75128
12	1106019	854829	792645	435067	319721
13	1177132	928445	855606	455829	373823
14	456390	398470	397333	186995	187278
15	3686560	4362733	4303507	2724579	3460088
16	1787230	1247315	1045929	497398	328269
17	3043087	2419130	2343046	1275075	900986
18	1144842	868485	770323	437099	308881
19	187512	116320	109786	41758	28203
20	819666	740794	589616	275532	207072
Total	92671159	92671159	92671159	92671159	92671159

(3) Signal remain (%)

	Experiment1					Experiment2					T50% (hrs)
Time (hr)	0	0.5	1	2	3	0	0.5	1	2	3	
Top bands	100	100	105	123	130	100	116	109	129	103	
1	100	93	100	67	51	100	83	91	54	45	3
2	100	102	97	65	44	100	91	88	53	39	2.8
3	100	100	88	54	35	100	90	80	44	31	2.4
4	100	100	84	49	33	100	89	77	40	30	2.2
5	100	95	91	54	39	100	85	83	43	34	2.4
6	100	115	114	77	56	100	102	104	62	49	3
7	100	101	100	80	61	100	90	91	64	54	3.3
8	100	113	111	100	72	100	101	101	81	64	3.5
9	100	95	95	68	51	100	85	87	55	45	3
10	100	84	79	47	33	100	75	72	38	28	2
11	100	73	71	48	29	100	65	64	38	25	1.8
12	100	87	79	49	33	100	77	72	39	29	2.5
13	100	88	80	48	36	100	79	73	39	32	2.2
14	100	98	96	51	47	100	87	87	41	41	2.6
15	100	132	128	92	105	100	118	117	74	94	>4
16	100	78	64	35	21	100	70	59	28	18	1.4
17	100	89	85	52	33	100	79	77	42	30	2.2
18	100	85	74	48	31	100	76	67	38	27	1.9
19	100	70	65	29	18	100	62	59	22	15	1.3
20	100	101	79	42	29	100	90	72	34	25	2

CPDs in the MFA2 TS in *htz1* strain (*Hae*III fragment)

(1) Band density values (peak areas)

	Experiment1				
Time (hr)	0	0.5	1	2	3
Top bands	70900955	67472946	66258436	76658787	72787916
1	1356172	1241811	1103087	906999	665135
2	2018977	1884316	1872059	1581442	1259390
3	13022504	11266306	10855498	9061173	7321822
4	4419760	3823773	3545524	2499638	1730805
5	519486	478531	420538	345805	235156
6	823809	780852	745035	682318	549637
7	3143983	2864992	2764279	2676557	2209893
8	277654	324104	347401	335912	321004
9	572439	505215	457756	385658	266885
10	565591	435883	349652	212238	136106
11	424606	344451	310085	206740	148303
12	1621339	1344668	1234260	879575	593509
13	1470979	1309990	1250658	956384	678083
14	605188	513739	540220	431582	317906
15	8149815	5317936	5556093	4647911	4991570
16	2187643	1759771	1588760	1128041	818609
17	3973140	3357873	3198178	2562892	1875423
18	1504261	1173950	1081928	879233	641807
19	275603	197322	159514	101146	60205
20	1149273	1001615	913237	660233	465287
Total	118983175	107400043	104552197	107800266	98074453
Ratio	1.00	0.90	0.88	0.91	0.82

	Experiment2				
Time (hr)	0	0.5	1	2	3
Top bands	61747028	68761451	54703690	72761733	76390451
1	1177956	1078354	957535	786754	576107
2	1755217	1637935	1627260	1374151	1093665
3	11338587	9809050	9451263	7888521	6373657
4	3846146	3327079	3084742	2173842	1504237
5	449256	413586	363078	297991	201622
6	714301	676889	645695	591072	475516
7	2735025	2492042	2404327	2327927	1921492
8	238635	279090	299380	289375	276391
9	495374	436826	395493	332700	229256
10	489410	376443	301341	181662	115356
11	366621	296811	266881	176874	125979
12	1408899	1167937	1071778	762870	513725
13	1277946	1137734	1086060	829766	587383
14	523897	444250	467313	372697	273693
15	7094785	4628399	4835819	4044851	4344156
16	1902114	1529465	1380525	979268	709772
17	3457168	2921310	2782225	2228932	1630190
18	1306932	1019252	939107	762572	555790
19	236849	168672	135743	84909	49251
20	997760	869159	792188	571837	402052
Total	103559907	103471737	87991445	99820306	98349743
Ratio	1.00	1.00	0.85	0.96	0.95

(2) Band density after adjustment

	Experiment1				
Time (hr)	0	0.5	1	2	3
Top bands	70900955	74749927	75403858	84611163	88305742
1	1356172	1375740	1255342	1001088	806937
2	2018977	2087540	2130452	1745496	1527882
3	13022504	12481381	12353845	10001155	8882778
4	4419760	4236168	4034900	2758944	2099799
5	519486	530140	478583	381678	285289
6	823809	865067	847870	753100	666816
7	3143983	3173983	3145823	2954215	2681025
8	277654	359059	395351	370759	389440
9	572439	559702	520939	425665	323782
10	565591	482893	397914	234255	165123
11	424606	381600	352885	228187	179920
12	1621339	1489691	1404620	970820	720041
13	1470979	1451273	1423282	1055596	822645
14	605188	569146	614784	476353	385682
15	8149815	5891477	6322982	5130073	6055734
16	2187643	1949563	1808051	1245061	993130
17	3973140	3720021	3639611	2828759	2275249
18	1504261	1300561	1231263	970442	778635
19	275603	218604	181531	111639	73040
20	1149273	1109639	1039288	728723	564482
Total	118983175	118983175	118983175	118983175	118983175

	Experiment2				
Time (hr)	0	0.5	1	2	3
Top bands	61747028	68820044	64382498	75487629	80437302
1	1177956	1079273	1126953	816229	606626
2	1755217	1639331	1915174	1425632	1151603
3	11338587	9817409	11123490	8184051	6711307
4	3846146	3329914	3630530	2255281	1583925
5	449256	413939	427318	309155	212303
6	714301	677466	759938	613216	500706
7	2735025	2494166	2829728	2415138	2023285
8	238635	279328	352350	300216	291033
9	495374	437199	465468	345164	241401
10	489410	376764	354658	188468	121467
11	366621	297064	314101	183500	132653
12	1408899	1168932	1261409	791450	540940
13	1277946	1138704	1278218	860851	618501
14	523897	444629	549996	386660	288192
15	7094785	4632343	5691428	4196384	4574291
16	1902114	1530768	1624783	1015955	747373
17	3457168	2923799	3274489	2312435	1716551
18	1306932	1020121	1105265	791141	585233
19	236849	168816	159760	88090	51860
20	997760	869900	932351	593260	423351
Total	103559907	103559907	103559907	103559907	103559907

(3) Signal remain (%)

Time (hr)	Experiment1					Experiment2					T50% (hrs)
	0	0.5	1	2	3	0	0.5	1	2	3	
Top bands	100	105	106	119	125	100	101	104	98	113	
1	100	101	93	74	60	100	92	96	69	51	3.4
2	100	103	106	86	76	100	93	109	81	66	3.9
3	100	96	95	77	68	100	87	98	72	59	>4
4	100	96	91	62	48	100	87	94	59	41	2.9
5	100	102	92	73	55	100	92	95	69	47	3.2
6	100	105	103	91	81	100	95	106	86	70	>4
7	100	101	100	94	85	100	91	103	88	74	>4
8	100	129	142	134	140	100	117	148	126	122	>4
9	100	98	91	74	57	100	88	94	70	49	3.3
10	100	85	70	41	29	100	77	72	39	25	1.9
11	100	90	83	54	42	100	81	86	50	36	2.5
12	100	92	87	60	44	100	83	90	56	38	2.7
13	100	99	97	72	56	100	89	100	67	48	3.2
14	100	94	102	79	64	100	85	105	74	55	3.5
15	100	72	78	63	74	100	65	80	59	64	>4
16	100	89	83	57	45	100	80	85	53	39	2.6
17	100	94	92	71	57	100	85	95	67	50	3.4
18	100	86	82	65	52	100	78	85	61	45	3
19	100	79	66	41	27	100	71	67	37	22	1.7
20	100	97	90	63	49	100	87	93	59	42	3

CPDs in the *MFA2* TS in *swr1Δ* strain (*HaeIII* fragment)

(1) Band density values (peak areas)

	Experiment1				
Time (hr)	0	0.5	1	2	3
Top bands	71633198	68935290	69424565	70009178	66960268
1	1668950	1340123	1234372	916955	666300
2	2080953	1978285	1835904	1480654	1082700
3	13098115	11645763	10760142	8563670	6376383
4	4491019	3924503	3534187	2382995	1578263
5	555310	464732	441838	302624	195646
6	847140	761235	756975	611726	467089
7	3326564	2913541	2833237	2498017	1860975
8	357173	397475	398589	364762	298687
9	595278	525176	474901	413642	272136
10	559933	445756	363089	245986	148445
11	454309	380034	324049	234388	163721
12	1642891	1379816	1188328	901453	567085
13	1564524	1461355	1291751	943160	672261
14	654564	648728	546149	387008	284857
15	6610092	6757146	5565453	5410369	3934956
16	2145416	1796108	1575421	1086837	655867
17	3907824	3482965	3166641	2376715	1552661
18	1407538	1172618	1031848	796721	518800
19	251392	198314	157915	90413	60449
20	1150495	1094368	914110	587195	355816
Total	119002680	111703329	107819467	100604470	88673370
Ratio	1.00	0.94	0.91	0.85	0.75

	Experiment2				
Time (hr)	0	0.5	1	2	3
Top bands	72384766	80035059	60461187	70970347	80314941
1	1450366	1163978	1071876	795426	577122
2	1809194	1719777	1595772	1286372	939780
3	11404440	10139534	9368214	7455227	5550240
4	3908208	3414808	3074868	2072253	1371383
5	480456	401568	381630	260382	167211
6	734622	659803	656094	529591	403622
7	2894042	2534325	2464386	2172430	1617607
8	307892	342992	343962	314501	256954
9	515266	454211	410425	357072	233830
10	484483	385041	313043	211054	126103
11	392491	327802	279043	200953	139407
12	1427670	1198548	1031774	781924	490711
13	1359417	1269564	1121849	818249	582313
14	566900	561817	472478	333876	244909
15	5753785	5881860	4843972	4708903	3423912
16	1865337	1561112	1368908	943382	568035
17	3400282	3030257	2754759	2066784	1349085
18	1222692	1018092	895490	690710	448658
19	215763	169535	134351	75561	49464
20	998825	949941	792948	508226	306710
Total	113576894	117219625	93837029	97553227	99161999
Ratio	1.00	1.03	0.83	0.86	0.87

(2) Band density after adjustment

	Experiment1				
Time (hr)	0	0.5	1	2	3
Top bands	71633198	73439926	76625396	82812222	89862959
1	1668950	1427694	1362403	1084644	894198
2	2080953	2107558	2026327	1751431	1453021
3	13098115	12406766	11876202	10129765	8557323
4	4491019	4180953	3900759	2818789	2118083
5	555310	495100	487667	357967	262563
6	847140	810978	835490	723597	626850
7	3326564	3103929	3127105	2954846	2497492
8	357173	423449	439931	431468	400848
9	595278	559494	524159	489288	365216
10	559933	474884	400749	290971	199219
11	454309	404868	357660	277252	219719
12	1642891	1469981	1311583	1066307	761047
13	1564524	1556849	1425734	1115642	902197
14	654564	691119	602797	457783	382288
15	6610092	7198697	6142711	6399800	5280844
16	2145416	1913476	1738827	1285594	880196
17	3907824	3710562	3495090	2811361	2083723
18	1407538	1249244	1138873	942423	696247
19	251392	211273	174295	106948	81125
20	1150495	1165880	1008923	694579	477518
Total	119002680	119002680	119002680	119002680	119002680

	Experiment2				
Time (hr)	0	0.5	1	2	3
Top bands	62384766	77547880	73180001	82627627	81990094
1	1450366	1127806	1297359	926079	661016
2	1809194	1666333	1931463	1497665	1076393
3	11404440	9824436	11338943	8679790	6357062
4	3908208	3308689	3721707	2412633	1570737
5	480456	389089	461911	303152	191518
6	734622	639299	794112	616579	462295
7	2894042	2455568	2982802	2529264	1852754
8	307892	332333	416319	366159	294307
9	515266	440096	496763	415724	267821
10	484483	373076	378896	245721	144434
11	392491	317615	337743	233961	159672
12	1427670	1161302	1248822	910360	562045
13	1359417	1230111	1357845	952651	666962
14	566900	544358	571870	388717	280511
15	5753785	5699074	5862965	5482367	3921636
16	1865337	1512598	1656876	1098338	650609
17	3400282	2936088	3334259	2406265	1545198
18	1222692	986454	1083869	804163	513878
19	215763	164267	162613	87972	56654
20	998825	920420	959755	591705	351295
Total	113576894	113576894	113576894	113576894	113576894

(3) Signal remain (%)

Time (hr)	Experiment1					Experiment2					T50% (hrs)
	0	0.5	1	2	3	0	0.5	1	2	3	
Top bands	100	103	107	116	125	100	124	117	125	126	
1	100	86	82	65	54	100	78	89	64	46	3.4
2	100	101	97	84	70	100	92	107	83	59	3.8
3	100	95	91	77	65	100	86	99	76	56	4
4	100	93	87	63	47	100	85	95	62	40	2.8
5	100	89	88	64	47	100	81	96	63	40	2.9
6	100	96	99	85	74	100	87	108	84	63	>4
7	100	93	94	89	75	100	85	103	87	64	>4
8	100	119	123	121	112	100	108	135	119	96	>4
9	100	94	88	82	61	100	85	96	81	52	3.6
10	100	85	72	52	36	100	77	78	51	30	2
11	100	89	79	61	48	100	81	86	60	41	2.8
12	100	89	80	65	46	100	81	87	64	39	2.8
13	100	100	91	71	58	100	90	100	70	49	3.3
14	100	106	92	70	58	100	96	101	69	49	3.3
15	100	109	93	97	80	100	99	102	95	68	>4
16	100	89	81	60	41	100	81	89	59	35	2.5
17	100	95	89	72	53	100	86	98	71	45	3.2
18	100	89	81	67	49	100	81	89	66	42	3
19	100	84	69	43	32	100	76	75	41	26	1.9
20	100	101	88	60	42	100	92	96	59	35	2.6

CPDs in the *HMRa1* NTS in WT strain (*RsaI*-*BglIII* fragment)

(1) Band density values (peak areas)

		Experiment1				
Time (hr)		0	0.5	1	2	3
Top bands		166514315	162382269	153109141	175758275	185468518
1		739622	1010654	891961	595286	158866
2		5000589	5609171	4517317	5465690	3923494
3		8647298	9505593	7879194	9086375	6834375
4		8439491	8583354	6593564	6679155	4896752
5		7033508	8488862	6309086	7376040	6396358
6		3386863	3571969	2670561	3279431	2503352
7		1638739	1810235	1344793	1619356	1604099
8		4177241	4597870	3399060	4126361	3023394
9		4376253	4423012	3402498	4084490	3273473
10		1265968	1300841	912894	1759654	1055331
11		1500374	1764874	1301111	1325488	1339938
12		3369761	3296165	2582321	2863222	2047182
13		5564244	6345185	5099551	5735737	4678076
14		7757480	8267316	6279628	7577893	5929318
15		2110116	2933777	2381340	2911756	2309083
16		2884772	3727506	3008248	3418586	2325880
Total		234406633	237618654	211682268	243662795	237767488
Ratio		1.00	1.01	0.90	1.04	1.01

		Experiment2				
Time (hr)		0	0.5	1	2	3
Top bands		178848925	165264837	180342372	186516399	188253411
1		778975	1070703	761903	547860	353532
2		5812262	6683916	5217176	5476637	3041425
3		10102026	10664355	8689625	8831655	5808186
4		9541793	10770531	8051569	7707321	4657104
5		8858973	9614295	6943122	7667456	6072423
6		4232555	4674737	3303285	3466114	2805261
7		1943999	2273239	1399840	1747022	1539095
8		5678822	6211075	4839981	4883764	3777052
9		4670849	5025965	4088620	4429152	3008361
10		1001704	1449939	1114903	971835	1039831
11		2242461	1858906	1495288	1580759	1481280
12		3720048	4029351	3407126	2907333	2526828
13		8149019	8129699	6085366	6943300	4682833
14		8338087	9238572	7698480	8944231	6922133
15		2423199	2649369	2251525	2667896	1985576
16		4050997	3923534	2962474	3827009	3235871
Total		260394693	253533022	248652654	259115744	241190200
Ratio		1.00	0.97	0.95	1.00	0.93

(2) Band density after adjustment

		Experiment1				
Time (hr)		0	0.5	1	2	3
Top bands		166514315	160187260	169545605	169081642	182846911
1		739622	996993	987714	572672	156620
2		5000589	5533348	5002257	5258062	3868035
3		8647298	9377101	8725036	8741205	6737771
4		8439491	8467328	7301392	6425430	4827536
5		7033508	8374113	6986375	7095842	6305945
6		3386863	3523685	2957249	3154853	2467967
7		1638739	1785765	1489158	1557841	1581425
8		4177241	4535718	3763953	3969610	2980658
9		4376253	4363223	3767761	3929330	3227202
10		1265968	1283257	1010894	1692809	1040414
11		1500374	1741017	1440787	1275136	1320998
12		3369761	3251609	2859536	2754455	2018245
13		5564244	6259414	5646995	5517850	4611951
14		7757480	8155562	6953755	7290027	5845507
15		2110116	2894120	2636980	2801145	2276444
16		2884772	3677119	3331187	3288723	2293003
Total		234406633	234406633	234406633	234406633	234406633

		Experiment2				
Time (hr)		0	0.5	1	2	3
Top bands		178848925	169737599	188858618	187437011	203242873
1		778975	1099681	797882	550564	381681
2		5812262	6864811	5463545	5503669	3283595
3		10102026	10952977	9099972	8875246	6270656
4		9541793	11062027	8431786	7745363	5027920
5		8858973	9874498	7270994	7705302	6555933
6		4232555	4801255	3459275	3483222	3028626
7		1943999	2334762	1465945	1755645	1661643
8		5678822	6379173	5068537	4907869	4077796
9		4670849	5161988	4281695	4451013	3247898
10		1001704	1489180	1167552	976632	1122626
11		2242461	1909216	1565899	1588561	1599225
12		3720048	4138402	3568019	2921684	2728023
13		8149019	8349723	6372733	6977570	5055698
14		8338087	9488606	8062022	8988378	7473299
15		2423199	2721072	2357848	2681064	2143675
16		4050997	4029721	3102370	3845899	3493524
Total		260394693	260394693	260394693	260394693	260394693

(3) Signal remain (%)

	Experiment1					Experiment2					T50% (hrs)
Time (hr)	0	0.5	1	2	3	0	0.5	1	2	3	
Top bands	100	96	102	102	110	100	95	106	105	114	
1	100	135	134	77	21	100	141	102	71	49	2.6
2	100	111	100	105	77	100	118	94	95	56	>4
3	100	108	101	101	78	100	108	90	88	62	3.9
4	100	100	87	76	57	100	116	88	81	53	3.4
5	100	119	99	101	90	100	111	82	87	74	3.8
6	100	104	87	93	73	100	113	82	82	72	3.4
7	100	109	91	95	97	100	120	75	90	85	6
8	100	109	90	95	71	100	112	89	86	72	3.9
9	100	100	86	90	74	100	111	92	95	70	4
10	100	101	80	134	82	100	149	117	97	112	>4
11	100	116	96	85	88	100	85	70	71	71	3.8
12	100	96	85	82	60	100	111	96	79	73	3.6
13	100	112	101	99	83	100	102	78	86	62	>4
14	100	105	90	94	75	100	114	97	108	90	>4
15	100	137	125	133	108	100	112	97	111	88	>4
16	100	127	115	114	79	100	99	77	95	86	4

CPDs in the *HMRa1* NTS in *htz1Δ* strain (*RsaI*-*BglII* fragment)

(1) Band density values (peak areas)

	Experiment1				
Time (hr)	0	0.5	1	2	3
Top bands	171605313	173596670	167655851	163512401	174919337
1	582569	1293245	463052	1377954	315124
2	5418383	7658251	4382676	7161654	3961966
3	8510665	12241675	7567476	11577720	7123279
4	8084920	11213279	6663828	7758172	4051194
5	7606418	10346853	6377730	10039489	6711774
6	3757768	4909372	2878881	4533995	2808275
7	1796571	2282847	1410443	2149430	1459146
8	5218947	6900354	4365011	6252841	3335183
9	4360516	5641059	3997643	4597781	2614816
10	1309827	1630532	921301	1649123	802927
11	1530132	1821463	1862903	2041792	1468879
12	3292073	4283591	3013596	5325665	2785015
13	7376595	9641860	6785099	8472360	4451708
14	8210242	10971262	7615864	10095504	5881608
15	2341758	2981633	2376462	3169102	2251822
16	3155100	3463753	2504599	3965728	2719849
Total	244157798	270877699	230842417	253680711	227661903
Ratio	1.00	1.11	0.95	1.04	0.93

	Experiment2				
Time (hr)	0	0.5	1	2	3
Top bands	180930054	168811049	200258086	173491359	204975597
1	510725	632976	384641	411351	228585
2	5612235	7975169	5519623	5451287	4575798
3	8874418	12810422	7879407	8109987	7410803
4	8425281	11725523	6926109	8080581	5169928
5	7420489	10811492	6624292	6487241	6976689
6	3860380	5575257	2933204	2679256	2858719
7	1791428	2304421	1684085	1463674	1435464
8	5401841	7175630	4500987	4492541	3414577
9	4496245	5847146	4513435	3746546	2854631
10	1377941	1616266	868068	835879	743190
11	1510350	1217688	1861405	1550123	1445731
12	3369099	4415094	3075321	3514422	2834181
13	7278038	10067765	7454043	7434008	4592447
14	8557488	11470208	7930453	6546333	6100912
15	2366570	3541602	2403181	2339371	2571692
16	3224600	3550211	2538358	4079766	2765434
Total	255007180	269547919	267354697	240713724	260954378
Ratio	1.00	1.06	1.05	0.94	1.02

(2) Band density after adjustment

	Experiment1				
Time (hr)	0	0.5	1	2	3
Top bands	171605313	156472759	177326524	157374314	187593618
1	582569	1165677	489762	1326227	337957
2	5418383	6902826	4635476	6892813	4249042
3	8510665	11034132	8003981	11143104	7639416
4	8084920	10107180	7048209	7466939	4344735
5	7606418	9326219	6745609	9662617	7198095
6	3757768	4425102	3044940	4363794	3011757
7	1796571	2057662	1491799	2068743	1564872
8	5218947	6219690	4616792	6018116	3576843
9	4360516	5084614	4228234	4425185	2804280
10	1309827	1469693	974443	1587217	861105
11	1530132	1641791	1970358	1965145	1575311
12	3292073	3861050	3187426	5125745	2986812
13	7376595	8690768	7176475	8154316	4774269
14	8210242	9889035	8055160	9716529	6307777
15	2341758	2687519	2513541	3050137	2414984
16	3155100	3122082	2649069	3816858	2916924
Total	244157798	244157798	244157798	244157798	244157798

	Experiment2				
Time (hr)	0	0.5	1	2	3
Top bands	180930054	159704552	191009361	183793186	200304166
1	510725	598830	366877	435776	223376
2	5612235	7544949	5264704	5774982	4471514
3	8874418	12119365	7515504	8591554	7241910
4	8425281	11092991	6606233	8560401	5052105
5	7420489	10228267	6318356	6872450	6817689
6	3860380	5274500	2797737	2838349	2793568
7	1791428	2180109	1606307	1550587	1402749
8	5401841	6788542	4293114	4759306	3336758
9	4496245	5531722	4304986	3969014	2789573
10	1377941	1529076	827977	885513	726252
11	1510350	1152000	1775437	1642168	1412783
12	3369099	4176922	2933290	3723107	2769589
13	7278038	9524660	7109785	7875435	4487785
14	8557488	10851449	7564193	6935051	5961871
15	2366570	3350550	2292192	2478281	2513083
16	3224600	3358695	2421126	4322020	2702410
Total	255007180	255007180	255007180	255007180	255007180

(3) Signal remain (%)

	Experiment1					Experiment2					T50% (hrs)
Time (hr)	0	0.5	1	2	3	0	0.5	1	2	3	
Top bands	100	91	103	92	109	100	88	106	102	111	
1	100	200	84	228	58	100	117	72	85	44	2.8
2	100	127	86	127	78	100	134	94	103	80	3.8
3	100	130	94	131	90	100	137	85	97	82	3.8
4	100	125	87	92	54	100	132	78	102	60	3.2
5	100	123	89	127	95	100	138	85	93	92	3.6
6	100	118	81	116	80	100	137	72	74	72	3.4
7	100	115	83	115	87	100	122	90	87	78	3.8
8	100	119	88	115	69	100	126	79	88	62	3.8
9	100	117	97	101	64	100	123	96	88	62	3.6
10	100	112	74	121	66	100	111	60	64	53	>4
11	100	107	129	128	103	100	76	118	109	94	3.6
12	100	117	97	156	91	100	124	87	111	82	3.6
13	100	118	97	111	65	100	131	98	108	62	>4
14	100	120	98	118	77	100	127	88	81	70	>4
15	100	115	107	130	103	100	142	97	105	106	>4
16	100	99	84	121	92	100	104	75	134	84	3.6

CPDs in the *HMRa1* NTS in *swr1A* strain (*RsaI*-*BglII* fragment)

(1) Band density values (peak areas)

	Experiment1				
Time (hr)	0	0.5	1	2	3
Top bands	178848925	171264837	158342372	196516399	218253411
1	778975	1070703	761903	547860	0
2	5812262	6683916	5217176	5476637	3041425
3	10102026	10664355	8689625	8831655	5808186
4	9541793	10770531	8051569	7707321	4657104
5	8858973	9614295	6943122	7667456	6072423
6	4232555	4674737	3303285	3466114	2805261
7	1943999	2273239	1399840	1747022	1539095
8	5678822	6211075	4839981	4883764	3777052
9	4670849	5025965	4088620	4429152	3008361
10	1001704	1449939	1114903	971835	1039831
11	2242461	1858906	1495288	1580759	1481280
12	3720048	4029351	3407126	2907333	2526828
13	8149019	8129699	6085366	6943300	4682833
14	8338087	9238572	7698480	8944231	6922133
15	2423199	2649369	2251525	2667896	1985576
16	4050997	3923534	2962474	3827009	3235871
Total	260394693	259533022	226652654	269115744	270836668
Ratio	1.00	1.00	0.87	1.03	1.04

	Experiment2				
Time (hr)	0	0.5	1	2	3
Top bands	176224554	199596351	168302611	171665250	180662567
1	598228	853188	583308	396243	229844
2	4997129	5758922	4477047	4603805	2575523
3	8746218	9037672	7511834	7635963	4993567
4	8256597	9330466	6954198	6653338	3987565
5	7359838	8319960	5985457	6618498	5224500
6	3616525	4002976	2004379	2946686	2169125
7	1616415	1904158	1140841	1444265	1262544
8	4880507	5345676	4147392	4185657	3218433
9	3999578	4309935	3490731	3788343	2546627
10	792885	1084625	891817	766781	826207
11	1877259	1542047	1224258	1398957	1212016
12	3668614	3438933	2895132	2458332	2125785
13	7039365	7022480	5235811	5985612	3810051
14	7204603	7991592	6645611	7834350	5967113
15	2035217	2232881	1885181	2249073	1652751
16	3457851	3146453	2306523	3262094	2745462
Total	246371383	274918316	225682132	233893248	225209679
Ratio	1.00	1.12	0.92	0.95	0.91

(2) Band density after adjustment

	Experiment1				
Time (hr)	0	0.5	1	2	3
Top bands	178848925	171833450	181914981	190148026	209838757
1	778975	1074258	875329	530106	0
2	5812262	6706108	5993863	5299159	2924164
3	10102026	10699761	9983259	8545453	5584254
4	9541793	10806290	9250215	7457555	4477551
5	8858973	9646215	7976752	7418982	5838304
6	4232555	4690258	3795049	3353790	2697105
7	1943999	2280786	1608236	1690408	1479756
8	5678822	6231696	5560514	4725499	3631430
9	4670849	5042651	4697297	4285619	2892375
10	1001704	1454752	1280880	940342	999741
11	2242461	1865078	1717893	1529532	1424170
12	3720048	4042729	3914349	2813117	2429407
13	8149019	8156690	6991301	6718293	4502289
14	8338087	9269244	8844561	8654381	6655253
15	2423199	2658165	2586712	2581439	1909023
16	4050997	3936560	3403500	3702990	3111114
Total	260394693	260394693	260394693	260394693	260394693

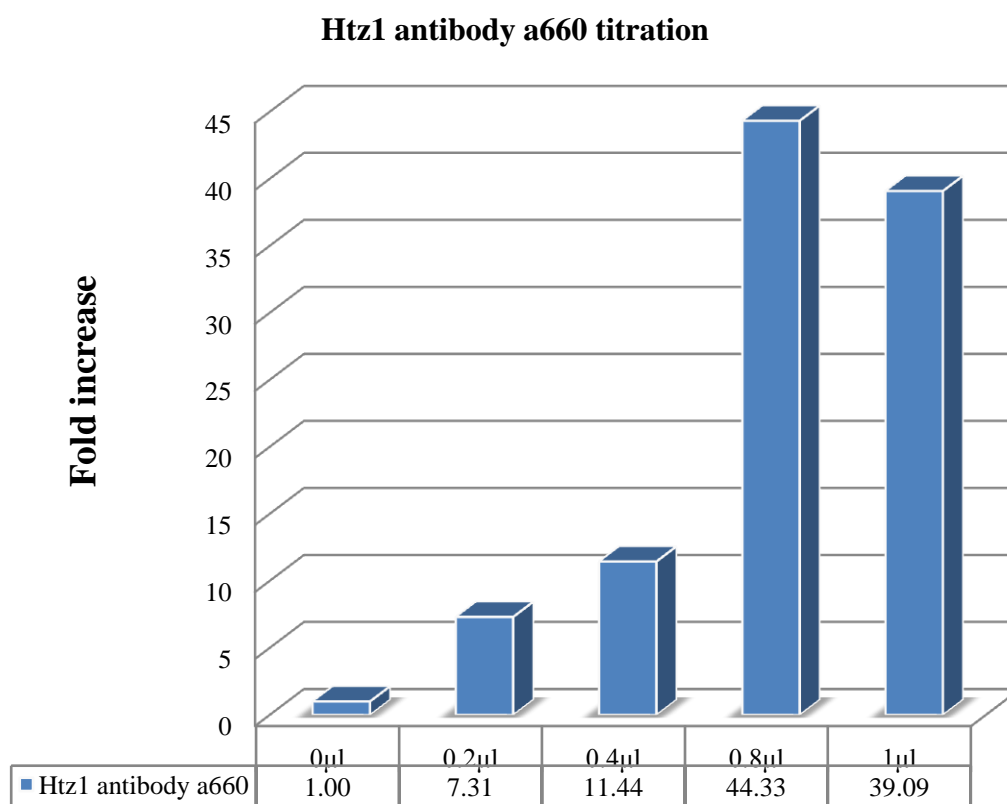
	Experiment2				
Time (hr)	0	0.5	1	2	3
Top bands	176224554	178870690	183731634	180823540	197638426
1	598228	764595	636783	417383	251441
2	4997129	5160927	4887477	4849417	2817531
3	8746218	8099220	8200476	8043339	5462785
4	8256597	8361611	7591719	7008292	4362254
5	7359838	7456033	6534170	6971593	5715417
6	3616525	3587315	2188129	3103890	2372945
7	1616415	1706434	1245427	1521316	1381178
8	4880507	4790592	4527601	4408960	3520852
9	3999578	3862400	3810742	3990450	2785919
10	792885	972000	973574	807689	903841
11	1877259	1381924	1336491	1473591	1325903
12	3668614	3081841	3160541	2589484	2325533
13	7039365	6293281	5715801	6304943	4168061
14	7204603	7161762	7254843	8252310	6527810
15	2035217	2001024	2058004	2369061	1808051
16	3457851	2819732	2517972	3436126	3003438
Total	246371383	246371383	246371383	246371383	246371383

(3) Signal remain (%)

	Experiment1					Experiment2					T50% (hrs)
Time (hr)	0	0.5	1	2	3	0	0.5	1	2	3	
Top bands	100	96	102	106	117	100	102	104	103	112	
1	100	138	112	68	0	100	128	106	70	42	2.4
2	100	115	103	91	50	100	103	98	97	56	3
3	100	106	99	85	55	100	93	94	92	62	3.2
4	100	113	97	78	47	100	101	92	85	53	3
5	100	109	90	84	66	100	101	89	95	78	3.8
6	100	111	90	79	64	100	99	61	86	66	3.6
7	100	117	83	87	76	100	106	77	94	85	3.8
8	100	110	98	83	64	100	98	93	90	72	3.4
9	100	108	101	92	62	100	97	95	100	70	3.4
10	100	145	128	94	100	100	123	123	102	114	>4
11	100	83	77	68	64	100	74	71	78	71	3.8
12	100	109	105	76	65	100	84	86	71	63	3.6
13	100	100	86	82	55	100	89	81	90	59	>4
14	100	111	106	104	80	100	99	101	115	91	3.8
15	100	110	107	107	79	100	98	101	116	89	3.8
16	100	97	84	91	77	100	82	73	99	87	3.8

Appendix IV - Raw data for experiment in Chapter 5

Antibody titration



Increasing volumes of antibody were added to optimize the amount of antibody for chromatin immunoprecipitation. This result was generated by qRT-PCR at MFA2 promoter region.

Data in the disc:

- 1.Htz1 pre-UV (3 biological repeats) after normalization whole-genome data
- 2.Htz1 pre-UV versus post-UV whole-genome data
- 3.Htz1 pre-UV and post-UV whole-genome data
- 4.Htz1 pre-UV versus *htz1Δ* control whole-genome data
- 5.Htz1 occupancy versus histone H3 acetylation whole-genome data
- 6.Htz1 occupancy versus CPD repair whole-genome data
- 7.Htz1 occupancy versus Gcn5 binding whole-genome data

qPCR quantification for microarray validation at *MFA2* and *HMRa1*

BY4742 (WT)	Time (hrs)	SQ mean			Fold change	Averaged Datasets	
		Input	IP	IP/Input		Average	SD
<i>MFA2</i>							
Expt 1	no UV	1.09E-01	2.47E-02	2.27E-01	1.72E+00	1.61E+00	1.02E-01
	0	1.09E-01	2.15E-02	1.98E-01	1.50E+00	1.37E+00	1.21E-01
	0.5	1.05E-01	1.42E-02	1.35E-01	1.02E+00	1.10E+00	1.27E-01
	1	6.90E-02	9.08E-03	1.32E-01	1.00E+00	1.00E+00	0.00E+00
Expt 2	no UV	1.07E-01	5.15E-02	4.82E-01	1.54E+00		
	0	9.20E-02	3.64E-02	3.96E-01	1.27E+00		
	0.5	8.45E-02	3.30E-02	3.91E-01	1.25E+00		
	1	9.47E-02	2.96E-02	3.13E-01	1.00E+00		
Expt 3	no UV	1.06E-01	1.82E-01	1.71E+00	1.55E+00		
	0	1.05E-01	1.55E-01	1.47E+00	1.34E+00		
	0.5	7.47E-02	8.51E-02	1.14E+00	1.04E+00		
	1	8.77E-02	9.65E-02	1.10E+00	1.00E+00		
<i>HMRa1</i>							
Expt 1	no UV	1.09E-01	1.24E-01	1.14E+00	2.72E-01	2.72E-01	3.23E-02
	0	7.38E-02	7.74E-02	1.05E+00	2.51E-01	2.54E-01	1.69E-02
	0.5	7.64E-02	5.69E-02	7.44E-01	1.78E-01	1.94E-01	1.42E-02
	1	7.62E-02	8.31E-02	1.09E+00	2.61E-01	2.43E-01	3.91E-02
Expt 2	no UV	7.40E-02	7.03E-03	9.50E-02	2.40E-01		
	0	5.07E-02	4.78E-03	9.43E-02	2.38E-01		
	0.5	1.20E-01	9.71E-03	8.06E-02	2.04E-01		
	1	9.05E-02	9.68E-03	1.07E-01	2.70E-01		
Expt 3	no UV	9.00E-02	2.33E-02	2.58E-01	3.05E-01		
	0	7.60E-02	1.75E-02	2.30E-01	2.72E-01		
	0.5	6.98E-02	1.19E-02	1.71E-01	2.01E-01		
	1	8.69E-02	1.46E-02	1.68E-01	1.98E-01		
Microarray		<i>MFA2</i> -log2	<i>HMRa1</i> -log2	<i>MFA2</i>	<i>HMRa1</i>		
	no UV	4.379091	0.1014931	20.81	1.08		
	0	3.866991	-0.4835903	14.59	0.72		
	0.5	2.924462	-1.096184	7.59	0.47		
	1	2.291658	-1.310162	4.89	0.40		

References:

- ABBOTT, D. W., IVANOVA, V. S., WANG, X., BONNER, W. M. & AUSIO, J. 2001. Characterization of the stability and folding of H2A.Z chromatin particles: implications for transcriptional activation. *J Biol Chem*, 276, 41945-9.
- ABOUSSEKHRA, A., BIGGERSTAFF, M., SHIVJI, M. K., VILPO, J. A., MONCOLLIN, V., PODUST, V. N., PROTIC, M., HUBSCHER, U., EGLY, J. M. & WOOD, R. D. 1995. Mammalian DNA nucleotide excision repair reconstituted with purified protein components. *Cell*, 80, 859-68.
- ADAM, M., ROBERT, F., LAROCHELLE, M. & GAUDREAU, L. 2001. H2A.Z Is Required for Global Chromatin Integrity and for Recruitment of RNA Polymerase II under Specific Conditions. *Mol Cell Biol*, 21, 6270-6279.
- AHMAD, K. & HENIKOFF, S. 2002. The histone variant H3.3 marks active chromatin by replication-independent nucleosome assembly. *Mol Cell*, 9, 1191-200.
- AKHMANOVA, A., MIEDEMA, K. & HENNIG, W. 1996. Identification and characterization of the Drosophila histone H4 replacement gene. *FEBS Lett*, 388, 219-22.
- ALBERT, I., MAVRICH, T. N., TOMSHO, L. P., QI, J., ZANTON, S. J., SCHUSTER, S. C. & PUGH, B. F. 2007. Translational and rotational settings of H2A.Z nucleosomes across the *Saccharomyces cerevisiae* genome. *Nature*, 446, 572-6.
- ALBERTS, B., JOHNSON, A., LEWIS, J., RAFF, M., ROBERTS, K. & WALTER, P. 2002. Molecular biology of the cell.
- ALBIG, W. & DOENECKE, D. 1997. The human histone gene cluster at the D6S105 locus. *Hum Genet*, 101, 284-94.
- ALEKSEEV, S., LUIJSTERBURG, M. S., PINES, A., GEVERTS, B., MARI, P. O., GIGLIA-MARI, G., LANS, H., HOUTSMULLER, A. B., MULLENDERS, L. H., HOEIJMAKERS, J. H. & VERMEULEN, W. 2008. Cellular concentrations of DDB2 regulate dynamic binding of DDB1 at UV-induced DNA damage. *Mol Cell Biol*, 28, 7402-13.
- ALLFREY, V. G., FAULKNER, R. & MIRSKY, A. E. 1964. ACETYLATION AND METHYLATION OF HISTONES AND THEIR POSSIBLE ROLE IN THE REGULATION OF RNA SYNTHESIS. *Proc Natl Acad Sci U S A*, 51, 786-94.
- ALLIS, C. D., GLOVER, C. V., BOWEN, J. K. & GOROVSKY, M. A. 1980. Histone variants specific to the transcriptionally active, amitotically dividing macronucleus of the unicellular eucaryote, *Tetrahymena thermophila*. *Cell*, 20, 609-17.
- ANGELOV, D., MOLLA, A., PERCHE, P. Y., HANS, F., COTE, J., KHOCHBIN, S., BOUVET, P. & DIMITROV, S. 2003. The histone variant macroH2A interferes with transcription factor binding and SWI/SNF nucleosome remodeling. *Mol Cell*, 11, 1033-41.
- ANINDYA, R., AYG N, O. & SVEJSTRUP, J. 2007. Damage-induced ubiquitylation of human RNA polymerase II by the ubiquitin ligase Nedd4, but not Cockayne syndrome proteins or BRCA1. *Mol Cell*, 28, 386-97.
- ANINDYA, R., MARI, P. O., KRISTENSEN, U., KOOL, H., GIGLIA-MARI, G., MULLENDERS, L. H., FOSTERI, M., VERMEULEN, W., EGLY, J. M. & SVEJSTRUP, J. Q. 2010. A ubiquitin-binding domain in Cockayne syndrome B required for transcription-coupled nucleotide excision repair. *Mol Cell*, 38, 637-48.
- ARAKI, M., MASUTANI, C., TAKEMURA, M., UCHIDA, A., SUGASAWA, K., KONDOH, J., OHKUMA, Y. & HANAOKA, F. 2001. Centrosome protein centrin 2/caltractin 1 is part of the xeroderma pigmentosum group C complex that initiates global genome nucleotide excision repair. *J Biol*

- Chem*, 276, 18665-72.
- ARAUJO, S. J., NIGG, E. A. & WOOD, R. D. 2001. Strong functional interactions of TFIIH with XPC and XPG in human DNA nucleotide excision repair, without a preassembled repairosome. *Mol Cell Biol*, 21, 2281-91.
- ARAUJO, S. J., TIRODE, F., COIN, F., POSPIECH, H., SYVAOJA, J. E., STUCKI, M., HUBSCHER, U., EGLY, J. M. & WOOD, R. D. 2000. Nucleotide excision repair of DNA with recombinant human proteins: definition of the minimal set of factors, active forms of TFIIH, and modulation by CAK. *Genes Dev*, 14, 349-59.
- ARENTS, G. & MOUDRIANAKIS, E. N. 1993. Topography of the histone octamer surface: repeating structural motifs utilized in the docking of nucleosomal DNA. *Proc Natl Acad Sci U S A*, 90, 10489-93.
- AUSIO, J. & ABBOTT, D. W. 2002. The many tales of a tail: carboxyl-terminal tail heterogeneity specializes histone H2A variants for defined chromatin function. *Biochemistry*, 41, 5945-9.
- BABIARZ, J. E., HALLEY, J. E. & RINE, J. 2006. Telomeric heterochromatin boundaries require NuA4-dependent acetylation of histone variant H2A.Z in *Saccharomyces cerevisiae*. *Genes Dev*, 20, 700-10.
- BAILLY, V., SOMMERS, C. H., SUNG, P., PRAKASH, L. & PRAKASH, S. 1992. Specific complex formation between proteins encoded by the yeast DNA repair and recombination genes RAD1 and RAD10. *Proc Natl Acad Sci U S A*, 89, 8273-7.
- BANASZYNSKI, L. A., ALLIS, C. D. & LEWIS, P. W. 2010. Histone variants in metazoan development. *Dev Cell*, 19, 662-74.
- BANG, D. D., VERHAGE, R., GOOSEN, N., BROUWER, J. & VAN DE PUTTE, P. 1992. Molecular cloning of RAD16, a gene involved in differential repair in *Saccharomyces cerevisiae*. *Nucleic Acids Res*, 20, 3925-31.
- BANNISTER, A. J. & KOUZARIDES, T. 2011. Regulation of chromatin by histone modifications. *Cell Res*, 21, 381-95.
- BARDWELL, A., BARDWELL, L., TOMKINSON, A. & FRIEDBERG, E. 1994. Specific cleavage of model recombination and repair intermediates by the yeast Rad1-Rad10 DNA endonuclease. *Science*, 265, 2082-2085.
- BARDWELL, L., COOPER, A. J. & FRIEDBERG, E. C. 1992. Stable and specific association between the yeast recombination and DNA repair protein Rad1 and protein Rad10 in vitro. *Mol Cell Biol*, 12, 3041-3049.
- BASTIN-SHANOWER, S. A. & BRILL, S. J. 2001. Functional analysis of the four DNA binding domains of replication protein A. The role of RPA2 in ssDNA binding. *J Biol Chem*, 276, 36446-53.
- BATTY, D., RAPIC-OTRIN, V., LEVINE, A. S. & WOOD, R. D. 2000. Stable binding of human XPC complex to irradiated DNA confers strong discrimination for damaged sites. *J Mol Biol*, 300, 275-90.
- BATTY, D. P. & WOOD, R. D. 2000. Damage recognition in nucleotide excision repair of DNA. *Gene*, 241, 193-204.
- BEDEZ, F., LINARD, B., BROCHET, X., RIPP, R., THOMPSON, J. D., MORAS, D., LECOMPTE, O. & POCH, O. 2013. Functional insights into the core-TFIIH from a comparative survey. *Genomics*, 101, 178-86.
- BEERENS, N., HOEIJMAKERS, J. H., KANAAR, R., VERMEULEN, W. & WYMAN, C. 2005. The CSB protein actively wraps DNA. *J Biol Chem*, 280, 4722-9.
- BENSON, L. J., GU, Y., YAKOVLEVA, T., TONG, K., BARROWS, C., STRACK, C. L., COOK, R. G., MIZZEN, C. A.

- & ANNUNZIATO, A. T. 2006. Modifications of H3 and H4 during chromatin replication, nucleosome assembly, and histone exchange. *J Biol Chem*, 281, 9287-96.
- BERGINK, S. & JENTSCH, S. 2009. Principles of ubiquitin and SUMO modifications in DNA repair. *Nature*, 458, 461-7.
- BERGINK, S., TOUSSAINT, W., LUIJSTERBURG, M. S., DINANT, C., ALEKSEEV, S., HOEIJMAKERS, J. H., DANTUMA, N. P., HOUTSMULLER, A. B. & VERMEULEN, W. 2012. Recognition of DNA damage by XPC coincides with disruption of the XPC-RAD23 complex. *J Cell Biol*, 196, 681-8.
- BERNSEN, C. E. & DENU, J. M. 2008. Catalysis and substrate selection by histone/protein lysine acetyltransferases. *Curr Opin Struct Biol*, 18, 682-9.
- BESPALOV, V. A., CONCONI, A., ZHANG, X., FAHY, D. & SMERDON, M. J. 2001. Improved method for measuring the ensemble average of strand breaks in genomic DNA. *Environ Mol Mutagen*, 38, 166-74.
- BHATIA, P. K., VERHAGE, R. A., BROUWER, J. & FRIEDBERG, E. C. 1996. Molecular cloning and characterization of *Saccharomyces cerevisiae* RAD28, the yeast homolog of the human Cockayne syndrome A (CSA) gene. *J Bacteriol*, 178, 5977-88.
- BHAUMIK, S. R., SMITH, E. & SHILATIFARD, A. 2007. Covalent modifications of histones during development and disease pathogenesis. *Nat Struct Mol Biol*, 14, 1008-16.
- BIRGER, Y., WEST, K. L., POSTNIKOV, Y. V., LIM, J. H., FURUSAWA, T., WAGNER, J. P., LAUFER, C. S., KRAEMER, K. H. & BUSTIN, M. 2003. Chromosomal protein HMG1 enhances the rate of DNA repair in chromatin. *EMBO J*, 22, 1665-75.
- BOCHKAREV, A., PFUETZNER, R. A., EDWARDS, A. M. & FRAPPIER, L. 1997. Structure of the single-stranded-DNA-binding domain of replication protein A bound to DNA. *Nature*, 385, 176-81.
- BOITEUX, S. & JINKS-ROBERTSON, S. 2013. DNA Repair Mechanisms and the Bypass of DNA Damage in *Saccharomyces cerevisiae*. *Genetics*, 193, 1025-64.
- BOSTELMAN, L. J., KELLER, A. M., ALBRECHT, A. M., ARAT, A. & THOMPSON, J. S. 2007. Methylation of histone H3 lysine-79 by Dot1p plays multiple roles in the response to UV damage in *Saccharomyces cerevisiae*. *DNA Repair (Amst)*, 6, 383-95.
- BOUDREAULT, A. A., CRONIER, D., SELLECK, W., LACOSTE, N., UTLEY, R. T., ALLARD, S., SAVARD, J., LANE, W. S., TAN, S. & COTE, J. 2003. Yeast enhancer of polycomb defines global Esa1-dependent acetylation of chromatin. *Genes Dev*, 17, 1415-28.
- BRADSHER, J. N., JACKSON, K. W., CONAWAY, R. C. & CONAWAY, J. W. 1993. RNA polymerase II transcription factor SIII. I. Identification, purification, and properties. *J Biol Chem*, 268, 25587-93.
- BRAND, M., MOGGS, J. G., OULAD-ABDELGHANI, M., LEJEUNE, F., DILWORTH, F. J., STEVENIN, J., ALMOUZNI, G. & TORA, L. 2001. UV-damaged DNA-binding protein in the TFTC complex links DNA damage recognition to nucleosome acetylation. *EMBO J*, 20, 3187-96.
- BRAND, M., YAMAMOTO, K., STAUB, A. & TORA, L. 1999. Identification of TATA-binding protein-free TAFII-containing complex subunits suggests a role in nucleosome acetylation and signal transduction. *J Biol Chem*, 274, 18285-9.
- BRICKNER, D. G., CAJIGAS, I., FONDUFE-MITTENDORF, Y., AHMED, S., LEE, P. C., WIDOM, J. & BRICKNER, J. H. 2007. H2A.Z-mediated localization of genes at the nuclear periphery confers epigenetic memory of previous transcriptional state. *PLoS Biol*, 5, e81.
- BROWN, D. T. 2003. Histone H1 and the dynamic regulation of chromatin function. *Biochem Cell Biol*,

- 81, 221-7.
- BROWN, T. A. 2002. *Genomes*. Oxford: Bios Scientific Publishers.
- BUDD, M. E. & CAMPBELL, J. L. 1995. DNA polymerases required for repair of UV-induced damage in *Saccharomyces cerevisiae*. *Mol Cell Biol*, 15, 2173-9.
- BURGESS, S. M., AJIMURA, M. & KLECKNER, N. 1999. GCN5-dependent histone H3 acetylation and RPD3-dependent histone H4 deacetylation have distinct, opposing effects on IME2 transcription, during meiosis and during vegetative growth, in budding yeast. *Proc Natl Acad Sci U S A*, 96, 6835-40.
- BUTERIN, T., MEYER, C., GIESE, B. & NAEGELI, H. 2005. DNA quality control by conformational readout on the undamaged strand of the double helix. *Chem Biol*, 12, 913-22.
- CAMENISCH, U., DIP, R., SCHUMACHER, S. B., SCHULER, B. & NAEGELI, H. 2006. Recognition of helical kinks by xeroderma pigmentosum group A protein triggers DNA excision repair. *Nat Struct Mol Biol*, 13, 278-84.
- CAMENISCH, U., TRAUTLEIN, D., CLEMENT, F. C., FEI, J., LEITENSTORFER, A., FERRANDO-MAY, E. & NAEGELI, H. 2009. Two-stage dynamic DNA quality check by xeroderma pigmentosum group C protein. *EMBO J*, 28, 2387-99.
- CANAU, R., ZHOU, J. X., ALLIS, C. D. & BERGER, S. L. 1997. Histone acetyltransferase activity and interaction with ADA2 are critical for GCN5 function in vivo. *EMBO J*, 16, 555-65.
- CARROZZA, M. J., LI, B., FLORENS, L., SUGANUMA, T., SWANSON, S. K., LEE, K. K., SHIA, W. J., ANDERSON, S., YATES, J., WASHBURN, M. P. & WORKMAN, J. L. 2005. Histone H3 methylation by Set2 directs deacetylation of coding regions by Rpd3S to suppress spurious intragenic transcription. *Cell*, 123, 581-92.
- CARROZZA, M. J., UTLEY, R. T., WORKMAN, J. L. & COTE, J. 2003. The diverse functions of histone acetyltransferase complexes. *Trends Genet*, 19, 321-9.
- CECCHINI, S., MASSON, C., LA MADELEINE, C., HUELS, M. A., SANCHE, L., WAGNER, J. R. & HUNTING, D. J. 2005. Interstrand cross-link induction by UV radiation in bromodeoxyuridine-substituted DNA: dependence on DNA conformation. *Biochemistry*, 44, 16957-66.
- CHADWICK, B. P. & WILLARD, H. F. 2001. A novel chromatin protein, distantly related to histone H2A, is largely excluded from the inactive X chromosome. *J Cell Biol*, 152, 375-84.
- CHANG, C. S. & PILLUS, L. 2009. Collaboration between the essential Esa1 acetyltransferase and the Rpd3 deacetylase is mediated by H4K12 histone acetylation in *Saccharomyces cerevisiae*. *Genetics*, 183, 149-60.
- CHAUDHURI, S., WYRICK, J. J. & SMERDON, M. J. 2009. Histone H3 Lys79 methylation is required for efficient nucleotide excision repair in a silenced locus of *Saccharomyces cerevisiae*. *Nucleic Acids Res*, 37, 1690-700.
- CHAURASIA, P., SEN, R. & BHAUMIK, S. R. 2013. Functional analysis of rad14p, a DNA damage recognition factor in nucleotide excision repair, in regulation of transcription in vivo. *J Biol Chem*, 288, 793-806.
- CHEN, L. & MADURA, K. 2002. Rad23 promotes the targeting of proteolytic substrates to the proteasome. *Mol Cell Biol*, 22, 4902-13.
- CHEN, L., SHINDE, U., ORTOLAN, T. G. & MADURA, K. 2001. Ubiquitin-associated (UBA) domains in Rad23 bind ubiquitin and promote inhibition of multi-ubiquitin chain assembly. *EMBO Rep*, 2, 933-8.
- CHEN, X., DING, B., LEJEUNE, D., RUGGIERO, C. & LI, S. 2009. Rpb1 sumoylation in response to UV

- radiation or transcriptional impairment in yeast. *PLoS One*, 4, e5267.
- CHEN, X., RUGGIERO, C. & LI, S. 2007. Yeast Rpb9 plays an important role in ubiquitylation and degradation of Rpb1 in response to UV-induced DNA damage. *Mol Cell Biol*, 27, 4617-25.
- CHOI, J. K. & HOWE, L. J. 2009. Histone acetylation: truth of consequences? *Biochem Cell Biol*, 87, 139-50.
- CHRISTIANS, F. C. & HANAWALT, P. C. 1992. Inhibition of transcription and strand-specific DNA repair by alpha-amanitin in Chinese hamster ovary cells. *Mutat Res*, 274, 93-101.
- CHURIKOV, D., SIINO, J., SVETLOVA, M., ZHANG, K., GINEITIS, A., MORTON BRADBURY, E. & ZALENSKY, A. 2004. Novel human testis-specific histone H2B encoded by the interrupted gene on the X chromosome. *Genomics*, 84, 745-56.
- CITTERIO, E., RADEMAKERS, S., VAN DER HORST, G. T., VAN GOOL, A. J., HOEIJMAKERS, J. H. & VERMEULEN, W. 1998. Biochemical and biological characterization of wild-type and ATPase-deficient Cockayne syndrome B repair protein. *J Biol Chem*, 273, 11844-51.
- CITTERIO, E., VAN DEN BOOM, V., SCHNITZLER, G., KANAAR, R., BONTE, E., KINGSTON, R. E., HOEIJMAKERS, J. H. & VERMEULEN, W. 2000. ATP-dependent chromatin remodeling by the Cockayne syndrome B DNA repair-transcription-coupling factor. *Mol Cell Biol*, 20, 7643-53.
- CLARKE, A. S., LOWELL, J. E., JACOBSON, S. J. & PILLUS, L. 1999. Esa1p is an essential histone acetyltransferase required for cell cycle progression. *Mol Cell Biol*, 19, 2515-26.
- CLARKSON, M. J., WELLS, J. R., GIBSON, F., SAINT, R. & TREMETHICK, D. J. 1999. Regions of variant histone His2AvD required for Drosophila development. *Nature*, 399, 694-7.
- CLEAVER, J. E. 1968. Defective repair replication of DNA in xeroderma pigmentosum. *Nature*, 218, 652-6.
- CLEAVER, J. E. 2012. Photosensitivity syndrome brings to light a new transcription-coupled DNA repair cofactor. *Nat Genet*, 44, 477-8.
- CLEAVER, J. E., LAM, E. T. & REVET, I. 2009. Disorders of nucleotide excision repair: the genetic and molecular basis of heterogeneity. *Nat Rev Genet*, 10, 756-68.
- COIN, F., OKSENYCH, V. & EGLY, J. M. 2007. Distinct roles for the XPB/p52 and XPD/p44 subcomplexes of TFIIH in damaged DNA opening during nucleotide excision repair. *Mol Cell*, 26, 245-56.
- COIN, F., OKSENYCH, V., MOCQUET, V., GROH, S., BLATTNER, C. & EGLY, J. M. 2008. Nucleotide excision repair driven by the dissociation of CAK from TFIIH. *Mol Cell*, 31, 9-20.
- CONAWAY, R. C. & CONAWAY, J. W. 1989. An RNA polymerase II transcription factor has an associated DNA-dependent ATPase (dATPase) activity strongly stimulated by the TATA region of promoters. *Proc Natl Acad Sci U S A*, 86, 7356-60.
- CONDE E SILVA, N., BLACK, B. E., SIVOLOB, A., FILIPSKI, J., CLEVELAND, D. W. & PRUNELL, A. 2007. CENP-A-containing nucleosomes: easier disassembly versus exclusive centromeric localization. *J Mol Biol*, 370, 555-73.
- CONSTANTINO, A., GUNZ, D., EVANS, E., LALLE, P., BATES, P. A., WOOD, R. D. & CLARKSON, S. G. 1999. Conserved residues of human XPG protein important for nuclease activity and function in nucleotide excision repair. *J Biol Chem*, 274, 5637-48.
- COSTANZI, C. & PEHRSON, J. R. 1998. Histone macroH2A1 is concentrated in the inactive X chromosome of female mammals. *Nature*, 393, 599-601.
- COUX, O., TANAKA, K. & GOLDBERG, A. L. 1996. Structure and functions of the 20S and 26S proteasomes. *Annu Rev Biochem*, 65, 801-47.
- COX, B. S. & PARRY, J. M. 1968. The isolation, genetics and survival characteristics of ultraviolet

- light-sensitive mutants in yeast. *Mutat Res*, 6, 37-55.
- CZAJA, W., MAO, P. & SMERDON, M. J. 2012. The Emerging Roles of ATP-Dependent Chromatin Remodeling Enzymes in Nucleotide Excision Repair. *Int J Mol Sci*, 13, 11954-73.
- DANTUMA, N. P., HEINEN, C. & HOOGSTRATEN, D. 2009. The ubiquitin receptor Rad23: at the crossroads of nucleotide excision repair and proteasomal degradation. *DNA Repair (Amst)*, 8, 449-60.
- DAVEY, C. A., SARGENT, D. F., LUGER, K., MAEDER, A. W. & RICHMOND, T. J. 2002. Solvent mediated interactions in the structure of the nucleosome core particle at 1.9 Å resolution. *J Mol Biol*, 319, 1097-113.
- DE BOER, J. & HOEIJMAKERS, J. H. 2000. Nucleotide excision repair and human syndromes. *Carcinogenesis*, 21, 453-60.
- DE LAAT W.L, JASPERS N.G & J.H, H. 1999. Molecular mechanisms of nucleotide excision repair. *Genes and Development*, 13, 768-785.
- DE LAAT, W. L., APPELDOORN, E., SUGASAWA, K., WETERINGS, E., JASPERS, N. G. & HOEIJMAKERS, J. H. 1998a. DNA-binding polarity of human replication protein A positions nucleases in nucleotide excision repair. *Genes Dev*, 12, 2598-609.
- DE LAAT, W. L., SIJBERS, A. M., ODIJK, H., JASPERS, N. G. & HOEIJMAKERS, J. H. 1998b. Mapping of interaction domains between human repair proteins ERCC1 and XPF. *Nucleic Acids Res*, 26, 4146-52.
- DECHASSA, M. L., WYNS, K., LI, M., HALL, M. A., WANG, M. D. & LUGER, K. 2011. Structure and Scm3-mediated assembly of budding yeast centromeric nucleosomes. *Nat Commun*, 2, 313.
- DECKER, P. V., YU, D. Y., IIZUKA, M., QIU, Q. & SMITH, M. M. 2008. Catalytic-site mutations in the MYST family histone Acetyltransferase Esa1. *Genetics*, 178, 1209-20.
- DEN DULK, B., SUN, S. M., DE RUIJTER, M., BRANDSMA, J. A. & BROUWER, J. 2006. Rad33, a new factor involved in nucleotide excision repair in *Saccharomyces cerevisiae*. *DNA Repair (Amst)*, 5, 683-92.
- DEN DULK, B., VAN EIJK, P., DE RUIJTER, M., BRANDSMA, J. A. & BROUWER, J. 2008. The NER protein Rad33 shows functional homology to human Centrin2 and is involved in modification of Rad4. *DNA Repair (Amst)*, 7, 858-68.
- DHILLON, N. & KAMAKAKA, R. T. 2000. A histone variant, Htz1p, and a Sir1p-like protein, Esc2p, mediate silencing at HMR. *Mol Cell*, 6, 769-80.
- DHILLON, N., OKI, M., SZYJKA, S. J., APARICIO, O. M. & KAMAKAKA, R. T. 2006. H2A.Z functions to regulate progression through the cell cycle. *Mol Cell Biol*, 26, 489-501.
- DIFFLEY, J. F. 1992. Global regulators of chromosome function in yeast. *Antonie Van Leeuwenhoek*, 62, 25-33.
- DING, B., RUGGIERO, C., CHEN, X. & LI, S. 2007. Tfb5 is partially dispensable for Rad26 mediated transcription coupled nucleotide excision repair in yeast. *DNA Repair (Amst)*, 6, 1661-9.
- DOUKI, T. & CADET, J. 2001. Individual Determination of the Yield of the Main UV-Induced Dimeric Pyrimidine Photoproducts in DNA Suggests a High Mutagenicity of CC Photolesions†. *Biochemistry*, 40, 2495-2501.
- DRAKER, R., NG, M. K., SARCINELLA, E., IGNATCHENKO, V., KISLINGER, T. & CHEUNG, P. 2012. A Combination of H2A.Z and H4 Acetylation Recruits Brd2 to Chromatin during Transcriptional Activation. *PLoS Genet*, 8, e1003047.
- DRYHURST, D., THAMBIRAJAH, A. A. & AUSIO, J. 2004. New twists on H2A.Z: a histone variant with a

- controversial structural and functional past. *Biochem Cell Biol*, 82, 490-7.
- DUNAND-SAUTHIER, I., HOHL, M., THOREL, F., JAQUIER-GUBLER, P., CLARKSON, S. G. & SCHARER, O. D. 2005. The spacer region of XPG mediates recruitment to nucleotide excision repair complexes and determines substrate specificity. *J Biol Chem*, 280, 7030-7.
- EGLY, J. M. & COIN, F. 2011. A history of TFIIH: two decades of molecular biology on a pivotal transcription/repair factor. *DNA Repair (Amst)*, 10, 714-21.
- EIRIN-LOPEZ, J. & AUSIO, J. 2007. H2A.Z-Mediated Genome-Wide Chromatin Specialization. *Curr Genomics*, 8, 59-66.
- EISEN, J. A., SWEDER, K. S. & HANAWALT, P. C. 1995. Evolution of the SNF2 family of proteins: subfamilies with distinct sequences and functions. *Nucleic Acids Res*, 23, 2715-23.
- EKWALL, K. 2005. Genome-wide analysis of HDAC function. *Trends Genet*, 21, 608-15.
- EL-MAHDY, M. A., ZHU, Q., WANG, Q. E., WANI, G., PRAETORIUS-IBBA, M. & WANI, A. A. 2006. Cullin 4A-mediated proteolysis of DDB2 protein at DNA damage sites regulates in vivo lesion recognition by XPC. *J Biol Chem*, 281, 13404-11.
- ELSASSER, S., CHANDLER-MILITELLO, D., MULLER, B., HANNA, J. & FINLEY, D. 2004. Rad23 and Rpn10 serve as alternative ubiquitin receptors for the proteasome. *J Biol Chem*, 279, 26817-22.
- ELSASSER, S., GALI, R. R., SCHWICKART, M., LARSEN, C. N., LEGGETT, D. S., MULLER, B., FENG, M. T., TUBING, F., DITTMAR, G. A. & FINLEY, D. 2002. Proteasome subunit Rpn1 binds ubiquitin-like protein domains. *Nat Cell Biol*, 4, 725-30.
- ESSERS, J., THEIL, A. F., BALDEYRON, C., VAN CAPPELLEN, W. A., HOUTSMULLER, A. B., KANAAR, R. & VERMEULEN, W. 2005. Nuclear dynamics of PCNA in DNA replication and repair. *Mol Cell Biol*, 25, 9350-9.
- EVANS, E., FELLOWS, J., COFFER, A. & WOOD, R. D. 1997a. Open complex formation around a lesion during nucleotide excision repair provides a structure for cleavage by human XPG protein. *EMBO J*, 16, 625-38.
- EVANS, E., MOGGS, J. G., HWANG, J. R., EGLY, J. M. & WOOD, R. D. 1997b. Mechanism of open complex and dual incision formation by human nucleotide excision repair factors. *EMBO J*, 16, 6559-73.
- FAAST, R., THONGLAIROAM, V., SCHULZ, T. C., BEALL, J., WELLS, J. R., TAYLOR, H., MATTHAEI, K., RATHJEN, P. D., TREMETHICK, D. J. & LYONS, I. 2001. Histone variant H2A.Z is required for early mammalian development. *Curr Biol*, 11, 1183-7.
- FAGBEMI, A. F., ORELLI, B. & SCHARER, O. D. 2011. Regulation of endonuclease activity in human nucleotide excision repair. *DNA Repair (Amst)*, 10, 722-9.
- FAN, J. Y., RANGASAMY, D., LUGER, K. & TREMETHICK, D. J. 2004. H2A.Z alters the nucleosome surface to promote HP1alpha-mediated chromatin fiber folding. *Mol Cell*, 16, 655-61.
- FAN, W. & LUO, J. 2010. SIRT1 regulates UV-induced DNA repair through deacetylating XPA. *Mol Cell*, 39, 247-58.
- FAN, Y., SIROTKIN, A., RUSSELL, R. G., AYALA, J. & SKOULTCHI, A. I. 2001. Individual somatic H1 subtypes are dispensable for mouse development even in mice lacking the H1(0) replacement subtype. *Mol Cell Biol*, 21, 7933-43.
- FARRELL, A. W., HALLIDAY, G. M. & LYONS, J. G. 2011. Chromatin Structure Following UV-Induced DNA Damage-Repair or Death? *Int J Mol Sci*, 12, 8063-85.
- FEAVER, W. J., GILEADI, O. & KORNBERG, R. D. 1991. Purification and characterization of yeast RNA polymerase II transcription factor b. *J Biol Chem*, 266, 19000-5.

- FEAVER, W. J., SVEJSTRUP, J. Q., BARDWELL, L., BARDWELL, A. J., BURATOWSKI, S., GULYAS, K. D., DONAHUE, T. F., FRIEDBERG, E. C. & KORNBERG, R. D. 1993. Dual roles of a multiprotein complex from *S. cerevisiae* in transcription and DNA repair. *Cell*, 75, 1379-87.
- FERNANDEZ-CAPETILLO, O., LEE, A., NUSSENZWEIG, M. & NUSSENZWEIG, A. 2004. H2AX: the histone guardian of the genome. *DNA Repair (Amst)*, 3, 959-67.
- FINLEY, D. 2009. Recognition and processing of ubiquitin-protein conjugates by the proteasome. *Annu Rev Biochem*, 78, 477-513.
- FITCH, M. E., NAKAJIMA, S., YASUI, A. & FORD, J. M. 2003. In vivo recruitment of XPC to UV-induced cyclobutane pyrimidine dimers by the DDB2 gene product. *J Biol Chem*, 278, 46906-10.
- FORTINI, P., PASCUCCI, B., PARLANTI, E., D'ERRICO, M., SIMONELLI, V. & DOGLIOTTI, E. 2003. The base excision repair: mechanisms and its relevance for cancer susceptibility. *Biochimie*, 85, 1053-1071.
- FOUSTERI, M., VERMEULEN, W., VAN ZEELAND, A. & MULLENDERS, L. 2006a. Cockayne syndrome A and B proteins differentially regulate recruitment of chromatin remodeling and repair factors to stalled RNA polymerase II in vivo. *Mol Cell*, 23, 471-82.
- FOUSTERI, M., VERMEULEN, W., VAN ZEELAND, A. A. & MULLENDERS, L. H. 2006b. Cockayne syndrome A and B proteins differentially regulate recruitment of chromatin remodeling and repair factors to stalled RNA polymerase II in vivo. *Mol Cell*, 23, 471-82.
- FRIEDBERG, E. C. 2000. Rous-Whipple Award Lecture. Nucleotide excision repair and cancer predisposition: A journey from man to yeast to mice. *Am J Pathol*, 157, 693-701.
- FRIEDBERG, E. C. 2006. *DNA repair and mutagenesis*, Washington, ASM Press.
- FRIEDBERG, E. C., WALKER, G. C., SIEDE, W., WOOD, R. D., SCHULTZ, R. A. & ELLENBERGER, T. 2005. *DNA Repair and Mutagenesis*, Washington DC, ASM Press.
- FRIT, P., BERGMANN, E. & EGLY, J. M. 1999. Transcription factor IIH: a key player in the cellular response to DNA damage. *Biochimie*, 81, 27-38.
- GALARNEAU, L., NOURANI, A., BOUDREAU, A. A., ZHANG, Y., HELIOT, L., ALLARD, S., SAVARD, J., LANE, W. S., STILLMAN, D. J. & COTE, J. 2000. Multiple links between the NuA4 histone acetyltransferase complex and epigenetic control of transcription. *Mol Cell*, 5, 927-37.
- GALE, J. M. & SMERDON, M. J. 1990. UV induced (6-4) photoproducts are distributed differently than cyclobutane dimers in nucleosomes. *Photochem Photobiol*, 51, 411-7.
- GANAPATHI, M., PALUMBO, M. J., ANSARI, S. A., HE, Q., TSUI, K., NISLOW, C. & MORSE, R. H. 2011. Extensive role of the general regulatory factors, Abf1 and Rap1, in determining genome-wide chromatin structure in budding yeast. *Nucleic Acids Res*, 39, 2032-44.
- GAUTIER, T., ABBOTT, D. W., MOLLA, A., VERDEL, A., AUSIO, J. & DIMITROV, S. 2004. Histone variant H2ABbd confers lower stability to the nucleosome. *EMBO Rep*, 5, 715-20.
- GIANNATTASIO, M., LAZZARO, F., PLEVANI, P. & MUZI-FALCONI, M. 2005. The DNA damage checkpoint response requires histone H2B ubiquitination by Rad6-Bre1 and H3 methylation by Dot1. *J Biol Chem*, 280, 9879-86.
- GILLET, L. C. & SCHARER, O. D. 2006. Molecular mechanisms of mammalian global genome nucleotide excision repair. *Chem Rev*, 106, 253-76.
- GILLETTE, T. G., HUANG, W., RUSSELL, S. J., REED, S. H., JOHNSTON, S. A. & FRIEDBERG, E. C. 2001. The 19S complex of the proteasome regulates nucleotide excision repair in yeast. *Genes Dev*, 15, 1528-39.
- GILLETTE, T. G., YU, S., ZHOU, Z., WATERS, R., JOHNSTON, S. A. & REED, S. H. 2006. Distinct functions of

- the ubiquitin-proteasome pathway influence nucleotide excision repair. *EMBO J*, 25, 2529-38.
- GILLJAM, K. M., MULLER, R., LIABAKK, N. B. & OTTERLEI, M. 2012. Nucleotide excision repair is associated with the replisome and its efficiency depends on a direct interaction between XPA and PCNA. *PLoS One*, 7, e49199.
- GINEITIS, A. A., ZALENSKAYA, I. A., YAU, P. M., BRADBURY, E. M. & ZALENSKY, A. O. 2000. Human sperm telomere-binding complex involves histone H2B and secures telomere membrane attachment. *J Cell Biol*, 151, 1591-8.
- GINSBURG, D. S., GOVIND, C. K. & HINNEBUSCH, A. G. 2009. NuA4 lysine acetyltransferase Esa1 is targeted to coding regions and stimulates transcription elongation with Gcn5. *Mol Cell Biol*, 29, 6473-87.
- GODON, C., MOURGUES, S., NONNEKENS, J., MOURCET, A., COIN, F., VERMEULEN, W., MARI, P. O. & GIGLIA-MARI, G. 2012. Generation of DNA single-strand displacement by compromised nucleotide excision repair. *EMBO J*, 31, 3550-63.
- GONG, F., FAHY, D. & SMERDON, M. J. 2006. Rad4-Rad23 interaction with SWI/SNF links ATP-dependent chromatin remodeling with nucleotide excision repair. *Nat Struct Mol Biol*, 13, 902-7.
- GOODSELL, D. S. 2001. The molecular perspective: ultraviolet light and pyrimidine dimers. *Stem Cells*, 19, 348-9.
- GORBALENYA, A. E. & KOONIN, E. V. 1993. Helicases: amino acid sequence comparisons and structure-function relationships. *Current Opinion in Structural Biology*, 3, 419-429.
- GORMAN, J., CHOWDHURY, A., SURTEES, J. A., SHIMADA, J., REICHMAN, D. R., ALANI, E. & GREENE, E. C. 2007. Dynamic basis for one-dimensional DNA scanning by the mismatch repair complex Msh2-Msh6. *Mol Cell*, 28, 359-70.
- GRANT, P. A., DUGGAN, L., COTE, J., ROBERTS, S. M., BROWNELL, J. E., CANDAU, R., OHBA, R., OWEN-HUGHES, T., ALLIS, C. D., WINSTON, F., BERGER, S. L. & WORKMAN, J. L. 1997. Yeast Gcn5 functions in two multisubunit complexes to acetylate nucleosomal histones: characterization of an Ada complex and the SAGA (Spt/Ada) complex. *Genes Dev*, 11, 1640-50.
- GREEN, C. M. & ALMOUZNI, G. 2003. Local action of the chromatin assembly factor CAF-1 at sites of nucleotide excision repair in vivo. *EMBO J*, 22, 5163-74.
- GREWAL, S. I. & JIA, S. 2007. Heterochromatin revisited. *Nat Rev Genet*, 8, 35-46.
- GROISMAN, R., KURAOKA, I., CHEVALLIER, O., GAYE, N., MAGNALDO, T., TANAKA, K., KISSELEV, A., HAREL-BELLAN, A. & NAKATANI, Y. 2006. CSA-dependent degradation of CSB by the ubiquitin-proteasome pathway establishes a link between complementation factors of the Cockayne syndrome. *Genes Dev*, 20, 1429-34.
- GROISMAN, R., POLANOWSKA, J., KURAOKA, I., SAWADA, J., SAIJO, M., DRAPKIN, R., KISSELEV, A. F., TANAKA, K. & NAKATANI, Y. 2003. The ubiquitin ligase activity in the DDB2 and CSA complexes is differentially regulated by the COP9 signalosome in response to DNA damage. *Cell*, 113, 357-67.
- GROTH, A., ROCHA, W., VERREAULT, A. & ALMOUZNI, G. 2007. Chromatin challenges during DNA replication and repair. *Cell*, 128, 721-33.
- GUERRERO-SANTORO, J., KAPETANAKI, M. G., HSIEH, C. L., GORBACHINSKY, I., LEVINE, A. S. & RAPIC-OTRIN, V. 2008. The cullin 4B-based UV-damaged DNA-binding protein ligase binds to UV-damaged chromatin and ubiquitinates histone H2A. *Cancer Res*, 68, 5014-22.

- GUILLEMETTE, B., BATAILLE, A. R., GEVRY, N., ADAM, M., BLANCHETTE, M., ROBERT, F. & GAUDREAU, L. 2005. Variant histone H2A.Z is globally localized to the promoters of inactive yeast genes and regulates nucleosome positioning. *PLoS Biol*, 3, e384.
- GUO, R., CHEN, J., MITCHELL, D. L. & JOHNSON, D. G. 2010. GCN5 and E2F1 stimulate nucleotide excision repair by promoting H3K9 acetylation at sites of damage. *Nucleic Acids Research*.
- GUO, R., CHEN, J., MITCHELL, D. L. & JOHNSON, D. G. 2011. GCN5 and E2F1 stimulate nucleotide excision repair by promoting H3K9 acetylation at sites of damage. *Nucleic Acids Res*, 39, 1390-7.
- GUTHRIE, O. W. 2008. Preincision complex-I from the excision nuclease reaction among cochlear spiral limbus and outer hair cells. *J Mol Histol*, 39, 617-25.
- GUZDER, S. N., HABRAKEN, Y., SUNG, P., PRAKASH, L. & PRAKASH, S. 1995. Reconstitution of yeast nucleotide excision repair with purified Rad proteins, replication protein A, and transcription factor TFIIF. *J Biol Chem*, 270, 12973-6.
- GUZDER, S. N., SOMMERS, C. H., PRAKASH, L. & PRAKASH, S. 2006. Complex formation with damage recognition protein Rad14 is essential for *Saccharomyces cerevisiae* Rad1-Rad10 nuclease to perform its function in nucleotide excision repair in vivo. *Mol Cell Biol*, 26, 1135-41.
- GUZDER, S. N., SUNG, P., BAILLY, V., PRAKASH, L. & PRAKASH, S. 1994. RAD25 is a DNA helicase required for DNA repair and RNA polymerase II transcription. *Nature*, 369, 578-81.
- GUZDER, S. N., SUNG, P., PRAKASH, L. & PRAKASH, S. 1993. Yeast DNA-repair gene RAD14 encodes a zinc metalloprotein with affinity for ultraviolet-damaged DNA. *Proc Natl Acad Sci U S A*, 90, 5433-7.
- GUZDER, S. N., SUNG, P., PRAKASH, L. & PRAKASH, S. 1996. Nucleotide excision repair in yeast is mediated by sequential assembly of repair factors and not by a pre-assembled repairosome. *J Biol Chem*, 271, 8903-10.
- GUZDER, S. N., SUNG, P., PRAKASH, L. & PRAKASH, S. 1998a. Affinity of yeast nucleotide excision repair factor 2, consisting of the Rad4 and Rad23 proteins, for ultraviolet damaged DNA. *J Biol Chem*, 273, 31541-6.
- GUZDER, S. N., SUNG, P., PRAKASH, L. & PRAKASH, S. 1998b. The DNA-dependent ATPase activity of yeast nucleotide excision repair factor 4 and its role in DNA damage recognition. *J Biol Chem*, 273, 6292-6.
- HABER, J. E. 2012. Mating-type genes and MAT switching in *Saccharomyces cerevisiae*. *Genetics*, 191, 33-64.
- HABER, J. E., THORBURN, P. C. & ROGERS, D. 1984. Meiotic and mitotic behavior of dicentric chromosomes in *Saccharomyces cerevisiae*. *Genetics*, 106, 185-205.
- HABRAKEN, Y., SUNG, P., PRAKASH, L. & PRAKASH, S. 1995. Structure-specific nuclease activity in yeast nucleotide excision repair protein Rad2. *J Biol Chem*, 270, 30194-8.
- HABRAKEN, Y., SUNG, P., PRAKASH, S. & PRAKASH, L. 1996. Transcription factor TFIIF and DNA endonuclease Rad2 constitute yeast nucleotide excision repair factor 3: implications for nucleotide excision repair and Cockayne syndrome. *Proc Natl Acad Sci U S A*, 93, 10718-22.
- HALLEY, J. E., KAPLAN, T., WANG, A. Y., KOBOR, M. S. & RINE, J. 2010. Roles for H2A.Z and its acetylation in GAL1 transcription and gene induction, but not GAL1-transcriptional memory. *PLoS Biol*, 8, e1000401.
- HAN, Q., LU, J., DUAN, J., SU, D., HOU, X., LI, F., WANG, X. & HUANG, B. 2008. Gcn5- and Elp3-induced histone H3 acetylation regulates hsp70 gene transcription in yeast. *Biochem J*, 409, 779-88.

- HANAWALT, P. C. 1994. Transcription-coupled repair and human disease. *Science*, 266, 1957-8.
- HANAWALT, P. C. & SPIVAK, G. 2008. Transcription-coupled DNA repair: two decades of progress and surprises. *Nat Rev Mol Cell Biol*, 9, 958-70.
- HAPPEL, N. & DOENECKE, D. 2009. Histone H1 and its isoforms: contribution to chromatin structure and function. *Gene*, 431, 1-12.
- HARA, R. & SANCAR, A. 2002. The SWI/SNF chromatin-remodeling factor stimulates repair by human excision nuclease in the mononucleosome core particle. *Mol Cell Biol*, 22, 6779-87.
- HAROSH, I., NAUMOVSKI, L. & FRIEDBERG, E. C. 1989. Purification and characterization of Rad3 ATPase/DNA helicase from *Saccharomyces cerevisiae*. *J Biol Chem*, 264, 20532-9.
- HARRIS, M. E., BOHNI, R., SCHNEIDERMAN, M. H., RAMAMURTHY, L., SCHUMPERLI, D. & MARZLUFF, W. F. 1991. Regulation of histone mRNA in the unperturbed cell cycle: evidence suggesting control at two posttranscriptional steps. *Mol Cell Biol*, 11, 2416-24.
- HARTIG, A., HOLLY, J., SAARI, G. & MACKAY, V. L. 1986. Multiple regulation of STE2, a mating-type-specific gene of *Saccharomyces cerevisiae*. *Mol Cell Biol*, 6, 2106-14.
- HASAN, S., HASSA, P. O., IMHOF, R. & HOTTIGER, M. O. 2001. Transcription coactivator p300 binds PCNA and may have a role in DNA repair synthesis. *Nature*, 410, 387-91.
- HASELTINE, W. A., GORDON, L. K., LINDAN, C. P., GRAFSTROM, R. H., SHAPER, N. L. & GROSSMAN, L. 1980. Cleavage of pyrimidine dimers in specific DNA sequences by a pyrimidine dimer DNA-glycosylase of *M. luteus*. *Nature*, 285, 634-41.
- HAYS, J. B. 2001. DNA Mismatch Repair: Eukaryotic. *eLS*. John Wiley & Sons, Ltd.
- HE, Z., HENRICKSEN, L. A., WOLD, M. S. & INGLES, C. J. 1995. RPA involvement in the damage-recognition and incision steps of nucleotide excision repair. *Nature*, 374, 566-9.
- HE, Z., WONG, J. M., MANIAR, H. S., BRILL, S. J. & INGLES, C. J. 1996. Assessing the requirements for nucleotide excision repair proteins of *Saccharomyces cerevisiae* in an in vitro system. *J Biol Chem*, 271, 28243-9.
- HEESSEN, S., MASUCCI, M. G. & DANTUMA, N. P. 2005. The UBA2 domain functions as an intrinsic stabilization signal that protects Rad23 from proteasomal degradation. *Mol Cell*, 18, 225-35.
- HENIKOFF, S. & AHMAD, K. 2005. Assembly of variant histones into chromatin. *Annu Rev Cell Dev Biol*, 21, 133-53.
- HENIKOFF, S., FURUYAMA, T. & AHMAD, K. 2004. Histone variants, nucleosome assembly and epigenetic inheritance. *Trends Genet*, 20, 320-6.
- HENNING, K. A., LI, L., IYER, N., MCDANIEL, L. D., REAGAN, M. S., LEGERSKI, R., SCHULTZ, R. A., STEFANINI, M., LEHMANN, A. R., MAYNE, L. V. & FRIEDBERG, E. C. 1995. The Cockayne syndrome group A gene encodes a WD repeat protein that interacts with CSB protein and a subunit of RNA polymerase II TFIIH. *Cell*, 82, 555-64.
- HEO, K., KIM, H., CHOI, S. H., CHOI, J., KIM, K., GU, J., LIEBER, M. R., YANG, A. S. & AN, W. 2008. FACT-mediated exchange of histone variant H2AX regulated by phosphorylation of H2AX and ADP-ribosylation of Spt16. *Mol Cell*, 30, 86-97.
- HESS, M. T., SCHWITTER, U., PETRETTA, M., GIESE, B. & NAEGELI, H. 1997. Bipartite substrate discrimination by human nucleotide excision repair. *Proc Natl Acad Sci U S A*, 94, 6664-9.
- HEY, T., LIPPS, G., SUGASAWA, K., IWAI, S., HANAOKA, F. & KRAUSS, G. 2002. The XPC-HR23B complex displays high affinity and specificity for damaged DNA in a true-equilibrium fluorescence assay. *Biochemistry*, 41, 6583-7.
- HEYER, W. D., EHMSSEN, K. T. & LIU, J. 2010. Regulation of homologous recombination in eukaryotes.

- Annu Rev Genet*, 44, 113-39.
- HIYAMA, H., YOKOI, M., MASUTANI, C., SUGASAWA, K., MAEKAWA, T., TANAKA, K., HOEIJMAKERS, J. H. & HANAOKA, F. 1999. Interaction of hHR23 with S5a. The ubiquitin-like domain of hHR23 mediates interaction with S5a subunit of 26 S proteasome. *J Biol Chem*, 274, 28019-25.
- HOHL, M., THOREL, F., CLARKSON, S. G. & SCHARER, O. D. 2003. Structural determinants for substrate binding and catalysis by the structure-specific endonuclease XPG. *J Biol Chem*, 278, 19500-8.
- HOLLOSY, F. 2002. Effects of ultraviolet radiation on plant cells. *Micron*, 33, 179-97.
- HOLSTEGE, F. C., JENNINGS, E. G., WYRICK, J. J., LEE, T. I., HENGARTNER, C. J., GREEN, M. R., GOLUB, T. R., LANDER, E. S. & YOUNG, R. A. 1998. Dissecting the regulatory circuitry of a eukaryotic genome. *Cell*, 95, 717-28.
- HOWE, L., AUSTON, D., GRANT, P., JOHN, S., COOK, R. G., WORKMAN, J. L. & PILLUS, L. 2001. Histone H3 specific acetyltransferases are essential for cell cycle progression. *Genes Dev*, 15, 3144-54.
- HUANG, J., SVOBODA, D., REARDON, J. & SANCAR, A. 1992. Human nucleotide excision nuclease removes thymine dimers from DNA by incising the 22nd phosphodiester bond 5' and the 6th phosphodiester bond 3' to the photodimer. *Proc Natl Acad Sci U S A*, 89, 3664-8.
- HUANG, J. C. & SANCAR, A. 1994. Determination of minimum substrate size for human excinuclease. *J Biol Chem*, 269, 19034-40.
- HUANG, X., MCLEAN, R. S. & ZHENG, M. 2005. High-resolution length sorting and purification of DNA-wrapped carbon nanotubes by size-exclusion chromatography. *Anal Chem*, 77, 6225-8.
- HUBSCHER, U., MAGA, G. & SPADARI, S. 2002. Eukaryotic DNA polymerases. *Annu Rev Biochem*, 71, 133-63.
- HUISINGA, K. L. & PUGH, B. F. 2004. A genome-wide housekeeping role for TFIID and a highly regulated stress-related role for SAGA in *Saccharomyces cerevisiae*. *Mol Cell*, 13, 573-85.
- HWANG, B. J., FORD, J. M., HANAWALT, P. C. & CHU, G. 1999. Expression of the p48 xeroderma pigmentosum gene is p53-dependent and is involved in global genomic repair. *Proc Natl Acad Sci U S A*, 96, 424-8.
- IOUZALEN, N., MOREAU, J. & MECHALI, M. 1996. H2A.ZI, a new variant histone expressed during *Xenopus* early development exhibits several distinct features from the core histone H2A. *Nucleic Acids Res*, 24, 3947-52.
- IRIZAR, A., YU, Y., REED, S. H., LOUIS, E. J. & WATERS, R. 2010. Silenced yeast chromatin is maintained by Sir2 in preference to permitting histone acetylations for efficient NER. *Nucleic Acids Res*, 38, 4675-86.
- ITO, S., KURAOKA, I., CHYMKOWITCH, P., COMPE, E., TAKEDACHI, A., ISHIGAMI, C., COIN, F., EGLY, J. M. & TANAKA, K. 2007. XPG stabilizes TFIID, allowing transactivation of nuclear receptors: implications for Cockayne syndrome in XP-G/CS patients. *Mol Cell*, 26, 231-43.
- IZZO, A., KAMIENIARZ, K. & SCHNEIDER, R. 2008. The histone H1 family: specific members, specific functions? *Biol Chem*, 389, 333-43.
- JACKSON, J. D., FALCIANO, V. T. & GOROVSKY, M. A. 1996. A likely histone H2A.F/Z variant in *Saccharomyces cerevisiae*. *Trends Biochem Sci*, 21, 466-7.
- JACKSON, J. D. & GOROVSKY, M. A. 2000. Histone H2A.Z has a conserved function that is distinct from that of the major H2A sequence variants. *Nucleic Acids Res*, 28, 3811-6.
- JACKSON, S. P. & DUROCHER, D. 2013. Regulation of DNA Damage Responses by Ubiquitin and SUMO. *Mol Cell*, 49, 795-807.
- JAGGER, J. 1958. Photoreactivation. *Bacteriol Rev*, 22, 99-142.

- JANSEN, L. E., VERHAGE, R. A. & BROUWER, J. 1998. Preferential binding of yeast Rad4.Rad23 complex to damaged DNA. *J Biol Chem*, 273, 33111-4.
- JAZAYERI, A. & JACKSON, S. P. 2002. Screening the yeast genome for new DNA-repair genes. *Genome Biol*, 3, REVIEWS1009.
- JENUWEIN, T. & ALLIS, C. D. 2001. Translating the histone code. *Science*, 293, 1074-80.
- JIANG, Y., WANG, X., BAO, S., GUO, R., JOHNSON, D. G., SHEN, X. & LI, L. 2010. INO80 chromatin remodeling complex promotes the removal of UV lesions by the nucleotide excision repair pathway. *Proc Natl Acad Sci U S A*, 107, 17274-9.
- JIN, C. & FELSENFELD, G. 2007. Nucleosome stability mediated by histone variants H3.3 and H2A.Z. *Genes Dev*, 21, 1519-29.
- JIRICNY, J. 2006. The multifaceted mismatch-repair system. *Nat Rev Mol Cell Biol*, 7, 335-46.
- JOHNSSON, A., DURAND-DUBIEF, M., XUE-FRANZEN, Y., RONNERBLAD, M., EKWALL, K. & WRIGHT, A. 2009. HAT-HDAC interplay modulates global histone H3K14 acetylation in gene-coding regions during stress. *EMBO Rep*, 10, 1009-14.
- JOSHI, A. A. & STRUHL, K. 2005. Eaf3 chromodomain interaction with methylated H3-K36 links histone deacetylation to Pol II elongation. *Mol Cell*, 20, 971-8.
- KADYROV, F. A., DZANTIEV, L., CONSTANTIN, N. & MODRICH, P. 2006. Endonucleolytic function of MutLalpha in human mismatch repair. *Cell*, 126, 297-308.
- KAMAKAKA, R. T. & BIGGINS, S. 2005. Histone variants: deviants? *Genes Dev*, 19, 295-310.
- KAMILERI, I., KARAKASILIOTI, I. & GARINIS, G. A. 2012. Nucleotide excision repair: new tricks with old bricks. *Trends Genet*.
- KAPETANAKI, M. G., GUERRERO-SANTORO, J., BISI, D. C., HSIEH, C. L., RAPIC-OTRIN, V. & LEVINE, A. S. 2006. The DDB1-CUL4ADDB2 ubiquitin ligase is deficient in xeroderma pigmentosum group E and targets histone H2A at UV-damaged DNA sites. *Proc Natl Acad Sci U S A*, 103, 2588-93.
- KELEHER, C. A., REDD, M. J., SCHULTZ, J., CARLSON, M. & JOHNSON, A. D. 1992. Ssn6-Tup1 is a general repressor of transcription in yeast. *Cell*, 68, 709-19.
- KELMAN, Z. 1997. PCNA: structure, functions and interactions. *Oncogene*, 14, 629-40.
- KEOGH, M. C., KURDISTANI, S. K., MORRIS, S. A., AHN, S. H., PODOLNY, V., COLLINS, S. R., SCHULDINER, M., CHIN, K., PUNNA, T., THOMPSON, N. J., BOONE, C., EMILI, A., WEISSMAN, J. S., HUGHES, T. R., STRAHL, B. D., GRUNSTEIN, M., GREENBLATT, J. F., BURATOWSKI, S. & KROGAN, N. J. 2005. Cotranscriptional set2 methylation of histone H3 lysine 36 recruits a repressive Rpd3 complex. *Cell*, 123, 593-605.
- KEOGH, M. C., MENNELLA, T. A., SAWA, C., BERTHELET, S., KROGAN, N. J., WOLEK, A., PODOLNY, V., CARPENTER, L. R., GREENBLATT, J. F., BAETZ, K. & BURATOWSKI, S. 2006. The *Saccharomyces cerevisiae* histone H2A variant Htz1 is acetylated by NuA4. *Genes Dev*, 20, 660-5.
- KEOHAVONG, P. & THILLY, W. G. 1989. Fidelity of DNA polymerases in DNA amplification. *Proc Natl Acad Sci U S A*, 86, 9253-7.
- KHOBT, A. & EPE, B. 2012. Interactions between DNA damage, repair, and transcription. *Mutation Research/Fundamental and Molecular Mechanisms of Mutagenesis*, 736, 5-14.
- KHORASANIZADEH, S. 2004. The nucleosome: from genomic organization to genomic regulation. *Cell*, 116, 259-72.
- KIM, C., PAULUS, B. F. & WOLD, M. S. 1994. Interactions of human replication protein A with oligonucleotides. *Biochemistry*, 33, 14197-206.
- KIM, C., SNYDER, R. O. & WOLD, M. S. 1992. Binding properties of replication protein A from human

- and yeast cells. *Mol Cell Biol*, 12, 3050-9.
- KIM, I., MI, K. & RAO, H. 2004. Multiple interactions of rad23 suggest a mechanism for ubiquitylated substrate delivery important in proteolysis. *Mol Biol Cell*, 15, 3357-65.
- KIM, J. H., SARAF, A., FLORENS, L., WASHBURN, M. & WORKMAN, J. L. 2010. Gcn5 regulates the dissociation of SWI/SNF from chromatin by acetylation of Swi2/Snf2. *Genes Dev*, 24, 2766-71.
- KOBOR, M. S., VENKATASUBRAHMANYAM, S., MENEGHINI, M. D., GIN, J. W., JENNINGS, J. L., LINK, A. J., MADHANI, H. D. & RINE, J. 2004. A protein complex containing the conserved Swi2/Snf2-related ATPase Swr1p deposits histone variant H2A.Z into euchromatin. *PLoS Biol*, 2, E131.
- KOUZARIDES, T. 2007. Chromatin modifications and their function. *Cell*, 128, 693-705.
- KROGAN, N. J., BAETZ, K., KEOGH, M. C., DATTA, N., SAWA, C., KWOK, T. C., THOMPSON, N. J., DAVEY, M. G., POOTOOLAL, J., HUGHES, T. R., EMILI, A., BURATOWSKI, S., HIETER, P. & GREENBLATT, J. F. 2004. Regulation of chromosome stability by the histone H2A variant Htz1, the Swr1 chromatin remodeling complex, and the histone acetyltransferase NuA4. *Proc Natl Acad Sci U S A*, 101, 13513-8.
- KROGAN, N. J., CAGNEY, G., YU, H., ZHONG, G., GUO, X., IGNATCHENKO, A., LI, J., PU, S., DATTA, N., TIKUISIS, A. P., PUNNA, T., PEREGR N-ALVAREZ, J. M., SHALES, M., ZHANG, X., DAVEY, M., ROBINSON, M. D., PACCANARO, A., BRAY, J. E., SHEUNG, A., BEATTIE, B., RICHARDS, D. P., CANADIEN, V., LALEV, A., MENA, F., WONG, P., STAROSTINE, A., CANETE, M. M., VLASBLOM, J., WU, S., ORSI, C., COLLINS, S. R., CHANDRAN, S., HAW, R., RILSTONE, J. J., GANDI, K., THOMPSON, N. J., MUSSO, G., ST ONGE, P., GHANNY, S., LAM, M. H. Y., BUTLAND, G., ALTAF-UL, A. M., KANAYA, S., SHILATIFARD, A., O'SHEA, E., WEISSMAN, J. S., INGLES, C. J., HUGHES, T. R., PARKINSON, J., GERSTEIN, M., WODAK, S. J., EMILI, A. & GREENBLATT, J. F. 2006. Global landscape of protein complexes in the yeast *Saccharomyces cerevisiae*. *Nature*, 440, 637-643.
- KROGAN, N. J., KEOGH, M. C., DATTA, N., SAWA, C., RYAN, O. W., DING, H., HAW, R. A., POOTOOLAL, J., TONG, A., CANADIEN, V., RICHARDS, D. P., WU, X., EMILI, A., HUGHES, T. R., BURATOWSKI, S. & GREENBLATT, J. F. 2003. A Snf2 family ATPase complex required for recruitment of the histone H2A variant Htz1. *Mol Cell*, 12, 1565-76.
- KROKAN, H. E., STANDAL, R. & SLUPPHAUG, G. 1997. DNA glycosylases in the base excision repair of DNA. *Biochem J*, 325 (Pt 1), 1-16.
- KUNKEL, T. A. 2004. DNA replication fidelity. *J Biol Chem*, 279, 16895-8.
- KUNKEL, T. A. & ERIE, D. A. 2005. DNA mismatch repair. *Annu Rev Biochem*, 74, 681-710.
- KUO, M.-H., BAUR, E. V., STRUHL, K. & ALLIS, C. D. 2000. Gcn4 Activator Targets Gcn5 Histone Acetyltransferase to Specific Promoters Independently of Transcription. *Molecular Cell*, 6, 1309-1320.
- KUO, M.-H., ZHOU, J., JAMBECK, P., CHURCHILL, M. E. A. & ALLIS, C. D. 1997. Histone acetyltransferase activity of yeast Gcn5p is required for the activation of target genes in vivo. *Genes and Development*, 12, 627-639.
- KURAOKA, I. 2008. Effects of DNA Lesions on Transcription Elongation by RNA Polymerases. *Genes and Environment*, 30, 63-70.
- KURDISTANI, S. K. & GRUNSTEIN, M. 2003. Histone acetylation and deacetylation in yeast. *Nat Rev Mol Cell Biol*, 4, 276-84.
- KURDISTANI, S. K., TAVAZOIE, S. & GRUNSTEIN, M. 2004. Mapping global histone acetylation patterns

- to gene expression. *Cell*, 117, 721-33.
- LAFRANCE-VANASSE, J., ARSENEAULT, G., CAPPADOCIA, L., LEGAULT, P. & OMICHINSKI, J. G. 2013. Structural and functional evidence that Rad4 competes with Rad2 for binding to the Tfb1 subunit of TFIIH in NER. *Nucleic Acids Res*, 41, 2736-45.
- LAGERWERF, S., VROUWE, M. G., OVERMEER, R. M., FOUSTERI, M. I. & MULLENDERS, L. H. 2011. DNA damage response and transcription. *DNA Repair (Amst)*, 10, 743-50.
- LAIN, J. & EGLY, J. 2006. Initiation of DNA repair mediated by a stalled RNA polymerase II. *EMBO J*, 25, 387-97.
- LAINE, J. P. & EGLY, J. M. 2006a. Initiation of DNA repair mediated by a stalled RNA polymerase II. *EMBO J*, 25, 387-97.
- LAINE, J. P. & EGLY, J. M. 2006b. When transcription and repair meet: a complex system. *Trends Genet*, 22, 430-6.
- LE MASSON, I., YU, D. Y., JENSEN, K., CHEVALIER, A., COURBEYRETTE, R., BOULARD, Y., SMITH, M. M. & MANN, C. 2003. Yaf9, a novel NuA4 histone acetyltransferase subunit, is required for the cellular response to spindle stress in yeast. *Mol Cell Biol*, 23, 6086-102.
- LEE, J. H., PARK, C. J., SHIN, J. S., IKEGAMI, T., AKUTSU, H. & CHOI, B. S. 2004. NMR structure of the DNA decamer duplex containing double T*G mismatches of cis-syn cyclobutane pyrimidine dimer: implications for DNA damage recognition by the XPC-hHR23B complex. *Nucleic Acids Res*, 32, 2474-81.
- LEE, K. B., WANG, D., LIPPARD, S. J. & SHARP, P. A. 2002. Transcription-coupled and DNA damage-dependent ubiquitination of RNA polymerase II in vitro. *Proc Natl Acad Sci U S A*, 99, 4239-44.
- LEE, S. K., YU, S. L., PRAKASH, L. & PRAKASH, S. 2001. Requirement for yeast RAD26, a homolog of the human CSB gene, in elongation by RNA polymerase II. *Mol Cell Biol*, 21, 8651-6.
- LEHMANN, A. R. 2008. XPD structure reveals its secrets. *DNA Repair (Amst)*, 7, 1912-5.
- LEJEUNE, D., CHEN, X., RUGGIERO, C., BERRYHILL, S., DING, B. & LI, S. 2009. Yeast Elc1 plays an important role in global genomic repair but not in transcription coupled repair. *DNA Repair (Amst)*, 8, 40-50.
- LI, B., CAREY, M. & WORKMAN, J. L. 2007. The Role of Chromatin during Transcription. *Cell*, 128, 707-719.
- LI, B., PATTENDEN, S. G., LEE, D., GUTIERREZ, J., CHEN, J., SEIDEL, C., GERTON, J. & WORKMAN, J. L. 2005. Preferential occupancy of histone variant H2AZ at inactive promoters influences local histone modifications and chromatin remodeling. *Proc Natl Acad Sci U S A*, 102, 18385-90.
- LI, J., WANG, Q. E., ZHU, Q., EL-MAHDY, M. A., WANI, G., PRAETORIUS-IBBA, M. & WANI, A. A. 2006a. DNA damage binding protein component DDB1 participates in nucleotide excision repair through DDB2 DNA-binding and cullin 4A ubiquitin ligase activity. *Cancer Res*, 66, 8590-7.
- LI, L., ELLEDGE, S. J., PETERSON, C. A., BALES, E. S. & LEGERSKI, R. J. 1994. Specific association between the human DNA repair proteins XPA and ERCC1. *Proc Natl Acad Sci U S A*, 91, 5012-6.
- LI, L., LU, X., PETERSON, C. A. & LEGERSKI, R. J. 1995a. An interaction between the DNA repair factor XPA and replication protein A appears essential for nucleotide excision repair. *Mol Cell Biol*, 15, 5396-402.
- LI, L., PETERSON, C. A., LU, X. & LEGERSKI, R. J. 1995b. Mutations in XPA that prevent association with ERCC1 are defective in nucleotide excision repair. *Mol Cell Biol*, 15, 1993-8.
- LI, S., CHEN, X., RUGGIERO, C., DING, B. & SMERDON, M. 2006b. Modulation of Rad26- and

- Rpb9-mediated DNA repair by different promoter elements. *J Biol Chem*, 281, 36643-51.
- LI, S., CHEN, X., RUGGIERO, C., DING, B. & SMERDON, M. J. 2006c. Modulation of Rad26- and Rpb9-mediated DNA repair by different promoter elements. *J Biol Chem*, 281, 36643-51.
- LI, S., DING, B., CHEN, R., RUGGIERO, C. & CHEN, X. 2006d. Evidence that the transcription elongation function of Rpb9 is involved in transcription-coupled DNA repair in *Saccharomyces cerevisiae*. *Mol Cell Biol*, 26, 9430-41.
- LI, S. & SHOGREN-KNAAK, M. A. 2009. The Gcn5 bromodomain of the SAGA complex facilitates cooperative and cross-tail acetylation of nucleosomes. *J Biol Chem*, 284, 9411-7.
- LI, S. & SMERDON, M. 2002a. Rpb4 and Rpb9 mediate subpathways of transcription-coupled DNA repair in *Saccharomyces cerevisiae*. *EMBO J*, 21, 5921-9.
- LI, S. & SMERDON, M. J. 2002b. Nucleosome structure and repair of N-methylpurines in the GAL1-10 genes of *Saccharomyces cerevisiae*. *J Biol Chem*, 277, 44651-9.
- LI, S. & SMERDON, M. J. 2002c. Rpb4 and Rpb9 mediate subpathways of transcription-coupled DNA repair in *Saccharomyces cerevisiae*. *EMBO J*, 21, 5921-9.
- LI, S. & SMERDON, M. J. 2004. Dissecting transcription-coupled and global genomic repair in the chromatin of yeast GAL1-10 genes. *J Biol Chem*, 279, 14418-26.
- LI, W., NAGARAJA, S., DELCUVE, G. P., HENDZEL, M. J. & DAVIE, J. R. 1993. Effects of histone acetylation, ubiquitination and variants on nucleosome stability. *Biochem J*, 296 (Pt 3), 737-44.
- LIEBER, M. R. 2010. The mechanism of double-strand DNA break repair by the nonhomologous DNA end-joining pathway. *Annu Rev Biochem*, 79, 181-211.
- LIN, Y. Y., QI, Y., LU, J. Y., PAN, X., YUAN, D. S., ZHAO, Y., BADER, J. S. & BOEKE, J. D. 2008. A comprehensive synthetic genetic interaction network governing yeast histone acetylation and deacetylation. *Genes Dev*, 22, 2062-74.
- LINDAHL, T. 1982. DNA-Repair Enzymes. *Annual Review of Biochemistry*, 51, 61-87.
- LIU, X., LI, B. & GOROVSKYMA 1996. Essential and nonessential histone H2A variants in *Tetrahymena thermophila*. *Mol Cell Biol*, 16, 4305-11.
- LIU, X., MANN, D. B., SUQUET, C., SPRINGER, D. L. & SMERDON, M. J. 2000. Ultraviolet damage and nucleosome folding of the 5S ribosomal RNA gene. *Biochemistry*, 39, 557-66.
- LIU, X. & SMERDON, M. J. 2000. Nucleotide excision repair of the 5 S ribosomal RNA gene assembled into a nucleosome. *J Biol Chem*, 275, 23729-35.
- LOMMEL, L., CHEN, L., MADURA, K. & SWEDER, K. 2000. The 26S proteasome negatively regulates the level of overall genomic nucleotide excision repair. *Nucleic Acids Res*, 28, 4839-45.
- LOMMEL, L., ORTOLAN, T., CHEN, L., MADURA, K. & SWEDER, K. S. 2002. Proteolysis of a nucleotide excision repair protein by the 26 S proteasome. *Curr Genet*, 42, 9-20.
- LUGER, K., MADER, A. W., RICHMOND, R. K., SARGENT, D. F. & RICHMOND, T. J. 1997. Crystal structure of the nucleosome core particle at 2.8 Å resolution. *Nature*, 389, 251-60.
- LUGER, K. & RICHMOND, T. J. 1998. The histone tails of the nucleosome. *Curr Opin Genet Dev*, 8, 140-6.
- LUIJSTERBURG, M. S., GOEDHART, J., MOSER, J., KOOL, H., GEVERTS, B., HOUTSMULLER, A. B., MULLENDERS, L. H., VERMEULEN, W. & VAN DRIEL, R. 2007. Dynamic in vivo interaction of DDB2 E3 ubiquitin ligase with UV-damaged DNA is independent of damage-recognition protein XPC. *J Cell Sci*, 120, 2706-16.
- LUK, E., RANJAN, A., FITZGERALD, P. C., MIZUGUCHI, G., HUANG, Y., WEI, D. & WU, C. 2010. Stepwise histone replacement by SWR1 requires dual activation with histone H2A.Z and canonical

- nucleosome. *Cell*, 143, 725-36.
- LUK, E., VU, N. D., PATTESON, K., MIZUGUCHI, G., WU, W. H., RANJAN, A., BACKUS, J., SEN, S., LEWIS, M., BAI, Y. & WU, C. 2007. Chz1, a nuclear chaperone for histone H2AZ. *Mol Cell*, 25, 357-68.
- LYNDAKER, A. M. & ALANI, E. 2009. A tale of tails: insights into the coordination of 3' end processing during homologous recombination. *Bioessays*, 31, 315-21.
- MACNEILL, S. A., BALDACCI, G., BURGERS, P. M. & HUBSCHER, U. 2001. A unified nomenclature for the subunits of eukaryotic DNA polymerase delta. *Trends Biochem Sci*, 26, 16-7.
- MADURA, K. & PRAKASH, S. 1990. Transcript levels of the *Saccharomyces cerevisiae* DNA repair gene RAD23 increase in response to UV light and in meiosis but remain constant in the mitotic cell cycle. *Nucleic Acids Res*, 18, 4737-42.
- MAILLARD, O., SOLYOM, S. & NAEGELI, H. 2007. An aromatic sensor with aversion to damaged strands confers versatility to DNA repair. *PLoS Biol*, 5, e79.
- MALIK, H. S. & HENIKOFF, S. 2003. Phylogenomics of the nucleosome. *Nat Struct Biol*, 10, 882-91.
- MALIK, S., CHAURASIA, P., LAHUDKAR, S., DURAIRAJ, G., SHUKLA, A. & BHAUMIK, S. R. 2010. Rad26p, a transcription-coupled repair factor, is recruited to the site of DNA lesion in an elongating RNA polymerase II-dependent manner in vivo. *Nucleic Acids Res*, 38, 1461-77.
- MALLOY, K. D., HOLMAN, M. A., MITCHELL, D. & DETRICH, H. W., 3RD 1997. Solar UVB-induced DNA damage and photoenzymatic DNA repair in antarctic zooplankton. *Proc Natl Acad Sci U S A*, 94, 1258-63.
- MALTSEVA, E. A., RECHKUNOVA, N. I., PETRUSEVA, I. O., SILNIKOV, V. N., VERMEULEN, W. & LAVRIK, O. I. 2006. Interaction of nucleotide excision repair factors RPA and XPA with DNA containing bulky photoreactive groups imitating damages. *Biochemistry (Mosc)*, 71, 270-8.
- MARTINEZ, E., KUNDU, T. K., FU, J. & ROEDER, R. G. 1998. A human SPT3-TAFII31-GCN5-L acetylase complex distinct from transcription factor IID. *J Biol Chem*, 273, 23781-5.
- MARTINEZ, E., PALHAN, V. B., TJERNBERG, A., LYMAR, E. S., GAMPER, A. M., KUNDU, T. K., CHAIT, B. T. & ROEDER, R. G. 2001. Human STAGA complex is a chromatin-acetylating transcription coactivator that interacts with pre-mRNA splicing and DNA damage-binding factors in vivo. *Mol Cell Biol*, 21, 6782-95.
- MASIH, P. J., KUNNEV, D. & MELENDY, T. 2008. Mismatch Repair proteins are recruited to replicating DNA through interaction with Proliferating Cell Nuclear Antigen (PCNA). *Nucleic Acids Res*, 36, 67-75.
- MASUTANI, C., ARAKI, M., SUGASAWA, K., VAN DER SPEK, P. J., YAMADA, A., UCHIDA, A., MAEKAWA, T., BOOTSMA, D., HOEIJMAKERS, J. H. & HANAOKA, F. 1997. Identification and characterization of XPC-binding domain of hHR23B. *Mol Cell Biol*, 17, 6915-23.
- MASUTANI, C., SUGASAWA, K., YANAGISAWA, J., SONOYAMA, T., UI, M., ENOMOTO, T., TAKIO, K., TANAKA, K., VAN DER SPEK, P. J., BOOTSMA, D. & ET AL. 1994. Purification and cloning of a nucleotide excision repair complex involving the xeroderma pigmentosum group C protein and a human homologue of yeast RAD23. *EMBO J*, 13, 1831-43.
- MATSUNAGA, T., MU, D., PARK, C. H., REARDON, J. T. & SANCAR, A. 1995. Human DNA repair excision nuclease. Analysis of the roles of the subunits involved in dual incisions by using anti-XPG and anti-ERCC1 antibodies. *J Biol Chem*, 270, 20862-9.
- MATSUNAGA, T., PARK, C. H., BESSHO, T., MU, D. & SANCAR, A. 1996. Replication protein A confers structure-specific endonuclease activities to the XPF-ERCC1 and XPG subunits of human DNA repair excision nuclease. *J Biol Chem*, 271, 11047-50.

- MATSUNO, M., KOSE, H., OKABE, M. & HIROMI, Y. 2007. TFIIF controls developmentally-regulated cell cycle progression as a holocomplex. *Genes Cells*, 12, 1289-300.
- MEAD, J., BRUNING, A. R., GILL, M. K., STEINER, A. M., ACTON, T. B. & VERSHON, A. K. 2002. Interactions of the Mcm1 MADS box protein with cofactors that regulate mating in yeast. *Mol Cell Biol*, 22, 4607-21.
- MEHTA, M., BRABERG, H., WANG, S., LOZSA, A., SHALES, M., SOLACHE, A., KROGAN, N. J. & KEOGH, M. C. 2010. Individual lysine acetylations on the N terminus of *Saccharomyces cerevisiae* H2A.Z are highly but not differentially regulated. *J Biol Chem*, 285, 39855-65.
- MEIJER, M. & SMERDON, M. J. 1999. Accessing DNA damage in chromatin: insights from transcription. *Bioessays*, 21, 596-603.
- MELLON, I., SPIVAK, G. & HANAWALT, P. C. 1987. Selective removal of transcription-blocking DNA damage from the transcribed strand of the mammalian DHFR gene. *Cell*, 51, 241-9.
- MENEGHINI, M. D., WU, M. & MADHANI, H. D. 2003. Conserved histone variant H2A.Z protects euchromatin from the ectopic spread of silent heterochromatin. *Cell*, 112, 725-36.
- MICHAELA, C., MARCUS, F. & THOMAS, C. 2003. DNA Damage and Repair. *CRC Handbook of Organic Photochemistry and Photobiology, Volumes 1 & 2, Second Edition*. CRC Press.
- MICHAELIS, S. & HERSKOWITZ, I. 1988. The a-factor pheromone of *Saccharomyces cerevisiae* is essential for mating. *Mol Cell Biol*, 8, 1309-18.
- MILLAR, C. B., XU, F., ZHANG, K. & GRUNSTEIN, M. 2006. Acetylation of H2AZ Lys 14 is associated with genome-wide gene activity in yeast. *Genes Dev*, 20, 711-22.
- MIN, J. H. & PAVLETICH, N. P. 2007. Recognition of DNA damage by the Rad4 nucleotide excision repair protein. *Nature*, 449, 570-5.
- MISSURA, M., BUTERIN, T., HINDGES, R., HUBSCHER, U., KASPARKOVA, J., BRABEC, V. & NAEGELI, H. 2001. Double-check probing of DNA bending and unwinding by XPA-RPA: an architectural function in DNA repair. *EMBO J*, 20, 3554-64.
- MITCHELL, D. L. & ROSENSTEIN, B. S. 1987. THE USE OF SPECIFIC RADIOIMMUNOASSAYS TO DETERMINE ACTION SPECTRA FOR THE PHOTOLYSIS OF (6-4) PHOTOPRODUCTS. *Photochemistry and Photobiology*, 45, 781-786.
- MIZUGUCHI, G., SHEN, X., LANDRY, J., WU, W. H., SEN, S. & WU, C. 2004. ATP-driven exchange of histone H2AZ variant catalyzed by SWR1 chromatin remodeling complex. *Science*, 303, 343-8.
- MOAN, J. & PEAK, M. J. 1989. Effects of UV radiation on cells. *Journal of Photochemistry and Photobiology B: Biology*, 4, 21-34.
- MOCQUET, V., KROPACHEV, K., KOLBANOVSKIY, M., KOLBANOVSKIY, A., TAPIAS, A., CAI, Y., BROYDE, S., GEACINTOV, N. E. & EGLY, J. M. 2007. The human DNA repair factor XPC-HR23B distinguishes stereoisomeric benzo[a]pyrenyl-DNA lesions. *EMBO J*, 26, 2923-32.
- MOCQUET, V., LAINE, J. P., RIEDL, T., YAJIN, Z., LEE, M. Y. & EGLY, J. M. 2008. Sequential recruitment of the repair factors during NER: the role of XPG in initiating the resynthesis step. *EMBO J*, 27, 155-67.
- MOGGS, J. G., YAREMA, K. J., ESSIGMANN, J. M. & WOOD, R. D. 1996. Analysis of incision sites produced by human cell extracts and purified proteins during nucleotide excision repair of a 1,3-intrastrand d(GpTpG)-cisplatin adduct. *J Biol Chem*, 271, 7177-86.
- MORILLO-HUESCA, M., CLEMENTE-RUIZ, M., ANDUJAR, E. & PRADO, F. 2010. The SWR1 histone replacement complex causes genetic instability and genome-wide transcription misregulation in the absence of H2A.Z. *PLoS One*, 5, e12143.

- MORRISON, A., ARAKI, H., CLARK, A. B., HAMATAKE, R. K. & SUGINO, A. 1990. A third essential DNA polymerase in *S. cerevisiae*. *Cell*, 62, 1143-51.
- MOSER, J., KOOL, H., GIAKZIDIS, I., CALDECOTT, K., MULLENDERS, L. H. & FOUSTERI, M. I. 2007. Sealing of chromosomal DNA nicks during nucleotide excision repair requires XRCC1 and DNA ligase III alpha in a cell-cycle-specific manner. *Mol Cell*, 27, 311-23.
- MOSER, J., VOLKER, M., KOOL, H., ALEKSEEV, S., VRIELING, H., YASUI, A., VAN ZEELAND, A. A. & MULLENDERS, L. H. 2005. The UV-damaged DNA binding protein mediates efficient targeting of the nucleotide excision repair complex to UV-induced photo lesions. *DNA Repair (Amst)*, 4, 571-82.
- MU, D., HSU, D. & SANCAR, A. 1996a. Reaction mechanism of human DNA repair excision nuclease. *J Biol Chem*, 271, 8285-94.
- MU, D., HSU, D. S. & SANCAR, A. 1996b. Reaction mechanism of human DNA repair excision nuclease. *J Biol Chem*, 271, 8285-94.
- MU, D. & SANCAR, A. 1997. Model for XPC-independent transcription-coupled repair of pyrimidine dimers in humans. *J Biol Chem*, 272, 7570-3.
- MU, D., WAKASUGI, M., HSU, D. & SANCAR, A. 1997. Characterization of reaction intermediates of human excision repair nuclease. *J Biol Chem*, 272, 28971-9.
- MUELLER, J. P. & SMERDON, M. J. 1996. Rad23 is required for transcription-coupled repair and efficient overall repair in *Saccharomyces cerevisiae*. *Mol Cell Biol*, 16, 2361-8.
- MUKHERJEE, S., BERGER, M. F., JONA, G., WANG, X. S., MUZZEY, D., SNYDER, M., YOUNG, R. A. & BULYK, M. L. 2004. Rapid analysis of the DNA-binding specificities of transcription factors with DNA microarrays. *Nat Genet*, 36, 1331-9.
- NAKATSU, Y., ASAHINA, H., CITTERIO, E., RADEMAKERS, S., VERMEULEN, W., KAMIUCHI, S., YEO, J. P., KHAW, M. C., SAIJO, M., KODO, N., MATSUDA, T., HOEIJMAKERS, J. H. & TANAKA, K. 2000. XAB2, a novel tetratricopeptide repeat protein involved in transcription-coupled DNA repair and transcription. *J Biol Chem*, 275, 34931-7.
- NASMYTH, K. A. 1982. Molecular genetics of yeast mating type. *Annu Rev Genet*, 16, 439-500.
- NEWMAN, J. C., BAILEY, A. D. & WEINER, A. M. 2006. Cockayne syndrome group B protein (CSB) plays a general role in chromatin maintenance and remodeling. *Proc Natl Acad Sci U S A*, 103, 9613-8.
- NG, J. M., VERMEULEN, W., VAN DER HORST, G. T., BERGINK, S., SUGASAWA, K., VRIELING, H. & HOEIJMAKERS, J. H. 2003. A novel regulation mechanism of DNA repair by damage-induced and RAD23-dependent stabilization of xeroderma pigmentosum group C protein. *Genes Dev*, 17, 1630-45.
- NISHI, R., OKUDA, Y., WATANABE, E., MORI, T., IWAI, S., MASUTANI, C., SUGASAWA, K. & HANAOKA, F. 2005. Centrin 2 stimulates nucleotide excision repair by interacting with xeroderma pigmentosum group C protein. *Mol Cell Biol*, 25, 5664-74.
- NOUSPIKEL, T. 2009. DNA repair in mammalian cells : Nucleotide excision repair: variations on versatility. *Cell Mol Life Sci*, 66, 994-1009.
- NUSINOW, D. A., HERNANDEZ-MUNOZ, I., FAZZIO, T. G., SHAH, G. M., KRAUS, W. L. & PANNING, B. 2007. Poly(ADP-ribose) polymerase 1 is inhibited by a histone H2A variant, MacroH2A, and contributes to silencing of the inactive X chromosome. *J Biol Chem*, 282, 12851-9.
- O'DONOVAN, A., DAVIES, A. A., MOGGS, J. G., WEST, S. C. & WOOD, R. D. 1994. XPG endonuclease makes the 3' incision in human DNA nucleotide excision repair. *Nature*, 371, 432-5.

- OGI, T. & LEHMANN, A. R. 2006. The Y-family DNA polymerase kappa (pol kappa) functions in mammalian nucleotide-excision repair. *Nat Cell Biol*, 8, 640-2.
- OGI, T., LIMSIRICHAIKUL, S., OVERMEER, R. M., VOLKER, M., TAKENAKA, K., CLONEY, R., NAKAZAWA, Y., NIIMI, A., MIKI, Y., JASPERS, N. G., MULLENDERS, L. H., YAMASHITA, S., FOSTERI, M. I. & LEHMANN, A. R. 2010. Three DNA polymerases, recruited by different mechanisms, carry out NER repair synthesis in human cells. *Mol Cell*, 37, 714-27.
- OGRYZKO, V. V., KOTANI, T., ZHANG, X., SCHILTZ, R. L., HOWARD, T., YANG, X. J., HOWARD, B. H., QIN, J. & NAKATANI, Y. 1998. Histone-like TAFs within the PCAF histone acetylase complex. *Cell*, 94, 35-44.
- OKSENYCH, V., BERNARDES DE JESUS, B., ZHOVMER, A., EGLY, J. M. & COIN, F. 2009a. Molecular insights into the recruitment of TFIIH to sites of DNA damage. *EMBO J*, 28, 2971-80.
- OKSENYCH, V., DE JESUS, B., ZHOVMER, A., EGLY, J. & COIN, F. 2009b. Molecular insights into the recruitment of TFIIH to sites of DNA damage. *EMBO J*, 28, 2971-80.
- ORELLI, B., MCCLENDON, T. B., TSODIKOV, O. V., ELLENBERGER, T., NIEDERNHOFER, L. J. & SCHARER, O. D. 2010. The XPA-binding domain of ERCC1 is required for nucleotide excision repair but not other DNA repair pathways. *J Biol Chem*, 285, 3705-12.
- ORREN, D. K., SELBY, C. P., HEARST, J. E. & SANCAR, A. 1992. Post-incision steps of nucleotide excision repair in Escherichia coli. Disassembly of the UvrBC-DNA complex by helicase II and DNA polymerase I. *J Biol Chem*, 267, 780-8.
- ORTOLAN, T. G., CHEN, L., TONGAONKAR, P. & MADURA, K. 2004. Rad23 stabilizes Rad4 from degradation by the Ub/proteasome pathway. *Nucleic Acids Res*, 32, 6490-500.
- ORTOLAN, T. G., TONGAONKAR, P., LAMBERTSON, D., CHEN, L., SCHAUBER, C. & MADURA, K. 2000. The DNA repair protein rad23 is a negative regulator of multi-ubiquitin chain assembly. *Nat Cell Biol*, 2, 601-8.
- OSLEY, M. A., TSUKUDA, T. & NICKOLOFF, J. A. 2007. ATP-dependent chromatin remodeling factors and DNA damage repair. *Mutat Res*, 618, 65-80.
- OVERMEER, R. M., GOURDIN, A. M., GIGLIA-MARI, A., KOOL, H., HOUTSMULLER, A. B., SIEGAL, G., FOSTERI, M. I., MULLENDERS, L. H. & VERMEULEN, W. 2010. Replication factor C recruits DNA polymerase delta to sites of nucleotide excision repair but is not required for PCNA recruitment. *Mol Cell Biol*, 30, 4828-39.
- OVERMEER, R. M., MOSER, J., VOLKER, M., KOOL, H., TOMKINSON, A. E., VAN ZEELAND, A. A., MULLENDERS, L. H. & FOSTERI, M. 2011. Replication protein A safeguards genome integrity by controlling NER incision events. *J Cell Biol*, 192, 401-15.
- PALMER, D. K., O'DAY, K. & MARGOLIS, R. L. 1990. The centromere specific histone CENP-A is selectively retained in discrete foci in mammalian sperm nuclei. *Chromosoma*, 100, 32-6.
- PAOLINELLI, R., MENDOZA-MALDONADO, R., CERSETO, A. & GIACCA, M. 2009. Acetylation by GCN5 regulates CDC6 phosphorylation in the S phase of the cell cycle. *Nat Struct Mol Biol*, 16, 412-20.
- PAPAMICHOS-CHRONAKIS, M., WATANABE, S., RANDO, O. J. & PETERSON, C. L. 2011. Global regulation of H2A.Z localization by the INO80 chromatin-remodeling enzyme is essential for genome integrity. *Cell*, 144, 200-13.
- PARK, Y. J., DYER, P. N., TREMETHICK, D. J. & LUGER, K. 2004. A new fluorescence resonance energy transfer approach demonstrates that the histone variant H2AZ stabilizes the histone octamer within the nucleosome. *J Biol Chem*, 279, 24274-82.

- PARSEGHIAN, M. H., NEWCOMB, R. L. & HAMKALO, B. A. 2001. Distribution of somatic H1 subtypes is non-random on active vs. inactive chromatin II: distribution in human adult fibroblasts. *J Cell Biochem*, 83, 643-59.
- PASSMORE, L. A. & BARFORD, D. 2004. Getting into position: the catalytic mechanisms of protein ubiquitylation. *Biochem J*, 379, 513-25.
- PEHRSON, J. R. & FUJI, R. N. 1998. Evolutionary conservation of histone macroH2A subtypes and domains. *Nucleic Acids Res*, 26, 2837-42.
- PENG, W., TOGAWA, C., ZHANG, K. & KURDISTANI, S. K. 2008. Regulators of cellular levels of histone acetylation in *Saccharomyces cerevisiae*. *Genetics*, 179, 277-89.
- PEROZZI, G. & PRAKASH, S. 1986. RAD7 gene of *Saccharomyces cerevisiae*: transcripts, nucleotide sequence analysis, and functional relationship between the RAD7 and RAD23 gene products. *Mol Cell Biol*, 6, 1497-507.
- PESTRYAKOV, P. E. & LAVRIK, O. I. 2008. Mechanisms of single-stranded DNA-binding protein functioning in cellular DNA metabolism. *Biochemistry (Mosc)*, 73, 1388-404.
- PETERSON, C. L. & LANIEL, M. A. 2004. Histones and histone modifications. *Curr Biol*, 14, R546-51.
- PETTIJOHN, D. & HANAWALT, P. 1964. EVIDENCE FOR REPAIR-REPLICATION OF ULTRAVIOLET DAMAGED DNA IN BACTERIA. *J Mol Biol*, 9, 395-410.
- PFEIFER, G. P. 1997. Formation and Processing of UV Photoproducts: Effects of DNA Sequence and Chromatin Environment. *Photochemistry and Photobiology*, 65, 270-283.
- PFEIFER, G. P., DROUIN, R., RIGGS, A. D. & HOLMQUIST, G. P. 1991. In vivo mapping of a DNA adduct at nucleotide resolution: detection of pyrimidine (6-4) pyrimidone photoproducts by ligation-mediated polymerase chain reaction. *Proc Natl Acad Sci U S A*, 88, 1374-8.
- PILLUS, L. 2008. MYSTs mark chromatin for chromosomal functions. *Curr Opin Cell Biol*, 20, 326-33.
- PLUCIENNIK, A., DZANTIEV, L., IYER, R. R., CONSTANTIN, N., KADYROV, F. A. & MODRICH, P. 2010. PCNA function in the activation and strand direction of MutLalpha endonuclease in mismatch repair. *Proc Natl Acad Sci U S A*, 107, 16066-71.
- POKHOLOK, D. K., HARBISON, C. T., LEVINE, S., COLE, M., HANNETT, N. M., LEE, T. I., BELL, G. W., WALKER, K., ROLFE, P. A., HERBOLSHEIMER, E., ZEITLINGER, J., LEWITTER, F., GIFFORD, D. K. & YOUNG, R. A. 2005a. Genome-wide Map of Nucleosome Acetylation and Methylation in Yeast. *Cell*, 122, 517-527.
- POKHOLOK, D. K., HARBISON, C. T., LEVINE, S., COLE, M., HANNETT, N. M., LEE, T. I., BELL, G. W., WALKER, K., ROLFE, P. A., HERBOLSHEIMER, E., ZEITLINGER, J., LEWITTER, F., GIFFORD, D. K. & YOUNG, R. A. 2005b. Genome-wide map of nucleosome acetylation and methylation in yeast. *Cell*, 122, 517-27.
- POPESCU, A., MIRON, S., BLOUQUIT, Y., DUCHAMBON, P., CHRISTOVA, P. & CRAESCU, C. T. 2003. Xeroderma pigmentosum group C protein possesses a high affinity binding site to human centrin 2 and calmodulin. *J Biol Chem*, 278, 40252-61.
- POWELL, N. G., FERREIRO, J., KARABETSOU, N., MELLOR, J. & WATERS, R. 2003. Transcription, nucleosome positioning and protein binding modulate nucleotide excision repair of the *Saccharomyces cerevisiae* MET17 promoter. *DNA Repair (Amst)*, 2, 375-86.
- PRAKASH, S. & PRAKASH, L. 2000. Nucleotide excision repair in yeast. *Mutat Res*, 451, 13-24.
- PRAKASH, S., SUNG, P. & PRAKASH, L. 1993. DNA repair genes and proteins of *Saccharomyces cerevisiae*. *Annu Rev Genet*, 27, 33-70.
- RADEMAKERS, S., VOLKER, M., HOOGSTRATEN, D., NIGG, A. L., MONE, M. J., VAN ZEELAND, A. A.,

- HOEIJMAKERS, J. H., HOUTSMULLER, A. B. & VERMEULEN, W. 2003. Xeroderma pigmentosum group A protein loads as a separate factor onto DNA lesions. *Mol Cell Biol*, 23, 5755-67.
- RAISNER, R. M., HARTLEY, P. D., MENEGHINI, M. D., BAO, M. Z., LIU, C. L., SCHREIBER, S. L., RANDO, O. J. & MADHANI, H. D. 2005. Histone variant H2A.Z marks the 5' ends of both active and inactive genes in euchromatin. *Cell*, 123, 233-48.
- RAMANATHAN, B. & SMERDON, M. J. 1986. Changes in nuclear protein acetylation in u.v.-damaged human cells. *Carcinogenesis*, 7, 1087-94.
- RAMANATHAN, B. & SMERDON, M. J. 1989. Enhanced DNA repair synthesis in hyperacetylated nucleosomes. *J Biol Chem*, 264, 11026-34.
- RAMSEY, K. L., SMITH, J. J., DASGUPTA, A., MAQANI, N., GRANT, P. & AUBLE, D. T. 2004. The NEF4 complex regulates Rad4 levels and utilizes Snf2/Swi2-related ATPase activity for nucleotide excision repair. *Mol Cell Biol*, 24, 6362-78.
- RANGASAMY, D., GREAVES, I. & TREMETHICK, D. J. 2004. RNA interference demonstrates a novel role for H2A.Z in chromosome segregation. *Nat Struct Mol Biol*, 11, 650-5.
- RAPIC-OTRIN, V., MCLENIGAN, M. P., BISI, D. C., GONZALEZ, M. & LEVINE, A. S. 2002. Sequential binding of UV DNA damage binding factor and degradation of the p48 subunit as early events after UV irradiation. *Nucleic Acids Res*, 30, 2588-98.
- RASMUSSEN, R. E. & PAINTER, R. B. 1964. EVIDENCE FOR REPAIR OF ULTRA-VIOLET DAMAGED DEOXYRIBONUCLEIC ACID IN CULTURED MAMMALIAN CELLS. *Nature*, 203, 1360-2.
- RASTOGI, R. P., RICHA, KUMAR, A., TYAGI, M. B. & SINHA, R. P. 2010. Molecular mechanisms of ultraviolet radiation-induced DNA damage and repair. *J Nucleic Acids*, 2010, 592980.
- RATNER, J. N., BALASUBRAMANIAN, B., CORDEN, J., WARREN, S. L. & BREGMAN, D. B. 1998. Ultraviolet radiation-induced ubiquitination and proteasomal degradation of the large subunit of RNA polymerase II. Implications for transcription-coupled DNA repair. *J Biol Chem*, 273, 5184-9.
- RAVINDRA, A., WEISS, K. & SIMPSON, R. T. 1999. High-resolution structural analysis of chromatin at specific loci: *Saccharomyces cerevisiae* silent mating-type locus HMRA. *Mol Cell Biol*, 19, 7944-50.
- REAGAN, M. S. & FRIEDBERG, E. C. 1997. Recovery of RNA polymerase II synthesis following DNA damage in mutants of *Saccharomyces cerevisiae* defective in nucleotide excision repair. *Nucleic Acids Res*, 25, 4257-63.
- REED, S. H. 2005. Nucleotide excision repair in chromatin: the shape of things to come. *DNA Repair (Amst)*, 4, 909-18.
- REED, S. H., AKIYAMA, M., STILLMAN, B. & FRIEDBERG, E. C. 1999. Yeast autonomously replicating sequence binding factor is involved in nucleotide excision repair. *Genes Dev*, 13, 3052-8.
- REED, S. H., YOU, Z. & FRIEDBERG, E. C. 1998. The yeast RAD7 and RAD16 genes are required for postincision events during nucleotide excision repair. In vitro and in vivo studies with rad7 and rad16 mutants and purification of a Rad7/Rad16-containing protein complex. *J Biol Chem*, 273, 29481-8.
- REYNOLDS, P., PRAKASH, L., DUMAIS, D., PEROZZI, G. & PRAKASH, S. 1985. Nucleotide sequence of the RAD10 gene of *Saccharomyces cerevisiae*. *EMBO J*, 4, 3549-52.
- RIDGWAY, P., BROWN, K. D., RANGASAMY, D., SVENSSON, U. & TREMETHICK, D. J. 2004. Unique residues on the H2A.Z containing nucleosome surface are important for *Xenopus laevis* development. *J Biol Chem*, 279, 43815-20.
- RIEDL, T., HANAOKA, F. & EGLY, J. 2003. The comings and goings of nucleotide excision repair factors

- on damaged DNA. *EMBO J*, 22, 5293-303.
- RIPPE, K., MAZURKIEWICZ, J. & KEPPEL, N. 2008. Interactions of Histones with DNA: Nucleosome Assembly, Stability, Dynamics, and Higher Order Structure. *DNA Interactions with Polymers and Surfactants*. John Wiley & Sons, Inc.
- RIZKI, R. M. & RIZKI, T. M. 1969. Somatic cell lesions induced by the base analog 5-bromodeoxyuridine. *Cancer Res*, 29, 201-8.
- RODRIGUEZ, A., DIEZ, C., CAAMANO, J. N., DE FRUTOS, C., ROYO, L. J., MUNOZ, M., IKEDA, S., FACAL, N., ALVAREZ-VIEJO, M. & GOMEZ, E. 2007. Retinoid receptor-specific agonists regulate bovine in vitro early embryonic development, differentiation and expression of genes related to cell cycle arrest and apoptosis. *Theriogenology*, 68, 1118-27.
- ROH, T. Y., NGAU, W. C., CUI, K., LANDSMAN, D. & ZHAO, K. 2004. High-resolution genome-wide mapping of histone modifications. *Nat Biotechnol*, 22, 1013-6.
- ROSENSTEIN, B. S. & MITCHELL, D. L. 1987. ACTION SPECTRA FOR THE INDUCTION OF PYRIMIDINE(6-4)PYRIMIDONE PHOTOPRODUCTS AND CYCLOBUTANE PYRIMIDINE DIMERS IN NORMAL HUMAN SKIN FIBROBLASTS. *Photochemistry and Photobiology*, 45, 775-780.
- RUSSELL, S. J., REED, S. H., HUANG, W., FRIEDBERG, E. C. & JOHNSTON, S. A. 1999. The 19S regulatory complex of the proteasome functions independently of proteolysis in nucleotide excision repair. *Mol Cell*, 3, 687-95.
- SAEKI, Y., SONE, T., TOH-E, A. & YOKOSAWA, H. 2002. Identification of ubiquitin-like protein-binding subunits of the 26S proteasome. *Biochem Biophys Res Commun*, 296, 813-9.
- SAIJO, M., KURAOKA, I., MASUTANI, C., HANAOKA, F. & TANAKA, K. 1996. Sequential binding of DNA repair proteins RPA and ERCC1 to XPA in vitro. *Nucleic Acids Res*, 24, 4719-24.
- SALAS, T. R., PETRUSEVA, I., LAVRIK, O. & SAINTOME, C. 2009. Evidence for direct contact between the RPA3 subunit of the human replication protein A and single-stranded DNA. *Nucleic Acids Res*, 37, 38-46.
- SAN FILIPPO, J., SUNG, P. & KLEIN, H. 2008. Mechanism of eukaryotic homologous recombination. *Annu Rev Biochem*, 77, 229-57.
- SANCHO, M., DIANI, E., BEATO, M. & JORDAN, A. 2008. Depletion of human histone H1 variants uncovers specific roles in gene expression and cell growth. *PLoS Genet*, 4, e1000227.
- SANTENARD, A., ZIEGLER-BIRLING, C., KOCH, M., TORA, L., BANNISTER, A. J. & TORRES-PADILLA, M. E. 2010. Heterochromatin formation in the mouse embryo requires critical residues of the histone variant H3.3. *Nat Cell Biol*, 12, 853-62.
- SANTISTEBAN, M. S., KALASHNIKOVA, T. & SMITH, M. M. 2000. Histone H2A.Z regulates transcription and is partially redundant with nucleosome remodeling complexes. *Cell*, 103, 411-22.
- SANTOS-ROSA, H., BANNISTER, A. J., DEHE, P. M., GELI, V. & KOUZARIDES, T. 2004. Methylation of H3 lysine 4 at euchromatin promotes Sir3p association with heterochromatin. *J Biol Chem*, 279, 47506-12.
- SARKAR, S., KIELY, R. & MCHUGH, P. J. 2010. The Ino80 chromatin-remodeling complex restores chromatin structure during UV DNA damage repair. *J Cell Biol*, 191, 1061-8.
- SARKER, A. H., TSUTAKAWA, S. E., KOSTEK, S., NG, C., SHIN, D. S., PERIS, M., CAMPEAU, E., TAINER, J. A., NOGALES, E. & COOPER, P. K. 2005. Recognition of RNA polymerase II and transcription bubbles by XPG, CSB, and TFIIH: insights for transcription-coupled repair and Cockayne Syndrome. *Mol Cell*, 20, 187-98.
- SCHAEFFER, L., MONCOLLIN, V., ROY, R., STAUB, A., MEZZINA, M., SARASIN, A., WEEDA, G.,

- HOEIJMAKERS, J. & EGLY, J. 1994. The ERCC2/DNA repair protein is associated with the class II BTF2/TFIIH transcription factor. *EMBO J*, 13, 2388-92.
- SCHAEFFER, L., ROY, R., HUMBERT, S., MONCOLLIN, V., VERMEULEN, W., HOEIJMAKERS, J., CHAMBON, P. & EGLY, J. 1993. DNA repair helicase: a component of BTF2 (TFIIH) basic transcription factor. *Science*, 260, 58-63.
- SCHARER, O. D. & JIRICNY, J. 2001. Recent progress in the biology, chemistry and structural biology of DNA glycosylases. *Bioessays*, 23, 270-81.
- SCHAUBER, C., CHEN, L., TONGAONKAR, P., VEGA, I., LAMBERTSON, D., POTTS, W. & MADURA, K. 1998. Rad23 links DNA repair to the ubiquitin/proteasome pathway. *Nature*, 391, 715-8.
- SCHENK, R., JENKE, A., ZILBAUER, M., WIRTH, S. & POSTBERG, J. 2011. H3.5 is a novel hominid-specific histone H3 variant that is specifically expressed in the seminiferous tubules of human testes. *Chromosoma*, 120, 275-85.
- SCHIEFERSTEIN, U. & THOMA, F. 1996. Modulation of cyclobutane pyrimidine dimer formation in a positioned nucleosome containing poly(dA.dT) tracts. *Biochemistry*, 35, 7705-14.
- SCHULZE, J. M., WANG, A. Y. & KOBOR, M. S. 2009. YEATS domain proteins: a diverse family with many links to chromatin modification and transcription. *Biochem Cell Biol*, 87, 65-75.
- SCHWEIZER, U., HEY, T., LIPPS, G. & KRAUSS, G. 1999. Photocrosslinking locates a binding site for the large subunit of human replication protein A to the damaged strand of cisplatin-modified DNA. *Nucleic Acids Res*, 27, 3183-9.
- SCRIMA, A., FISCHER, E. S., LINGARAJU, G. M., BOHM, K., CAVADINI, S. & THOMA, N. H. 2011. Detecting UV-lesions in the genome: The modular CRL4 ubiquitin ligase does it best! *FEBS Lett*, 585, 2818-25.
- SCRIMA, A., KONICKOVA, R., CZYZEWSKI, B. K., KAWASAKI, Y., JEFFREY, P. D., GROISMAN, R., NAKATANI, Y., IWAI, S., PAVLETICH, N. P. & THOMA, N. H. 2008. Structural basis of UV DNA-damage recognition by the DDB1-DDB2 complex. *Cell*, 135, 1213-23.
- SEKULIC, N., BASSETT, E. A., ROGERS, D. J. & BLACK, B. E. 2010. The structure of (CENP-A-H4)(2) reveals physical features that mark centromeres. *Nature*, 467, 347-51.
- SELBY, C. P. & SANCAR, A. 1997. Human transcription-repair coupling factor CSB/ERCC6 is a DNA-stimulated ATPase but is not a helicase and does not disrupt the ternary transcription complex of stalled RNA polymerase II. *J Biol Chem*, 272, 1885-90.
- SHIA, W. J., LI, B. & WORKMAN, J. L. 2006. SAS-mediated acetylation of histone H4 Lys 16 is required for H2A.Z incorporation at subtelomeric regions in *Saccharomyces cerevisiae*. *Genes Dev*, 20, 2507-12.
- SHILATIFARD, A. 2006. Chromatin modifications by methylation and ubiquitination: implications in the regulation of gene expression. *Annu Rev Biochem*, 75, 243-69.
- SHIOTA, S. & NAKAYAMA, H. 1997. UV endonuclease of *Micrococcus luteus*, a cyclobutane pyrimidine dimer-DNA glycosylase/abasic lyase: cloning and characterization of the gene. *Proc Natl Acad Sci U S A*, 94, 593-8.
- SHIVASWAMY, S. & IYER, V. R. 2007. Genome-wide analysis of chromatin status using tiling microarrays. *Methods*, 41, 304-11.
- SHRIVASTAV, D., LI D FAU - ESSIGMANN, J. M. & ESSIGMANN, J. M. 2010. Chemical biology of mutagenesis and DNA repair: cellular responses to DNA alkylation.
- SIDDIQ, Z. H. 2005. Mechanisms of Action of Cancer Chemotherapeutic Agents: DNA-Interactive Alkylating Agents and Antitumour Platinum-Based Drugs. *The Cancer Handbook*. John Wiley

- & Sons, Ltd.
- SIJBERS, A. M., DE LAAT, W. L., ARIZA, R. R., BIGGERSTAFF, M., WEI, Y. F., MOGGS, J. G., CARTER, K. C., SHELL, B. K., EVANS, E., DE JONG, M. C., RADEMAKERS, S., DE ROOIJ, J., JASPERS, N. G., HOEIJMAKERS, J. H. & WOOD, R. D. 1996a. Xeroderma pigmentosum group F caused by a defect in a structure-specific DNA repair endonuclease. *Cell*, 86, 811-22.
- SIJBERS, A. M., VAN DER SPEK, P. J., ODIJK, H., VAN DEN BERG, J., VAN DUIN, M., WESTERVELD, A., JASPERS, N. G., BOOTSMA, D. & HOEIJMAKERS, J. H. 1996b. Mutational analysis of the human nucleotide excision repair gene ERCC1. *Nucleic Acids Res*, 24, 3370-80.
- SMERDON, M. J. 1991. DNA repair and the role of chromatin structure. *Curr Opin Cell Biol*, 3, 422-8.
- SMERDON, M. J., LAN, S. Y., CALZA, R. E. & REEVES, R. 1982. Sodium butyrate stimulates DNA repair in UV-irradiated normal and xeroderma pigmentosum human fibroblasts. *J Biol Chem*, 257, 13441-7.
- SOMESH, B. P., REID, J., LIU, W. F., SOGAARD, T. M., ERDJUMENT-BROMAGE, H., TEMPST, P. & SVEJSTRUP, J. Q. 2005. Multiple mechanisms confining RNA polymerase II ubiquitylation to polymerases undergoing transcriptional arrest. *Cell*, 121, 913-23.
- STARESINCIC, L., FAGBEMI, A. F., ENZLIN, J. H., GOURDIN, A. M., WIJGERS, N., DUNAND-SAUTHIER, I., GIGLIA-MARI, G., CLARKSON, S. G., VERMEULEN, W. & SCHARER, O. D. 2009. Coordination of dual incision and repair synthesis in human nucleotide excision repair. *EMBO J*, 28, 1111-20.
- STERNER, D. E., NATHAN, D., REINDLE, A., JOHNSON, E. S. & BERGER, S. L. 2006. Sumoylation of the yeast Gcn5 protein. *Biochemistry*, 45, 1035-42.
- STRAHL, B. D. & ALLIS, C. D. 2000. The language of covalent histone modifications. *Nature*, 403, 41-5.
- STRAUBE, K., BLACKWELL, J. S., JR. & PEMBERTON, L. F. 2010. Nap1 and Chz1 have separate Htz1 nuclear import and assembly functions. *Traffic*, 11, 185-97.
- STRYER, L., BERG, J. M. & TYMOCZKO, J. L. 2006. *Biochemistry: International edition*, New York, W.H. Freeman & Co Ltd.
- SU, D. G., KAO, J. L., GROSS, M. L. & TAYLOR, J. S. 2008. Structure determination of an interstrand-type cis-anti cyclobutane thymine dimer produced in high yield by UVB light in an oligodeoxynucleotide at acidic pH. *J Am Chem Soc*, 130, 11328-37.
- SUGASAWA, K. 2006. UV-induced ubiquitylation of XPC complex, the UV-DDB-ubiquitin ligase complex, and DNA repair. *J Mol Histol*, 37, 189-202.
- SUGASAWA, K. 2009. Regulation of damage recognition in mammalian global genomic nucleotide excision repair. *Mutat Res*.
- SUGASAWA, K., AKAGI, J., NISHI, R., IWAI, S. & HANAOKA, F. 2009. Two-step recognition of DNA damage for mammalian nucleotide excision repair: Directional binding of the XPC complex and DNA strand scanning. *Mol Cell*, 36, 642-53.
- SUGASAWA, K., MASUTANI, C. & HANAOKA, F. 1993. Cell-free repair of UV-damaged simian virus 40 chromosomes in human cell extracts. I. Development of a cell-free system detecting excision repair of UV-irradiated SV40 chromosomes. *J Biol Chem*, 268, 9098-104.
- SUGASAWA, K., MASUTANI, C., UCHIDA, A., MAEKAWA, T., VAN DER SPEK, P. J., BOOTSMA, D., HOEIJMAKERS, J. H. & HANAOKA, F. 1996. HHR23B, a human Rad23 homolog, stimulates XPC protein in nucleotide excision repair in vitro. *Mol Cell Biol*, 16, 4852-61.
- SUGASAWA, K., NG, J. M., MASUTANI, C., IWAI, S., VAN DER SPEK, P. J., EKER, A. P., HANAOKA, F., BOOTSMA, D. & HOEIJMAKERS, J. H. 1998. Xeroderma pigmentosum group C protein complex is the initiator of global genome nucleotide excision repair. *Mol Cell*, 2, 223-32.

- SUGASAWA, K., OKAMOTO, T., SHIMIZU, Y., MASUTANI, C., IWAI, S. & HANAOKA, F. 2001. A multistep damage recognition mechanism for global genomic nucleotide excision repair. *Genes Dev*, 15, 507-21.
- SUGASAWA, K., OKUDA, Y., SAIJO, M., NISHI, R., MATSUDA, N., CHU, G., MORI, T., IWAI, S., TANAKA, K. & HANAOKA, F. 2005. UV-induced ubiquitylation of XPC protein mediated by UV-DDB-ubiquitin ligase complex. *Cell*, 121, 387-400.
- SUGASAWA, K., SHIMIZU, Y., IWAI, S. & HANAOKA, F. 2002. A molecular mechanism for DNA damage recognition by the xeroderma pigmentosum group C protein complex. *DNA Repair (Amst)*, 1, 95-107.
- SUKA, N., SUKA, Y., CARMEN, A. A., WU, J. & GRUNSTEIN, M. 2001. Highly Specific Antibodies Determine Histone Acetylation Sites Usage in Yeast Heterochromatin and Euchromatin. *Molecular Cell*, 8, 473-479.
- SUNG, J.-S. & DEMPSEY, B. 2006. Roles of base excision repair subpathways in correcting oxidized abasic sites in DNA. *FEBS Journal*, 273, 1620-1629.
- SUNG, P., BAILLY, V., WEBER, C., THOMPSON, L., PRAKASH, L. & PRAKASH, S. 1993. Human xeroderma pigmentosum group D gene encodes a DNA helicase. *Nature*, 365, 852-5.
- SUNG, P., PRAKASH, L., MATSON, S. W. & PRAKASH, S. 1987. RAD3 protein of *Saccharomyces cerevisiae* is a DNA helicase. *Proc Natl Acad Sci U S A*, 84, 8951-5.
- SUQUET, C. & SMERDON, M. J. 1993. UV damage to DNA strongly influences its rotational setting on the histone surface of reconstituted nucleosomes. *J Biol Chem*, 268, 23755-7.
- SUTHERLAND, B. M. & SHIH, A. G. 1983. Quantitation of pyrimidine dimer contents of nonradioactive deoxyribonucleic acid by electrophoresis in alkaline agarose gels. *Biochemistry*, 22, 745-9.
- SUTO, R. K., CLARKSON, M. J., TREMETHICK, D. J. & LUGER, K. 2000. Crystal structure of a nucleosome core particle containing the variant histone H2A.Z. *Nat Struct Biol*, 7, 1121-4.
- SVEJSTRUP, J. Q. 2002. Mechanisms of transcription-coupled DNA repair. *Nat Rev Mol Cell Biol*, 3, 21-9.
- SVEJSTRUP, J. Q. 2003. Rescue of arrested RNA polymerase II complexes. *J Cell Sci*, 116, 447-51.
- SVEJSTRUP, J. Q. 2007. Contending with transcriptional arrest during RNAPII transcript elongation. *Trends Biochem Sci*, 32, 165-71.
- SVEJSTRUP, J. Q., VICHI, P. & EGLY, J. M. 1996. The multiple roles of transcription/repair factor TFIIH. *Trends Biochem Sci*, 21, 346-50.
- SVOTELIS, A., GEVRY, N. & GAUDREAU, L. 2009. Regulation of gene expression and cellular proliferation by histone H2A.Z. *Biochem Cell Biol*, 87, 179-88.
- SWEDER, K. S. & HANAWALT, P. C. 1992. Preferential repair of cyclobutane pyrimidine dimers in the transcribed strand of a gene in yeast chromosomes and plasmids is dependent on transcription. *Proc Natl Acad Sci U S A*, 89, 10696-700.
- SZUMIEL, I. 2008. Intrinsic radiation sensitivity: cellular signaling is the key. *Radiat Res*, 169, 249-58.
- TAGAMI, H., RAY-GALLET, D., ALMOUZNI, G. & NAKATANI, Y. 2004. Histone H3.1 and H3.3 complexes mediate nucleosome assembly pathways dependent or independent of DNA synthesis. *Cell*, 116, 51-61.
- TALBERT, P. B. & HENIKOFF, S. 2010. Histone variants--ancient wrap artists of the epigenome. *Nat Rev Mol Cell Biol*, 11, 264-75.
- TANAKA, K. & WOOD, R. D. 1994. Xeroderma pigmentosum and nucleotide excision repair of DNA. *Trends Biochem Sci*, 19, 83-6.
- TANG, J. & CHU, G. 2002. Xeroderma pigmentosum complementation group E and UV-damaged

- DNA-binding protein. *DNA Repair (Amst)*, 1, 601-16.
- TANG, M. S., BOHR, V. A., ZHANG, X. S., PIERCE, J. & HANAWALT, P. C. 1989. Quantification of aminofluorene adduct formation and repair in defined DNA sequences in mammalian cells using the UVRABC nuclease. *J Biol Chem*, 264, 14455-62.
- TANTIN, D. 1998. RNA polymerase II elongation complexes containing the Cockayne syndrome group B protein interact with a molecular complex containing the transcription factor IIH components xeroderma pigmentosum B and p62. *J Biol Chem*, 273, 27794-9.
- TAPIAS, A., AURIOL, J., FORGET, D., ENZLIN, J. H., SCHARER, O. D., COIN, F., COULOMBE, B. & EGLY, J. M. 2004. Ordered conformational changes in damaged DNA induced by nucleotide excision repair factors. *J Biol Chem*, 279, 19074-83.
- TASCHNER, M., HARREMAN, M., TENG, Y., GILL, H., ANINDYA, R., MASLEN, S. L., SKEHEL, J. M., WATERS, R. & SVEJSTRUP, J. Q. 2010. A role for checkpoint kinase-dependent Rad26 phosphorylation in transcription-coupled DNA repair in *Saccharomyces cerevisiae*. *Mol Cell Biol*, 30, 436-46.
- TATUM, D. & LI, S. 2011. Evidence that the histone methyltransferase Dot1 mediates global genomic repair by methylating histone H3 on lysine 79. *J Biol Chem*, 286, 17530-5.
- TENG, Y., BENNETT, M., EVANS, K. E., ZHUANG-JACKSON, H., HIGGS, A., REED, S. H. & WATERS, R. 2010. A novel method for the genome-wide high resolution analysis of DNA damage. *Nucleic Acids Res.*
- TENG, Y., LI, S., WATERS, R. & REED, S. H. 1997. Excision repair at the level of the nucleotide in the *Saccharomyces cerevisiae* MFA2 gene: mapping of where enhanced repair in the transcribed strand begins or ends and identification of only a partial rad16 requisite for repairing upstream control sequences. *J Mol Biol*, 267, 324-37.
- TENG, Y., LIU, H., GILL, H. W., YU, Y., WATERS, R. & REED, S. H. 2008a. *Saccharomyces cerevisiae* Rad16 mediates ultra-violet histone H3 acetylation required for efficient global genome nucleotide-excision repair. *EMBO reports*, 9, 97-102.
- TENG, Y., LIU, H., GILL, H. W., YU, Y., WATERS, R. & REED, S. H. 2008b. *Saccharomyces cerevisiae* Rad16 mediates ultraviolet-dependent histone H3 acetylation required for efficient global genome nucleotide-excision repair. *EMBO Rep*, 9, 97-102.
- TENG, Y., LONGHESE, M., MCDONOUGH, G. & WATERS, R. 1998. Mutants with changes in different domains of yeast replication protein A exhibit differences in repairing the control region, the transcribed strand and the non-transcribed strand of the *Saccharomyces cerevisiae* MFA2 gene. *J Mol Biol*, 280, 355-63.
- TENG, Y. & WATERS, R. 2000. Excision repair at the level of the nucleotide in the upstream control region, the coding sequence and in the region where transcription terminates of the *Saccharomyces cerevisiae* MFA2 gene and the role of RAD26. *Nucleic Acids Res*, 28, 1114-9.
- TENG, Y., YU, S., REED, S. H. & WATERS, R. 2009. Lux ex tenebris: nucleotide resolution DNA repair and nucleosome mapping. *Methods*, 48, 23-34.
- TENG, Y., YU, S. & WATERS, R. 2001. The mapping of nucleosomes and regulatory protein binding sites at the *Saccharomyces cerevisiae* MFA2 gene: a high resolution approach. *Nucleic Acids Res*, 29, E64-4.
- TENG, Y., YU, Y., FERREIRO, J. A. & WATERS, R. 2005. Histone acetylation, chromatin remodelling, transcription and nucleotide excision repair in *S. cerevisiae*: studies with two model genes. *DNA Repair (Amst)*, 4, 870-83.
- TENG, Y., YU, Y. & WATERS, R. 2002. The *Saccharomyces cerevisiae* histone acetyltransferase Gcn5 has

- a role in the photoreactivation and nucleotide excision repair of UV-induced cyclobutane pyrimidine dimers in the MFA2 gene. *J Mol Biol*, 316, 489-99.
- THAMBIRAJAH, A. A., DRYHURST, D., ISHIBASHI, T., LI, A., MAFFEY, A. H. & AUSIO, J. 2006. H2A.Z stabilizes chromatin in a way that is dependent on core histone acetylation. *J Biol Chem*, 281, 20036-44.
- THATCHER, T. H. & GOROVSKY, M. A. 1994. Phylogenetic analysis of the core histones H2A, H2B, H3, and H4. *Nucleic Acids Res*, 22, 174-9.
- THOMA, F. 1999. Light and dark in chromatin repair: repair of UV-induced DNA lesions by photolyase and nucleotide excision repair. *EMBO J*, 18, 6585-98.
- THOMAS, M. & CHIANG, C. 2006. The general transcription machinery and general cofactors. *Crit Rev Biochem Mol Biol*, 41, 105-78.
- THORNE, A. W., SAUTIERE, P., BRIAND, G. & CRANE-ROBINSON, C. 1987. The structure of ubiquitinated histone H2B. *EMBO J*, 6, 1005-10.
- TIJSTERMAN, M., DE PRIL, R., TASSERON-DE JONG, J. G. & BROUWER, J. 1999. RNA polymerase II transcription suppresses nucleosomal modulation of UV-induced (6-4) photoproduct and cyclobutane pyrimidine dimer repair in yeast. *Mol Cell Biol*, 19, 934-40.
- TIJSTERMAN, M., TASSERON-DE JONG, J. G., VERHAGE, R. A. & BROUWER, J. 1998. Defective Kin28, a subunit of yeast TFIIF, impairs transcription-coupled but not global genome nucleotide excision repair. *Mutat Res*, 409, 181-8.
- TOMKINSON, A. E., BARDWELL, A. J., TAPPE, N., RAMOS, W. & FRIEDBERG, E. C. 1994. Purification of Rad1 protein from *Saccharomyces cerevisiae* and further characterization of the Rad1/Rad10 endonuclease complex. *Biochemistry*, 33, 5305-11.
- TORNALETTI, S. 2009. DNA repair in mammalian cells: Transcription-coupled DNA repair: directing your effort where it's most needed. *Cell Mol Life Sci*, 66, 1010-20.
- TORNALETTI, S., REINES, D. & HANAWALT, P. C. 1999. Structural characterization of RNA polymerase II complexes arrested by a cyclobutane pyrimidine dimer in the transcribed strand of template DNA. *J Biol Chem*, 274, 24124-30.
- TRAN, H. T., DEGTYAREVA, N. P., GORDENIN, D. A. & RESNICK, M. A. 1999. Genetic factors affecting the impact of DNA polymerase delta proofreading activity on mutation avoidance in yeast. *Genetics*, 152, 47-59.
- TREMBLAY, M., TENG, Y., PAQUETTE, M., WATERS, R. & CONCONI, A. 2008. Complementary roles of yeast Rad4p and Rad34p in nucleotide excision repair of active and inactive rRNA gene chromatin. *Mol Cell Biol*, 28, 7504-13.
- TREMEAU-BRAVARD, A., RIEDL, T., EGLY, J. M. & DAHMUS, M. E. 2004. Fate of RNA polymerase II stalled at a cisplatin lesion. *J Biol Chem*, 279, 7751-9.
- TREMETHICK, D. J. 2007. Higher-order structures of chromatin: the elusive 30 nm fiber. *Cell*, 128, 651-4.
- TROELSTRA, C., VAN GOOL, A., DE WIT, J., VERMEULEN, W., BOOTSMAN, D. & HOEIJMAKERS, J. H. 1992. ERCC6, a member of a subfamily of putative helicases, is involved in Cockayne's syndrome and preferential repair of active genes. *Cell*, 71, 939-53.
- TSODIKOV, O. V., IVANOV, D., ORELLI, B., STARESINCIC, L., SHOSHANI, I., OBERMAN, R., SCHARER, O. D., WAGNER, G. & ELLENBERGER, T. 2007. Structural basis for the recruitment of ERCC1-XPF to nucleotide excision repair complexes by XPA. *EMBO J*, 26, 4768-76.
- URA, K., ARAKI, M., SAEKI, H., MASUTANI, C., ITO, T., IWAI, S., MIZUKOSHI, T., KANEDA, Y. & HANAOKA,

- F. 2001. ATP-dependent chromatin remodeling facilitates nucleotide excision repair of UV-induced DNA lesions in synthetic dinucleosomes. *EMBO J*, 20, 2004-14.
- URA, K. & HAYES, J. J. 2002. Nucleotide excision repair and chromatin remodeling. *Eur J Biochem*, 269, 2288-93.
- VAN DEN BOOM, V., CITTERIO, E., HOOGSTATEN, D., ZOTTER, A., EGLY, J. M., VAN CAPPELLEN, W. A., HOEIJMAKERS, J. H., HOUTSMULLER, A. B. & VERMEULEN, W. 2004. DNA damage stabilizes interaction of CSB with the transcription elongation machinery. *J Cell Biol*, 166, 27-36.
- VAN GOOL, A. J., CITTERIO, E., RADEMAKERS, S., VAN OS, R., VERMEULEN, W., CONSTANTINO, A., EGLY, J. M., BOOTSMA, D. & HOEIJMAKERS, J. H. 1997. The Cockayne syndrome B protein, involved in transcription-coupled DNA repair, resides in an RNA polymerase II-containing complex. *EMBO J*, 16, 5955-65.
- VAN GOOL, A. J., VERHAGE, R., SWAGEMAKERS, S. M., VAN DE PUTTE, P., BROUWER, J., TROELSTRA, C., BOOTSMA, D. & HOEIJMAKERS, J. H. 1994. RAD26, the functional *S. cerevisiae* homolog of the Cockayne syndrome B gene ERCC6. *EMBO J*, 13, 5361-9.
- VAN LEEUWEN, F., GAFKEN, P. R. & GOTTSCHLING, D. E. 2002. Dot1p modulates silencing in yeast by methylation of the nucleosome core. *Cell*, 109, 745-56.
- VAN VUUREN, A. J., APPELDOORN, E., ODIJK, H., YASUI, A., JASPERS, N. G., BOOTSMA, D. & HOEIJMAKERS, J. H. 1993. Evidence for a repair enzyme complex involving ERCC1 and complementing activities of ERCC4, ERCC11 and xeroderma pigmentosum group F. *EMBO J*, 12, 3693-701.
- VANDEMARK, A. P., KASTEN, M. M., FERRIS, E., HEROUX, A., HILL, C. P. & CAIRNS, B. R. 2007. Autoregulation of the rsc4 tandem bromodomain by gcn5 acetylation. *Mol Cell*, 27, 817-28.
- VENEMA, J., MULLENDERS, L. H., NATARAJAN, A. T., VAN ZEELAND, A. A. & MAYNE, L. V. 1990. The genetic defect in Cockayne syndrome is associated with a defect in repair of UV-induced DNA damage in transcriptionally active DNA. *Proc Natl Acad Sci U S A*, 87, 4707-11.
- VENEMA, J., VAN HOFFEN, A., KARACAGI, V., NATARAJAN, A. T., VAN ZEELAND, A. A. & MULLENDERS, L. H. 1991. Xeroderma pigmentosum complementation group C cells remove pyrimidine dimers selectively from the transcribed strand of active genes. *Mol Cell Biol*, 11, 4128-34.
- VENTERS, B. J., WACHI, S., MAVRICH, T. N., ANDERSEN, B. E., JENA, P., SINNAMON, A. J., JAIN, P., ROLLERI, N. S., JIANG, C., HEMERYCK-WALSH, C. & PUGH, B. F. 2011. A comprehensive genomic binding map of gene and chromatin regulatory proteins in *Saccharomyces*. *Mol Cell*, 41, 480-92.
- VERHAGE, R., ZEEMAN, A. M., DE GROOT, N., GLEIG, F., BANG, D. D., VAN DE PUTTE, P. & BROUWER, J. 1994. The RAD7 and RAD16 genes, which are essential for pyrimidine dimer removal from the silent mating type loci, are also required for repair of the nontranscribed strand of an active gene in *Saccharomyces cerevisiae*. *Mol Cell Biol*, 14, 6135-42.
- VERHAGE, R. A., VAN GOOL, A. J., DE GROOT, N., HOEIJMAKERS, J. H., VAN DE PUTTE, P. & BROUWER, J. 1996. Double mutants of *Saccharomyces cerevisiae* with alterations in global genome and transcription-coupled repair. *Mol Cell Biol*, 16, 496-502.
- VERMA, R., OANIA, R., GRAUMANN, J. & DESHAIES, R. J. 2004. Multiubiquitin chain receptors define a layer of substrate selectivity in the ubiquitin-proteasome system. *Cell*, 118, 99-110.
- VERMEULEN, W., BERGMANN, E., AURIOL, J., RADEMAKERS, S., FRIT, P., APPELDOORN, E., HOEIJMAKERS, J. H. & EGLY, J. M. 2000. Sublimiting concentration of TFIIH transcription/DNA repair factor causes TTD-A trichothiodystrophy disorder. *Nat Genet*, 26, 307-13.

- VOLKER, M., MONE, M. J., KARMAKAR, P., VAN HOFFEN, A., SCHUL, W., VERMEULEN, W., HOEIJMAKERS, J. H., VAN DRIEL, R., VAN ZEELAND, A. A. & MULLENDERS, L. H. 2001. Sequential assembly of the nucleotide excision repair factors in vivo. *Mol Cell*, 8, 213-24.
- WAKASUGI, M., KAWASHIMA, A., MORIOKA, H., LINN, S., SANCAR, A., MORI, T., NIKAIDO, O. & MATSUNAGA, T. 2002. DDB accumulates at DNA damage sites immediately after UV irradiation and directly stimulates nucleotide excision repair. *J Biol Chem*, 277, 1637-40.
- WAKASUGI, M. & SANCAR, A. 1998. Assembly, subunit composition, and footprint of human DNA repair excision nuclease. *Proc Natl Acad Sci U S A*, 95, 6669-74.
- WAKASUGI, M. & SANCAR, A. 1999. Order of assembly of human DNA repair excision nuclease. *J Biol Chem*, 274, 18759-68.
- WAN, Y., SALEEM, R. A., RATUSHNY, A. V., RODA, O., SMITH, J. J., LIN, C. H., CHIANG, J. H. & AITCHISON, J. D. 2009. Role of the histone variant H2A.Z/Htz1p in TBP recruitment, chromatin dynamics, and regulated expression of oleate-responsive genes. *Mol Cell Biol*, 29, 2346-58.
- WANG, H., ZHAI, L., XU, J., JOO, H. Y., JACKSON, S., ERDJUMENT-BROMAGE, H., TEMPST, P., XIONG, Y. & ZHANG, Y. 2006. Histone H3 and H4 ubiquitylation by the CUL4-DDB-ROC1 ubiquitin ligase facilitates cellular response to DNA damage. *Mol Cell*, 22, 383-94.
- WANG, Q. E., PRAETORIUS-IBBA, M., ZHU, Q., EL-MAHDY, M. A., WANI, G., ZHAO, Q., QIN, S., PATNAIK, S. & WANI, A. A. 2007. Ubiquitylation-independent degradation of Xeroderma pigmentosum group C protein is required for efficient nucleotide excision repair. *Nucleic Acids Res*, 35, 5338-50.
- WANG, Q. E., ZHU, Q., WANI, G., EL-MAHDY, M. A., LI, J. & WANI, A. A. 2005. DNA repair factor XPC is modified by SUMO-1 and ubiquitin following UV irradiation. *Nucleic Acids Res*, 33, 4023-34.
- WANG, Z., WEI, S., REED, S. H., WU, X., SVEJSTRUP, J. Q., FEAVER, W. J., KORNBERG, R. D. & FRIEDBERG, E. C. 1997. The RAD7, RAD16, and RAD23 genes of *Saccharomyces cerevisiae*: requirement for transcription-independent nucleotide excision repair in vitro and interactions between the gene products. *Mol Cell Biol*, 17, 635-43.
- WANG, Z., ZANG, C., CUI, K., SCHONES, D. E., BARSKI, A., PENG, W. & ZHAO, K. 2009. Genome-wide mapping of HATs and HDACs reveals distinct functions in active and inactive genes. *Cell*, 138, 1019-31.
- WARD, J. F. 1994. The complexity of DNA damage: relevance to biological consequences. *Int J Radiat Biol*, 66, 427-32.
- WARD, J. F. 2000. Complexity of damage produced by ionizing radiation. *Cold Spring Harb Symp Quant Biol*, 65, 377-82.
- WATANABE, S., RADMAN-LIVAJA, M., RANDO, O. J. & PETERSON, C. L. 2013. A histone acetylation switch regulates H2A.Z deposition by the SWR-C remodeling enzyme. *Science*, 340, 195-9.
- WATERS, R., EVANS, K., BENNETT, M., YU, S. & REED, S. 2012. Nucleotide Excision Repair in Cellular Chromatin: Studies with Yeast from Nucleotide to Gene to Genome. *Int J Mol Sci*, 13, 11141-11164.
- WATERS, R., REED, S. H., YU, Y. & TENG, Y. 2008. Chromatin modifications and nucleotide excision repair. *SEB Exp Biol Ser*, 59, 189-201.
- WATERS, R., TENG, Y., YU, Y., YU, S. & REED, S. H. 2009. Tilting at windmills? The nucleotide excision repair of chromosomal DNA. *DNA Repair (Amst)*, 8, 146-52.
- WATKINS, J. F., SUNG, P., PRAKASH, L. & PRAKASH, S. 1993. The *Saccharomyces cerevisiae* DNA repair gene RAD23 encodes a nuclear protein containing a ubiquitin-like domain required for

- biological function. *Mol Cell Biol*, 13, 7757-65.
- WEIBEZAHN, K. F., LOHRER, H. & HERRLICH, P. 1985. Double-strand break repair and G2 block in Chinese hamster ovary cells and their radiosensitive mutants. *Mutat Res*, 145, 177-83.
- WEISS, K. & SIMPSON, R. T. 1998. High-resolution structural analysis of chromatin at specific loci: *Saccharomyces cerevisiae* silent mating type locus HMLalpha. *Mol Cell Biol*, 18, 5392-403.
- WELLINGER, R. E. & THOMA, F. 1997. Nucleosome structure and positioning modulate nucleotide excision repair in the non-transcribed strand of an active gene. *EMBO J*, 16, 5046-56.
- WEST, M. H. & BONNER, W. M. 1980. Histone 2A, a heteromorphous family of eight protein species. *Biochemistry*, 19, 3238-45.
- WETERINGS, E. & VAN GENT, D. C. 2004. The mechanism of non-homologous end-joining: a synopsis of synapsis. *DNA Repair*, 3, 1425-1435.
- WIEDEMANN, S. M., MILDNER, S. N., BONISCH, C., ISRAEL, L., MAISER, A., MATHEISL, S., STRAUB, T., MERKL, R., LEONHARDT, H., KREMMER, E., SCHERMELLEH, L. & HAKE, S. B. 2010. Identification and characterization of two novel primate-specific histone H3 variants, H3.X and H3.Y. *J Cell Biol*, 190, 777-91.
- WINKLER, G. S., ARAÑJO, S. J., FIEDLER, U., VERMEULEN, W., COIN, F., EGLY, J.-M., HOEIJMAKERS, J. H. J., WOOD, R. D., TIMMERS, H. T. M. & WEEDA, G. 2000. TFIIF with Inactive XPD Helicase Functions in Transcription Initiation but Is Defective in DNA Repair. *Journal of Biological Chemistry*, 275, 4258-4266.
- WITTSCHIEBEN, B. O., IWAI, S. & WOOD, R. D. 2005. DDB1-DDB2 (xeroderma pigmentosum group E) protein complex recognizes a cyclobutane pyrimidine dimer, mismatches, apurinic/apyrimidinic sites, and compound lesions in DNA. *J Biol Chem*, 280, 39982-9.
- WOLD, M. S. 1997. Replication protein A: a heterotrimeric, single-stranded DNA-binding protein required for eukaryotic DNA metabolism. *Annu Rev Biochem*, 66, 61-92.
- WONG, L. H., MCGHIE, J. D., SIM, M., ANDERSON, M. A., AHN, S., HANNAN, R. D., GEORGE, A. J., MORGAN, K. A., MANN, J. R. & CHOO, K. H. 2010. ATRX interacts with H3.3 in maintaining telomere structural integrity in pluripotent embryonic stem cells. *Genome Res*, 20, 351-60.
- WOODCOCK, C. L. & DIMITROV, S. 2001. Higher-order structure of chromatin and chromosomes. *Curr Opin Genet Dev*, 11, 130-5.
- WOUDSTRA, E. C., GILBERT, C., FELLOWS, J., JANSEN, L., BROUWER, J., ERDJUMENT-BROMAGE, H., TEMPST, P. & SVEJSTRUP, J. Q. 2002. A Rad26-Def1 complex coordinates repair and RNA pol II proteolysis in response to DNA damage. *Nature*, 415, 929-33.
- WU, W. H., ALAMI, S., LUK, E., WU, C. H., SEN, S., MIZUGUCHI, G., WEI, D. & WU, C. 2005. Swc2 is a widely conserved H2AZ-binding module essential for ATP-dependent histone exchange. *Nat Struct Mol Biol*, 12, 1064-71.
- WU, X., SHELL, S. M., YANG, Z. & ZOU, Y. 2006. Phosphorylation of nucleotide excision repair factor xeroderma pigmentosum group A by ataxia telangiectasia mutated and Rad3-related-dependent checkpoint pathway promotes cell survival in response to UV irradiation. *Cancer Res*, 66, 2997-3005.
- XIE, Z., LIU, S., ZHANG, Y. & WANG, Z. 2004. Roles of Rad23 protein in yeast nucleotide excision repair. *Nucleic Acids Res*, 32, 5981-90.
- XU, Y., AYRAPETOV, M. K., XU, C., GURSOY-YUZUGULLU, O., HU, Y. & PRICE, B. D. 2012. Histone H2A.Z Controls a Critical Chromatin Remodeling Step Required for DNA Double-Strand Break Repair. *Mol Cell*.

- YAMAMOTO, J., HITOMI, K., HAYASHI, R., GETZOFF, E. D. & IWAI, S. 2009. Role of the Carbonyl Group of the (6–4) Photoproduct in the (6–4) Photolyase Reaction. *Biochemistry*, 48, 9306-9312.
- YAN, Y., HARPER, S., SPEICHER, D. W. & MARMORSTEIN, R. 2002. The catalytic mechanism of the ESA1 histone acetyltransferase involves a self-acetylated intermediate. *Nat Struct Biol*, 9, 862-9.
- YANG, X. J. 2004. Lysine acetylation and the bromodomain: a new partnership for signaling. *Bioessays*, 26, 1076-87.
- YANG, X. J. & SETO, E. 2008. The Rpd3/Hda1 family of lysine deacetylases: from bacteria and yeast to mice and men. *Nat Rev Mol Cell Biol*, 9, 206-18.
- YANG, Z., ROGINSKAYA, M., COLIS, L. C., BASU, A. K., SHELL, S. M., LIU, Y., MUSICH, P. R., HARRIS, C. M., HARRIS, T. M. & ZOU, Y. 2006. Specific and efficient binding of xeroderma pigmentosum complementation group A to double-strand/single-strand DNA junctions with 3'- and/or 5'-ssDNA branches. *Biochemistry*, 45, 15921-30.
- YANG, Z. G., LIU, Y., MAO, L. Y., ZHANG, J. T. & ZOU, Y. 2002. Dimerization of human XPA and formation of XPA2-RPA protein complex. *Biochemistry*, 41, 13012-20.
- YARRAGUDI, A. & MORSE, R. 2006. Chromatin opening and potentiation of transcriptional activation by the General Regulatory Factors, ABF1 and RAP1, in the budding yeast *Saccharomyces cerevisiae*. *Proc Indian Natn Sci Acad*, 72, 13-17.
- YASUDA, G., NISHI, R., WATANABE, E., MORI, T., IWAI, S., ORIOLI, D., STEFANINI, M., HANAOKA, F. & SUGASAWA, K. 2007. In vivo destabilization and functional defects of the xeroderma pigmentosum C protein caused by a pathogenic missense mutation. *Mol Cell Biol*, 27, 6606-14.
- YEH, J. I., LEVINE, A. S., DU, S., CHINTE, U., GHODKE, H., WANG, H., SHI, H., HSIEH, C. L., CONWAY, J. F., VAN HOUTEN, B. & RAPIC-OTRIN, V. 2012. Damaged DNA induced UV-damaged DNA-binding protein (UV-DDB) dimerization and its roles in chromatinized DNA repair. *Proc Natl Acad Sci U S A*, 109, E2737-46.
- YOKOI, M., MASUTANI, C., MAEKAWA, T., SUGASAWA, K., OHKUMA, Y. & HANAOKA, F. 2000. The xeroderma pigmentosum group C protein complex XPC-HR23B plays an important role in the recruitment of transcription factor IIH to damaged DNA. *J Biol Chem*, 275, 9870-5.
- YOU, J. S., WANG, M. & LEE, S. H. 2003. Biochemical analysis of the damage recognition process in nucleotide excision repair. *J Biol Chem*, 278, 7476-85.
- YU, S., OWEN-HUGHES, T., FRIEDBERG, E. C., WATERS, R. & REED, S. H. 2004. The yeast Rad7/Rad16/Abf1 complex generates superhelical torsion in DNA that is required for nucleotide excision repair. *DNA Repair (Amst)*, 3, 277-87.
- YU, S., SMIRNOVA, J. B., FRIEDBERG, E. C., STILLMAN, B., AKIYAMA, M., OWEN-HUGHES, T., WATERS, R. & REED, S. H. 2009. ABF1-binding sites promote efficient global genome nucleotide excision repair. *J Biol Chem*, 284, 966-73.
- YU, S., TENG, Y., WATERS, R. & REED, S. H. 2011. How chromatin is remodelled during DNA repair of UV-induced DNA damage in *Saccharomyces cerevisiae*. *PLoS Genet*, 7, e1002124.
- YU, S. L., LEE, S. K., JOHNSON, R. E., PRAKASH, L. & PRAKASH, S. 2003. The stalling of transcription at abasic sites is highly mutagenic. *Mol Cell Biol*, 23, 382-8.
- YU, Y., DENG, Y., REED, S. H., MILLAR, C. B. & WATERS, R. 2013. Histone variant Htz1 promotes histone H3 acetylation to enhance nucleotide excision repair in Htz1 nucleosomes. *Nucleic Acids Res*.
- YU, Y., TENG, Y., LIU, H., REED, S. H. & WATERS, R. 2005a. UV irradiation stimulates histone acetylation and chromatin remodeling at a repressed yeast locus. *Proc Natl Acad Sci U S A*, 102, 8650-5.

- YU, Y., TENG, Y., LIU, H., REED, S. H. & WATERS, R. 2005b. UV irradiation stimulates histone acetylation and chromatin remodelling at a repressed yeast locus. *PNAS*, 102, 8650-8655.
- YUAN, G. & ZHU, B. 2012. Histone variants and epigenetic inheritance. *Biochim Biophys Acta*, 1819, 222-9.
- YUAN, G. C., LIU, Y. J., DION, M. F., SLACK, M. D., WU, L. F., ALTSCHULER, S. J. & RANDO, O. J. 2005. Genome-scale identification of nucleosome positions in *S. cerevisiae*. *Science*, 309, 626-30.
- ZHANG, H., RICHARDSON, D. O., ROBERTS, D. N., UTLEY, R., ERDJUMENT-BROMAGE, H., TEMPST, P., COTE, J. & CAIRNS, B. R. 2004. The Yaf9 component of the SWR1 and NuA4 complexes is required for proper gene expression, histone H4 acetylation, and Htz1 replacement near telomeres. *Mol Cell Biol*, 24, 9424-36.
- ZHANG, H., ROBERTS, D. N. & CAIRNS, B. R. 2005. Genome-wide dynamics of Htz1, a histone H2A variant that poises repressed/basal promoters for activation through histone loss. *Cell*, 123, 219-31.
- ZHANG, L., JONES, K., SMERDON, M. J. & GONG, F. 2009. Assays for chromatin remodeling during nucleotide excision repair in *Saccharomyces cerevisiae*. *Methods*, 48, 19-22.
- ZHANG, W., BONE, J. R., EDMONDSON, D. G., TURNER, B. M. & ROTH, S. Y. 1998. Essential and redundant functions of histone acetylation revealed by mutation of target lysines and loss of the Gcn5p acetyltransferase. *The EMBO Journal*, 17, 3155-3167.
- ZHOU, Y., KOU, H. & WANG, Z. 2007. Tfb5 interacts with Tfb2 and facilitates nucleotide excision repair in yeast. *Nucleic Acids Res*, 35, 861-71.
- ZIERLER, S., KLEIN, B., FURTNER, T., BRESGEN, N., LUTZ-MEINDL, U. & KERSCHBAUM, H. H. 2006. Ultraviolet irradiation-induced apoptosis does not trigger nuclear fragmentation but translocation of chromatin from nucleus into cytoplasm in the microglial cell-line, BV-2. *Brain Res*, 1121, 12-21.
- ZLATANOVA, J. & THAKAR, A. 2008. H2A.Z: view from the top. *Structure*, 16, 166-79.